

**Exploration of neuromuscular plasticity: an examination of acetylcholine
receptor and skeletal muscle fiber adaptations**

Ewa M. Kulig

A Thesis
In The Department
of
Chemistry and Biochemistry

Presented in Partial Fulfillment of the Requirements
for the Degree of
Doctor of Philosophy (Chemistry)
at
Concordia University
Montreal, Quebec, Canada

April 2012

© Ewa M. Kulig, 2012

CONCORDIA UNIVERSITY
School of Graduate Studies

This is to certify that the thesis prepared

By: **Ewa M. Kulig**

Entitled: **Exploration of neuromuscular plasticity: an examination of acetylcholine receptor and skeletal muscle fiber adaptations.**

and submitted in partial fulfillment of the requirements for the degree of

Doctor of Philosophy (Chemistry)

complies with the regulations of the University and meets the accepted standards with respect to originality and quality.

Signed by the final Examining Committee:

Dr. P. Wood-Adams	Chair
Dr. F. Ambrasio	External Examiner
Dr. J. Pfaus	External to Program
Dr. A. Piekny	Examiner
Dr. P. Joyce	Examiner
Dr. J. Turnbull	Examiner
Dr. H. Muchall	Thesis Supervisor

Approved by

Chair of Department or Graduate Program Director

Dean of Faculty

Abstract

Exploration of neuromuscular plasticity: an examination of acetylcholine receptor and skeletal muscle fiber adaptations.

Ewa M. Kulig, PhD
Concordia University, 2012

Muscle is an example of a beautifully orchestrated biological system whose main role is to convey a chemical stimulus into a mechanical response. Skeletal muscles carry out the function of moving the bones of the skeleton. Skeletal muscles display remarkable levels of adaptability and plasticity. The regulation of neuromuscular plasticity is influenced by signals coming from the motor neuron and from within the muscles. In this thesis, different transgenic and surgical mice models are used to investigate key aspects of muscle plasticity. Firstly, transgenic mice expressing a calmodulin-binding peptide are used to demonstrate that calmodulin regulates the aggregation of acetylcholine receptors. Secondly, the roles of Nuclear Factor of activated-Tcells (NFAT) transcription factors are investigated in adaptive muscle growth using mice knockouts for these transcription factors. The results presented indicate that NFATc2 and NFATc3 are essential for muscle hypertrophy and that they have distinct roles in the regulation of muscle growth. Thirdly, novel roles for the nerve-derived trophic factor agrin are explored in healthy and deteriorating muscles. Overall, the results presented in this thesis provide original information on the regulation of muscle plasticity and serve to point to novel potential targets in the regulation of various neuromuscular diseases.

Acknowledgments

I want to express my sincere gratitude to my thesis committee members Dr. Paul Joyce and Dr. Joanne Turnbull for their precious advice and insightful comments. A special thanks to the Chemistry Graduate Program Director, Dr. Heidi Muchall. I also wish to thank all other professors, faculty members and staff from Concordia University who helped me in this journey. Thank you to the members of Dr. Michel's lab, past and present, for their comments, technical help and friendships.

I am forever grateful to my boyfriend Artur for all his love, his everlasting support, his precious help and limitless patience. I also want to thank my beloved family for all their support and for always believing in me. Thank you to all my friends for their constant encouragement.

I wish to express my thanks to Aileen Murray for teaching and helping me with the animal care and Dr. Marc Champagne for his expertise in microscopy. Finally, I would like to thank everyone I encountered in my journey and who allowed me to become a stronger and better person in life.

I also wish to acknowledge the funding from Concordia University and the Canadian Institute of Health Research.

Contribution of Authors

All experiments presented in this thesis were carried out in the laboratory of Dr. Robin Michel, in the Department of Exercise Science at Concordia University.

All experiments presented in this thesis were performed by me with the exception of:

Chapter 2:

Raphael Vezina-Audette (McGill) collaborated on experiments presented in Figure 2.2. I performed all animal extractions; he carried out all cell cultures experiments. Histochemistry experiments were performed by both of us. Raphael conducted all statistical analysis in this figure.

Chapter 3:

Dr. Robin Michel performed all overload surgeries, with my assistance in wound suturing and animal care. In addition, Dr. Mathieu St-Louis helped me during muscle extractions.

Table of Contents

List of Figures	x
List of Tables	xii
List of Abbreviations	xiii
Chapter 1 : General Introduction	1
1.1 Skeletal muscle development and structure	2
1.1.1 Muscle structure	2
1.1.2 Development of skeletal muscle	6
1.1.3 Acetylcholine Receptors	8
1.1.4 Muscle fiber types	12
1.2 Skeletal muscle plasticity and signal transduction	14
1.2.1 Calmodulin	14
1.2.2 Calcium/calmodulin dependent protein kinase	16
1.2.3 Ca ²⁺ /CaM regulation of neuromuscular junction	19
1.2.4 Calcineurin	23
1.2.5 Nuclear Factor of Activated T-cells	26
1.2.6 Cn / NFAT signaling in muscle fiber remodelling	29
1.2.7 Agrin	33
1.2.8 Agrin structure	34
1.2.9 Agrin in skeletal muscles	37
1.3 Thesis organization, scope and hypotheses	43
Chapter 2 : Calmodulin signaling regulates acetylcholine receptor organization in CaMBP expressing mice	44
2.1 Background	45
2.2 Abstract	46
2.3 Introduction	47

2.4 Methods	50
2.4.1 Animal Care, Protocols and Extractions	50
2.4.2 Cell culture	51
2.4.3 RNA extraction and semi-quantitative RT-PCR	52
2.4.4 Histochemistry of NMJ	54
2.4.5 Protein Extraction and Western Blotting	55
2.4.6 Statistical Analysis	57
2.5 Results	57
2.5.1 Characterization of CaMBP-TG mice	57
2.5.2 Transgenic expression of CaMBP increases endplate complexity	60
2.5.3 The expression of selected transcripts is not altered in CaMBP-TG mice	62
2.5.4 CaMBP-TG mice do not show altered signaling of JNK and ERK kinase	64
2.5.5 Larger AChR aggregates are not caused by increased expression of AChR	65
2.6 Discussion	68
2.7 Future Directions	76
<i>Chapter 3 : NFATc2 and NFATc3 have essential roles in the regulation of adaptive skeletal muscle fiber growth</i>	78
3.1 Background	79
3.2 Abstract	80
3.3 Introduction	81
3.4 Methods	83
3.4.1 Animal Care and Protocols	83
3.4.2 Animal Surgeries and Extractions	84
3.4.3 Immunohistochemistry	86
3.4.4 Immunofluorescence	87
3.4.5 RNA extraction and semi-quantitative RT-PCR	88
3.4.6 Protein extraction and Western Blotting	90
3.4.7 Statistical Analysis	91
3.5 Results	92

3.5.1 NFATc2 ^{-/-} and NFATc3 ^{-/-} mice show blunted muscle growth following functional overload	92
3.5.2 NFATc2 ^{-/-} and NFATc3 ^{-/-} mice show altered growth that is fiber type specific	94
3.5.3 NFATc2 and NFATc3 knockout mice maintain the ability to remodel muscle fibers toward oxidative metabolic profiles	97
3.5.4 NFATc2 ^{-/-} and NFATc3 ^{-/-} mice display distinct nuclear localization of NFAT isoforms	99
3.5.5 NFATc2 ^{-/-} and NFATc3 ^{-/-} mice display an alteration in the expression of myogenic regulatory factors	104
3.5.6 NFATc2 ^{-/-} and NFATc3 ^{-/-} mice do not exhibit modification in Akt signaling in the overload growth model	107
3.6 Discussion	109
3.7 Future Directions	128
<i>Chapter 4 : Agrin regulates skeletal muscle signaling</i>	131
4.1 Background	132
4.2 Abstract	133
4.3 Introduction	134
4.4 Methods	136
4.4.1 Animal Care, Surgeries and Extractions	136
4.4.2 Animal Surgeries and Extractions	137
4.4.3 Immunohistochemistry	137
4.4.4 Protein extraction and Western Blotting	139
4.4.5 Statistical Analysis	141
4.5 Results	141
4.5.1 Agrin injection is not regulating muscle fiber growth in healthy adult mice	141
4.5.2 Agrin may regulate Akt signaling in muscles of healthy adult mice	142
4.5.3 Agrin does not activate Akt signaling in a sarcopenia model	144
4.5.4 Agrin treatment regulates central nucleation in dystrophic muscles	147
4.6 Discussion	150
4.7 Future Directions	157

<i>Chapter 5 : Conclusion</i>	158
Statistical Analysis	162
<i>Chapter 2: PCR</i>	162
<i>Chapter 2: Western Blotting</i>	164
<i>Chapter 3: Muscle Weights</i>	168
<i>Chapter 3: Fibers Size</i>	172
<i>Chapter 3: Fiber Number</i>	174
<i>Chapter 3: Analysis of MyHC IIa fibers</i>	176
<i>Chapter 3: Analysis of MyHC IIb fibers</i>	179
<i>Chapter 3: PCR</i>	182
<i>Chapter 3: Nuclear Localization</i>	193
<i>Chapter 3: Western Blotting</i>	197
<i>Chapter 4: Agrin in adult healthy mice</i>	199
<i>Chapter 4: Characterization of sarcopenia</i>	204
<i>Chapter 4: Agrin in sarcopenia</i>	206
<i>Chapter 4: Characterization of mdx mice</i>	208
<i>Chapter 4: Agrin in mdx mice</i>	211
References	214

List of Figures

Figure 1.1: Structure of skeletal muscle contractile unit (Marieb, 2001).	3
Figure 1.2: Dystrophin associated protein complex (Blake <i>et al.</i> , 2002).....	5
Figure 1.3: Myogenesis (Sabourin & Rudnicki, 2000).....	7
Figure 1.4: Crystal structure of muscle AChR (Lindstrom, 2010)	9
Figure 1.5: AChR aggregates topographic maturation (Kummer <i>et al.</i> , 2004).....	11
Figure 1.6: Properties of major fiber types (Gundersen, 2010)	12
Figure 1.7: Calmodulin secondary structure (Al-Shanti & Stewart, 2009).....	15
Figure 1.8: Schematic of multifunctional CaMK structure (Hook & Means, 2001)	17
Figure 1.9: CaMKII-HDAC4-Mgn signaling loop (Tang <i>et al.</i> , 2009)	21
Figure 1.10: Calcineurin structure (Al-Shanti & Stewart, 2009).....	24
Figure 1.11: Model of Cn activation (Li <i>et al.</i> , 2011).....	25
Figure 1.12: Schematic structure of NFAT protein (Hogan <i>et al.</i> , 2003)	28
Figure 1.13: Agrin functional domains (Ngo <i>et al.</i> , 2007).....	36
Figure 1.14: Agrin and α -DG signaling (Pilgram <i>et al.</i> , 2010).....	38
Figure 1.15: Agrin and LRP4/MuSK signaling (Song & Balice-Gordon, 2008).....	40
Figure 2.1: Decreased calmodulin signaling in CaMBP-TG mice	59
Figure 2.2: Expression of CaMBP leads to larger endplate structures <i>in vitro</i> and <i>in vivo</i>	61
Figure 2.3: The expression of selected gene targets is not changed in CaMBP-TG mice	63
Figure 2.4: Signaling of ERK and JNK are not altered in CaMBP-TG mice	65
Figure 2.5: Neither the AChR gene or AChR protein levels are altered in CaMBP-TG mice.	67
Figure 2.6: Schematic of signaling pathways investigated	72
Figure 3.1: Schematic of the functional overload model (Lieber, 2010).....	85
Figure 3.2: Blunted compensatory muscle growth in NFATc2 and NFATc3 knockout mice.....	93
Figure 3.3: Muscle fibers expressing MyHC Iia maintain their ability to grow in NFATc2 and NFATc3 knockout mice.....	95
Figure 3.4: Muscle fibers expressing MyHC Iib lose their ability to grow in NFATc2 and NFATc3 knockout mice.....	96
Figure 3.5: Remodeling toward oxidative muscle profiles is maintained in NFATc2 and NFATc3 knockout mice	98
Figure 3.6: NFATc2 and NFATc3 knockout mice do not display compensatory changes in the expression of <i>NFAT</i> mRNA levels.	100

Figure 3.7: Nuclear trafficking of NFAT protein family members is altered in NFATc2 ^{-/-} and NFATc3 ^{-/-} mice.....	103
Figure 3.8: NFATc2 influences <i>Myf5</i> levels while NFATc3 regulates <i>Mgn</i> levels.....	106
Figure 3.9: Akt signaling is not responsible for altered growth in NFAT knockout mice.....	108
Figure 4.1: Agrin is not promoting muscle growth in adult, healthy mice.	142
Figure 4.2: Agrin may regulate Akt signaling in muscles of adult, healthy mice.....	143
Figure 4.3: Characterization of the sarcopenia model	145
Figure 4.4: Agrin does not activate Akt signaling in aging muscles	146
Figure 4.5: Characterization of the dystrophic model.....	148
Figure 4.6: Agrin decrease central nucleation in mdx mice.....	149

List of Tables

Table 1-1: Properties of multifunctional CaMK: adapted from (Hook & Means, 2001).....	18
Table 1-2: NFAT protein nomenclature (from HGNC and PubMed).....	27
Table 2-1: Primers and RT-PCR conditions	53
Table 2-2: Western Blotting Conditions	57
Table 3-1: Primers and cycling conditions	89
Table 3-2: Western Blotting Conditions	91
Table 4-1: Western Blotting Conditions	140

List of Abbreviations

ACh	Acetylcholine
AChR	Acetylcholine Receptor
AGR	Agrin
BSA	Bovine Serum Albumin
CaM	Calmodulin
CaMBP	Calmodulin Binding Protein
CaMK	Calcium-Calmodulin Dependent Protein Kinase
CaMKK	CaMK Kinase
Cdk5	Cyclin-dependent kinase 5
cDNA	complementary DNA
CK1	Casein Kinase-1
CMD	Congenital Muscular Dystrophy
CMS	Congenital Myasthenia Syndrome
Cn	Calcineurin
CNS	Central Nervous System
CsA	Cyclosporine A
CSA	Cross Sectional Area
CTL	Control
DBD	DNA Binding Domain
DG	Dystroglycan
DGC	Dystrophin-Associated Glycoprotein Complex
dH ₂ O	Distilled Water
DMD	Duchenne Muscular Dystrophy
DNA	Deoxyribonucleic Acid
dNTP	Deoxyribonucleotide triphosphate
Dok-7	Downstream of tyrosine kinase-7
ECM	Extracellular Matrix
EDL	Extensor Digitorum Longus
ERK	Extracellular signal-Regulated Kinase
GABP	GA-Binding Protein
GSK3	Glycogen Synthase Kinase-3
HDAC	Histone Deacetylase
HRP	Horseradish Peroxidase
IGF	Insulin Growth Factor
JNK	c-Jun Terminal Kinase
LDL	Low-density lipoprotein

LRP4	LDL-receptor Related Protein 4
MAPK	Mitogen-Activated Protein Kinase
MG	Myasthenia Gravis
MMLV	Moloney Murine Leukemia Virus
MRF	Muscle Regulatory Factors
mRNA	messenger RNA
MuSK	Muscle Specific Kinase
MyHC	Myosin Heavy Chain
NES	Nuclear Export Signal
NFAT	Nuclear Factor of Activated T cells
NHR	NFAT Homology Region
NLS	Nuclear Localization Signal
NMJ	Neuromuscular Junction
NRG	Neuregulin
OV	Overload
PBS	Phosphate Buffered Saline
PCR	Polymerase Chain Reaction
PLA	Plantaris
PVDF	Polyvinylidene fluoride
Rapsyn	Receptor-associated protein of the synapse
RIPA	Radioimmunoprecipitation Assay
RNA	Ribonucleic Acid
RT	Reverse Transcription
SDS	Sodium Dodecyl Sulfate
SOL	Soleus
TA	Tibialis Anterior
TA	Transactivation Domain
TBS	Tris Buffered Saline
Tid1	Timorous imaginal disc-1
TnIs	Troponin I Slow

Chapter 1: ***General Introduction***

1.1 Skeletal muscle development and structure

1.1.1 Muscle structure

Muscle is an example of a beautifully orchestrated biological system whose main role is to convey a chemical stimulus into a mechanical response. Three types of muscle tissues exist: skeletal, cardiac and smooth. These three categories differ in their microscopic anatomy, location and control by the nervous and endocrine systems (Jenkins *et al.*, 2010). Skeletal muscles contract voluntarily, are striated and carry the function of moving the bones of the skeleton. Cardiac muscles are also striated and form the heart wall. These muscles carry heart contractions that serve to propel blood into the body's circulatory system. Finally, smooth muscle tissue is located in the walls of hollow internal structures such as blood vessels, the respiratory and the gastrointestinal track. Smooth muscles lack striations and perform involuntary movements that regulate the movement of liquids in internal body structures.

Skeletal muscle fibers are made up of bundles of myofibrils composed of a network of contractile myofilaments. The sarcomere is the functional unit of muscle contraction (Jenkins *et al.*, 2010) and it is defined as the region between successive Z-discs (also called Z-bands or Z-lines) (Figure 1.1). The Z-disc structural backbone is formed by α -actinin dimers where structural and signaling proteins, such as actin filaments, titin or nebulin, are inserted (Frank *et al.*, 2006). The thick filaments of the sarcomere are composed of myosin and are situated in the central portion of the sarcomere, while the thin actin containing filaments are situated toward the extremities of

the functional unit with one end attached to the Z line and the other binding myosin. Myosin and actin are contractile proteins of skeletal muscle that carry out the process of skeletal muscle contraction. More specifically, myosin is the motor protein that converts the chemical energy of ATP into the mechanical energy of motion, while using the actin filaments to perform a sliding motion that leads to muscle contraction (Jenkins *et al.*, 2010). This cycle of sarcomere contraction and relaxation is repeated to achieve muscle movement.

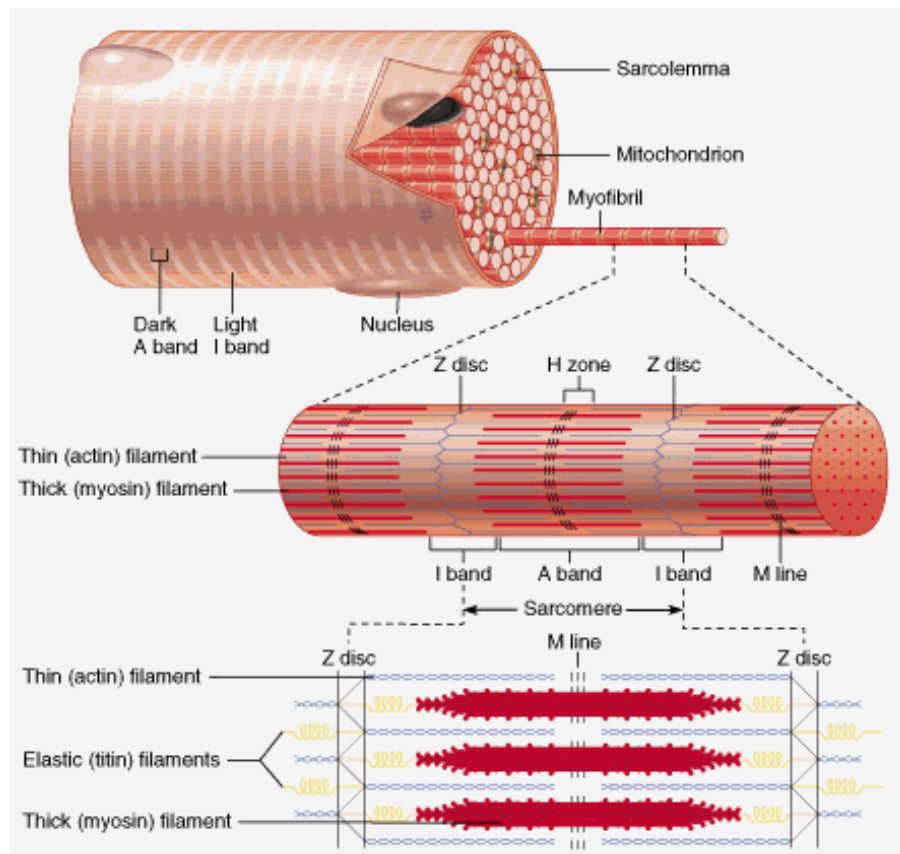


Figure 1.1: Structure of skeletal muscle contractile unit (Marieb, 2001).

Muscle contraction events are initiated by electrical signals coming from the nerve: a process referred to as excitation-contraction coupling (Jenkins *et al.*, 2010). Briefly, a nerve impulse will trigger the release of the neurotransmitter acetylcholine (ACh) from the presynaptic terminal into the synaptic cleft. Acetylcholine will bind to its receptor (AChR), situated on the postsynaptic muscle surface, and induce a conformational change opening this channel and allowing ion exchange. Most notably, the influx of Na^+ will lead to membrane depolarization and the propagation of an action potential. This action potential will travel down the muscle sarcolemma (muscle fiber plasma membrane) into the T-tubules (special extensions of the sarcolemma) where it will open sarcoplasmic reticulum Ca^{2+} channels. Ca^{2+} moving into the sarcoplasm (muscle fiber cytoplasm) will bind to the troponin-tropomyosin protein complex and move this complex away from the myosin binding site on actin. This process allows free myosin heads to bind and initiate the sliding motion cycle of muscle contraction.

In addition to muscle contractile proteins and their regulatory proteins, skeletal muscle also consists of a vast number of structural proteins that contribute to stability, elasticity, extensibility and alignment of muscle myofibrils (Jenkins *et al.*, 2010; Singhal & Martin, 2011). Some of these proteins assemble the extracellular matrix (ECM), while others form the muscle basement membrane that is linked to the muscle sarcolemma. The list of these proteins is extensive but includes agrin, laminin, collagen, perlecan, integrin, dystroglycan, rapsyn, and dystrophin (Pilgram *et al.*, 2010; Singhal & Martin, 2011). ECM proteins can form signaling complexes, for example laminins regulate, via

dystroglycan and integrins, the Akt signaling cascade (Langenbach & Rando, 2002). Furthermore, agrin and rapsyn modulate post-synaptic receptor density at muscle synapses (Moransard *et al.*, 2003). The complexity of the ECM highlights its essential roles in muscle development, muscle growth, neuromuscular junction formation and synaptic transmission (Singhal & Martin, 2011).

The most extensive and well-characterized complex formed by some of these proteins is the dystrophin-associated glycoprotein complex (DGC) (Figure 1.2). This complex links the sarcomere actin filaments to the integral membrane proteins of the sarcolemma, which in turn is connected to the connective tissue in the ECM, providing reinforcement to muscle structure.

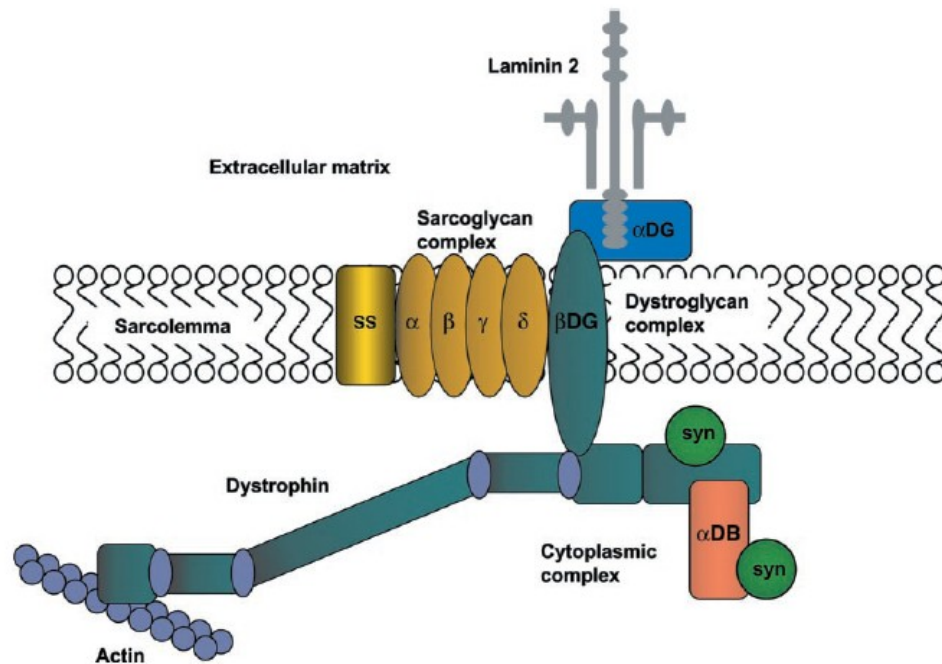


Figure 1.2: Dystrophin associated protein complex (Blake *et al.*, 2002)

Figure legend: DG, dystroglycan; syn, syntrophin; SS, sarcoglycan

This DGC is formed by proteins highly conserved between species and this highlights its important role in the maintenance of muscle fiber integrity (Pilgram *et al.*, 2010). A lack of, or mutation in, almost any of these proteins leads to muscular dystrophies such as Duchenne Muscular Dystrophy (characterized by the absence of functional dystrophin) or Limb Girdle Muscular Dystrophy (characterized by the absence of functional sarcoglycan). Moreover, it is now established that the DGC also serves as a platform for the proteins calmodulin and insulin, involved in muscle signaling (Pilgram *et al.*, 2010). Additionally, the DGC provides a scaffold for anchoring and regulating calcium transporters such as the store-operated channel (SOC) or the stretch-activated channel (SAC) regulating intracellular calcium concentration (Constantin *et al.*, 2006). As such, a better understanding of muscle structure can also provide a better comprehension of muscle and nerve communication.

1.1.2 Development of skeletal muscle

Skeletal muscles carry out numerous essential functions in the body including locomotor activity, posture and breathing. The development of skeletal muscle involves the simultaneous processes of myogenesis that forms muscle cells, and synaptogenesis that forms neuromuscular junctions (NMJ).

Skeletal muscle cells are derived from mesodermal precursor cells of the embryo's somites (Figure 1.3). All myogenic precursor cells express the transcription factor *Pax7* (Seale *et al.*, 2000; Yokoyama & Asahara, 2011). During the process of

myogenesis, the expression of *Pax7* decreases and myogenic precursor cells are determined to become myoblasts through the signaling of transcription factors *myoD* (myogenic determination) and *myf5* (myogenic factor 5) (Sabourin & Rudnicki, 2000; Charge & Rudnicki, 2004; Lieber, 2010; Yokoyama & Asahara, 2011). Myoblasts are primitive, proliferating, mononucleated muscle fiber precursor cells that differentiate into myocytes. This differentiation of myoblasts into myocytes is promoted by the expression of two other myogenic regulator factors, *mrf4* and *myogenin* (Sabourin & Rudnicki, 2000; Charge & Rudnicki, 2004; Lieber, 2010). This controlled timing of expression of the myogenic factors leads to clustering and fusion of myocytes into multinucleated myofibers. Myofibers continue their maturation into contractile muscle fibers that express muscle-specific genes such as the ones encoding myosin heavy chains (MyHC).

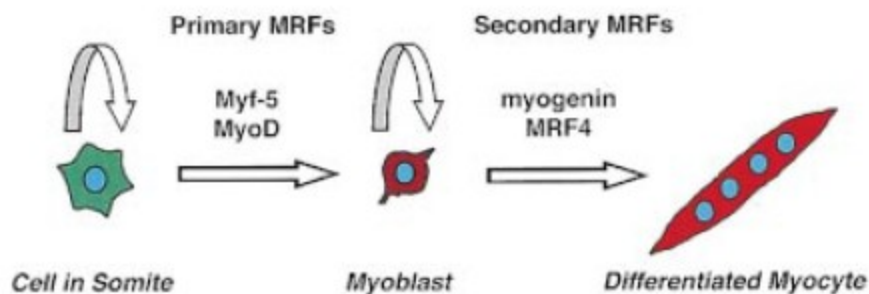


Figure 1.3: Myogenesis (Sabourin & Rudnicki, 2000)

Alternatively, a subpopulation of muscle precursor cells do not differentiate into myoblasts but form muscle stem cells termed satellite cells. Satellite cells are localized within the basal lamina surrounding muscle fibers. Satellite cells remain mitotically

quiescent and become activated under conditions of muscle growth or repair (Charge & Rudnicki, 2004; Al-Shanti & Stewart, 2009; Yokoyama & Asahara, 2011). Activated satellite cells divide and differentiate into myoblasts. These myoblasts can fuse with pre-existing myofibers, or they can fuse together and give rise to new muscle fibers.

Synaptogenesis starts with axonal outgrowth arising from the ventral horn of the spinal cord. Axons grow towards the location of a specific target muscle, following a pre-determined direction but also being guided by additional cues coming from muscle cells. This process will lead to the formation of a NMJ where a motor neuron innervates specific muscle fibers. The formed end plate is a cholinergic synapse since the presynaptic nerve releases the chemical neurotransmitter acetylcholine (ACh) that conveys information through a synaptic cleft to a postsynaptic muscle fiber. The NMJ is the site of communication between the nerve and the muscle and where excitation-contraction coupling events are initiated.

1.1.3 Acetylcholine Receptors

Acetylcholine receptors (AChR) mediate the communication between motor neurons and skeletal muscle fibers, and thus the levels, distribution and properties of these receptors influence the efficacy of synaptic transmission. The importance of these receptors is highlighted in Myasthenia Gravis, a disease characterized by defects in NMJ synaptic transmission. This disease is caused by an autoimmune response against AChR or other important proteins found at the NMJ (McConville & Vincent, 2002; Newsom-

Davis, 2007). This autoimmune response leads to the inhibition and loss of AChR at the muscle surface. This in turn leads to a defective communication between the nerve and the muscle. Muscles do not respond adequately to the nerve signals, and muscles become weaker and unable to sustain to the mechanical demands of the body. A combination of mechanisms influences the density of AChR at endplates, ranging from increase in mRNA synthesis, protein translation, and increase in protein stability to the lateral migration of receptors, receptors insertion, degradation, and recycling. AChR dynamics are controlled by muscle nerve activity, by phosphorylation events and by the action of scaffolding proteins (Bruneau & Akaaboune, 2006b; Bruneau *et al.*, 2009).

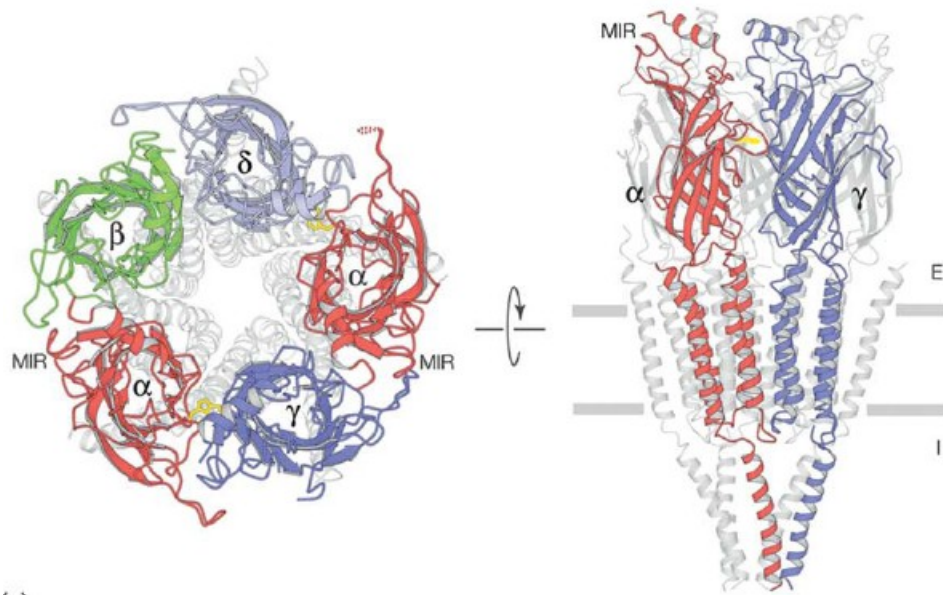


Figure 1.4: Crystal structure of muscle AChR (Lindstrom, 2010)

On left is presented a top view illustrating the channel formed by the assembly of AChR subunits: $\alpha\beta\gamma\delta$. On right is depicted the side view of the pentameric structure. Here the embryonic form is shown, in adults the γ subunit is replaced by the ϵ subunit.

AChRs are ligand-gated ion channels composed of four different subunits that assemble to form a pentameric structure (Figure 1.4). The neurotransmitter Ach binds at the interface formed between α / γ and α / δ subunits. Viewed from the side, each receptor subunit consists of a large extracellular amino-terminal domain, four helical transmembrane domains and a cytoplasmic domain formed between the third and fourth transmembrane helices (Lindstrom, 2010).

Early in development, the entire muscle surface expresses AChR however these receptors will become localized to junctional regions. Various factors are thought to regulate the decrease in extrajunctional receptors and the increase in junctional receptors. For instance, it has been proposed that nerve endplate potential or electrical activity clusters receptors under the muscle-nerve contacts through a dispersal of extrajunctional receptors mediated by the neurotransmitter acetylcholine (Sanes *et al.*, 1991; Misgeld *et al.*, 2002; Misgeld *et al.*, 2005). Expression of ACh was shown to promote the signaling of cyclin-dependent kinase 5 (cdk5), which acts to inhibit AChR expression (Fu *et al.*, 2005; Cheung *et al.*, 2006). Concurrently, a local increase in the synthesis of receptors is observed at junctional regions (Sanes & Lichtman, 2001; Lieber, 2010). Skeletal muscles and motor nerves also secrete various ECM proteins (eg. agrin, rapsyn, laminin and dystroglycan) that act to stabilize the formed NMJ (Singhal & Martin, 2011).

Moreover, synaptogenesis transforms the NMJ, structurally and functionally, to ensure that synaptic transmission occurs with high fidelity each time the motor nerve is excited. A change in AChR subunit composition occurs to allow the expression of

receptors with shorter open times and higher conductance in adult muscles as compared to embryonic muscles (Mishina *et al.*, 1986; Martinou & Merlie, 1991). In neonatal, embryonic and denervated muscles the subunits are assembled in the order $\alpha\beta\alpha\gamma\delta$, but in the first two post-natal weeks the fetal γ subunit is replaced by the adult ϵ subunit (Mishina *et al.*, 1986; Gu & Hall, 1988; Martinou & Merlie, 1991). In addition, during NMJ maturation, the aggregation of AChRs becomes more complex and the endplate topography is transformed from an oval “plaque-like” structure to a branched “pretzel-like” structure (Figure 1.5) (Balice-Gordon & Lichtman, 1993; Sanes & Lichtman, 1999, 2001). This transformation occurs independently of nerve activity, by mechanisms regulated by postsynaptic muscle cell signaling (Kummer *et al.*, 2004). All of these changes, reorganize the localization and concentration of AChR to a density of 10 000-20 000/ μm^2 in a synaptic region, as compared to only 10/ μm^2 in an extrajunctional region (Fertuck & Salpeter, 1976; Kummer *et al.*, 2006; Singhal & Martin, 2011); thus ensuring efficient and adequate nerve to muscle communication.

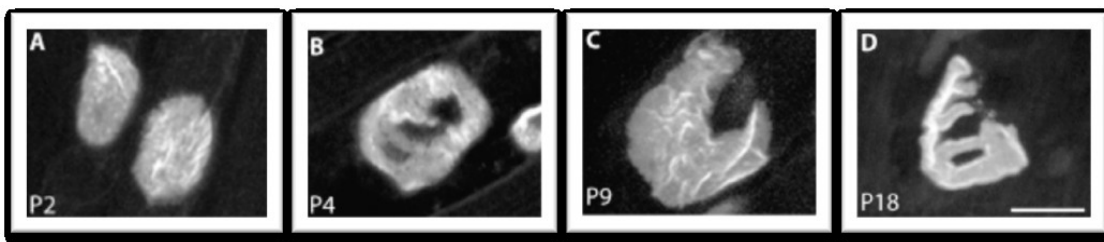


Figure 1.5: AChR aggregates topographic maturation (Kummer *et al.*, 2004)

AChR aggregates at the NMJ are initially plaque-shaped (A), perforated or ring (B), C-shaped or broken-ring and finally branched pretzel-like (D) structures become more prevalent. Postnatal Ages = P. Bar = 20 μm

1.1.4 Muscle fiber types

Skeletal muscle fibers differ in their biochemical and physiological properties. Muscle fibers are divided into types based on their metabolic, contractile and electrical properties. Muscle fibers contract and relax at different speeds and these properties of muscles result from to the ability of different isoforms of myosin heavy chain ATPase to perform the chemical breakdown of ATP with different speeds. Hence, a reliable method of muscle fiber classification is based on the type of myosin heavy chain (MyHC) isoform it expresses (Pette & Staron, 2001; Schiaffino *et al.*, 2007). This method of classification is readily used since it defines muscle fibers specifically on various characteristics, some of which are summarized in Figure 1.6. According to this classification system, muscles used for posture or regular aerobic endurance activities are predominantly high endurance, oxidative fibers consisting of MyHC type I and IIa, whereas muscles used for rapid, intense movements of short duration are predominantly formed by glycolytic, low endurance MyHC type IIb expressing fibers.

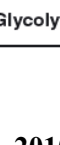
MyHC type	Twitch duration	Shortening velocity	Cross-sectional area	Metabolism	Endurance	Energy efficiency
I	Slow 	Slow 	Small 	Oxidative 	High 	High 
IIa						
IIx						
IIb						
	Fast 	Fast 	Large 	Glycolytic 	Low 	Low 

Figure 1.6: Properties of major fiber types (Gundersen, 2010)

A motor axon innervates many muscle fibers within a single muscle forming a motor unit. An important characteristic of motor units is that the properties of each motor neuron are matched to those of the muscle fibers it innervates. For example, slow motor neurons release neurotransmitters continuously at low rates, and are matched to slow muscle fibers, which are fatigue resistant and contract slowly. By contrast, fast motor neurons release neurotransmitters intermittently in high-frequency bursts and, are linked to fast muscle fibers, which contract rapidly and are fatigue susceptible (Mendell *et al.*, 1994; Gundersen, 2010). This motor unit homogeneity is influenced by both anterograde (from the nerve) and retrograde (from the muscle fiber) mechanisms (Chakkalakal *et al.*, 2010), further illustrating the importance of the communication that occurs at the NMJ. Moreover, skeletal muscles possess the remarkable ability to adapt to increased load or neural input by increasing fiber size and/or by undergoing fiber type switching (Pette & Staron, 2001; Schiaffino *et al.*, 2007). For instance, endurance/aerobic exercise training promotes muscle fiber type remodeling from fast glycolytic to slow oxidative fibers, whereas strength/resistance exercise training promotes the opposite conversion. Muscle fiber type remodeling usually occurs following a sequential transition in order from I↔IIa↔IIx↔IIb fiber types and is also accompanied by increased expression of hybrid fibers which express more than one MyHC isoform (Pette & Staron, 2001). A better understanding of mechanisms that regulate muscle ability to respond to functional demands awaits further research.

1.2 Skeletal muscle plasticity and signal transduction

1.2.1 Calmodulin

Skeletal muscle cell survival and normal function depend on the strict regulation of intracellular calcium (Ca^{2+}) levels. In fact, calcium is the main regulatory and signaling molecule in skeletal muscle. While the fluctuation of Ca^{2+} levels determines the contraction and relaxation properties of muscle fibers (Berchtold *et al.*, 2000), Ca^{2+} also serves as a second messenger molecule that interacts with specific targets to initiate cascades of biochemical events. Information encoded in transient Ca^{2+} signals is decoded by various intracellular Ca^{2+} binding proteins, and converted to biochemical signaling events.

Calmodulin (CaM) is a small 17kDa, evolutionarily highly conserved, calcium binding protein (Chin & Means, 2000; Al-Shanti & Stewart, 2009). This protein is composed of four EF hand motifs, a signature helix-loop-helix structure which is found in numerous other Ca^{2+} binding proteins such as parvalbumin and troponin C (Chin & Means, 2000; Al-Shanti & Stewart, 2009). Specifically, each pair of EF hand motifs is associated with the amino- or carboxy-terminal domain of the protein. Respective terminal regions are tethered together by a long central helix hinge region. In the absence of Ca^{2+} , the protein amino-terminus adopts a closed conformation, where the two EF hand motifs are tightly packed together (Al-Shanti & Stewart, 2009). In contrast, the carboxy-terminus adopts a “semi-open” conformation partly exposing hydrophobic

residues and allowing for the binding of some targets under resting conditions (Figure 1.7A) (Chin *et al.*, 1997; Al-Shanti & Stewart, 2009).

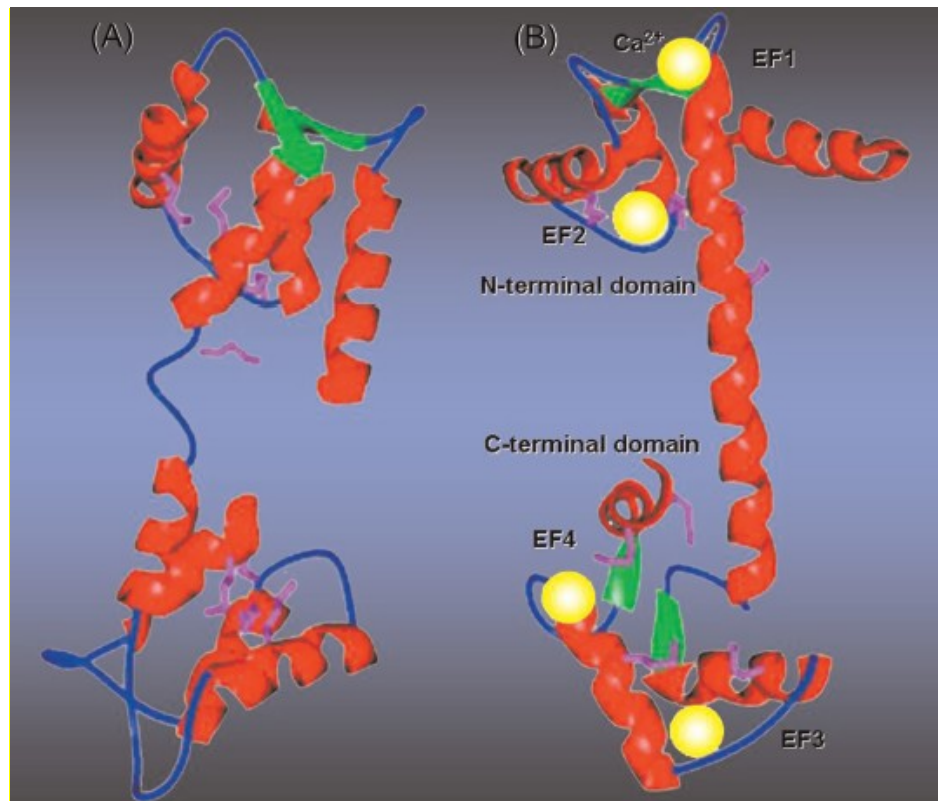


Figure 1.7: Calmodulin secondary structure (Al-Shanti & Stewart, 2009)

On the left calmodulin is shown (A) in the closed conformation while on the right (B) calmodulin is illustrated in the open conformation induced by Ca²⁺ binding.

With an increase in intracellular Ca²⁺ levels, Ca²⁺ binds to the central loop of each EF hand motif, leading to a more “open” protein confirmation that exposes additional hydrophobic regions, further promoting the binding of other target proteins (Figure 1.7B) (Chin & Means, 2000; Al-Shanti & Stewart, 2009). In skeletal muscle, these target proteins include ion channels (ryanodine receptors), kinases (calcium-calmodulin kinase),

phosphatases (calcineurin) and structural proteins (dystrophin) (Berchtold *et al.*, 2000; Chin & Means, 2000). The vast list of CaM targets, coupled with different mechanisms of calcium interaction and modes of regulation (Chin & Means, 2000), provide CaM with the ability to play various roles in the cell by activating numerous signaling molecules in response to calcium influx.

1.2.2 Calcium/calmodulin dependent protein kinase

A distinct group of CaM effectors is the calcium-calmodulin dependent protein kinase (CaMK) family (Hanson & Schulman, 1992; Braun & Schulman, 1995; Chin & Means, 2000; Means, 2000; Hook & Means, 2001). The CaMK family consists of four serine threonine kinases: CaMKI, II and IV are multifunctional kinases possessing several substrate proteins, while CaMKIII is a dedicated kinase that recognizes a single substrate; elongation factor-2 (Hanson & Schulman, 1992; Braun & Schulman, 1995). All three multifunctional kinases share a similar general structure (Figure 1.8): an amino-terminal catalytic domain followed by an autoinhibitory domain and an overlapping CaM binding site (Means, 2000; Hook & Means, 2001). CaMKII also possesses, at its carboxy-terminal region, an additional association domain essential for its oligomerization. CaM activates the CaMK family of enzymes by binding to them and removing the autoinhibitory domain from the catalytic pocket, thus promoting substrate protein binding (Hook & Means, 2001). Furthermore, CaMKI and CaMKIV are phosphorylated (at Thr177 and Thr196, respectively) in their activation loops by CaMK

kinases (CaMKK) leading to enhanced activity (Means, 2000; Hook & Means, 2001). CaMKII and CaMKIV also possess autophosphorylation sites (Thr286) within their autoinhibitory regions. Upon phosphorylation at these sites, these kinases can acquire an autonomous, Ca²⁺ independent, activity (Means, 2000; Hook & Means, 2001). Table 1.1 summarizes the main differences between these multifunctional kinases.

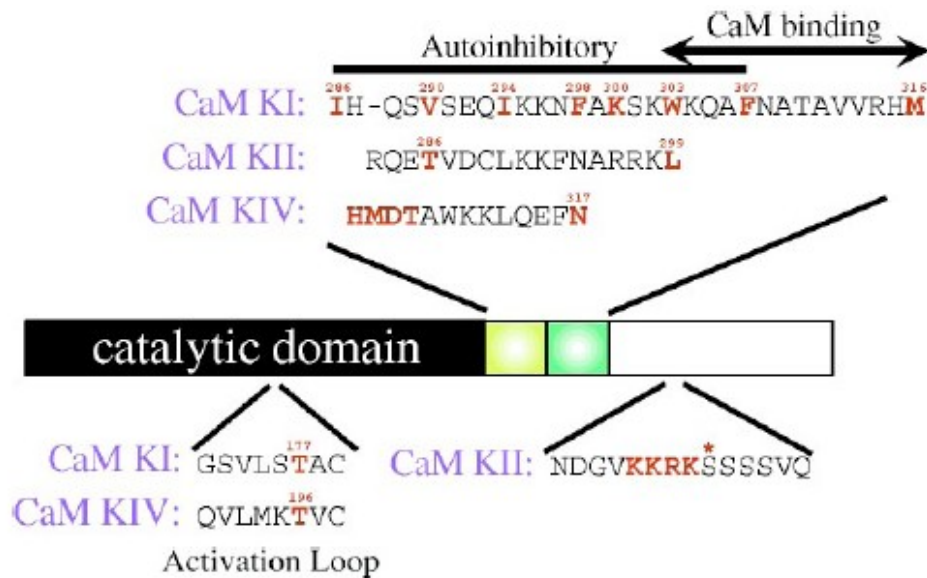


Figure 1.8: Schematic of multifunctional CaMK structure (Hook & Means, 2001)

In red are indicated important residues for CaMK activation and/or regulation by CaM (for details see Hook & Means, 2001). Numbers indicate the positions of these residues in these kinases. Within the catalytic domain of CaMKI and CaMKII is the activation loop. CaMKII alone possesses a C-terminal association domain essential for its multimerization. This C-terminal region also contains an NLS that can be hidden by phosphorylation of a serine residue (indicated by *).

	CaMKI	CaMKII	CaMKIV
Tissue Distribution	Ubiquitous	Ubiquitous (isoform specific)	Limited
Subcellular Localization	Cytoplasmic	Cytoplasmic (some isoforms nuclear)	Nuclear and cytoplasmic
Subunit Composition	Monomeric	Homo- and heteromultimeric	Monomeric
Requirement for Activation	Ca ²⁺ /CaM binding; activation loop phosphorylation	Ca ²⁺ /CaM binding; autophosphorylation	Ca ²⁺ /CaM binding; activation loop phosphorylation; autophosphorylation
Gains Ca²⁺/CaM Independence	No	Yes (up to 80%)	Yes (up to 20%)

Table 1-1: Properties of multifunctional CaMK: adapted from (Hook & Means, 2001)

CaMKII is the most well characterized multifunctional kinase of the CaMK family. This kinase is recognized to regulate various cellular events including neuronal plasticity, myofilament contraction, and gene expression (Braun & Schulman, 1995; Means, 2000; Chin, 2004). In skeletal muscle, CaMKII was shown to be the predominant isoform activated by exercise in humans (Rose & Hargreaves, 2003; Rose *et al.*, 2006; Rose *et al.*, 2007a; Rose *et al.*, 2007b). Similar results were observed in rodent models, leading to the hypothesis that CaMKII signaling is important in mediating contractile adaptation associated with muscle hypertrophic growth (Fluck *et al.*, 2000). CaMKII is a very sensitive calcium sensor that can detect not only the concentration of Ca²⁺ but also the frequency, amplitude and duration of Ca²⁺ oscillations (De Koninck & Schulman, 1998; Dupont & Goldbeter, 1998). This enzyme is encoded by four separate genes (α , β ,

γ , δ) that undergo alternative splicing to generate up to 24 distinct splice variants (Braun & Schulman, 1995; Carafoli & Klee, 1999; Hook & Means, 2001). CaMKII is the sole kinase of this family that requires homo- or hetero- oligomerization of 8 to 12 subunits into a pinwheel-like structure for activity (Kanaseki *et al.*, 1991; Means, 2000; Hook & Means, 2001). Moreover, it does not require the presence of CaMKK for its activity since it can undergo inter-subunit phosphorylation. CaMKII modulates its own activity levels due to its multimerization and autophosphorylation abilities. Indeed, CaMKII autophosphorylation of Thr286 requires both inter-subunit interactions and cooperative calmodulin binding. These events increase the enzyme's affinity for CaM and partly disrupt the enzyme autoinhibitory domain. Both of these events allow the kinase to retain partial, Ca^{2+} - independent activity (Hanson & Schulman, 1992; Braun & Schulman, 1995). These unique mechanisms allow this kinase to potentiate transient increases in Ca^{2+} levels and make CaMKII a very sensitive sensor of Ca^{2+} frequency oscillations in the cell.

1.2.3 Ca^{2+} /CaM regulation of neuromuscular junction

As described previously, CaM acts as a very efficient second messenger of Ca^{2+} signaling. In this section, CaM regulation of neuromuscular junction development, stability and plasticity will be discussed.

In the 1980s, experiments conducted *in vitro* using calcium-coated beads showed that, by a CaM-mediated mechanism, Ca^{2+} induces the formation of new AChR clusters

without major effects on existing clusters (Peng, 1984). Similar results were observed when monitoring AChR clustering induced by the nerve-derived trophic factor agrin (AGR) (Megeath & Fallon, 1998). Some data have implicated the Ca^{2+} /CaM dependent phosphatase calcineurin in this process (Madhavan *et al.*, 2003). Subsequently, it was shown that Ca^{2+} binds the nerve-derived trophic factor agrin (AGR) and alters its conformation, leading to activation of its biological activity (Tseng *et al.*, 2003; Stetefeld *et al.*, 2004; Tseng *et al.*, 2011). Specifically, AGR was shown to regulate phosphorylation of the AChR β subunit, which promotes AChR binding to the scaffolding protein rapsyn, and this in turn induces stabilization of the receptor clusters increasing receptor density at the synapse (Borges & Ferns, 2001; Borges *et al.*, 2002; Moransard *et al.*, 2003; Borges *et al.*, 2008). This AGR clustering activity was shown to signal through LRP4/MuSK receptor complex (DeChiara *et al.*, 1996; Glass *et al.*, 1996a; Glass *et al.*, 1996b; Kim *et al.*, 2008; Zhang *et al.*, 2008; Wu *et al.*, 2010). In addition, nerve-activity independent AChR clustering was shown to be activated by two other important ECM proteins: dystroglycan and laminin (Jacobson *et al.*, 2001; Kummer *et al.*, 2004; Bruneau *et al.*, 2005b; Tremblay & Carbonetto, 2006; Nishimune *et al.*, 2008).

A key aspect of AChR redistribution during NMJ maturation involves the selective accumulation of AChR subunits in junctional regions, with simultaneous suppression of expression in extrajunctional regions. Nerve-electrical activity leads to a rise in intracellular Ca^{2+} levels that acts to suppress expression of *AChR* genes in the extrajunctional regions (Walke *et al.*, 1994). Calcium signaling through CaMKII can

repress AChR promoter activity by inhibiting myogenin transcriptional activity (Tang *et al.*, 2001). CaMKII phosphorylates myogenin, decreasing myogenin's ability to bind to DNA and reducing myogenin's activity, and leading to a decrease in *AChR* gene expression (Macpherson *et al.*, 2002; Tang *et al.*, 2004). These results were further expanded and shown to implicate the signaling of a histone deacetylase pathway: the HDAC4 – Dach2 – Mgn loop (Figure 1.9) (Tang & Goldman, 2006; Cohen *et al.*, 2007; Tang *et al.*, 2009). This signaling pathway was shown to specifically coordinate phenotypic changes in muscle following denervation (Tang *et al.*, 2009), but could potentially regulate gene expression in conditions of synaptic adaptation.

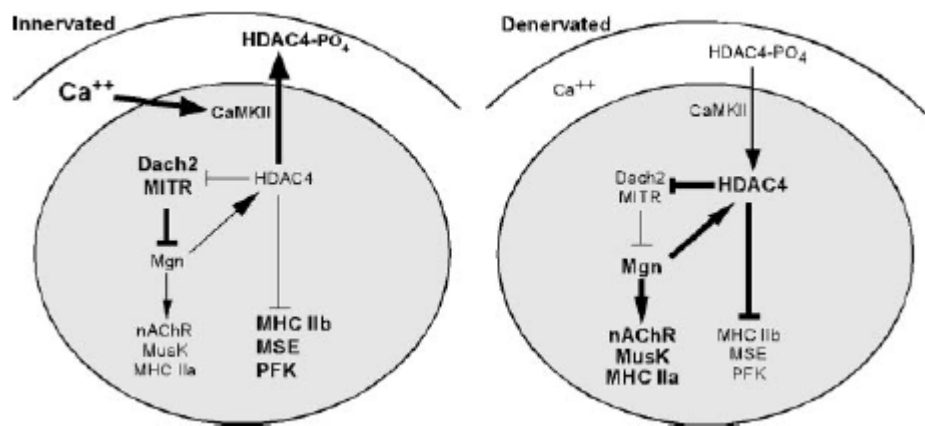


Figure 1.9: CaMKII-HDAC4-Mgn signaling loop (Tang *et al.*, 2009)

In conditions of normal innervations, Ca²⁺ activates CaMKII promoting downstream signaling that decreases synaptic gene expression and promotes glycolytic genes. During denervation, Ca²⁺ levels decrease and trigger expression of synaptic genes.

Additionally, the nerve-derived trophic factor neuregulin (NRG) (also called ARIA or heuregulin) has been identified as a key factor that promotes expression of synaptic genes independently of nerve electrical activity (Martinou *et al.*, 1991; Martinou & Merlie, 1991; Jo *et al.*, 1995). NRG acts through receptors of the ErbB family and activates the expression of *AChR* subunit genes through an ERK signaling cascade that recruits the activation of the *Ets* transcription factor GABP (GA-binding protein) (Tansey *et al.*, 1996; Sapru *et al.*, 1998; Briguet & Ruegg, 2000; Lacazette *et al.*, 2003). Similarly, AGR/MuSK signaling was shown to converge on this signaling pathway and cooperatively regulate GABP activation through JNK signaling (Lacazette *et al.*, 2003).

AChR density also can be regulated by mechanisms that involve receptor dynamic movements and/or recycling. Extensive fluorescence labelling experiments have shown that AChR receptors can be recycled in conditions of nerve activity (Bruneau *et al.*, 2005a; Bruneau & Akaaboune, 2006a). Under conditions of muscle stimulation, intracellular Ca^{2+} levels increase and prevent AChR removal from the muscle surface. This is achieved by promoting receptor recycling, and maintaining the synthesis and insertion of new receptors (Bruneau & Akaaboune, 2006a). It has been shown that muscle activity regulates the recycling process through CaMKII activity (Martinez-Pena y Valenzuela *et al.*, 2010). It is proposed that CaMKII might modulate proteins involved in sorting, targeting and/or fusion of endocytic vesicles with the muscle membrane or that it itself acts as a scaffolding protein as suggested by its localization at the NMJ (Fertuck & Salpeter, 1976; Martinez-Pena y Valenzuela *et al.*, 2010).

Consequently, current research has identified some possible pathways that can regulate AChR expression. It appears the muscle fiber's intrinsic signaling contributes to the formation of NMJ structures (Kummer *et al.*, 2006; Wu *et al.*, 2010). Nevertheless, an in depth understanding of the events that regulate AChR density, and in turn synaptic communication, still requires further investigation since parallel and complementary mechanisms exist and need to be fully explained in the perspective of disease or compromised signaling models.

1.2.4 Calcineurin

Calcineurin (Cn), a Ca^{2+} /CaM-dependent phosphatase, is another well-characterized modulator of skeletal muscle phenotypes. Cn (Figure 1.10) is a heterodimeric serine / threonine protein phosphatase comprised of a catalytic A subunit (CnA) of ~60 kDa and a calcium-binding regulatory B subunit (CnB) of ~19 kDa (Sakuma & Yamaguchi, 2010). An amino-terminal catalytic domain and a carboxy-terminal regulatory domain form the CnA subunit. The regulatory domain of CnA contains a CnB interacting domain, a calmodulin binding site and an autoinhibitory domain (Al-Shanti & Stewart, 2009; Li *et al.*, 2011). The CnB subunit has four EF-hand motifs: the two carboxy-terminal motifs bind Ca^{2+} with high affinity and serve to stabilize the heterodimeric structure, while the two amino-terminal motifs bind Ca^{2+} with low affinity and serve as regulatory sites (Li *et al.*, 2011).

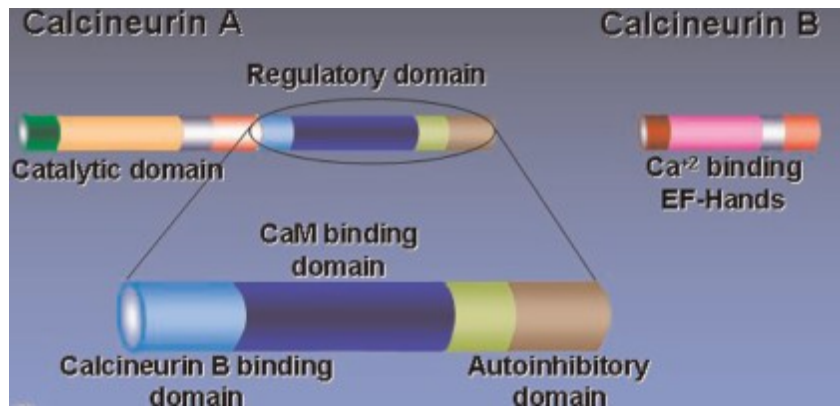


Figure 1.10: Calcineurin structure (Al-Shanti & Stewart, 2009)

The proposed model of calcineurin activation involves a series of conformational changes illustrated in Figure 1.11. In resting skeletal muscle cells, intracellular Ca²⁺ levels are low and the Cn heterodimer adopts an inactive conformation state (Form I). In this state, A) the autoinhibitory domain of CnA masks the catalytic site of the protein and B) the calmodulin binding site is associated with CnB. During physical activity, intracellular levels of Ca²⁺ increase and bind the low affinity EF-hand motifs on CnB inducing a conformational change that un masks the catalytic site and exposes the calmodulin binding site (Form II). This process promotes calmodulin binding to CnA (Form III) which is followed by a displacement of the CnA autoinhibitory domain (Form IV) and full activation of the protein phosphatase activity (Li *et al.*, 2011).

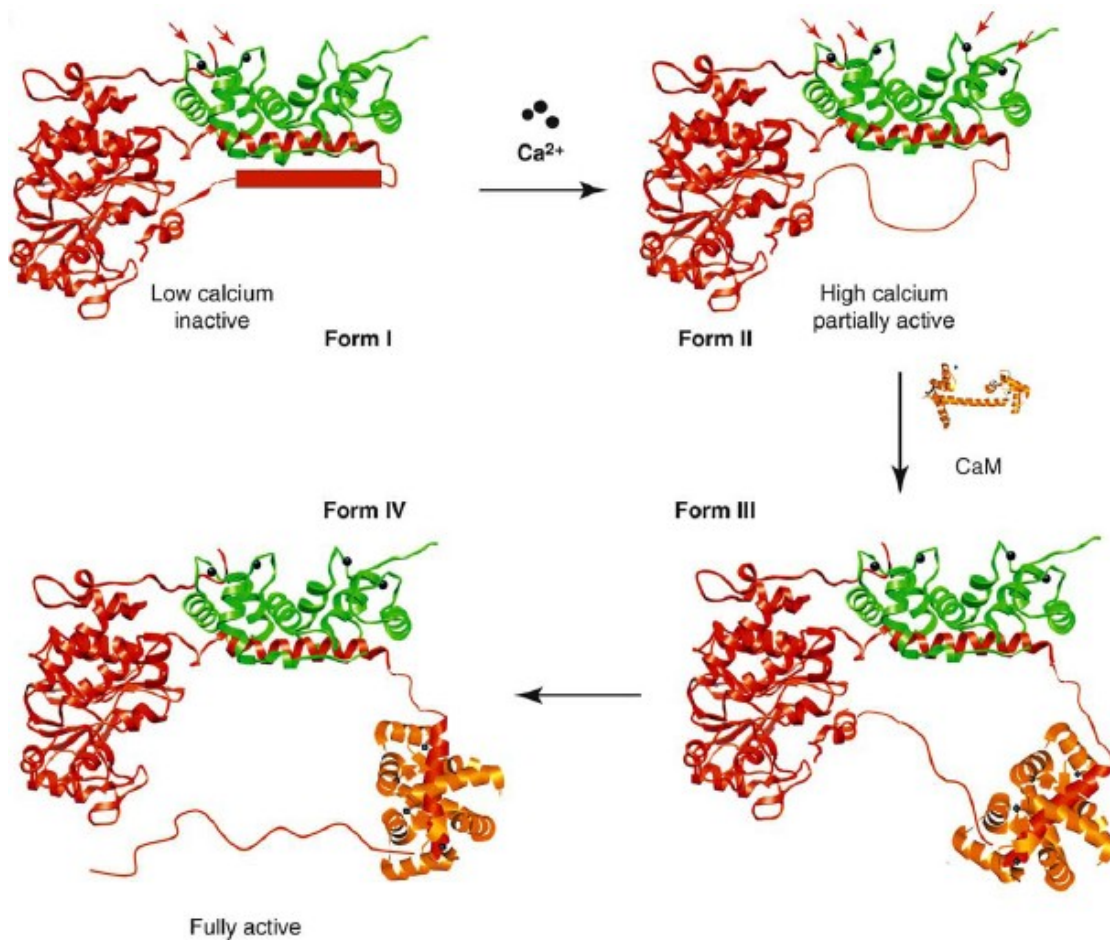


Figure 1.11: Model of Cn activation (Li *et al.*, 2011)

CnA is color coded in red; CnB in green; CaM in orange, Ca^{2+} as black circles. Ca^{2+} binds EF-hand motifs of CnB. CaM interacts with the carboxy-terminal of CnA and leads to the displacement of the autoinhibitory domain from the catalytic site.

Three genes have been identified for CnA: CnA α and CnA β that are both ubiquitously expressed and CnA γ which is expressed in brain and testes (Guerini & Klee, 1989; Lara-Pezzi *et al.*, 2007). The CnA β isoform exists in two splice variants, CnA β 1 and CnA β 2, which differ in their carboxy-terminal regions (Guerini & Klee, 1989). Specifically, the CnA β 1 isoform lacks the typical autoinhibitory domain and has a novel

unrelated carboxy-terminal domain that allows this isoform to be constitutively active (Lara-Pezzi *et al.*, 2007).

Calcineurin regulates a vast number of functions in various cell types because it interacts with numerous substrates, such as transcription factors, scaffolding proteins, ion channels, cell cycle regulators, and cytoskeleton proteins (Li *et al.*, 2011). As such, dysregulation of calcineurin signaling is associated with numerous diseases, for instance cardiac disorders, osteoporosis, Alzheimer's, Down syndrome, autoimmune diseases and cancer (Li *et al.*, 2011). One of the most recognized targets of calcineurin is the Nuclear Factor of Activated T cells (NFAT) family of transcription factors and these transcription factors have been used as models of signal transmission in various cell types.

1.2.5 Nuclear Factor of Activated T-cells

The NFAT protein was originally identified as an inducible factor of T cell activation (Shaw *et al.*, 1988). Subsequently, a whole family of these transcription factors was identified and its members were found to regulate the development and function of various tissues including the cardiovascular, musculoskeletal and nervous systems (Crabtree & Olson, 2002). Each NFAT protein exists as multiple isoforms and splice variants that share a conserved DNA binding domain (DBD) (Jain *et al.*, 1995) and an NFAT homology region (NHR) (Luo *et al.*, 1996a). The nomenclature of these proteins is confusing due to various names given to distinct isoforms through time. For simplicity, this nomenclature was standardized by the Human Genome Organization (HUGO) Gene

Nomenclature Committee (HGNC) in 2000 to define the proteins as NFATc1, NFATc2, NFATc3, NFATc4 and NFAT5. Table 1-2 presents a summary of all alternative names used in the literature. All NFAT proteins, for the exception of NFAT5 (that lacks the “c” annotation in its name), are found in the cytoplasm until activated by dephosphorylation.

Current Name	Alternative Names
NFATc1	NFAT2; NFATc; NF-ATC
NFATc2	NFAT1; NFATp; NF-ATP
NFATc3	NFAT4; NFATx;
NFATc4	NFAT3
NFAT5	TonEBP; OREBP; NFATz, NF-AT5; NFATL1; KIAA0827

Table 1-2: NFAT protein nomenclature (from HGNC and PubMed).

As indicated above, NFAT proteins share sequence similarity and functional domain homology. The region of highest sequence similarity within the NFAT protein family is the DBD, which also shares moderate similarity with the Rel-family of transcription factors (Rao *et al.*, 1997). The NHR, situated amino-terminal to the DBD, shows a strong conservation of sequence motifs (Rao *et al.*, 1997). The NHR is also often called the regulatory domain since it contains the nuclear localization signal (NLS), a possible nuclear export signal (NES), numerous phosphorylation sites (serine-rich region and SP-motifs) and the calcineurin binding sites (Figure 1.12) (Rao *et al.*, 1997; Hogan *et al.*, 2003). In fact, NFAT proteins contain two conserved calcineurin binding sites: a conserved sequence of PxIxIT at the N-terminal end of the NHR and an LxVP motif located closer to the DBD site (presented using amino acid single letter code where x is any amino acid): (Hogan *et al.*, 2003; Li *et al.*, 2011). The LxVP site shows different Cn

binding strengths and could be a source of differential regulation between the NFAT isoforms (Rodriguez *et al.*, 2009). Finally, NFAT proteins also contain an amino-terminal transactivation domain (and possibly another one at the carboxy-terminal end) (Luo *et al.*, 1996b). This region of variable sequence provides an additional site for distinct regulation and distinct interaction with co-activators or other components of the transcriptional machinery.

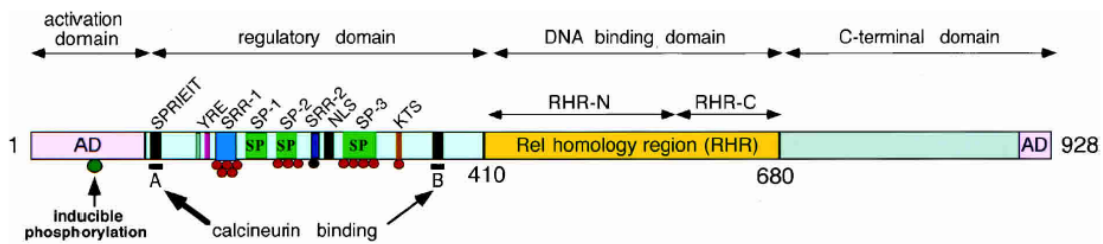


Figure 1.12: Schematic structure of NFAT protein (Hogan *et al.*, 2003)

NFATc2 is shown as a model. Regulatory-domain phosphorylation sites are shown as circles under the scheme. In red are serine residues regulated by Cn, while the black circle is a Cn-independent serine site. Black bars under the scheme indicate the two Cn binding regions. The conserved sequences are shown with the amino acid single letter code where x represents any amino acid. Region A is the PxIxIT sequence, while region B is the LxVP sequence. The transactivation domain is indicated by AD (activation domain).

Finally, it is worth noting that the NFAT5 isoform lacks the PxIxIT calcineurin binding site, the transactivation domain and is constitutively nuclear in localization (Lopez-Rodriguez *et al.*, 1999). This isoform is not regulated by calcium / Cn signaling and will not be further considered here.

NFAT protein activation occurs in three steps: dephosphorylation, nuclear translocation and increased affinity for DNA binding (Rao *et al.*, 1997). In resting cells, NFAT proteins are phosphorylated at multiple sites in their regulatory domain, are

localized to the cytoplasm and show a low affinity for DNA binding. Upon physical activity, intracellular Ca^{2+} levels increase and activate calcineurin, the major phosphatase that dephosphorylates NFATs. This process exposes the NLS, promotes NFAT's nuclear translocation and increases DNA binding affinity. Alternatively, NFATs can be phosphorylated by various kinases to be exported back out of the nucleus. Four kinases are known to phosphorylate NFATs: the constitutive kinases casein kinase-1 (CK1) and glycogen synthase kinase-3 (GSK3), and the inducible kinases MAPK p38 and JNK (Hogan *et al.*, 2003). The selective activation of these export kinases provides an additional level of regulation of NFAT proteins. Furthermore, NFAT transcriptional activity also can be regulated by modification of the TA domain. Less information is available on this mechanism, but inducible activation of the TA domain has been shown (Okamura *et al.*, 2000; de Gregorio *et al.*, 2001; Rainio *et al.*, 2002). Additionally, NFAT transcriptional activity also can be regulated by cooperative binding with other transcription factors. Indeed, NFAT can bind DNA as monomers, as homo- or heterodimers with other NFAT isoforms, or as cooperative complexes with other transcription factors such as the AP-1 family (Fos and Jun), GATA or MEF2 family (Hogan *et al.*, 2003)

1.2.6 Cn / NFAT signaling in muscle fiber remodelling

Calcium signaling plays crucial roles in determining, maintaining and transforming muscle fiber types (Bassel-Duby & Olson, 2003) and Cn acts as an intermediate factor in this process. Numerous groups have shown the importance of Cn in

the regulation of skeletal muscle fiber remodeling. For instance, the overexpression of activated Cn in muscle cell culture myocytes was shown to promote the slow muscle, oxidative gene program (Chin *et al.*, 1998). Furthermore, *in vivo* over-expression of activated Cn, driven by a muscle specific promoter, was shown to upregulate endogenous oxidative proteins such as myoglobin or troponin I slow (Naya *et al.*, 2000). In contrast, transgenic mice lacking CnA showed decreased expression of slow fiber types (Parsons *et al.*, 2003). Similarly, blocking Cn activity *in vivo*, using the specific pharmacological Cn inhibitor cyclosporine (CsA), led to transformation towards fast, glycolytic muscle profiles (Chin *et al.*, 1998; Bigard *et al.*, 2000). It is important to point out that the regulation of muscle fiber metabolic profiles by Cn does not induce a fiber type remodeling displaying a complete sequential transition of MyHC (in order from IIb→IIx→IIa→I fiber types). Instead Cn seems to regulate fibers type remodeling of slow oxidative (type I) and fast oxidative (type IIa) MyHC profiles (Bigard *et al.*, 2000). In addition, muscles with different metabolic properties display a different response to Cn activity (Bigard *et al.*, 2000; Talmadge *et al.*, 2004). This observation indicates that Cn can distinguish between fiber types and offers distinct regulation based on their metabolic profiles. These results imply that other calcium-regulated pathways also play important roles in the process of fiber type remodeling. Nevertheless, the importance of Cn signaling in oxidative fibers is defined.

In contrast, while Cn appears to play defined roles in muscle fiber type remodelling, its function in skeletal muscle fiber growth is more controversial (Schiaffino

& Serrano, 2002; Bassel-Duby & Olson, 2003; Tidball, 2005; Sakuma & Yamaguchi, 2010). The contribution of Cn alone to skeletal muscle fiber hypertrophy is supported by three main observations. Firstly, Cn was shown to mediate skeletal muscle hypertrophy induced by IGF treatment in skeletal muscle cell cultures (Musaro *et al.*, 1999; Semsarian *et al.*, 1999). Secondly, Cn has been shown to mediate muscle hypertrophy *in vivo*, in a model of adaptive muscle growth: the functional overload model. In this model, Cn activity was blocked using pharmacological inhibitors (FK506 and CsA), and in the absence of Cn activity overload induced hypertrophy was prevented in both fast plantaris and slow soleus muscles (Dunn *et al.*, 1999; Sakuma *et al.*, 2008). Thirdly, numerous groups showed that Cn is important for growth recovery following atrophy (Mitchell *et al.*, 2002; Miyazaki *et al.*, 2006; Oishi *et al.*, 2008). In contrast, other results suggest that Cn is not mediating fiber hypertrophy alone and that it requires collaborative signaling events. For instance, transgenic mice over-expressing an activated Cn did not display fiber hypertrophy under normal weight-bearing conditions (Dunn *et al.*, 1999; Naya *et al.*, 2000). Similarly, a genetic loss of Cn did not block skeletal muscle hypertrophy induced by functional overload (Parsons *et al.*, 2004). Meanwhile, *in vitro* experiments that induced skeletal muscle hypertrophy by IGF, but performed in different cell culture lines than Musaro *et al.* (1999) and Semsarian *et al.* (1999), failed to show an activation of Cn (Bodine *et al.*, 2001; Rommel *et al.*, 2001). These same experiments also used different dosages of pharmacological Cn inhibitors (CsA or FK506) and failed to prevent IGF induced hypertrophy. The observed contradicting results are probably due to the

usage of different cell line backgrounds or by smaller dosages of Cn pharmacological inhibitors. Additionally, the vehicle for CsA drug delivery was also different and might further explain the observed discrepancies (Sanchez *et al.*, 2000). Overall, it appears the Cn has a certain ability to regulate muscle fiber hypertrophy but the exact signaling pathways are not clearly defined. Cn regulation of muscle growth differs between muscle types (Mitchell *et al.*, 2002; Talmadge *et al.*, 2004) or growth model used, and is probably necessary but not sufficient alone to mediate muscle fiber hypertrophy (Naya *et al.*, 2000).

Involvement of Cn signaling in the regulation of the skeletal muscle fiber phenotype is recognized, however the elucidation of the roles of Cn-regulated NFAT isoforms in this process remains rudimentary. Previous literature has reviewed in detail the phenotypes of NFAT-deficient mice (Crabtree & Olson, 2002; Horsley & Pavlath, 2002), but it appears important to briefly highlight the importance of some NFAT isoforms in the regulation of skeletal muscle. NFATc1-deficient mice have deficient heart valve development and abnormalities in heart septum, which leads to embryonic death. Nevertheless, cell culture work, has identified a potential role for NFATc1 in the regulation of Myf5 expression (Friday & Pavlath, 2001). In addition, NFATc2-deficient mice display defects in the recruitment of myoblasts to fuse with multinucleated myofibers; a process required for postnatal myotube growth (Horsley *et al.*, 2001). On the other hand, NFATc3-deficient mice show defects in development of myoblasts; thus NFATc3 seems to regulate primary myogenesis (Kegley *et al.*, 2001). Finally, NFATc4-

deficient mice did not show any abnormalities in skeletal muscles (Graef *et al.*, 2001), but overexpression of NFATc4 induced hypertrophy of the heart (Molkentin *et al.*, 1998).

At last, the involvement of Cn in regulation of muscle phenotypes is documented. Cn is involved in the regulation of oxidative remodeling and seems to have the potential to regulate muscle growth. NFAT proteins are recognized as the main transcriptional targets downstream of Cn, yet the importance and exact roles of NFAT protein isoforms in the regulation of skeletal muscle adaptive remodeling still awaits further investigation.

1.2.7 Agrin

Agrin (AGR) is a large (~225 kDa) heparan sulfate proteoglycan. This protein is widely expressed in different tissues such as brain, spinal cord, retina, muscle, liver, kidney and lung (Ferns *et al.*, 1993; Hoch *et al.*, 1993). Agrin exists in numerous different splice variants displaying different biological activities and tissue distributions (Ferns *et al.*, 1993; Hoch *et al.*, 1993). Agrin has been extensively studied in the context of NMJ regulation but its broad expression indicates that it also can regulate other processes. For instance, agrin is necessary for hypertrophic differentiation of chondrocytes (Hausser *et al.*, 2007) and it can regulate blood vessel angiogenesis (Iozzo *et al.*, 2009). Agrin is also important in the activation of the T cell immune response (Khan *et al.*, 2001; Jury & Kabouridis, 2010). In addition, agrin mediates axonal guidance in the CNS (McCroskery *et al.*, 2006; McCroskery *et al.*, 2009) and controls the maintenance of the blood-brain barrier (Rascher *et al.*, 2002). The best characterized role

for agrin is its involvement in the stabilization of neuromuscular junctions (Bezakova & Ruegg, 2003; Lin *et al.*, 2008). Indeed, agrin was discovered as a trophic factor sufficient to instruct pre- and post-synaptic NMJ assembly (Godfrey *et al.*, 1984; Nitkin *et al.*, 1987) and later it was shown that agrin induces the clustering of AChR aggregates (Ferns *et al.*, 1992; Ferns *et al.*, 1993). The clustering of AChR at NMJ is the predominant biological activity of agrin.

The recognition of the varied functions of agrin led to the implication of this protein in several diseases (Williams *et al.*, 2008) such as cancer (Iozzo *et al.*, 2009; Somoracz *et al.*, 2010), Alzheimer's (Verbeek *et al.*, 1999; Reilly, 2000; Rauch *et al.*, 2011), Myasthenia Gravis (MG) (Hoch *et al.*, 2001; McConville & Vincent, 2002; Romi *et al.*, 2008), various forms of Congenital Myasthenia Syndrome (CMS) (Moll *et al.*, 2001; Meinen & Ruegg, 2006; Maselli *et al.*, 2011; Meinen *et al.*, 2011) and some forms of muscular dystrophy (Moll *et al.*, 2001; Bentzinger *et al.*, 2005; Qiao *et al.*, 2005; Meinen & Ruegg, 2006; Meinen *et al.*, 2011). Yet, precise and exact details about agrin's roles and/or regulation in these varied contexts still require more in depth research.

1.2.8 Agrin structure

The agrin gene shares high sequence similarity between different species ranging from chicks to mice, rats and humans (Bezakova & Ruegg, 2003). Agrin is a large protein containing numerous functional domains (Figure 1.13) homologous to motifs found in other proteins of the ECM (Bezakova & Ruegg, 2003; Ngo *et al.*, 2007). These conserved

motifs present in agrin can regulate agrin's ability to bind numerous proteins of the ECM such as dystroglycan, laminins and integrins (Bezakova & Ruegg, 2003). The N-terminus of agrin can be N- and O- glycosylated. The glycolysation sites serve as docking sites for glycoaminoglycan (GAG) groups and increase the size of the protein to ~400-600kDa (Winzen *et al.*, 2003). These modifications probably induce conformational changes in the protein structure that regulate agrin interactions with its binding partners, or the stability of the protein by preventing rapid degradation (Winzen *et al.*, 2003).

Agrin transcripts can be alternatively spliced at four different sites (Ferns *et al.*, 1993; Bezakova & Ruegg, 2003; Iozzo *et al.*, 2009). The N-terminal end of agrin can be spliced to generate a short or long protein isoform that displays differential localization (Burgess *et al.*, 2000) (Figure 1.13). The longer form is able to bind laminin and is localized to the basal lamina of the ECM while the shorter form is a Type II transmembrane protein expressed in the central nervous system (Burgess *et al.*, 2000; Bezakova & Ruegg, 2003; Iozzo *et al.*, 2009). Additionally, agrin has three alternative splice sites localized at its C-terminus: X, Y and Z sites (Figure 1.13). Alternative splicing of the C-terminal end of agrin forms protein isoforms that differ in localization and/or ability to cluster AChR receptors (Ferns *et al.*, 1992; Ferns *et al.*, 1993). At the X position, alternative splicing can lead to insertion of 3 or 12 amino acids (Rupp *et al.*, 1991; Ferns *et al.*, 1993), the Y site can contain an insert of 4 amino acids (Ferns *et al.*, 1993) and the Z site can include or exclude two separate exons, and lead to possible inserts of 8, 11 or 19 amino acids (Ferns *et al.*, 1992). Alternative splicing at the X site is

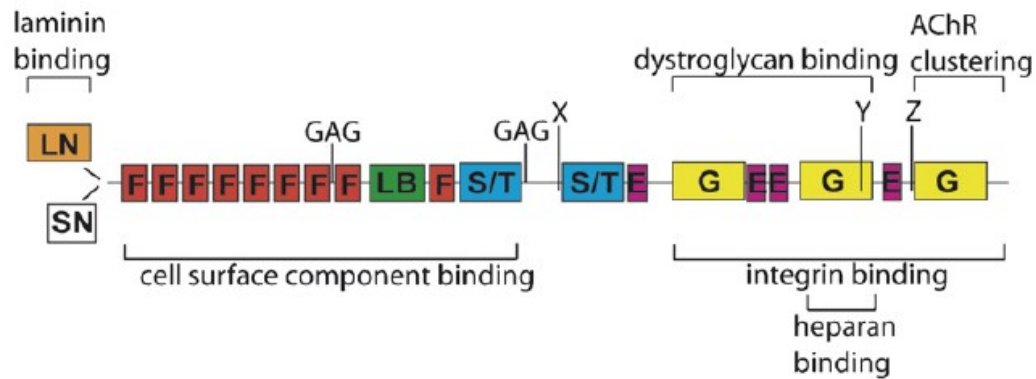


Figure 1.13: Agrin functional domains (Ngo *et al.*, 2007)

Agrin contains follistatin-like cysteine-rich repeats (F), repeats homologous to epidermal growth factor EGF (E), laminin B (LB) and laminin AG domains (G). Agrin also has two serine/threonine (S/T) rich regions and glycosaminoglycan side chains (GAG). Alternative RNA splice sites (X, Y and Z) are indicated. Alternative transcriptional start sites give rise to short and long N-terminal (SN and LN) agrin variants.

not tissue specific and does not regulate agrin biological activity (Ferns *et al.*, 1993). The insert at the Y site shows tissue specific expression and is found predominantly in neuronal tissues (Ferns *et al.*, 1993; Hoch *et al.*, 1993). Finally, alternative splicing at the Z site controls agrin biological activity that mediates the assembly and stabilization of NMJ (Ferns *et al.*, 1993; Hoch *et al.*, 1993). An insert of 8 amino acids at the Z site is essential to the formation of AChR aggregates at the postsynaptic muscle surface (Ferns *et al.*, 1993). The agrin isoforms that include the 8, 11 or 19 amino acid inserts at the Z site are called “neural agrin”. These neural isoforms of agrin are secreted by the motor neurons and they display different biological activities. The rank order for the efficacy in AChR clustering activity of the Z splicing variants is $8 \geq 19 > 11 > 0$ (Ferns *et al.*, 1993). Muscles synthesize the isoform lacking the insert at the Z site and this isoform is called

“muscle agrin”. The function of muscle agrin still remains unclear but it might act to amplify and/or sustain the activity of neural agrin (Ferns *et al.*, 1993; Bezakova & Lomo, 2001; Williams *et al.*, 2008). Currently, neural agrin is the sole isoform recognized to display biological activity.

1.2.9 Agrin in skeletal muscles

In skeletal muscles agrin is crucial for the organization and stabilization of the NMJ where it functions to assemble diverse molecules required for efficient nerve-muscle communication. Agrin is released from the motor neuron into the presynaptic cleft where it binds the muscle surface. On the muscle surface, agrin interacts with two receptors (Hoch, 1999): α -dystroglycan (α -DG) (Gee *et al.*, 1994) and LDL-receptor related protein 4 (LRP4) (Kim *et al.*, 2008; Zhang *et al.*, 2008). Over the past two decades, work carried out by varied groups elucidated some major signaling partners for agrin signaling in skeletal muscles. In addition, recent discoveries indicate that agrin might have novel, yet unidentified roles, in skeletal muscles.

Firstly, the association of agrin with α -DG serves to aggregate the dystrophin-associated glycoprotein complex (DGC) (Figure 1.14) (Campanelli *et al.*, 1994; Hoch, 1999). The main function of this complex is to stabilize skeletal muscle structure but it also serves as a scaffold for various signaling molecules (Pilgram *et al.*, 2010). The assembly of this structural complex at the NMJ concentrates synaptic molecules such as AChR (Campanelli *et al.*, 1994). Dystroglycan is synthesized as a precursor propeptide

that is post-translationally cleaved to generate α - and β -DB (Holt *et al.*, 2000). Agrin binds the C-terminal end of α -DG that interacts with β -DG, which in turn binds rapsyn (Figure 1.14) (Hopf & Hoch, 1996; Bartoli *et al.*, 2001). Rapsyn is a peripheral protein expressed on the muscle surface that binds the actin cytoskeleton and facilitates AChR attachment to the muscle surface (Peng & Froehner, 1985).

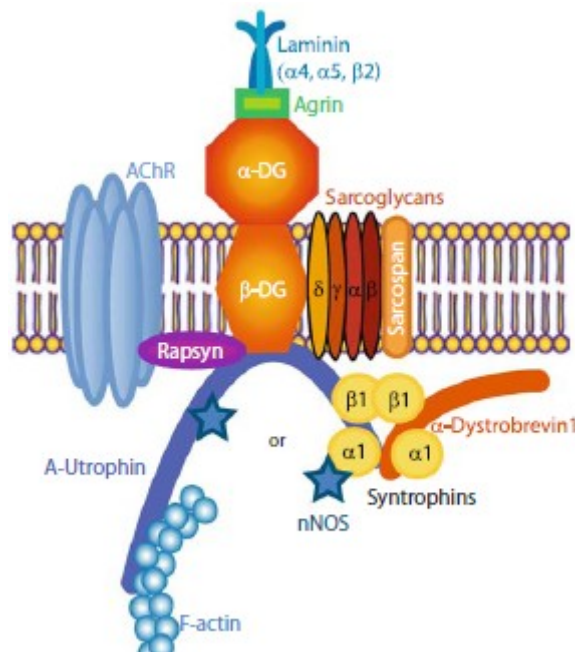


Figure 1.14: Agrin and α -DG signaling (Pilgram *et al.*, 2010)

Figure legend: DG, dystroglycan; AChR, acetylcholine receptor complex; NOS, nitric oxide synthase

In addition, the amino-terminal end of agrin interacts with laminins, that in turn bind integrins (Denzer *et al.*, 1997) and this further stabilizes the formed DGC ensuring adequate force transmission between the ECM and the muscle actin cytoskeleton. In summary, agrin interaction with α -DG functions to stabilize the NMJ by concentrating

protein found in the DGC and by promoting the concentration of AChR aggregates at synaptic sites (Apel *et al.*, 1995; Fuhrer *et al.*, 1999; Moransard *et al.*, 2003).

Secondly, agrin interacts with the LRP4/MuSK receptor complex to initiate a signaling cascade that drives the aggregation of AChR. Specifically, agrin directly interacts with LRP4 which in turn binds the muscle specific kinase (MuSK) co-receptor (Figure 1.15) (Kim *et al.*, 2008; Zhang *et al.*, 2008). MuSK is as a tyrosine kinase receptor specifically localized at the NMJ of adult skeletal muscles (Valenzuela *et al.*, 1995). The first suggestion that it might act as a receptor for agrin came from the similarity in NMJ defects observed in MuSK-deficient mice (DeChiara *et al.*, 1996) and agrin-deficient mice (Gautam *et al.*, 1996). Subsequently, MuSK was shown to mediate the agrin induced phosphorylation of AChR β -subunit (Wallace *et al.*, 1991) but this signaling was demonstrated to occur without direct binding between agrin and MuSK (Glass *et al.*, 1996a; Glass *et al.*, 1996b). Recently, LRP4 was shown to be the receptor that binds directly to agrin and is necessary and sufficient for agrin-induced tyrosine phosphorylation of MuSK and downstream AChR β (Kim *et al.*, 2008; Zhang *et al.*, 2008). The signaling events downstream of agrin/LRP4/MuSK are beginning to be elucidated (Figure 1.15) and involve the adaptor protein downstream of tyrosine kinase-7 (Dok-7) (Okada *et al.*, 2006) that binds directly to MuSK and promotes activation of timorous imaginal disc-1 (Tid1) (Linnoila *et al.*, 2008). Tid1 activity regulates the phosphorylation of AChR β and modulates cytoskeletal dynamics to promote clustering of AChR through cytoskeleton protein adenomatous polyposis coli (APC) (Wang *et al.*,

2003), by regulating the activity of small GTPases (Weston *et al.*, 2000; Weston *et al.*, 2003; Linnoila *et al.*, 2008) and by activating heat shock proteins (Liang & MacRae, 1997; Linnoila *et al.*, 2008). The phosphorylation of AChR β regulates the binding to the scaffolding protein rapsyn and acts to further stabilize AChR clusters (Borges & Ferns, 2001; Borges *et al.*, 2002; Moransard *et al.*, 2003; Friese *et al.*, 2007; Borges *et al.*, 2008).

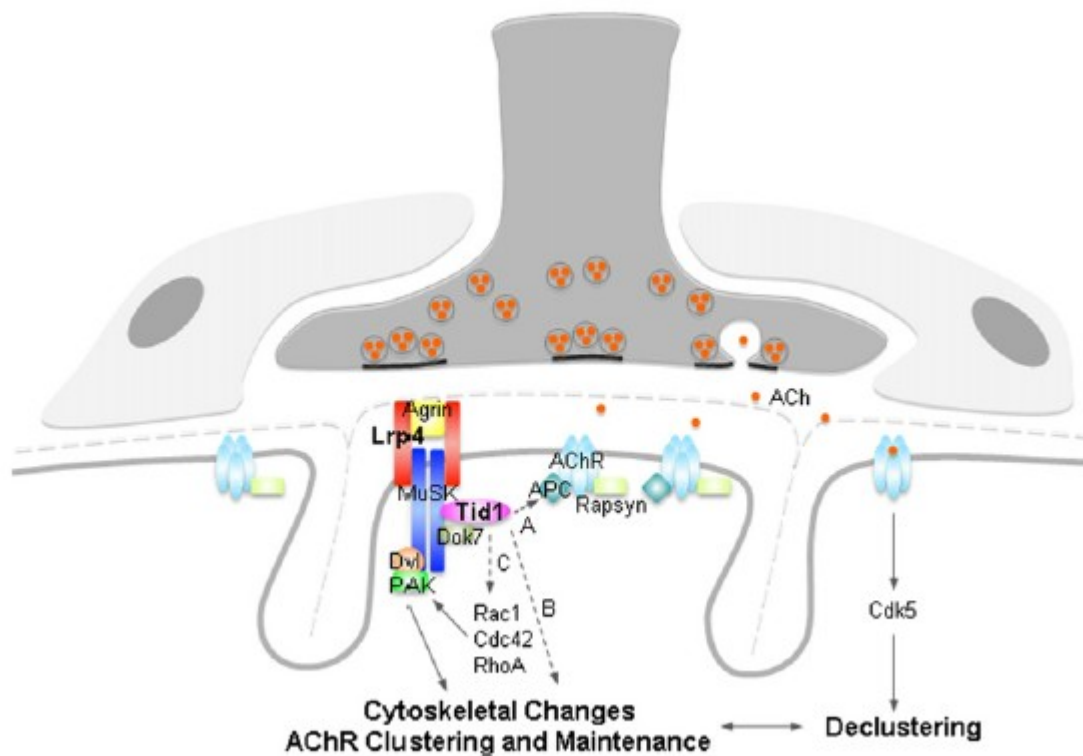


Figure 1.15: Agrin and LRP4/MuSK signaling (Song & Balice-Gordon, 2008)

Downstream of agrin/LRP4/MuSK proteins Dok-7 and Tid1 regulate postsynaptic reorganization by regulating (A) APC, (B) heat-shock proteins, (C) and by activating small GTPase Rac1, Cdc42 and RhoA. The neurotransmitter ACh acts to disperse non-synaptic clusters through Cdk5 signaling. Legend: APC, Adenomatous Polyposis Coli; PAK, p21-activated kinase; Dvl, disheveled; ACh, acetylcholine

Alternatively, agrin promotes the expression of AChR genes by localizing the trophic factor neuregulin (NRG) at synaptic sites (Meier *et al.*, 1998; Rimer *et al.*, 1998). Recently, the protein erbin was demonstrated to interact with MuSK and erbin was shown to regulate signaling events between AGR and NRG (Simeone *et al.*, 2010). At the NMJ, NRG binds the ErbB family of receptors and signals to activate the expression of *AChR* subunit genes through an ERK signaling cascade that recruits the activation of the *Ets* transcription factor GABP (GA-binding protein) (Tansey *et al.*, 1996; Sapru *et al.*, 1998; Briguët & Ruegg, 2000; Lacazette *et al.*, 2003). In summary, signaling downstream of agrin/LRP4 influences skeletal muscle properties by regulating the clustering of AChR aggregates through rearrangement of the cytoskeleton and by promoting expression of AChR genes.

Finally, studies have indicated that agrin also can regulate aspects of skeletal muscles other than the maintenance and development of nerve-muscle communication. As such, agrin treatment was sufficient to improve dystrophic muscle pathology observed in congenital muscular dystrophy (Moll *et al.*, 2001; Bentzinger *et al.*, 2005; Qiao *et al.*, 2005; Meinen & Ruegg, 2006). This disease is characterized by the absence of the ECM structural protein laminin- α 2. In this dystrophic model, using transgenic mice expressing a miniagrin gene or using adeno-associated virus mediated-overexpression of miniagrin, it was shown that agrin can restore muscle structure, improve whole body growth, and ameliorate locomotor and contractile functions of the dystrophic muscles (Moll *et al.*, 2001; Bentzinger *et al.*, 2005; Qiao *et al.*, 2005). In addition, whole-cell patch-clamp

experiments have demonstrated that agrin regulates the electrical properties of skeletal muscle cells *in vitro* by altering excitation-contraction coupling and regulating ion channels expression (Bandi et al., 2008; Jurdana et al., 2009). In addition, recent data showed that agrin can enhance the contractile functions of an engineered aneural muscle tissue system (Bian & Bursac, 2011). These novel roles of agrin are still emerging and more research is required in this field.

1.3 Thesis organization, scope and hypotheses

The ability of skeletal muscle and nerve to adapt to functional demand is a noteworthy characteristic that can be viewed as a significant evolutionary achievement. Future research is needed to better understand the underlying mechanisms and molecular elements responsible for mediating the remarkable neuromuscular adaptation.

In this thesis, using transgenic and surgical models, we seek to explore some of the signaling components of neuromuscular plasticity.

Chapter 2: The function of calmodulin in the regulation of AChR density at the adult NMJ is investigated using a transgenic mouse model that expresses an inhibitor peptide for CaM. We hypothesize that calmodulin can influence endplate morphology by regulating the expression of AChR.

Chapter 3: The specific functions of NFAT transcription factors are investigated in adaptive growth of adult muscles using a surgical synergistic ablation overload model. Muscle growth is compared between wild-type mice and mice deficient for NFATc2 or NFATc3 isoforms. We hypothesize that NFATc2 and NFATc3 have essential and distinct functions in adaptive growth of skeletal muscles.

Chapter 4: The roles of the nerve-derived trophic factor agrin in the regulation of muscle growth are revealed, in healthy muscles and in models of muscle aging and Duchenne muscular dystrophy. We hypothesize that agrin can regulate signaling events that regulate skeletal muscle mass.

Chapter 2: ***Calmodulin signaling regulates acetylcholine receptor organization in CaMBP expressing mice***

Ewa M. Kulig¹, Raphael Vezina-Audette², Salvatore Carbonetto² and Robin N. Michel³

1. *Department of Chemistry and Biochemistry, Concordia University, Montreal, Quebec, Canada*
2. *Centre for Research in Neuroscience, McGill University Health Centre, Montreal, Quebec, Canada*
3. *Department of Exercise Science, Concordia University, Montreal, Quebec, Canada*

2.1 Background

In this Chapter we seek to better understand the regulation of acetylcholine receptors (AChR) density at the adult neuromuscular junction (NMJ) using an *in vivo* transgenic mouse model. The results provide novel findings illustrating that calmodulin (CaM) alter AChR aggregate morphology in a transgenic mouse model. Our findings suggest that CaM regulates adult NMJ morphology through mechanisms independent of synaptic transcription and translation.

The results of this chapter are to be submitted for publication in *Muscle & Nerve*. This journal specializes in original research studies focused on neuromuscular disorders and/or on their treatment options. Our work provides new insights into the regulation of NMJ morphology in adult mice and identifies a new direction for future research. A better understanding of mechanisms that regulate AChR maintenance and recruitment is of foremost importance for treatment of disease such as Myasthenia Gravis or Congenital Myasthenia Syndrome.

2.2 Abstract

The NMJ is the interface between motor neurons and their target muscle fibers. AChR mediate nerve-muscle communication, and the density and properties of these receptors regulate synaptic efficiency. The density and morphology of AChR aggregates can change based on functional demands, as is seen during muscle development and growth. Adequate expression and recruitment of AChR are important for appropriate synaptic communication and normal muscle function.

The calcium-regulated protein CaM, by modifying its downstream signaling events, has the potential to alter AChR expression. In the present study, a transgenic mouse model that displayed a decrease in CaM activity was used to evaluate the role of CaM in the regulation of AChR expression in adult muscles. Larger and more complex endplates were observed in the muscles of transgenic mice as compared to wild-type mice. The data showed that the increased complexity of endplates is most likely regulated by post-translational mechanisms in transgenic mice since two major signaling pathways that regulate AChR expression were not altered in transgenic mice. Consistent with this, the results did not indicate increased expression for AChR genes and proteins. These collective findings present new insights into the regulation of AChR density *in vivo* in adult muscles and suggest that CaM regulates adult NMJ morphology by regulating AChR localization.

2.3 Introduction

Acetylcholine receptors (AChR) mediate the communication between the motor neuron and skeletal muscle fibers. These ligand-gated ion channels are made of four different types of subunits that form a pentameric structure. In neonatal, embryonic and denervated muscle the subunits are assembled in the order $\alpha\beta\alpha\gamma\delta$, whereas in the first post-natal week the fetal γ subunit is replaced by the adult ε subunit. This γ - to ε - subunit conversion during muscle development allows for the expression, in adult muscles, of receptors with shorter open times and higher conductance (Mishina *et al.*, 1986; Gu & Hall, 1988). In addition, during NMJ maturation, the aggregation of AChRs becomes more complex and the endplate topography is transformed from an oval “plaque-like” structure to a branched “pretzel-like” structure (Balice-Gordon & Lichtman, 1993; Sanes & Lichtman, 1999, 2001).

The density of AChRs at the postsynaptic muscle membrane influences the efficacy of synaptic transmission. Various diseases illustrate the importance of adequate AChR maintenance and recruitment for the appropriate synaptic function of the adult NMJ. For instance, the main symptoms of Myasthenia Gravis are muscle fatigue and muscle weakness. This autoimmune disease is characterized by an inhibition and loss of AChR at the surface of muscle which leads to defects in neuromuscular communication (Strohlic *et al.*, 2005). Additionally, recent data have shown that AChR expression is also reduced in certain forms of muscular dystrophies (Lane *et al.*, 2011). Finally, decreased expression of AChR is also seen in aging muscles (Doran *et al.*, 2009;

McMullen & Andrade, 2009) and this further highlights the importance of an in-depth understanding of the regulation of AChR expression.

The localization of AChRs at the neuromuscular junction (NMJ) appears to be regulated by mechanisms that reorganize AChR proteins within the muscle fiber membrane and directs them to synaptic regions (reviewed in (Wu *et al.*, 2010)). Nerve activity is known to regulate the levels, distribution and properties of the AChR. Previous research has identified some signaling pathways that influence the expression of synaptic genes. For instance, the HDAC4/myogenin cascade drives activity-dependent gene expression of AChR subunits (Tang *et al.*, 2004; Tang & Goldman, 2006; Tang *et al.*, 2009). Similarly, signaling pathways downstream of agrin (AGR) or neuregulin (NRG), act through the transcription factor GA-binding protein (GABP) to regulate transcription of AChR and other synapse-specific genes (Schaeffer *et al.*, 1998; Briguet & Ruegg, 2000; Schaeffer *et al.*, 2001; Lacazette *et al.*, 2003; Mejat *et al.*, 2003). Additionally, several calcium-sensitive molecules can regulate synaptic receptor density by activating downstream signaling pathways, after detecting even subtle changes in calcium concentration inside the cell (Peng, 1984; Malenka *et al.*, 1989; Walke *et al.*, 1994; Borges *et al.*, 2002; Madhavan *et al.*, 2003).

One such calcium-sensitive molecule is calmodulin (CaM). CaM is a protein with four EF hand calcium-binding motifs (Chin & Means, 2000; Al-Shanti & Stewart, 2009) that readily detects calcium oscillations in skeletal muscle. In this study, we used an *in vivo* transgenic mouse model to determine the influence of decreased calmodulin

signaling on the expression of AChR. More specifically, transgenic mice used express a small peptide inhibitor for CaM, known as the CaM-binding protein (CaMBP), under the control of the slow fiber-specific troponin I slow (TnIs) promoter (Corin *et al.*, 1994; Corin *et al.*, 1995; Levitt *et al.*, 1995; Wang *et al.*, 1995; Dunn *et al.*, 2000). In these transgenic CaMBP-expressing mice, downstream pathways involving Ca^{2+} /CaM-regulated enzymes such as calcineurin and CaMKII are attenuated (Wang *et al.*, 1995; Dunn *et al.*, 2000).

We hypothesized that a reduction of calmodulin would alter AChR aggregates morphology and could regulate synaptic plasticity. The involvement of a transcriptional signaling mechanism was explored in this study. Our results indicate that in the CaMBP transgenic mouse model, the reduced calmodulin activity decreases CaMKII signaling and leads to an increased density of AChR at the NMJ. CaM regulation of AChR aggregates does not alter the levels of the AChR gene or protein. The data suggest that CaM likely regulates NMJ morphology by mechanisms that regulate the distribution and localization of receptors at the muscle surface. These results identify a new transgenic model that should be further investigated to better understand mechanisms that regulate the expression and density of AChR at the adult NMJ. This in turn could help in the identification of novel therapeutic targets for the treatment of neuromuscular disorders.

2.4 Methods

2.4.1 Animal Care, Protocols and Extractions

All animal care and experimental procedures were performed in accordance with the guidelines established by the Canadian Council of Animal Care. These procedures were approved by the University Animal Research Ethics Committee (UAREC) of Concordia University. Animals were housed in temperature and humidity controlled conditions on a 14:10 hour light: dark cycle and had access to water and food *ad libitum*. Mice were bred using standard breeding methods and identified to express the calmodulin binding peptide (CaMBP) transgene through PCR screening of genomic DNA extracted from tails (Dunn *et al.*, 2000). The expression of CaMBP was also confirmed in the soleus muscle using genotyping cycling conditions and primers: Fwd 5'-cctttacttctaggcctgtagg -3' and Rvs 5'-gcattttttcactgcattctagttgt -3'. In all experimental procedures, male mice aged between 3-9 months were used. Mice were anesthetized by intramuscular injection (1.2 µl/g) of 100 mg/ml ketamine hydrochloride and 10 mg/ml xylazine in a volume ratio of 1.6:1 and selected muscles were extracted for biochemical analysis. Muscles were either fixed in 4% paraformaldehyde for histological analysis or frozen directly in liquid nitrogen for RT-PCR and Western blotting purposes. Upon completion of tissues extraction, mice were euthanized by cervical dislocation under anesthesia and all tissues were stored at -86°C until processed.

2.4.2 Cell culture

Primary mouse myoblast cultures were prepared from postnatal day 1 mice that were euthanized by asphyxiation with carbon dioxide. Using surgical scissors, the skin around the ankles of their hindlimbs was cut and stripped off to expose the muscles of the limbs. Special attention was given to keep the muscles moist at all times with Dulbecco's Phosphate Buffered Saline (DPBS). The muscles were minced to slurry in a culture dish using a razor blade. The slurry was transferred to a 15 ml conical vial containing 5 ml of a 0.25% Trypsin/EDTA solution at 37°C and incubated at 37°C for 5 minutes and vortexed until the solution became cloudy. The solution was transferred to a new 15 ml conical vial and the trypsin inhibited with proliferation media. The dissociation procedure was repeated using the leftover tissue and fresh 0.25% Trypsin/EDTA solution. The two dissociation solutions were combined and filtered through a 70 mm nylon mesh to remove large pieces of tissue. The suspension of cells was centrifuged at 1000 rpm for 5 minutes and the pellet was resuspended in 20 ml of proliferation medium (80% Dulbecco's Modified Eagle Medium (DMEM) high glucose supplemented with 20% fetal bovine serum and 1% Penicillin/Streptomycin) and cultured in a flask. The cells were incubated in a 37°C incubator with 5% carbon dioxide overnight. In order to purify the myoblast culture and eliminate fibroblasts, after 12-18 hours of culture, we collected the medium that contained the yet unattached myoblasts from the flask. The myoblasts were resuspended in 8-10 ml of growth medium and seeded on gelatin-coated substrate. The cultures were left incubating for 2 days before substituting the medium to fresh proliferation medium. When myoblasts reached confluence, the medium was changed to

fusion medium (98% DMEM high glucose supplemented with 2% horse serum and 1% penicillin/streptomycin) and incubated for 3 day.

These myotubes grown on gelatin substrate were then used to assay the formation of complex AChR aggregates in response to laminin as previously described (Vogel *et al.*, 1983). All cell samples were incubated with soluble laminin for 18 hours and subsequently AChR aggregates visualized.

This section is adapted from Vezina-Audette (2009).

2.4.3 RNA extraction and semi-quantitative RT-PCR

Total RNA was extracted from soleus (SOL) and extensor digitorum longus (EDL) muscles as previously described (Gauthier *et al.*, 1997; Dunn *et al.*, 1999). RNA concentration and purity were determined using an Eppendorf Biophotometer. Subsequently, RT-PCR was carried using 2 µg of each RNA sample. The final volume of the RT mixture (40 µl) contained of 0.625 µM random primer hexamers (Invitrogen, Burlington, ON, Canada), 1 X RT buffer (Ambion, Streetsville, ON, Canada), 0.5 µM dNTP mix (Invitrogen, Burlington, ON, Canada), 40U of RNase inhibitor (Ambion, Streetsville, ON, Canada), and 100U of MMLV reverse transcriptase (Ambion, Streetsville, ON, Canada). Subsequently, PCR amplifications were carried out using 1.5 µl of the cDNA generated in a master mix containing 1X Taq buffer with KCl (Fermentas, Burlington, ON, Canada), 1.5 mM MgCl₂ (Fermentas, Burlington, ON, Canada), 0.1 mM dNTP mix (Invitrogen, Burlington, ON, Canada), 0.2 mM primers

(custom synthesized by Sigma Genosys, St-Louis, MO, USA) and 0.05U/μl of Taq DNA polymerase (Fermentas, Burlington, ON, Canada) yielding a total volume of 25 μl.

GENE NAME	PRIMER PAIR SEQUENCES	SIZE (bp)	T _M (°C)	CYCLE #	ACCESSION NUMBER
28S	Fwd: 5'-TTGTTGCCATGGTAATCCTGCTCAGTACG-3' Rvs: 5'-TCTGACTTAGAGGCGTTCAGTCATAATCCC-3'	132	55	16	NR_003279.1
HDAC4¹	Fwd: 5'-CAGGAGATGCTGGCCATGAA-3' Rvs: 5'-GCACTCTCTTTGCCCTTCTC-3'	189	55	32	NM_207225.1
Dach2¹	Fwd: 5'-ACTGAAAGTGGCTTTGGATAA-3' Rvs: 5'-TTCAGACGCTTTTGCATTGTA-3'	165	55	34	NM_001142570.1 NM_033605.2
Mgn²	Fwd: 5'-CTCAGCTTAGCACCGGAAGCCCGA-3' Rvs: 5'-ATTGCCCCACTCCGGAGCGCAGGAG-3'	392	55	36	NM_031189.1
AGR³	Fwd: 5'-CAGTGGGGGACCTAGAAACA-3' Rvs: 5'-GCCATGTAGTCTGCACGTTCT-3'	181	60	40	NM_021604.2
NRG	Fwd: 5'-ACTCGCTGCTACTCGCCC-3' Rvs: 5'-CGCCGCTGCCTCACACTTG-3'	457	55	45	NM_001167891.1
GABP⁴	Fwd: 5'-GGGGAACAGAACAGGAAACA-3' Rvs: 5'-CCGTAATGCACGGCTAAGTT-3'	208	55	36	NM_008065.2
MuSK	Fwd: 5'-ATGCTGTTTCTTCAGGTTCC-3' Rvs: 5'-CTTCCATTGCCAGCCATTCC-3'	495	60	30	NM_001165996.1 NM_001037130.1 NM_010944.2 NM_001037129.1 NM_001037128.1
AChRα²	Fwd: 5'-CGTCTGGTGGCAAAGCT-3' Rvs: 5'-CCGCTCTCCATGAAGTT-3'	506	55	28	NM_007389.4
AChRγ²	Fwd: 5'-ACGGTTGTATCTACTGGCTG-3' Rvs: 5'-GATCCACTCAATGGCTTGC-3'	176	55	45	NM_009604.3
AChRε²	Fwd: 5'-AGACCTACAATGCTGAGGAGG-3' Rvs: 5'-GGATGATGAGCGTATAGATGA-3'	204	55	30	NM_009603.1

Table 2-1: Primers and RT-PCR conditions

Superscript number following a gene name indicates the paper from which the sequences were obtained. When no number is indicated, primers were designed by our lab. 1) (Tang *et al.*, 2009) 2) (Tang & Goldman, 2006) 3) (Hausser *et al.*, 2007) 4) (Angus *et al.*, 2005)

Amplification conditions consisted of an initial denaturation at 95°C for 3 minutes, followed by cycles of 1 minute denaturation at 94°C, 1 minute annealing at primer specific temperature and 1 minute extension at 72°C (Table2-1), followed by a final extension at 72°C for 10 minutes. For each set of primers, cycle number was adjusted to

permit comparison of PCR products within their linear range of amplification across samples (Table 2-1). Amplification of the ribosomal 28S RNA was used as an internal control. PCR products were separated by electrophoresis on 1.5% agarose gels and visualized with ethidium bromide. Band intensities were quantitated by densitometry with the AlphaInnotech system and FluorChem software (San Leonardo, CA, USA).

2.4.4 Histochemistry of NMJ

Muscle tissues, fixed with paraformaldehyde (4%), were used to carry out the staining for cholinesterase (Karnovsky & Roots, 1964). Following fixation, muscles were washed with distilled water (dH₂O) and placed in an incubation medium until the endplates became visible as white areas on the muscle surface. All muscle samples were treated in the same incubation solutions in order to stain acetylcholinesterase uniformly across samples. The incubation medium was prepared from 1.6 ml of a solution of 0.5 M glycine and 0.1 M copper sulfate pentahydrate, 3.2 ml of substrate solution consisting of 0.05 M acetylthiocholine iodide and 0.025 M copper sulfate, 20 ml of 0.2 M acetate buffer (pH 4.8) and 15.2 ml of dH₂O. Following the incubation period, samples were washed in dH₂O, stained for 2 minutes in 1% ammonium sulfide and washed once more. ImageJ software was used with the MultiCell outliner plug-in to outline and measure the size of endplates detected with the cholinesterase staining.

Additionally, AChRs were labeled using fluorescent rhodamine-conjugated α -bungarotoxin (r-BTX). Myotubes or muscle bundles were incubated with 1 μ g/ml r-BTX for 15 minutes at 37°C. Tissues were then washed twice in PBS and mounted with a

glycerol solution containing 1,4-diaminobutane dihydrochloride (P5780, Sigma) to reduce bleaching of fluorescent samples. Pictures of AChR endplates were acquired using a Zeiss axioskop epifluorescence microscope with a X63 objective (Zeiss). The system was equipped with a Retiga 1300R camera (Qimaging) and images were captured using Northern Eclipse software (Empix). All pictures were acquired at a fixed exposure for all specimens. Fluorescence analysis was carried out using ImageJ software to compare the fluorescence intensity of r-BTX staining across samples.

All histochemistry images were quantified using NMJ randomly selected from 5 experimental samples per condition. All quantifications were performed blind to the experimental condition.

2.4.5 Protein Extraction and Western Blotting

Muscles were homogenized using a hand-held Tissue Tearor homogenizer (ColeParmer, Montreal, QC, Canada) in RIPA buffer consisting of 1XPBS, 1% Igepal, 0.5% sodium deoxycholate, 0.1% sodium dodecyl sulfate (SDS), 0.001 M sodium orthovanadate, 0.01 M sodium fluoride, 0.01 mg/ml aprotinin, 0.01 mg/ml leupeptin and 1 mM phenylmethanesulfonyl fluoride (all reagents from Sigma-Aldrich, St-Louis, MO, USA). Homogenates were incubated on ice for 30 minutes followed by two 4°C centrifugations at 15 000 x g for 20 minutes. The supernatants were collected and protein concentration determined using Quick Start Bradford dye reagent (Bio-Rad, Mississauga, ON, Canada).

For protein expression analysis, 150 µg of protein were separated by SDS polyacrylamide gel electrophoresis (SDS-PAGE) on a gel consisting of a 5% stacking gel and an 8% separating gel. Samples were electrophoresed at 120V and Amersham Full-Range Rainbow (GE Healthcare, Baie d'Urfe, QC, Canada) molecular weight markers were used to define the protein sizes. Subsequently, proteins were transferred to a PVDF membrane (Millipore, Billerica, MA, USA) at 100V for one hour and a successful transfer was confirmed using Ponceau S staining. Membranes were blocked for one hour using 5% non-fat milk in 0.1% Tween-Tris Buffered Saline (T-TBS) and incubated with primary antibody overnight at 4°C on a shaker as indicated in Table 2-2. The following day the membranes were washed three times for five minutes each using 0.1% T-TBS and were then incubated with the appropriate horseradish peroxidase-conjugated secondary antibody: anti-rabbit IgG #7074 (Cell Signaling Technology, Danvers, MA, USA) or anti-mouse IgG #A8924 (Sigma-Aldrich, St-Louis, MO, USA). Subsequently, membranes were developed using the chemiluminescent Immobilon HRP substrate kit (Millipore, MA, USA) as per the manufacturer's instructions. Images were captured and protein expression quantified by densitometry with the AlphaInnotech system and FluorChem software (San Leonardo, CA, USA).

PROTEIN NAME	SUPPLIER	SIZE (kDa)	1°ANTIBODY	2°ANTIBODY
α-tubulin	Cell Signaling #2125	52	1:2000 in 5% milk	1:2000 in 5% milk for 1hr (anti-rabbit)
pCaMKII (thr286)	Cell Signaling #3361	$\alpha = 50$ $\gamma, \delta = 55-60$ $\beta_M = 73$	1:1000 in 5% BSA	1:2000 in 5% milk for 1hr (anti-rabbit)
CaMKII	Cell Signaling #4436	$\alpha = 50$ $\gamma, \delta = 55-60$ $\beta_M = 73$	1:1000 in 5% BSA	1:2000 in 5% milk for 1hr (anti-rabbit)
pERK1/2 (thr202/tyr204)	Cell Signaling #4370	42/44	1:1000 in 5% BSA	1:1000 in 5% milk for 1hr (anti-rabbit)
ERK1/2	Cell Signaling #9696	42/44	1:1000 in 5% BSA	1:1000 in 5% milk for 1hr (anti-rabbit)
pJNK (tyr183)	Santa Cruz #sc-6254	54	1:500 in 5% BSA	1:2000 in 5% milk for 1hr (anti-mouse)
JNK	Santa Cruz #sc-827	54	1:500 in 5% BSA	1:2000 in 5% milk for 1hr (anti-rabbit)
AChRα	Abcam #ab65832	54	1:1000 in 5% milk	1:1000 in 5% milk for 1hr (anti-rabbit)

Table 2-2: Western Blotting Conditions

2.4.6 Statistical Analysis

All data were analyzed using independent samples two-tailed Student's T-test. All statistics were performed using SPSS statistics software version 17.0 (IBM SPSS, Chicago, IL, USA).

2.5 Results

2.5.1 Characterization of CaMBP-TG mice

In this study, transgenic mice used express a small peptide inhibitor for CaM, known as the CaM-binding protein (CaMBP) under the control of the slow fiber-specific promoter troponin I slow (TnIs). (Corin *et al.*, 1994; Corin *et al.*, 1995; Levitt *et al.*,

1995; Wang *et al.*, 1995; Dunn *et al.*, 2000). RNA was extracted from selected muscles and RT-PCR was carried out to validate the expression of the inhibitory peptide exclusively in transgenic muscles. The 28S ribosomal RNA served as a loading control. Results confirmed the expression of CaMBP predominantly in the slow fiber expressing muscle soleus (SOL), with very little in the fast fiber expressing muscle extensor digitorum longus (EDL) (Figure 2.1A). To further demonstrate alterations in CaM signaling, immunoblotting for CaMKII phosphorylated at Thr286 was performed. This phosphorylation provides CaMKII with the ability to be autonomously active and it is the form of CaMKII displaying maximal activity (Means, 2000; Hook & Means, 2001). The SOL muscle of CaMBP-TG mice displayed a 30% decrease in the level of this active pCaMKII form (Figure 2.1B and C). Several bands, corresponding to different isoforms of CaMKII were detected on this Western blot (Figure 2.1B), however as CaMKII β_M is a skeletal muscle specific isoform (Bayer *et al.*, 1998; Rose *et al.*, 2006), found localized at endplates regions (Martinez-Pena y Valenzuela *et al.*, 2010), it was the sole isoform quantified (Figure 2.1C). Note that changes in the amount of the other CaMKII isoforms followed a similar trend to the response observed for CaMKII β_M (Figure 2.1B). The results did not indicate a significant alteration of pCaMKII levels in the fast muscle EDL, supporting the fact that the observed changes are mediated by the expression of CaMBP under the control of a slow fiber-specific promoter. Additionally, no alterations levels of total CaMKII were observed between the wild-type and transgenic muscles (Figure 2.1B and C). The assessment of CaMKII activity in the SOL muscle (expressed as the ratio of

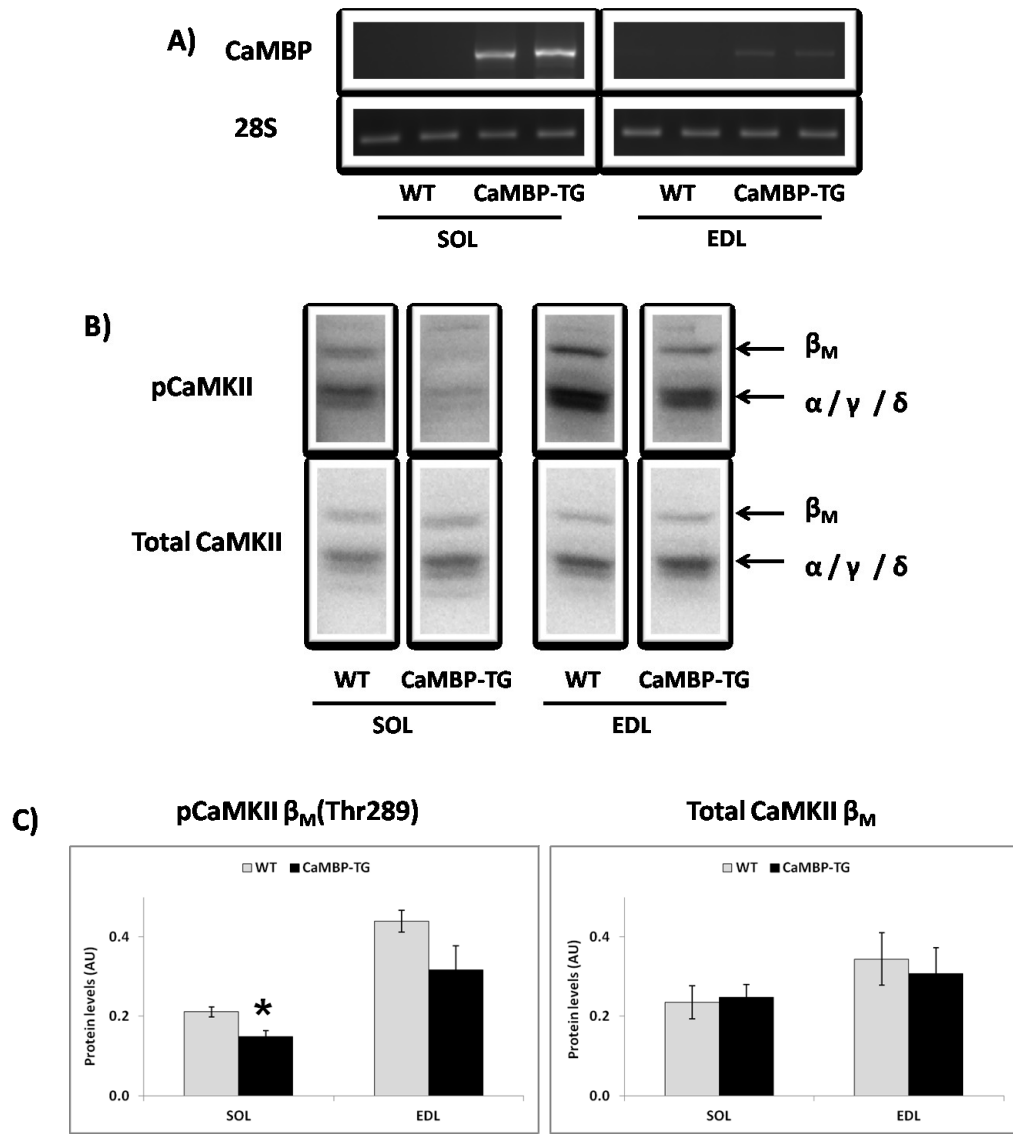


Figure 2.1: Decreased calmodulin signaling in CaMBP-TG mice

A) Representative agarose gel images comparing the expression of CaMBP in SOL and EDL muscles of wild-type and transgenic mice. Shown are images for two mice per group. Ribosomal 28S RNA served as a loading control. B) Representative Western blot images C) and quantifications of relative protein expression for pCaMKII and total CaMKII in SOL and EDL muscles of wild-type and transgenic mice. All quantifications were standardized to tubulin loading control and are expressed as mean \pm SE. (* sig. diff. from WT, $p < 0.05$, $n = 3$)

pCaMKII to total CaMKII) indicated a 35% drop of protein activity in CaMBP-TG mice as compared to wild-type mice. In contrast, the EDL muscle only displayed a 20% drop of protein activity in CaMBP-TG mice as compared to wild-type mice. These results confirmed the expression of CaMBP in the SOL muscle of transgenic mice and showed a compromised CaM signaling, as detected by decreased levels of pCaMKII in CaMBP-expressing mice.

2.5.2 Transgenic expression of CaMBP increases endplate complexity

Previous research has implicated calcium in the modulation of AChR aggregates formation (Peng, 1984) and in AChR gene expression (Walke *et al.*, 1994). In this study the hypothesis that calmodulin is altering the morphology of AChR aggregates on the muscle surface was further explored.

Initial experiments were performed *in vitro* on muscle cell cultures using a simplified model that used soluble laminin, an extracellular matrix protein, to induce AChR aggregates. The clustering of AChR induced on cultured myotubes by soluble laminin occurs independently of nerve activity (Vogel *et al.*, 1983; Sugiyama *et al.*, 1997; Montanaro *et al.*, 1998; Kummer *et al.*, 2004). The formation of AChR aggregates was observed using bungaratoxin (BTX) staining after 18 hours of incubation with soluble laminin. The complexity of endplates was compared between myotubes produced from wild-type or CaMBP-expressing myoblasts. Wild-type myotubes formed simple, “plaque-like” AChR aggregates (Figure 2.2A). In contrast, CaMBP-expressing myotubes formed

complex, branched, “pretzel-like” AChR aggregates (Figure 2.2A). These results suggest that calmodulin can regulate the complexity of AChR aggregates *in vitro* independently of nerve activity.

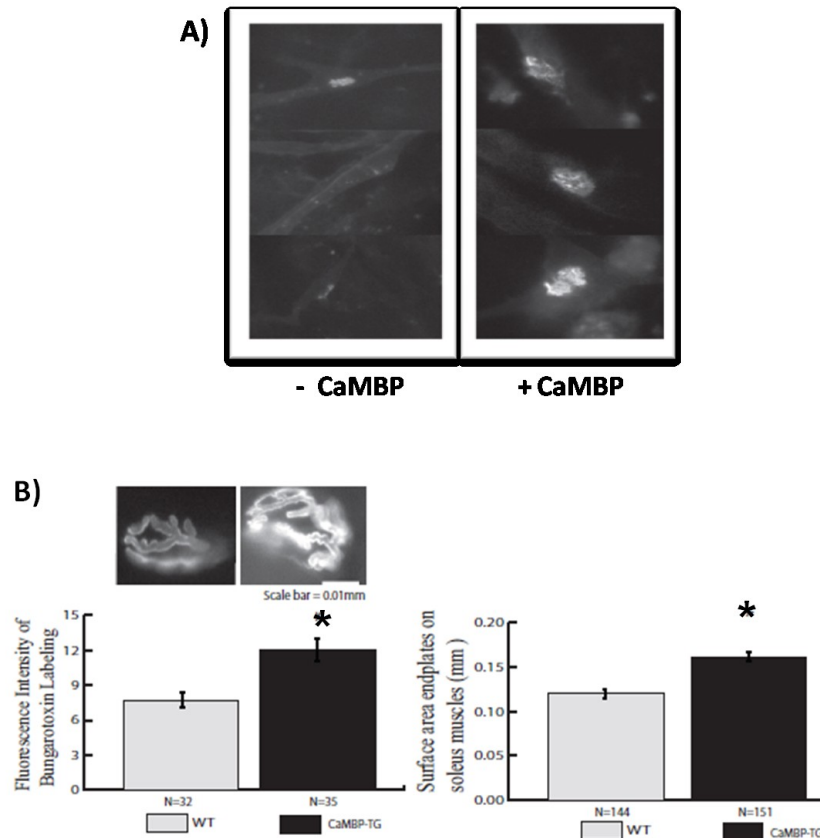


Figure 2.2: Expression of CaMBP leads to larger endplate structures *in vitro* and *in vivo*.

Figure modified from (Vezina-Audette, 2009) as authorized per author.

A) Primary myotubes were stained for AChR using BTX. Formation of AChR aggregates was induced by incubation with soluble laminin. Shown are myotubes from wild-type mice and myotubes prepared from CaMBP-TG mice. B) Representative images of SOL muscle bundles isolated from mice and stained using BTX. The quantification of the fluorescent intensity of the BTX stain is presented. Additionally, staining for acetylcholinesterase identified the surface area of endplates and the quantification is shown. All quantification are expressed as mean \pm SE (* sig. diff. from WT, $p < 0.05$, N = indicates the number of NMJ analysed randomly selected from 5 experimental samples per condition)

To investigate if a similar response was observed *in vivo*, muscle fiber bundles were teased from adult soleus muscles and their NMJ were visualized by staining AChR using bungaratoxin (BTX); a toxin that binds specifically AChRs. Additionally, staining for acetylcholinesterase identified the surface area of endplates. Acetylcholinesterase is the enzyme that degrades the neurotransmitter acetylcholine and it is localized at endplates. A comparison of soleus muscles of wild-type and transgenic mice indicated that a reduction of calmodulin signaling leads to more complex AChR clusters (Figure 2.2B). The fluorescence intensity of bungaratoxin staining was greater in transgenic muscles and the surface area of endplates was increased in transgenic mice. Taken together these findings indicate that CaM regulates the density of AChR aggregates both *in vitro* and *in vivo*.

2.5.3 The expression of selected transcripts is not altered in CaMBP-TG mice

Calmodulin, by altering CaMKII activity, appears as a candidate in the conversion of muscle activity into intracellular signaling events that modulate gene expression at the neuromuscular junction (Tang *et al.*, 2001; Tang *et al.*, 2004; Tang & Goldman, 2006; Tang *et al.*, 2009). We hypothesized that altered gene expression at the NMJ could lead to changes in the morphology of AChR aggregates on the muscle surface. Semi-quantitative RT-PCR analysis was conducted on RNA isolated from SOL muscle of wild-type and CaMBP-TG mice. The expression of transcripts from the HDAC/myogenin pathway was investigated and results failed to detect alterations in the target genes measured (Figure 2.3A). Additionally, agrin and neuregulin have been shown to

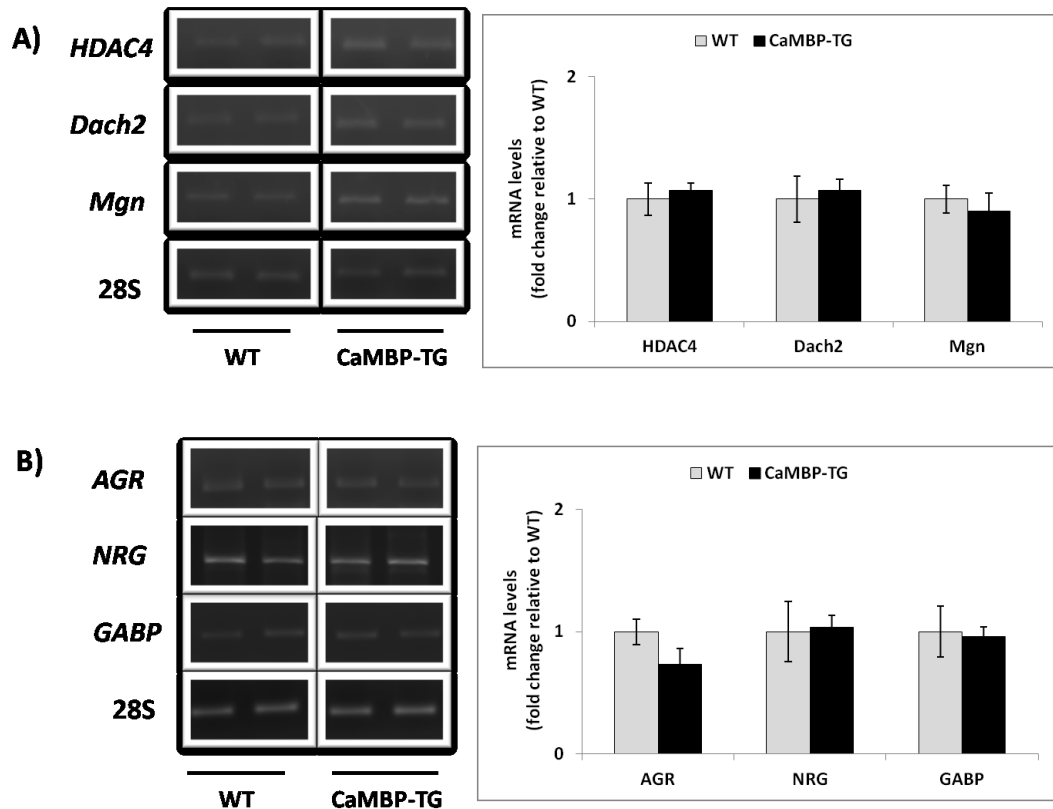


Figure 2.3: The expression of selected gene targets is not changed in CaMBP-TG mice

Representative agarose gel images of PCR products and quantifications are shown for the (A) HDAC/Mgn pathway and for (B) AGR and NRG signaling. All quantifications are standardized to ribosomal 28S RNA. Data were normalized to wild-type and expressed as mean \pm SE. (* sig. diff. from WT, $p < 0.05$, $n = 3$ to $n = 5$)

influence AChR aggregates by signaling through the GABP transcription factor (Schaeffer *et al.*, 1998; Briguet & Ruegg, 2000; Schaeffer *et al.*, 2001; Lacazette *et al.*, 2003; Mejat *et al.*, 2003). Thus mRNA levels of these targets were measured and again results did not indicate changes in gene expression, as compared to wild-type mice (Figure 2.3B). Overall, these findings indicate that genes previously shown to regulate

AChR expression are not differentially expressed in CaMBP-TG mice, suggesting a post-transcriptional regulation of the observed morphological changes in endplate structures.

2.5.4 CaMBP-TG mice do not show altered signaling of JNK and ERK kinase

Signaling pathways of agrin and neuregulin converge and act cooperatively to activate signaling events through MAPK kinases ERK and JNK (Lacazette *et al.*, 2003). These pathways have been shown to regulate expression of AChR. Accordingly, it is thus possible that levels of ERK and JNK are altered in our transgenic model of compromised CaM. Immunoblotting of whole cell muscle protein extracts was performed and protein expression analysed. The results indicated a trend towards increased levels of pERK1 and pERK2 (Figure 2.4A) without a significant difference, and without changes in total protein levels. Similarly, a significant alteration in the levels of pJNK or total JNK protein was not observed (Figure 2.4B). These findings indicate that neither ERK nor JNK signaling are perturbed in the CaMBP-TG mice model. These outcomes suggest that CaM regulates AChR density at NMJ independently of MAPK signaling.

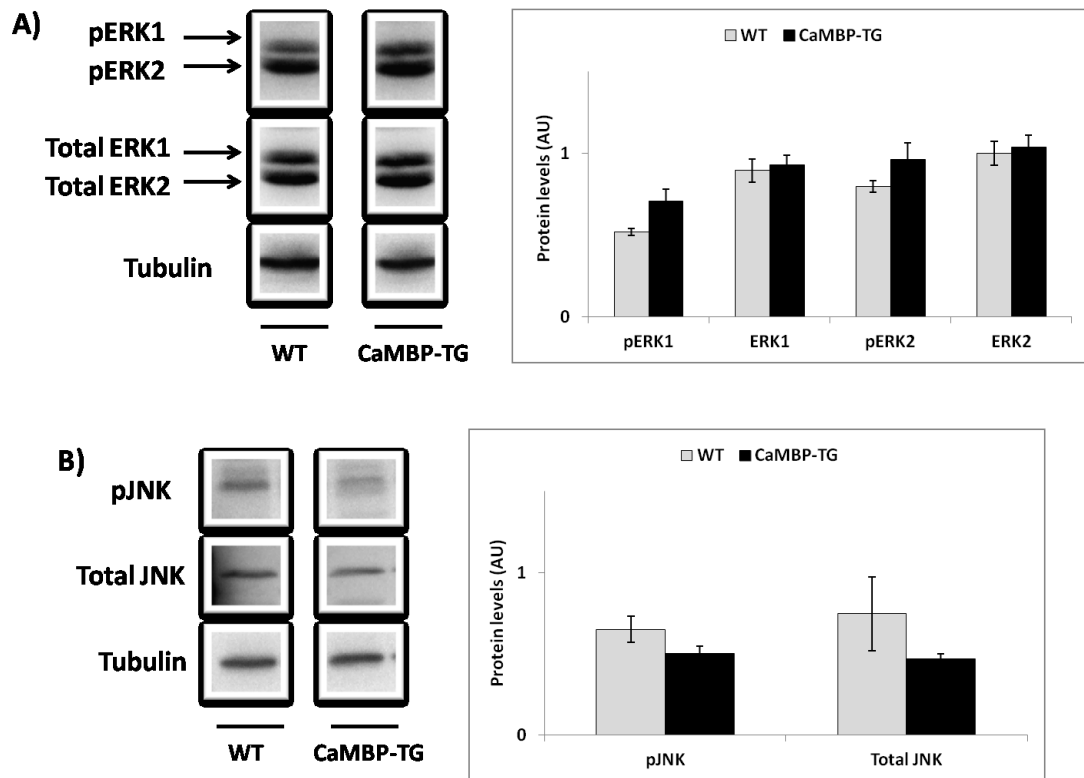


Figure 2.4: Signaling of ERK and JNK are not altered in CaMBP-TG mice

Representative Western blot images and quantifications for A) phosphorylated ERK1/2 (pERK1/2) and total ERK1/2 B) pJNK and total JNK. All quantifications were standardized to tubulin loading control and are expressed as mean \pm SE (* sig. diff. from WT, $p < 0.05$, $n=3$).

2.5.5 Larger AChR aggregates are not caused by increased expression of AChR

The larger endplates observed *in vitro* and *in vivo* in our model of compromised CaM (Figure 2.2) could be mediated by remodeling processes that lead to a change in AChR localization without a change in the expression of AChR genes and proteins. To support the idea that there is no transcriptional mechanism involved, levels of synaptic genes were measured in CaMBP-TG mice using semi-quantitative RT-PCR analysis. MuSK mRNA levels were also measured as this receptor is found localized at the NMJ,

its expression is known to be influenced by nerve activity and it is recognized as the central organizer of synaptic differentiation. Additionally, mRNA levels of the major subunit forming the pentameric receptor structure, subunit α , were determined. Both *MuSK* and *AChR α* mRNA levels were unchanged in CaMBP-TG mice as compared to wild-type mice, (Figure 2.5A). The AChR pentameric structure is formed by distinct subunits that differ with respect to their time of expression and their properties. The fetal γ subunit and the adult ϵ subunit are also reported to be regulated by distinct regulatory mechanisms (Martinou *et al.*, 1991; Martinou & Merlie, 1991). Measurements of the expression levels of these two subunits did not indicate changes of expression between the wild-type and CaMBP-TG mice (Figure 2.5A). Overall, these results support the conclusion that the observed morphological changes in endplate structures are not regulated at the level of transcription.

To address the possibility that the larger endplates are caused by an overall increase of AChR protein level, mediated by an increased efficacy of translation, immunoblotting of whole cell muscle protein extract was performed and expression of the major *AChR α* subunit was measured. Similarly to transcript levels, no alteration in protein levels was observed between the wild-type and CaMBP-TG mice (Figure 2.5B). Note that the commercially available antibodies for AChR subunits recognize uncharacterized targets that appear as multiple non-specific bands on the Western blot. For this reason, expression analysis of other AChR subunits was not possible. These findings indicated that the larger endplate morphology in CaMBP-TG mice was not

mediated by changes in AChR transcript or protein levels. The results presented imply that CaM regulates AChR aggregate morphology in an *in vivo* transgenic mouse model and suggest involvement of mechanisms independent of synaptic transcription and translation as mediators of this remodeling.

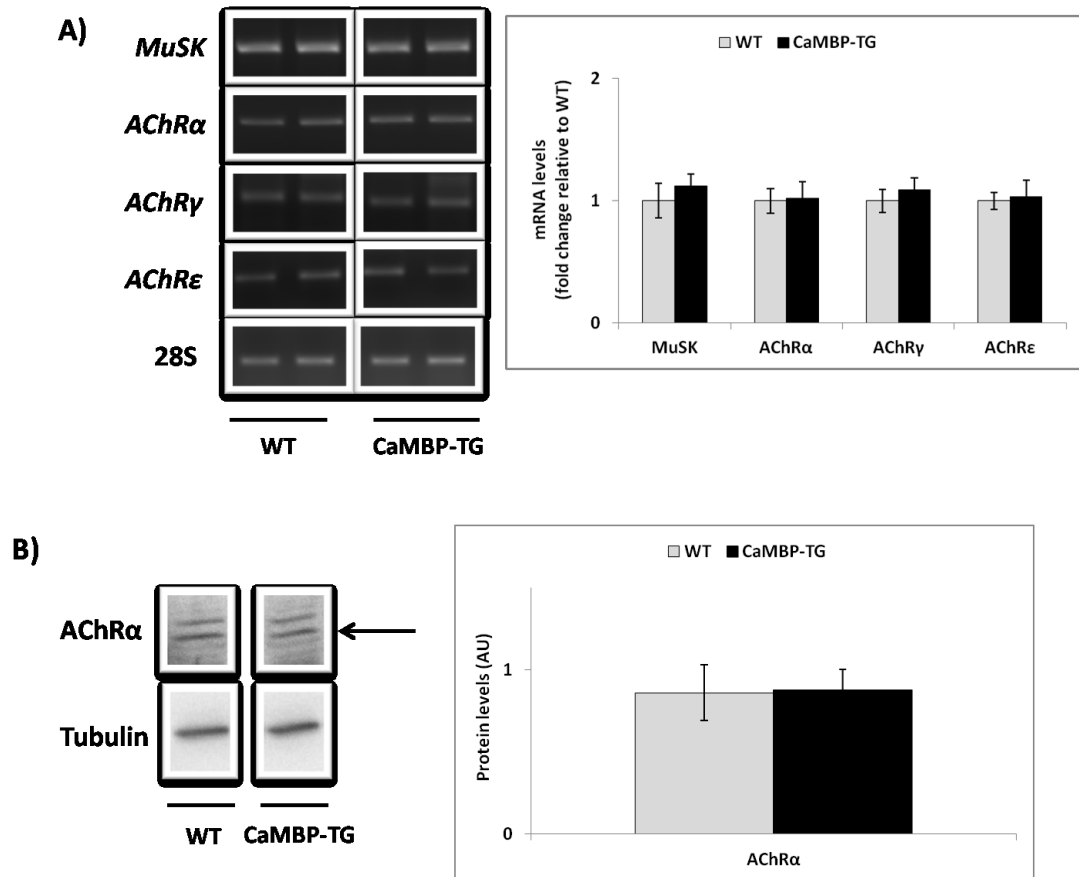


Figure 2.5: Neither the AChR gene or AChR protein levels are altered in CaMBP-TG mice.

A) Representative agarose gel images of PCR products and quantifications for synaptic gene levels. All quantifications are standardized to ribosomal 28S RNA. Data were normalized to wild-type and expressed as mean \pm SE. (* sig. diff. from WT, $p < 0.05$, $n = 3$ to $n = 5$). B) Representative Western blot images for AChR α subunit and the quantification normalized to tubulin loading control. The arrow points to the specific band of interest. All data are expressed as mean \pm SE. ($n = 3$, * statistical significant, $p < 0.05$)

2.6 Discussion

Research has highlighted the importance of maintaining an adequate density of AChR receptor at the NMJ for efficient synaptic communication (reviewed in (McConville & Vincent, 2002; Newsom-Davis, 2007)). In this study, our aim was to investigate the regulation of AChR expression by calmodulin, a second messenger of Ca^{2+} signaling. We hypothesize that calmodulin can influence expression of AChR at adult muscle endplates. This is the first study that uses an *in vivo* transgenic mouse model, displaying compromised CaM signaling, to elucidate CaM involvement in regulation of AChR density at the adult NMJ.

The transgenic mice used express a small peptide inhibitor for CaM, known as the CaM-binding protein (CaMBP), under the control of the slow fiber-specific promoter troponin I slow (TnIs). (Corin *et al.*, 1994; Corin *et al.*, 1995; Levitt *et al.*, 1995; Wang *et al.*, 1995; Dunn *et al.*, 2000). Previous characterization of CaMBP-transgenic mice has indicated that under resting conditions, muscles of these animals display a normal phenotype (Dunn *et al.*, 2000). In the initial phase of our experiments, we confirmed the alteration of CaM signaling in the animals used. The findings presented in Figure 2.1 indicated that the SOL muscle of transgenic mice was expressing CaMBP at high levels and this was leading to decreased expression of active pCaMKII, thus confirming a decrease in CaM signaling. CaMKII was chosen as a target since previous data have indicated that this kinase is localized at the NMJ (Fertuck & Salpeter, 1976; Martinez-Pena y Valenzuela *et al.*, 2010), therefore, this suggests CaMKII involvement in the

regulation of endplate morphology or function. Additionally, the role of CaMKII in the regulation of synaptic plasticity of the central nervous system (CNS) has been shown (Lisman *et al.*, 2002) and this also suggests its possible function in the much simpler, neuromuscular synapse.

Next, we sought to determine if calmodulin can lead to alterations in the formation of AChR aggregates. Preliminary experiments were conducted *in vitro* on cultured myotubes with AChR aggregation induced using soluble laminin (Vogel *et al.*, 1983; Sugiyama *et al.*, 1997; Montanaro *et al.*, 1998). Laminin is a potent nerve-independent model of synaptic development that has the ability to promote formation of complex, branched, pretzel-like AChR aggregates that are characteristic of adult NMJ (Kummer *et al.*, 2004). Myoblasts from CaMBP-TG mice were isolated and differentiated into myotubes. The AChR aggregates formed on CaMBP expressing myotubes were larger than wild-type controls and displayed branched like structures (Figure 2.2A). These findings suggest that in cultured myotubes, CaM acts to regulate the morphology of endplates by suppressing formation of mature pretzel-like structures.

To determine if a similar response is observed *in vivo*, we analysed the NMJ on muscle bundles isolated from wild-type and CaMBP-TG mice. As in the *in vitro* results, the NMJ of CaMBP-TG muscles displayed larger surface areas, as measured by AChE staining, as well as an increased density of AChR at NMJ, as measured by BTX labeling experiments. These results (Figure 2.2B) indicated that CaM signaling influences the morphology of AChR aggregates both *in vitro* and *in vivo*. In wild-type mice, CaM likely

serves to suppress the formation of aberrant pretzel-like structures. These results support a novel and important regulatory role for CaM.

A tight regulation of the number and structure of neuromuscular junctions is a fundamental aspect of efficient and appropriate synaptic transmission (Sanes & Lichtman, 1999, 2001). An inadequate regulation of NMJ formation and the presence of aberrant AChR aggregates have been shown in Fukuyama-type congenital muscular dystrophy (Taniguchi *et al.*, 2006). In addition, a deregulation in AChR localization or expression are the hallmark of numerous neuromuscular junction disorders such as Myasthenia Gravis (reviewed in (McConville & Vincent, 2002; Newsom-Davis, 2007). Furthermore, more complex NMJ could represent fragmented endplates that are caused by a loss of nerve terminals followed by novel nerve sprouting. Overall, the formation of more complex NMJ in CaMBP-TG mice may be preliminary symptoms of a disease. Muscles of CaMBP-TG mice display a normal phenotype under resting conditions (Dunn *et al.*, 2000), but it is possible that under exercise or stress conditions, the muscles of these mice are more susceptible to damage or fatigue. Future studies should address these questions.

Subsequent experiments were performed to identify the signaling pathways implicated in the observed alteration of AChR aggregate morphology in CaMBP-TG mice. The hypothesis that CaM regulates signaling pathways influencing the expression of synaptic genes was tested. The first pathway investigated was the HDAC/Mgn pathway (Figure 2.6A) that is regulated by CaMKII activity (Tang *et al.*, 2001; Tang *et*

al., 2004; Tang & Goldman, 2006; Tang *et al.*, 2009). Under normal innervation and signaling conditions, CaMKII activity induces phosphorylation of HDAC4, which promotes HDAC4 shuttling out of the nucleus (Tang *et al.*, 2001; Tang *et al.*, 2004; Tang & Goldman, 2006; Tang *et al.*, 2009). This, in turn, stimulates expression of the *Dach2* gene that inhibits expression of *Mgn* that drives expression of AChR genes (Tang *et al.*, 2001; Tang *et al.*, 2004; Tang & Goldman, 2006; Tang *et al.*, 2009). Results previously discussed (Figure 2.1) indicated that CaMKII signaling is compromised in CaMBP-TG mice, thus we hypothesized that similarly to the denervated condition, CaMBP-TG mice would display decreased *Dach2* and increased *Mgn* levels, and this in turn would increase levels of AChR genes. Results (Figure 2.3A) failed to show alterations in the signaling targets of this pathway. Myogenin signaling was previously characterized to regulate gene expression in innervated versus denervated muscle (Tang *et al.*, 2009) thus the HDAC/*Mgn* signaling appears important for adaptive fiber remodeling associated with denervation, whereas suppression of glycolytic genes and induction of oxidative and synaptic genes is observed. This pathway is not regulating expression of AChRs in models of normal innervations.

Alternatively, AGR and NRG, two trophic factors synthesized by the nerve also influence AChR clustering and the transcription of AChR genes (Figure 2.6B) (reviewed in (Williams *et al.*, 2008)). AGR and NRG interact with distinct receptors and activate distinct signaling cascades, but their signaling events converge and cooperatively regulate

the GABP transcription factor (Lacazette *et al.*, 2003). The mRNA expression of *AGR*, *NRG* and *GABP* was compared between wild-type and CaMBP-expressing SOL muscles

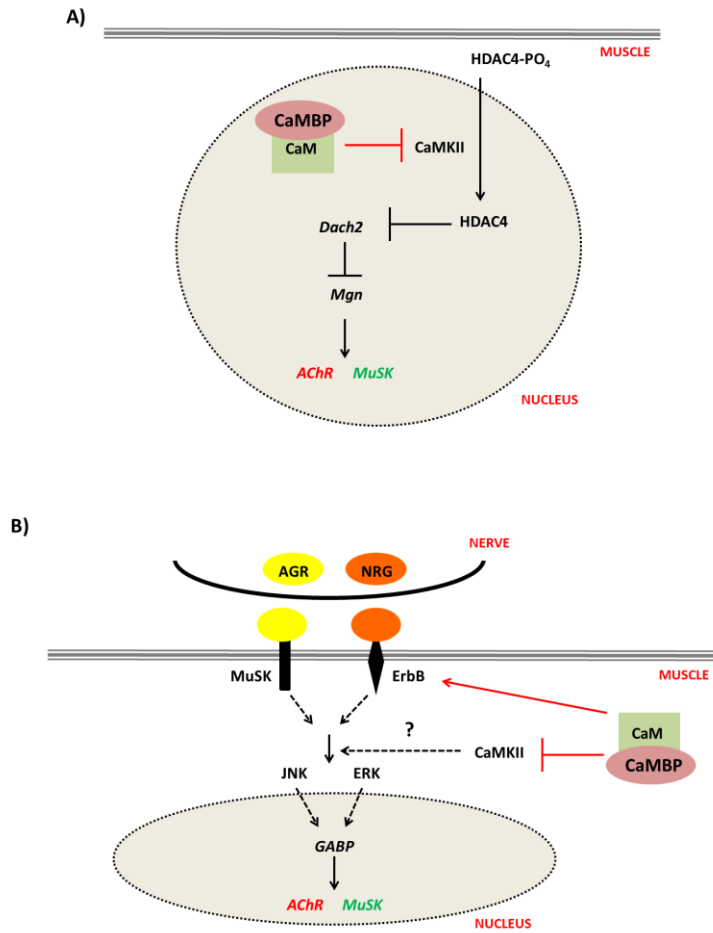


Figure 2.6: Schematic of signaling pathways investigated

Signaling pathway hypothesized in this study to influence the expression of AChR expression: A) HDAC4/Mgn pathway and B) signaling downstream of AGR and NRG.

and no differences were observed for any target (Figure 2.3B). MAPK kinases ERK and JNK are downstream signaling partners of AGR and NRG. ERK and JNK promote expression of AChR genes by stimulating GABP binding to promoter regions (Schaeffer *et al.*, 2001; Lacazette *et al.*, 2003; Mejat *et al.*, 2003). The levels of phosphorylated and total proteins ERK and JNK (Figure 2.4) were not changed in CaMBP-TG mice and are in agreement with the absence of modification in the amount of *GABP* mRNA. Collectively, two pathways that regulate the expression of AChR are not modified in CaMBP-TG mice and this data suggest that the expression of AChR may not be altered in our model.

These results urged us to measure changes in the expression of synaptic genes in CaMBP-TG mice. *MuSK* mRNA levels were measured since this receptor is recognized as a central organizer of synaptic differentiation (reviewed in (Strohlic *et al.*, 2005)) and its expression levels correlate with AChR gene expression (Valenzuela *et al.*, 1995; Ip *et al.*, 2000; Moore *et al.*, 2001). The mRNA levels of *AChR* subunits also were measured. The fetal γ subunit and the adult ϵ subunit were chosen since they differ in their expression time, properties and also have been shown to be differently regulated (Mishina *et al.*, 1986; Gu & Hall, 1988; Martinou *et al.*, 1991; Martinou & Merlie, 1991). In addition, *AChR* α subunit was chosen since it is the main subunit forming the receptor pentameric structure. Outcomes did not identify any alteration of expression in these targets and indicated that expression of synaptic genes is not altered in CaMBP-TG mice (Figure 2.5A). Finally, the larger endplate morphology could be mediated by increased

synthesis of AChR protein, but here again our findings did not detect an increase in protein levels using immunoblotting analysis (Figure 2.5B). Overall these results suggest that neither modifications of signaling events that promote synaptic gene transcription, nor variations in AChR protein translation, are the cause for increased NMJ complexity in CaMBP-TG mice. These findings are in agreement with published results that indicate that AChR density at the muscle surface is regulated by recycling mechanisms (Bruneau *et al.*, 2005a; Bruneau & Akaaboune, 2006a). Furthermore, it has been proposed that CaMKII could modulate the levels or activities of proteins involved in sorting, targeting and/or fusion of endocytic vesicles at the muscle membrane and thus play regulatory roles in AChR recycling events (Martinez-Pena y Valenzuela *et al.*, 2010). Given the findings presented in this investigation, further research in the CaMBP-TG mouse model should aim to study AChR movement and recycling events using techniques such as confocal microscopy and selective receptor labeling.

In conclusion, the results presented here support the idea that CaM regulates AChR aggregates morphology. The data imply that transcriptional or translational mechanisms are not involved and point toward mechanisms of receptor movement or recycling. CaMKII activity is shown to be decreased in CaMBP-TG mice and thus CaMKII signaling may be implicated in the organization of AChR at NMJ. Yet, it may not be the sole pathway regulating this process since additional pathways downstream of CaM have been shown to regulate AChR clustering activity. For instance, calcineurin (Cn) is a well known CaM dependent phosphatase (reviewed in (Al-Shanti & Stewart,

2009) that has been implicated in the regulation of AChR distribution *in vitro* (Madhavan *et al.*, 2003). The findings presented in this study demonstrate for the first time that a transgenic inhibition of CaM signaling has the ability to regulate NMJ morphology. These results are important since they identify a new model that should be further investigated to better understand mechanisms that regulate the dynamics of AChRs at the adult NMJ. This in turn could help in the identification of novel therapeutic targets for the treatment of neuromuscular disorders. In addition, many of the molecules expressed at NMJ are also expressed in the CNS, and thus studies of NMJ assembly might provide information on the mechanisms of synaptogenesis in the brain.

2.7 Future Directions

In conclusion, it is important to specify the limitations of the experiments presented here and to identify additional experiments that would address these limitations. The skeletal muscle tissue is heterogeneous and composed of many cell types that include muscle fibers, fibroblasts, vascular cells and interstitial space. In addition, NMJ assembly has been shown to be regulated by signaling from a specific subtype of nuclei situated solely at the motor nerve contact sites (reviewed in (Schaeffer *et al.*, 2001; Mejat *et al.*, 2003)). These synaptic nuclei form a small portion of the whole muscle tissue investigated. Similarly, synaptic proteins that mediate the assembly and/or maintenance of NMJ are localized and concentrated at nerve-muscle contact sites (reviewed in (Sanes & Lichtman, 1999, 2001). In this study, whole muscle samples analysis were carried out and thus it is possible that alterations in gene and/or protein levels in a specific subset of cells are not detected, or only subtle variations are noted. A recent and more precise technique called Laser Capture Microdissection (LCM) (Espina *et al.*, 2006a; Espina *et al.*, 2006b; Espina *et al.*, 2007; Decarlo *et al.*, 2011) is now available in the laboratory. This methodology permits a simple and rapid isolation of selected cell types by direct microscope visualization (Espina *et al.*, 2006a; Espina *et al.*, 2006b; Espina *et al.*, 2007; Decarlo *et al.*, 2011). Subsequently, gene or protein analysis can be performed on samples of pure enriched cell populations. This technique can be used to selectively isolate NMJ enriched regions (Nazarian *et al.*, 2005; Ketterer *et al.*,

2011) and thus an in depth analysis of synaptic genes and proteins of CaMBP-TG mice can be carried out and compared to wild-type mice.

In addition, the data presented in this study suggest that CaM signaling regulates movement of AChR at the muscle surface. For this reason, the sequential labeling of AChR localized at the surface of wild-type and CaMBP-TG muscles should be carried out. Sequential labeling of receptor can be performed using bungaratoxin conjugated to different fluorophores as described in detail by Akaaboune group (Bruneau *et al.*, 2005a). This technique can distinguish pre-existing, new and recycled receptor aggregates and provides information on AChR movement at the muscle surface. Alteration in receptor dynamics could contribute to the larger and more complex NMJ observed in CaMBP-TG mice as compared to wild-type mice.

Chapter 3: NFATc2 and NFATc3 *have essential roles in the regulation of adaptive skeletal muscle fiber growth*

Ewa M. Kulig¹ and Robin N. Michel²

1. *Department of Chemistry and Biochemistry, Concordia University, Montreal, Quebec, Canada*
2. *Department of Exercise Science, Concordia University, Montreal, Quebec, Canada*

3.1 Background

In this Chapter the functions of different isoforms of NFAT transcription factors are investigated in the regulation of adaptive muscle growth. A surgical overload growth model is used to induce adaptive muscle remodeling. We assessed the expression, localization and function of NFAT isoforms in muscle fibers of wild-type, NFATc2 and NFATc3 knockout mice under normal weight-bearing or functional compensatory work overload conditions. The results provide novel findings that suggest distinct and essential roles for the members of the NFAT family of transcription factors in conditions of rapid fiber growth.

These results are to be included in a paper written for future submission to The Journal of Physiology. This journal presents original work devoted to demonstrating new physiological mechanisms. Alternatively, the work presented in this chapter could be separated into smaller studies that might be published separately. Some of the data presented has been included in previous poster presentations (Kulig *et al.*, 2009; Kulig *et al.*, 2010). Overall, the findings presented here provide new insights into the roles and regulation of NFAT transcription factors in adaptive muscle remodeling.

3.2 Abstract

Calcineurin (Cn) is a calcium-regulated serine/threonine phosphatase that acts via its substrate the Nuclear Factor of Activated T-cells (NFAT) family of transcription factors. Involvement of Cn / NFAT signaling in the regulation of the skeletal muscle fiber phenotype is recognized, however, little is known about the roles of the various Cn-regulated NFAT isoforms (NFATc1-c4) in this process.

In this study, mice deficient for the NFATc2 or NFATc3 isoform displayed blunted muscle growth following functional work overload while maintaining fiber remodeling towards oxidative phenotypes. Furthermore, NFATc2 and NFATc3 regulated the hypertrophic growth specifically in glycolytic, but not oxidative, muscle fiber types. RT-PCR did not reveal compensatory upregulation of any surviving NFAT isoform mRNA in knockout mice, but immunofluorescence data showed that the nuclear localization of NFAT proteins is differentially regulated during compensatory growth in knockout mice. Analysis of the mRNA levels of several myogenic regulatory factors indicated that NFATc2 may regulate *Myf5* expression during adaptive muscle growth, while NFATc3 may control *Mgn* expression during developmental muscle growth. Furthermore, immunoblotting did not detect altered overload-induced Akt signaling in NFATc2^{-/-} and NFATc3^{-/-} mice, as compared to wild-type mice. Taken together, these results show that members of the NFAT family of transcription factors have distinct roles in the remodeling of the muscle fiber phenotype. In addition, the data demonstrate essential roles for NFATc2 and NFATc3 in the regulation of the adaptive muscle growth.

3.3 Introduction

Skeletal muscle fibers are composed of myofibers that can adapt and remodel their biochemical, physiological and metabolic properties to meet functional demands (reviewed in (Bassel-Duby & Olson, 2006)). The remodeling of skeletal muscles results from the activation of signaling pathways that reprogram gene and/or protein expression to sustain muscle performance. Calcium-dependent signaling is well characterized for regulation of muscle function and plasticity (Berchtold *et al.*, 2000) and calcineurin (Cn) is a calcium/calmodulin-activated serine-threonine phosphatase that has been implicated in modulation of myofiber growth and remodeling (reviewed in (Olson & Williams, 2000; Bassel-Duby & Olson, 2003, 2006; Michel *et al.*, 2007)). More specifically, previous experiments have implicated calcineurin in muscle cell differentiation (Delling *et al.*, 2000; Friday *et al.*, 2000; Friday & Pavlath, 2001; Friday *et al.*, 2003), muscle hypertrophy (Dunn *et al.*, 1999; Musaro *et al.*, 1999; Semsarian *et al.*, 1999; Dunn *et al.*, 2000) and in the regulation of the muscle oxidative gene program (Chin *et al.*, 1998; Bigard *et al.*, 2000; Delling *et al.*, 2000; Naya *et al.*, 2000).

Downstream targets of calcineurin signaling include the nuclear factors of activated T-cells (NFAT) family of transcription factors (Crabtree & Olson, 2002; Bassel-Duby & Olson, 2003). Originally identified in T cells, NFATs are now also well characterized for their roles in various other cell types including skeletal muscles (Rao *et al.*, 1997; Crabtree & Olson, 2002; Horsley & Pavlath, 2002). Calcium regulated NFATs are activated by a direct calcineurin induced dephosphorylation that promotes nuclear translocation, and subsequent DNA binding that activates gene expression. Four different

Cn-regulated isoforms: NFATc1, NFATc2, NFATc3 and NFATc4, are expressed in skeletal muscles (Hoey *et al.*, 1995; Calabria *et al.*, 2009). Previous research showed that a knockout of NFATc1 lead to embryonic lethality due to defects in cardiogenesis (de la Pompa *et al.*, 1998). In addition, disruption of NFATc2 or NFATc3 lead to an alteration in muscle mass without changes in fiber type proportions (Horsley *et al.*, 2001; Kegley *et al.*, 2001). More specifically, this alteration in muscle mass was caused by a reduced fiber cross sectional area in NFATc2^{-/-} mice, and a reduced number of fibers in NFATc3^{-/-} mice. Meanwhile, mice with an NFATc4 knockout display a normal phenotype without evident defects in muscles (Graef *et al.*, 2001). Furthermore, recently it has been shown that NFAT isoforms have differential sensitivity to nerve electrical activity patterns and that different combinations of NFAT isoforms are necessary for maintenance of both slow and fast muscle fibers (Calabria *et al.*, 2009).

Various models can be used to induce muscle growth, however, the synergist ablation or overload model is a potent and well-characterized model that leads to increased muscle load, while simultaneously doubling nerve mediated fiber activation (Gardiner *et al.*, 1986). This model has been shown to promote muscle fiber hypertrophy (Dunn & Michel, 1997; Dunn *et al.*, 1999) and hyperplasia (Antonio & Gonyea, 1993; Kelley, 1996) as well as muscle remodeling toward the oxidative phenotype (Dunn & Michel, 1997).

The aim of the present study was to assess the role of the NFATc2 and NFATc3 in the regulation of adaptive muscle growth. Results indicate that NFATc2 and NFATc3

knockout mice undergo a blunted plantaris muscle hypertrophy, while maintaining oxidative fiber type remodeling following 28 days of functional overload. In NFATc2^{-/-} or NFATc3^{-/-} mice, nuclear trafficking of NFAT isoforms was altered following overload in comparison to wild-type mice. In addition, changes in the expression of myogenic regulatory factor (MRF) mRNA levels were observed in NFATc2 and NFATc3 knockout mice in comparison to wild-type mice. Taken together, these results illustrate that members of the NFAT family of transcription factors have distinct and important roles in the regulation of muscle fiber phenotypes in an adaptive growth model.

3.4 Methods

3.4.1 Animal Care and Protocols

All animal care and experimental procedures were performed in accordance with the guidelines established by the Canadian Council of Animal Care. These procedures were approved by the University Animal Research Ethics Committee (UAREC) of Concordia University. Transgenic mice models deficient for functional NFATc2 (NFATc2^{-/-}) were a gift from Dr. L. Glimcher (Harvard University) whereas mice deficient for functional NFATc3 (NFATc3^{-/-}) were a gift from Dr. G. Pavlath (Emory University). Both NFATc2 and NFATc3 knockout mice were generated by the insertion of a neomycin resistance gene into the Rel homology region leading to a disruption of the DNA-binding domain of NFATc2 or NFATc3 protein (Hodge *et al.*, 1996; Oukka *et al.*, 1998). The truncated proteins generated in mutant mice are unable to bind DNA but can still

potentially interact with other accessory binding partners; however the characterization of the mutant mice confirmed a loss of function mutation in these animals (Hodge *et al.*, 1996; Oukka *et al.*, 1998). Animals were housed in temperature and humidity controlled conditions on a 14:10 hour light: dark cycle and had access to water and food *ad libitum*. Mice were bred using standard breeding methods and identified as deficient for specific NFAT isoform by screening of genomic DNA extracted from tails (Dunn *et al.*, 2000). For all experimental procedures, male mice aged between 4-8 months were used.

3.4.2 Animal Surgeries and Extractions

All surgical procedures were performed under aseptic conditions on animals anesthetized by intramuscular injection (1.2 μ l / g) of 100 mg/ml ketamine hydrochloride and 10 mg/ml xylazine in a volume ratio of 1.6:1. Functional compensatory work overload of plantaris muscle was induced by bilateral surgical ablation of the synergistic muscles: soleus and a major portion of the gastrocnemius muscle (Figure 3.1). The mice were overloaded for periods of 7 and 28 days. During these periods, following a period of convalescence (3-5 days), the overload mice were exercised daily for 60 minutes by placing them in an exercise ball (12 cm diameter). At the end of the experimental period, mice were anesthetized as previously described and lower limb muscles of control and overloaded animals were extracted, either frozen directly in liquid nitrogen or embedded

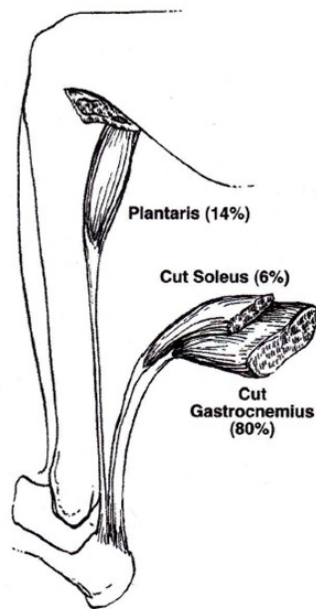


Figure 3.1: Schematic of the functional overload model (Lieber, 2010)

In normal conditions, the plantaris, soleus and gastrocnemius muscles carry jointly weight bearing functions in mice hindlimbs (the percentage indicate the contribution of each muscle).

in OCT (Tissue-Tek, Torrance, CA, USA) and frozen in melting isopentane cooled in liquid nitrogen. At the end of the experimental period, mice were anesthetized as previously described and lower limb muscles of control and overloaded animals were extracted, either frozen directly in liquid nitrogen or embedded in OCT (Tissue-Tek, Torrance, CA, USA) and frozen in melting isopentane cooled in liquid nitrogen. Upon completion of tissue extractions, mice were euthanized by cervical dislocation under anesthesia and all tissues were stored at -86°C until processed.

3.4.3 Immunohistochemistry

To determine muscle fiber type and size, muscle cryosections (10 μm) were cut from each plantaris muscle midbelly anatomical location. Sections were blocked for 30 minutes in 5% goat serum in a carrier solution consisting of 0.5% bovine serum albumin (BSA) in 25 mM phosphate buffer solution (PBS) (pH = 7.4). Subsequently, the sections were incubated overnight at 4°C in carrier solution with a primary antibody raised against the appropriate MyHC type. All antibodies used (MyHC I: A4.840 using 1:25 dilution; MyHC IIa: SC71 using 2:25 dilution; MyHC IIx: 6H1 without dilution; MyHC IIb: BF-F3 using 1:25 dilution) were from the Developmental Study Hybridoma Bank (DSHB, University of Iowa, Iowa city, IA). After three 10 minutes rinses in PBS, sections were incubated for two hours in secondary antibodies, horseradish peroxidase-conjugated goat anti-mouse IgG (MyHC type IIa) or IgM (MyHC type I, IIx, IIb) (Sigma-Aldrich, St-Louis, MO, USA) using a 1:25 dilution. The sections then were rinsed three times with PBS for ten minutes, and the bound antibody complexes were visualized using 1 mg/ml of diaminobenzidine tetrahydrochloride (DAB). Slides were analyzed with an Olympus BX-60 light microscope. Three distinct regions were selected randomly from the midbelly of each plantaris muscle and images were captured across serial sections using a Retiga SRV camera (QImaging, Surrey, ON, Canada). All fibers in those regions were classified according to the type of MyHC expressed and fiber cross-sectional size was measured using ImagePro Plus version 6.2 software (Olympus, Markham, ON, Canada).

3.4.4 Immunofluorescence

To determine NFAT nuclear localization, muscle cryosections (10 μm) were cut from each plantaris muscle midbelly anatomical location. Sections were fixed in 2% paraformaldehyde (PFA) for 20 minutes, washed three times five minutes with PBS and blocked for one hour in PBS containing 1% normal goat serum and 0.2% Triton X-100. Slides were subsequently washed and incubated overnight with a primary antibody at 4°C (1:50 dilution) in an antibody solution of 1% normal goat serum and 0.1% Triton X-100. Antibodies (NFATc1 #sc-13033, NFATc2 #sc-13034, NFATc3 #sc-8321 and NFATc4 #sc-13036) were all from Santa Cruz Biotechnology (Santa Cruz, CA, USA). The sections then were rinsed three times five minutes with PBS and incubated with secondary anti-rabbit Alexa488 conjugated antibody #A-1108 (Invitrogen, Burlington, ON, Canada) using a 1:100 dilution. Slides were mounted using DAPI-Vectashield (#H-1200 from Vector Laboratories, Burlingame, CA, USA). Three distinct regions were selected randomly from each plantaris muscle and images were captured using a Zeiss Axioplan fluorescence microscope mounted with a Lumenera Infinity 3-1C1.4 camera (Ottawa, ON, Canada). Control slides, omitting primary antibodies revealed the absence of background staining at the acquisition time used. Co-localization analysis of NFAT and nuclei was performed using ImagePro Plus version 6.2 software (Olympus, Markham, ON, Canada). In all analysis, the researcher was blinded to the experimental condition.

3.4.5 RNA extraction and semi-quantitative RT-PCR

Total RNA was extracted from each plantaris muscle as previously described (Gauthier *et al.*, 1997; Dunn *et al.*, 1999). RNA concentration and purity were determined using the Eppendorf Biophotometer. Subsequently, RT-PCR was carried out using 2 µg of each RNA sample. The final volume of the RT mixture (40 µL) contained 0.625 µM of random primer hexamers (Invitrogen, Burlington, ON, Canada), 1X RT buffer (Ambion, Streetsville, ON, Canada), 0.5 µM dNTP mix (Invitrogen, Burlington, ON, Canada), 40U of RNase inhibitor (Ambion, Streetsville, ON, Canada), and 100U of MMLV reverse transcriptase (Ambion, Streetsville, ON, Canada). Subsequently, PCR amplification was carried out using 1.5 µl of the cDNA generated in a master mix containing 1X Taq buffer with KCl (Fermentas, Burlington, ON, Canada), 1.5 mM MgCl₂ (Fermentas, Burlington, ON, Canada), 0.1 mM dNTP (Invitrogen, Burlington, ON, Canada), 0.2 mM primers (custom synthesized by Sigma Genosys, St-Louis, MO, USA) and 0.05 U/µl of Taq DNA polymerase (Fermentas, Burlington, ON, Canada) yielding a total volume of 25 µl. Amplification conditions consisted of an initial denaturation at 95°C for 3 minutes, followed by cycles of 1 minute denaturation at 94°C, 1 minute annealing at primer specific temperature and 1 minute extension at 72°C (Table 3-1), followed by a final extension at 72°C for 10 minutes. For each set of primers, cycle number was adjusted to permit comparison of PCR products within their linear range of amplification across animals (Table 3-1). Amplification of the ribosomal 28S RNA was used as an internal control. PCR products were separated by electrophoresis on 1.5% agarose gels and visualized with ethidium bromide. Band intensities were quantified by

densitometry with the AlphaInnotech system and FluorChem software (San Leonardo, CA, USA).

GENE NAME	PRIMER PAIR SEQUENCES	SIZE (bp)	T_M (°C)	CYCLE #	ACCESSION NUMBER
28S	Fwd: 5'-TTGTTGCCATGGTAATCCTGCTCAGTACG-3' Rvs: 5'-TCTGACTTAGAGGCGTTTCAGTCATAATCCC-3'	132	55	16	NR_003279.1
MyHC IIa¹	Fwd: 5'-GAACCTCCCAAGTACGACA-3' Rvs: 5'-TAAGGGTTGACGGTGACACA-3'	147	55	32	NM_001039545.1
MyHC IIb¹	Fwd: 5'-CCAGAGTCACCTTCCAGCTC-3' Rvs: 5'-CTTCCCTTTGCTTTTGCTTG-3'	300	55	20	NM_010855.2
TnIs	Fwd: 5'-TGCTGAAGAGCCTGATGCTA-3' Rvs: 5'-GAACATCTTCTTGCGACCTTC-3'	485	55	32	NM_021467.4
NFATc1	Fwd: 5'-TTCCAGCACCTTCGGAAGGGT-3' Rvs: 5'-AGTGAGCCCTGTGGTGAGAC-3'	205	55	34	NM_016791.4 NM_001164109.1 NM_001164111.1 NM_001164112.1 NM_198429.2 NM_001164110.1
NFATc2	Fwd: 5'-TCTGCTGTTCTCATGGATGCCCC-3' Rvs: 5'-GGATGCAGTCACAGGGATGCT-3'	282	55	30	NM_001037177.1 NM_001037178.1 NM_001136073.1 NM_010899.2
NFATc3	Fwd: 5'-CGATCTGCTCAAGAACTCCC-3' Rvs: 5'-GGCAGATGTAAGTCTGGGT-3'	246	55	28	NM_010901.2
NFATc4	Fwd: 5'-CTGAGGATCGAGGTACAGCC-3' Rvs: 5'-TTGTTCTCTGGGAGCAAGGT-3'	293	55	33	NM_023699.3 NM_001168346.1
Pax7	Fwd: 5'-GTAAGCAGGCAGGAGCTAAC-3' Rvs: 5'-GGTTCATGAAGCTGTCAGAG-3'	285	55	38	NM_011039.2
Myf5	Fwd: 5'-CTGTCTGGTCCCGAAAGAAC-3' Rvs: 5'-GTCTTTCCTTCAGCTTCAGGGC-3'	328	55	38	NM_008656.5
MyoD	Fwd: 5'-TACCCAAGGTGGAGATCCT-3' Rvs: 5'-GCGGTGTCGTAGCCATTCT-3'	253	55	32	NM_010866.2
Mgn²	Fwd: 5'-GAAGAAAAGGGACTGGGG-3' Rvs: 5'-GGACCGAACTCCAGTGCAT-3'	392	55	35	NM_031189.1

Table 3-1: Primers and cycling conditions

Superscript number following a gene name indicates the paper from which the sequences were obtained. When no number is indicated, primers were designed by our lab. 1) (Murphy *et al.*, 2010) 2) (Tang & Goldman, 2006).

3.4.6 Protein extraction and Western Blotting

Muscles were homogenized using a hand-held Tissue Tearor homogenizer (ColeParmer, Montreal, QC, Canada) in RIPA buffer consisting of 1XPBS, 1% igeal, 0.5% sodium deoxycholate, 0.1% sodium dodecyl sulfate (SDS), 0.001 M sodium orthovanadate, 0.01 M sodium fluoride, 0.01 mg/ml aprotinin, 0.01 mg/ml leupetin and 1 mM phenylmethanesulfonyl fluoride (all reagents from Sigma-Aldrich, St-Louis, MO, USA). Homogenates were incubated on ice for 30 minutes followed by two 4°C centrifugations at 15 000 x g for 20 minutes. The supernatants were collected and the protein concentration determined using Quick Start Bradford dye reagent (Bio-Rad, Mississauga, ON, Canada).

For protein expression analysis, 150 µg of protein were separated by SDS polyacrylamide gel electrophoresis (SDS-PAGE) on a gel consisting of a 5% stacking gel and an 8% separating gel. Samples were electrophoresed (buffer: 25mM Tris, 192 mM glycine, 0.1% SDS, pH 8.3) at 120V and Amersham Full-Range Rainbow (GE Healthcare, Baie d'Urfe, QC, Canada) molecular weight markers were used to define the protein sizes. Subsequently, proteins were transferred (buffer: 25 mM Tris, 192 mM glycine and 20% methanol) to a PVDF membrane (Millipore, Billerica, MA, USA) at 100V for one hour and a successful transfer was confirmed using Ponceau S staining. Membranes were blocked for one hour using 5% non-fat milk in 0.1% Tween-Tris Buffered Saline (T-TBS) and incubated with primary antibody overnight at 4°C on a shaker as indicated in Table 3.2. The following day, the membranes were washed three times five minutes using 0.1% T-TBS and were then incubated with the appropriate

horseradish peroxidase-conjugated secondary antibody: anti-rabbit IgG #7074 (Cell Signaling Technology, Danvers, MA, USA) or anti-mouse IgG #A8924 (Sigma-Aldrich, St-Louis, MO, USA). Subsequently, membranes were developed using chemiluminescent Immobilon HRP substrate kit (Millipore, MA, USA) as per the manufacturer's instructions. Images were captured and protein expression quantified by densitometry with the AlphaInnotech system and FluorChem software (San Leonardo, CA, USA).

PROTEIN NAME	SUPPLIER	SIZE (kDa)	1°ANTIBODY	2°ANTIBODY
α-tubulin	Cell Signaling #2125	52	1:2000 in 5% milk	1:2000 in 5% milk for 1hr (anti-rabbit)
pAkt (ser473)	Cell Signaling #4060	60	1:1000 in 5% BSA	1:2000 in 5% milk for 2hrs (anti-rabbit)
Akt	BD Bioscience #610861	60	1:1000 in 5% milk	1:2000 in 5% milk for 2hrs (anti-mouse)
pGSK3β (ser9)	Cell Signaling #9323	46	1:1000 in 5% BSA	1:2000 in 5% milk for 1hr (anti-rabbit)
GSK3β	Cell Signaling #9315	46	1:1000 in 5% BSA	1:2000 in 5% milk for 1hr (anti-rabbit)

Table 3-2: Western Blotting Conditions

3.4.7 Statistical Analysis

The data were tested for homogeneity of variance using Levene's test. In the case where variance between groups was homogenous one-way ANOVA was used followed by Tukey HSD (or Tukey-Kramer if uneven sample size) *post hoc* test. In the case where the variance between groups was not homogenous, the Welch's T test was used followed by Dunnett T3 *post hoc* test. All statistics were performed using SPSS statistics software version 17.0. (IBM SPSS, Chicago, IL, USA)

3.5 Results

3.5.1 NFATc2^{-/-} and NFATc3^{-/-} mice show blunted muscle growth following functional overload

The hypothesis explored was that an absence of the downstream Cn signaling partners NFATc2 or NFATc3 would prevent or blunt overload-induced muscle growth. Plantaris muscle weights were measured following 7 and 28 days of functional overload in wild-type and NFATc2 or NFATc3 knockout mice. Values were expressed relative to total body weight and compared to wild-type mice. Wild-type mice showed a significant progressive muscle growth from 7 days to 28 days of overload, reaching a 2.1 fold growth after 28 days as compared to control, normal weight-bearing muscles (Figure 3.2A). On the other hand, NFATc2^{-/-} and NFATc3^{-/-} mice displayed blunted muscle growth after 7 and 28 days of functional overload (Figure 3.2A).

The increase in fiber size (Figure 3.2B) and fiber number at the midbelly area (Figure 3.2C) confirms that ablation of synergistic muscles induces a growth characterized by both fiber hypertrophy and hyperplasia in wild-type mice. Fiber size and number were also measured in the NFATc2 and NFATc3 knockout mice to determine if either blocked fiber hypertrophy or blocked fiber hyperplasia are the mechanisms responsible for the blunted muscle growth in these mice. The results indicated that the plantaris muscles of NFATc2 and NFATc3 knockout mice are not displaying hypertrophic fiber growth (Figure 3.2B) but maintain overload induced fiber hyperplasia (Figure 3.2C). It should also be noted that in the overload condition, NFATc2 deficient

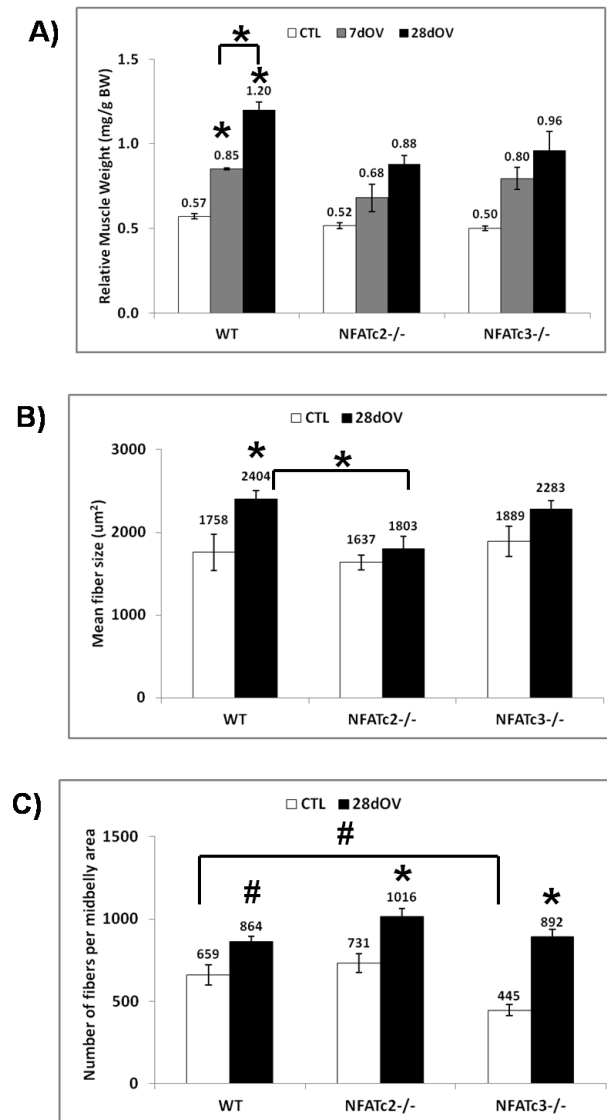


Figure 3.2: Blunted compensatory muscle growth in NFATc2 and NFATc3 knockout mice

A) Comparison of relative muscle weights following 7 days or 28 days of functional overload in wild-type, NFATc2^{-/-} and NFATc3^{-/-} mice B) Measurement of mean fiber cross sectional area size for all fiber types comparing control and 28 days overloaded muscles of wild-type, NFATc2^{-/-} and NFATc3^{-/-} mice. C) Fiber number count at the midbelly area comparing control and 28 days overloaded muscles of wild-type, NFATc2^{-/-} and NFATc3^{-/-} mice. All results are expressed as the mean \pm SE. Numbers above bars indicate the data value. (* or # sig. diff. from respective normal weight-bearing CTL unless otherwise indicated, * $p \leq 0.05$, # < 0.09 WT: CTL n=6, 7dOV n=3, 28dOV n=4; NFATc2^{-/-}: CTL n=7, 7dOV n=3, 28dOV n=4; NFATc3^{-/-}: CTL n=5, 7dOV n=3, 28dOV n=3).

fibers are significantly smaller than wild-type overloaded fibers, although this is not the case of NFATc3 deficient fibers (Figure 3.2B). Additionally, as expected (Kegley *et al.*, 2001), there was a decrease in the number of fibers in NFATc3^{-/-} mice in the normal weight-bearing condition in comparison to wild-type and NFATc2^{-/-} mice (Figure 3.2C). These findings show that NFATc2 and NFATc3 transcription factors have essential roles in adaptive muscle growth. Additionally, our data suggest that adaptive muscle growth is regulated by a distinct mechanism in NFATc2^{-/-} mice than in wild-type or NFATc3 knockout mice.

3.5.2 NFATc2^{-/-} and NFATc3^{-/-} mice show altered growth that is fiber type specific

Given the observed reduced hypertrophic growth in both NFATc2 and NFATc3 knockout mice, we sought to determine if this regulation is fiber type specific. Fiber typing was carried out based on the type of MyHC expressed and the fibers cross sectional area (CSA) and the percentage expression of fibers were compared between experimental groups. Muscle fibers classified as MyHC type IIa are characterized by an oxidative metabolism. These oxidative fibers maintained the ability to carry out overload-induced hypertrophic growth in NFATc2 and NFATc3 knockout mice (Figure 3.3B) but this growth was reduced in NFATc2^{-/-} mice as compared to wild-type mice. Meanwhile, a marked but not significant increase in the percentage of fibers expressing MyHC IIa was observed in all mice investigated following 28 days of overload (Figure 3.3C).

Similar results (data not shown) were obtained for fibers expressing MyHC type I. These fibers are also oxidative fibers but display slower contraction times.

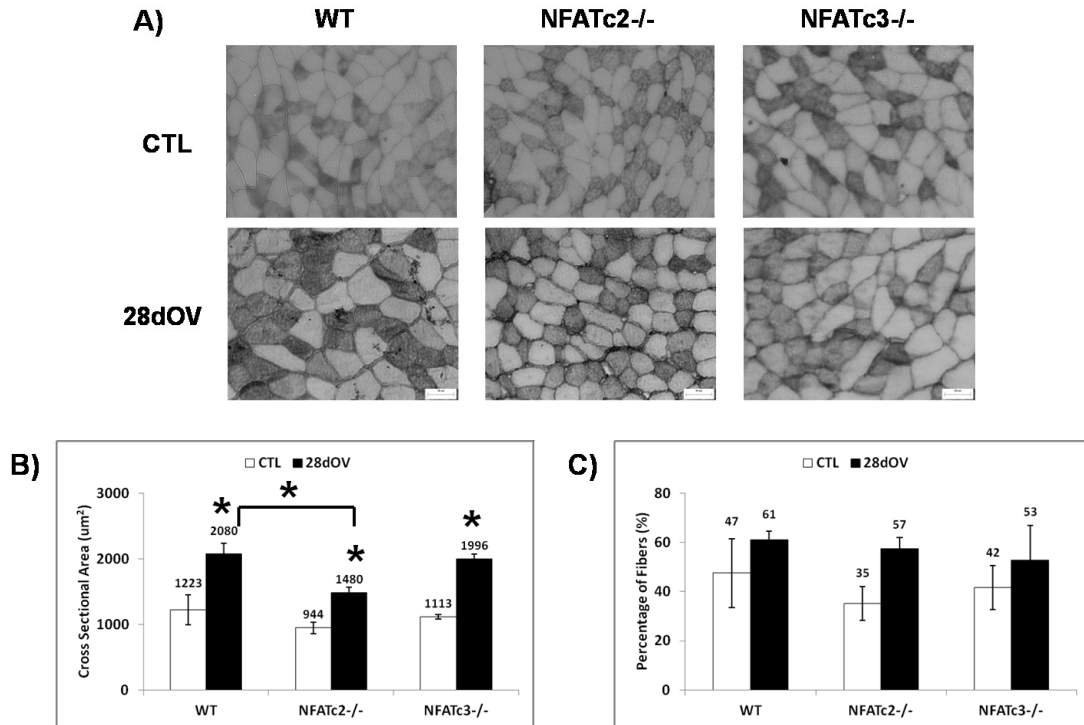


Figure 3.3: Muscle fibers expressing MyHC IIa maintain their ability to grow in NFATc2 and NFATc3 knockout mice

A) Representative images of histological sections stained for MyHC IIa fibers. Scale bar 50 µm. Quantification of B) fiber cross sectional area and C) percentage of fibers expressing MyHC IIa comparing wild-type, NFATc2^{-/-} and NFATc3^{-/-} transgenic mice under control normal weight-bearing and 28 days of functional overload conditions. All results are expressed as the mean ±SE. Numbers above bars indicate the data value. (* sig. diff. from respective normal weight-bearing CTL unless otherwise indicated, $p \leq 0.05$, WT: CTL n=3 & 28dOV n=4; NFATc2^{-/-}: CTL n=4 & 28dOV n=4; NFATc3^{-/-}: CTL n=3 & 28dOV n=3).

Next, analysis of glycolytic fibers, classified as expressing MyHC type IIb indicated a block of overload-induced hypertrophic growth in NFATc2 and NFATc3 knockout mice (Figure 3.4B). It should be noted that overloaded muscles of NFATc2^{-/-}

mice were significantly smaller than wild-type overloaded muscles, but this was not the case for NFATc3^{-/-} overloaded muscles (Figure 3.4B). Meanwhile, all mice displayed a marked but not significant decrease in the number of MyHC Iib expressing fibers (Figure 3.4C) following 28 days of overload (Figure 3.4C).

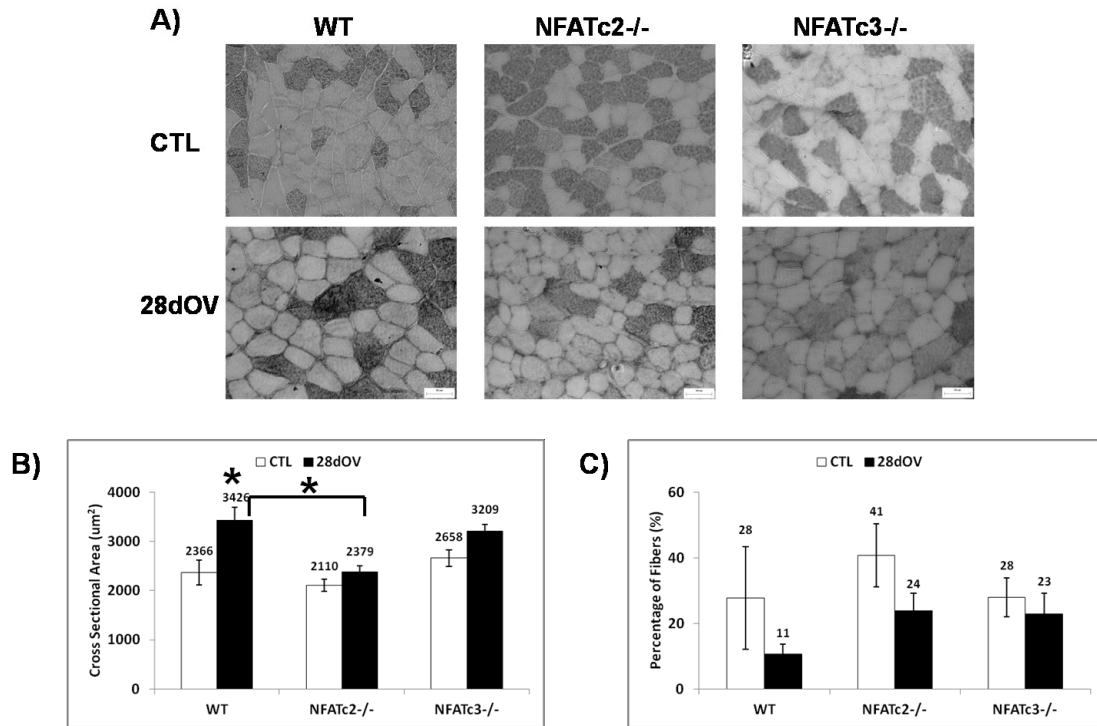


Figure 3.4: Muscle fibers expressing MyHC Iib lose their ability to grow in NFATc2 and NFATc3 knockout mice.

A) Representative images of histological sections stained for MyHC Iib fibers. Scale bar 50 um. Quantification of B) fiber cross sectional area and C) percentage of fibers expressing MyHC Iib comparing wild-type, NFATc2^{-/-} and NFATc3^{-/-} transgenic mice under control normal weight-bearing and 28 days of functional overload conditions. All results are expressed as the mean \pm SE. Numbers above bars indicate the data value. (* sig. diff. from respective CTL, $p \leq 0.05$, WT: CTL n=3 & 28dOV n=4; NFATc2^{-/-}: CTL n=3 & 28dOV n=4; NFATc3^{-/-}: CTL n=3 & 28dOV n=3).

Overall these findings indicate that NFATc2 and NFATc3 isoforms are essential for the maintenance of adaptive hypertrophy of fast glycolytic muscle fibers but do not influence

the hypertrophic growth of fast oxidative fibers. Also, these data showed differences in the hypertrophic growth response between NFATc2^{-/-} and NFATc3^{-/-} mice and suggest distinct roles for NFAT transcription factors in muscle adaptive growth.

3.5.3 NFATc2 and NFATc3 knockout mice maintain the ability to remodel muscle fibers toward oxidative metabolic profiles

Based on the observed tendencies for increased MyHC IIa and decreased MyHC IIb expressing fibers, we sought to determine if the expected overload-induced oxidative fiber type remodeling is maintained in mice deficient for functional NFATc2 or NFATc3. First, the levels of slow oxidative fibers, expressing MyHC I, were markedly increase (3-10%) in all mice investigated following 28 days of overload (data not showed). Next, the amount of transcripts coding for MyHC IIa and IIb were measured. Following 7 days of functional overload, the levels of *MyHC IIa* transcripts remained unchanged (Figure 3.5A) while a marked not significant down-regulation of *MyHC IIb* transcripts was observed in overloaded muscles of all mice investigated (Figure 3.5B). Specifically, all animals showed similar decrease of *MyHC IIb* mRNA levels in the overload condition displaying a ~60% decrease in comparison to respective normal weight bearing condition (Figure 3.5B). These findings suggest that fiber type remodeling toward oxidative metabolism is occurring in NFATc2 and NFATc3 knockout mice, as is observed in wild-type animals.

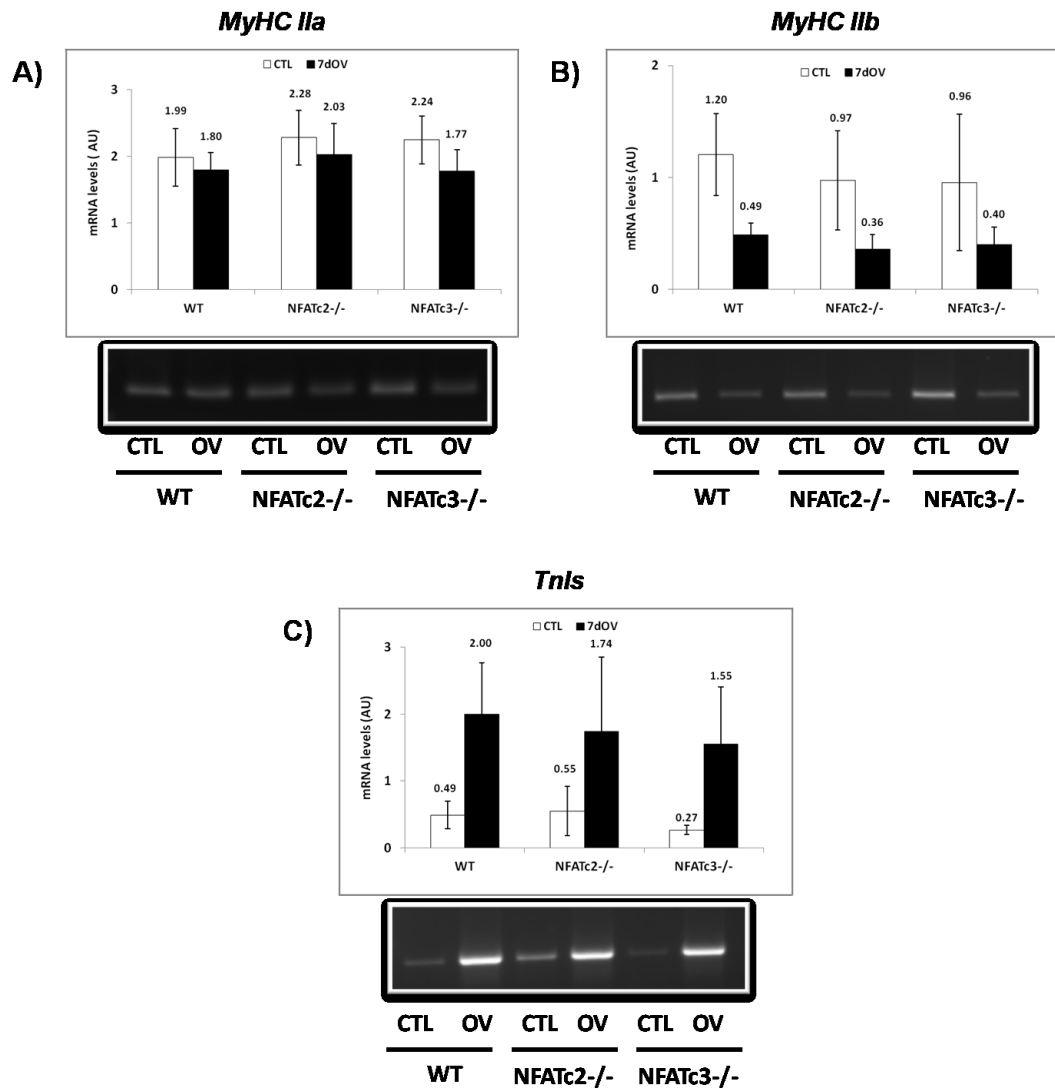


Figure 3.5: Remodeling toward oxidative muscle profiles is maintained in NFATc2 and NFATc3 knockout mice

Representative agarose gel images of PCR products with quantification are shown comparing wild-type, NFATc2^{-/-} and NFATc3^{-/-} mice under control normal weight-bearing and 7 days of functional overload conditions. A) Expression of mRNA levels for *MyHC IIa*, B) *MyHC IIb* and C) *TnIs*. All quantifications are standardized to the ribosomal 28S RNA. Data are expressed as the mean \pm SE. Numbers above bars indicate the data value. ($p \leq 0.05$, $n=3$ per group)

Changes in metabolic profiles often precede changes in expression of myosins (Gundersen, 1998) hence the amount of mRNA coding for the slow muscle specific contractile protein troponin I slow (TnIs) were measured to further validate an increase in oxidative muscle profile. The levels of *TnIs* displayed a large (3 to 5 fold) increase following overload in muscles of all genetic backgrounds (Figure 3.5C).

These collective findings indicate that fiber type remodeling is maintained in the NFAT knockout mice. All mice displayed the characteristic muscle metabolic remodeling observed in the overload condition, marked by an increase in the oxidative profiles and a decrease in the glycolytic profiles.

3.5.4 NFATc2^{-/-} and NFATc3^{-/-} mice display distinct nuclear localization of NFAT isoforms

All four isoforms of calcium-regulated NFAT are present in skeletal muscle. To determine the ability of NFAT isoforms to compensate for the absence of functional NFATc2 or NFATc3 in the knockout mice investigated, RT-PCR analysis was carried out (Figure 3.6). It is important to indicate that both NFATc2 and NFATc3 knockout mice are capable of producing a mutated transcript for their respective isoforms (Hodge *et al.*, 1996; Oukka *et al.*, 1998) and the PCR primers used in this study were designed in a manner to detect these mutant transcripts. In addition, it should also be noted that this assay is comparing the overall expression of NFAT isoforms between the different groups and it is not providing a comparison of the relative amounts of each isoform in the

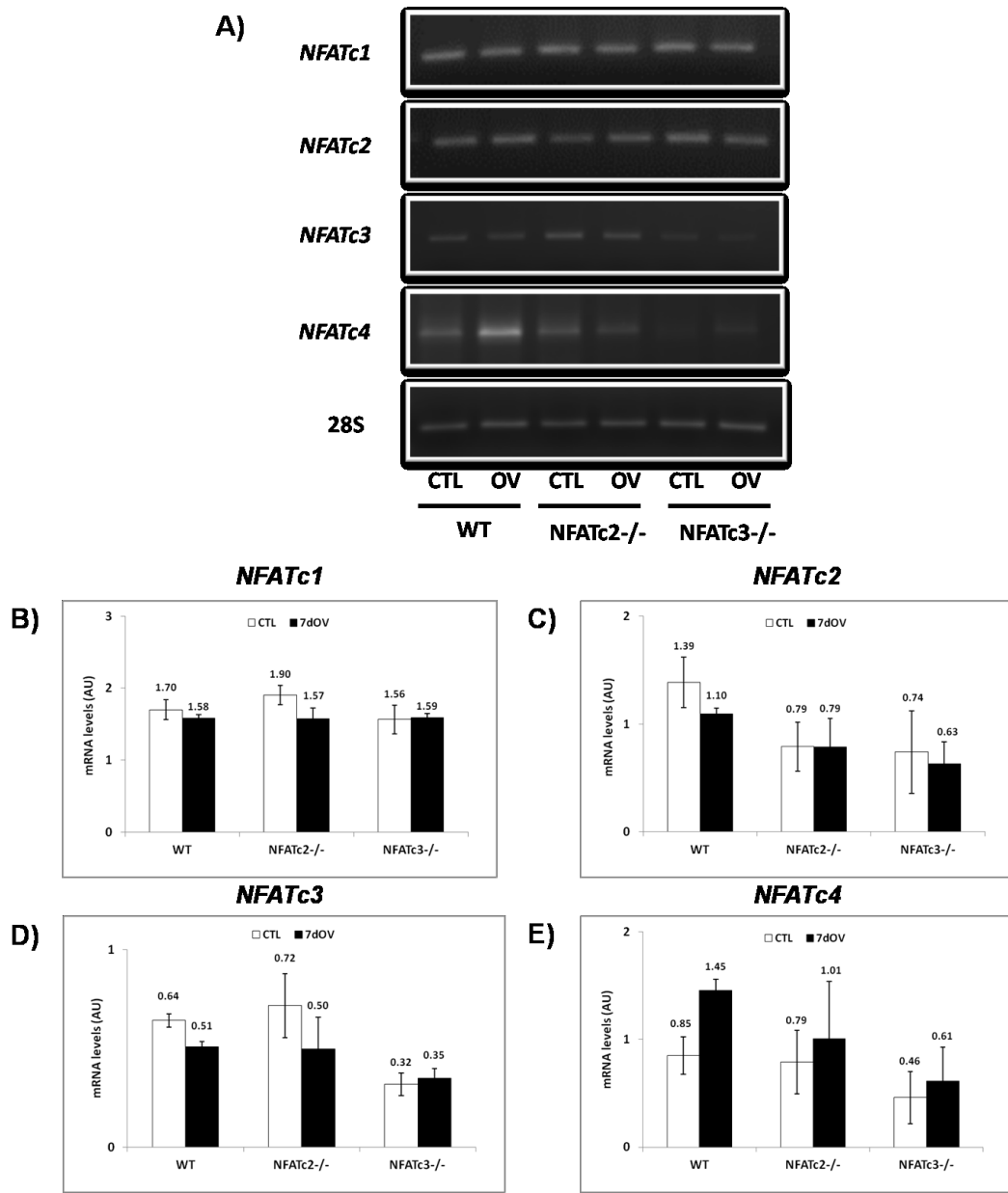
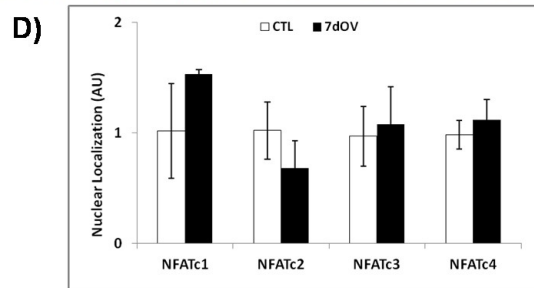
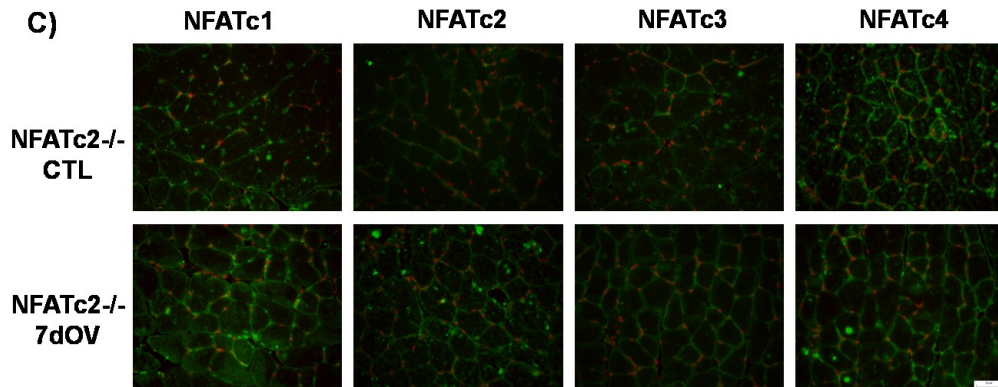
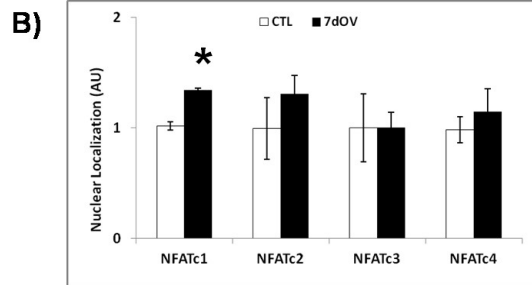
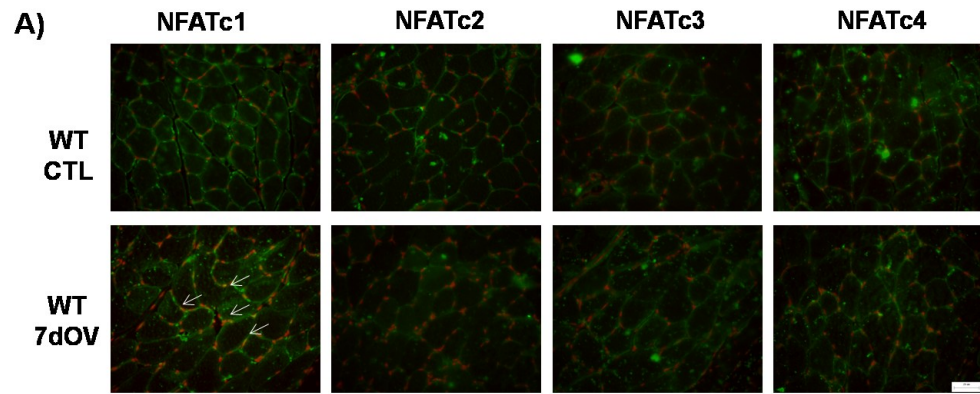


Figure 3.6: NFATc2 and NFATc3 knockout mice do not display compensatory changes in the expression of *NFAT* mRNA levels.

A) Representative agarose gel images of PCR products and quantifications comparing mRNA levels for B) *NFATc1*, C) *NFATc2*, D) *NFATc3* and E) *NFATc4* under normal weight-bearing or 7 days functional overload condition for all genetic background of mice investigated. All quantifications are standardized to ribosomal 28S RNA. Data are expressed as the mean \pm SE. Numbers above bars indicate the data value. ($p \leq 0.05$, $n=3$ per group)

plantaris muscle. Overall these data did not indicate that NFAT isoforms have the ability to compensate for the absence of functional NFATc2 or NFATc3 at the mRNA levels in normal weight bearing or functional overload condition.

The NFAT transcription factors are found in the cytoplasm in a phosphorylated state. The activity of these proteins is controlled through dephosphorylation that leads to the translocation of NFATs to the nucleus. In addition, the activity of these transcription factors is regulated by selective activation of export kinases. The study of the cellular distribution of the members of the NFAT protein family is important to better understand the functions and regulation of these transcription factors. Immunofluorescence was carried out to assess the nuclear localization of the members of the NFAT protein family and to evaluate if compensatory alterations in cellular distribution are observed in NFATc2 or NFATc3 knockout mice (Figure 3.7). The levels of NFAT isoforms co-localized with nuclei were compared between the different groups. It should be noted that this assay is solely comparing the levels of nuclear-localized NFAT isoforms between the normal weight-bearing and overloaded condition in each mice group. This assay is not providing a comparison of the relative amounts of nuclear-localized NFAT isoforms in the plantaris muscle of different genetic background of mice. Also, the antibodies used in this study detected protein epitopes localized outside of the mutated region and hence these antibodies recognized mutant and wild-type proteins. All antibodies used were previously characterized for NFAT isoform specificity (data not shown).



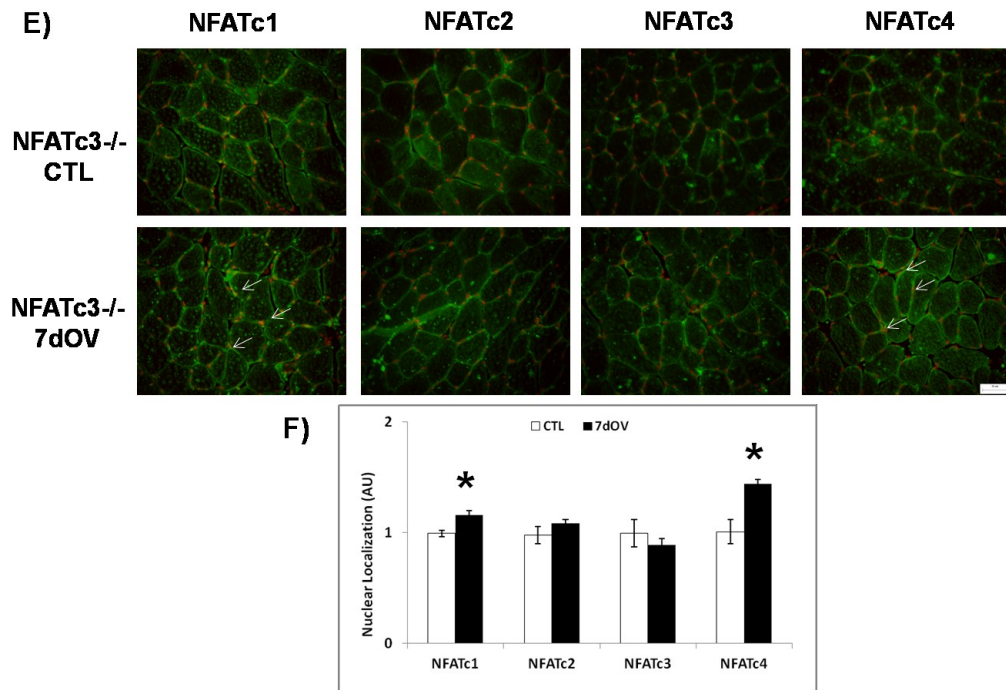


Figure 3.7: Nuclear trafficking of NFAT protein family members is altered in NFATc2^{-/-} and NFATc3^{-/-} mice.

A, C and E) are representative immunofluorescence images that showed the overlay of images stained for nuclei (red) and specific NFAT isoforms (green) as indicated. Scale bar is 50 μ m. Arrows point to some of the nuclear-localized NFAT proteins (yellow). B, D and F) present the quantification of nuclear localization. A, B) are wild-type mice, C, D) are NFATc2 knockout mice and E, F) are NFATc3 knockout mice. All results are expressed as the mean \pm SE. (* sig. diff. from respective CTL, n=3 per group, $p \leq 0.05$).

In wild-type mice, following 7 days of functional overload, a significant 1.3 fold increase in nuclear-localized NFATc1 isoform was observed (Figure 3.7A and B). High amount of nuclear-localized NFATc2 also were observed but due to the high variability in the normal weight-bearing condition significance was not reached. Finally, the other NFAT isoforms did not display alteration in their nuclear localization in the wild-type mice. NFATc2 knockout mice also had a 1.5 fold increase in nuclear-localized NFATc1 following functional overload. However, NFATc2^{-/-} mice displayed an alteration in the

nuclear-localized levels of NFATc1 in the normal weight-bearing condition and, therefore, no significant change in nuclear translocation is observed after overload (Figure 3.7C and D). NFATc3 knockout mice displayed a 1.2 fold increase in nuclear-localized NFATc1 and an interesting 1.4 fold increase in nuclear-localized NFATc4 (Figure 3.7E and F). Collectively, these findings suggest that NFATc1 is the main isoform translocated to the nucleus in the overload response. These results also suggest that NFATc2 and NFATc3 may regulate the overload induced signaling by an indirect mechanism that depends on NFATc1 nuclear localization. In addition, these results imply a novel role for NFATc4 isoform in the overload response.

3.5.5 NFATc2^{-/-} and NFATc3^{-/-} mice display an alteration in the expression of myogenic regulatory factors

NFATc2 and NFATc3 knockout mice have been shown to display defects in various steps of myogenesis. While NFATc2 knockout mice display defects in the recruitment of myoblasts to fuse with multinucleated myofibers; a process required for postnatal myotube growth (Horsley *et al.*, 2001), NFATc3 knockout mice show defects in development of myoblasts; thus NFATc3 seems to regulate primary myogenesis (Kegley *et al.*, 2001). To address these differences, the transcript levels of several members of the myogenic regulator factors were measured. The results described in this section are preliminary data that require a larger sample size to achieve statistical

significance, but that suggest important novel regulatory roles for NFATc2 and NFATc3 transcription factors in the expression of muscle regulatory factors.

Firstly, the amount of *Pax7* was slightly increased in all genetic backgrounds of mice following 7 days of overload (Figure 3.8A and B). This suggests that all mice maintained the ability to carry out satellite cell self-renewal. The expression of *Myf5* was increased 1.7 fold in both wild-type and NFATc3^{-/-} mice in the overload condition as compared to normal weight bearing state, but this increase was blocked in NFATc2^{-/-} mice (Figure 3.8A and C), implying that NFATc2 is important in the regulation of *Myf5* expression during adaptive muscle growth. The levels of *MyoD* mRNA were not altered following 7 days of functional overload in any genetic background of mice (Figure 3.8A and D). Finally, NFATc3 knockout mice displayed decrease levels of *Mgn* transcripts in the normal weight-bearing condition while maintaining the ability to promote the expression of *Mgn* transcript in the functional overload condition (Figure 3.8A and E).

These results imply that NFATc2 and NFATc3 transcription factors can regulate the expression of myogenic regulatory factors. The data suggest that a larger block of overload induced hypertrophy observed in NFATc2^{-/-} mice (Figure 3.2B) could be mediated by a decrease in *Myf5* expression. Meanwhile, the decreased number of fibers seen in NFATc3^{-/-} mice in normal weight-bearing muscles (Figure 3.2C) could be caused by a decrease in expression of *Mgn*.

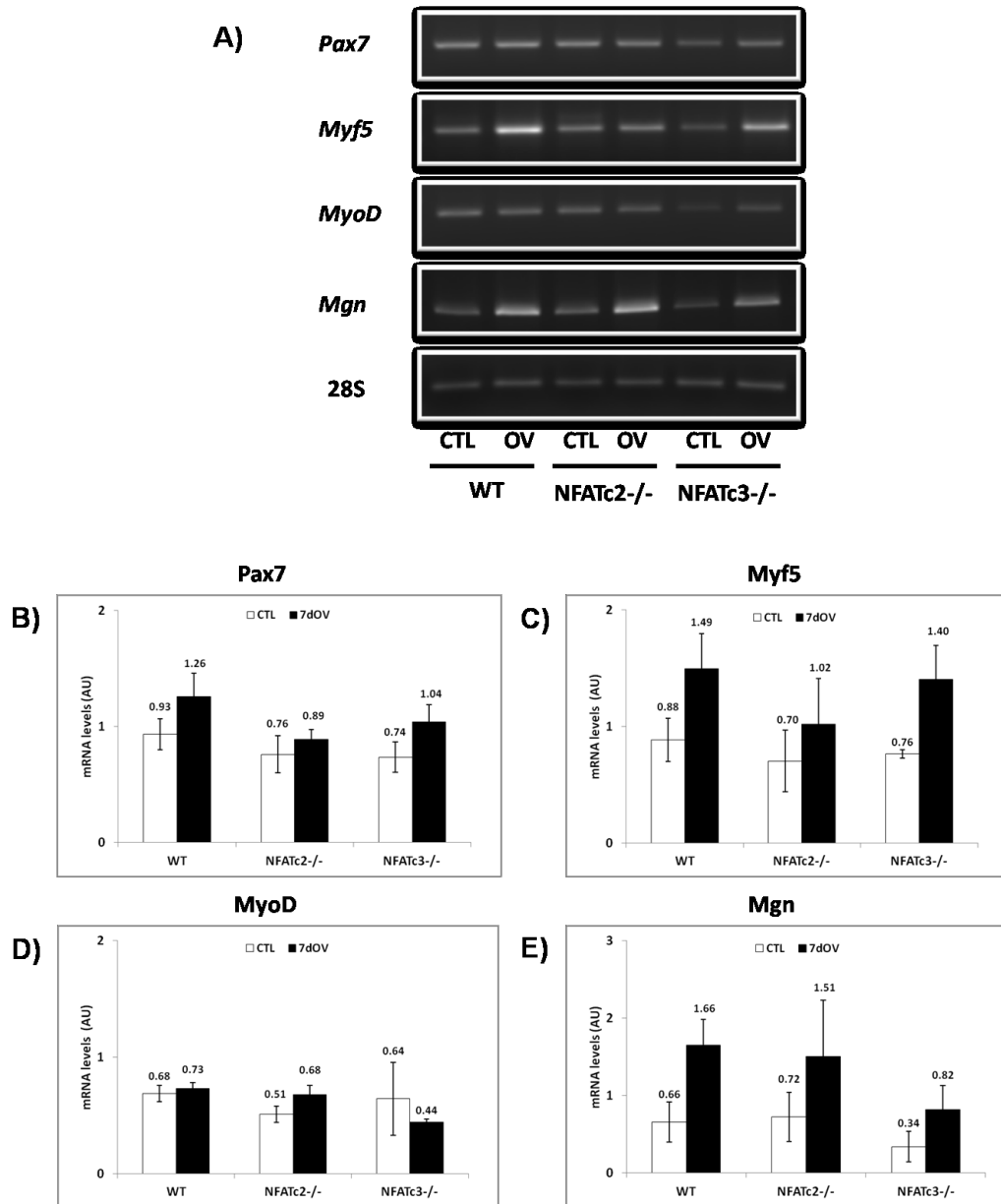


Figure 3.8: NFATc2 influences *Myf5* levels while NFATc3 regulates *Mgn* levels.

A) Representative agarose gel images of PCR products and quantifications comparing mRNA levels for B) *Pax7*, C) *Myf5*, D) *MyoD* and E) *Mgn* under normal weight-bearing or 7 days functional overload condition for all genetic background of mice investigated. All quantifications are standardized to ribosomal 28S RNA. Numbers above bars indicate the data value. Data are expressed as the mean \pm SE. ($p \leq 0.05$, $n=3$ per group for exception of *Pax7* and *MyoD* NFATc3^{-/-} CTL $n=2$).

3.5.6 NFATc2^{-/-} and NFATc3^{-/-} mice do not exhibit modification in Akt signaling in the overload growth model

The Akt signaling pathway is the best characterized skeletal muscle growth pathway and it has been shown important in the overload-induced muscle growth response (Bodine *et al.*, 2001). Protein levels of pAkt and total Akt were measured since NFAT knockout mice displayed blunted overload induced muscle growth. In addition, the levels of the Akt downstream signaling target, GSK3 β , were determined. The results described in this section are preliminary data that require a larger sample size to achieve statistical significance, but these data point out that Akt signaling pathway is most likely not altered in the adaptive muscle growth response of NFATc2^{-/-} or NFATc3^{-/-} mice, as compared to wild-type mice.

First, results indicated a 2 fold increased in the level of pAkt in the overloaded wild-type muscles (Figure 3.9A and B). NFATc2 and NFATc3 knockout mice displayed similar amounts of pAkt as wild-type mice in the overloaded condition but these mice displayed larger variability in the amount of pAkt under normal weight-bearing conditions, particularly in the case of NFATc3^{-/-} mice (Figure 3.9A and B). The levels of total Akt protein also display higher expression levels in the overloaded condition in all genetic backgrounds of mice (Figure 3.9A and C). Finally, pGSK3 β or total GSK3 β levels were not modified in the normal weight-bearing or overloaded conditions between mice investigated (Figure 3.9A, D and E). These findings suggest that reduced Akt activity is not responsible for the blunted growth in NFAT knockout mice in the adaptive functional overload growth model.

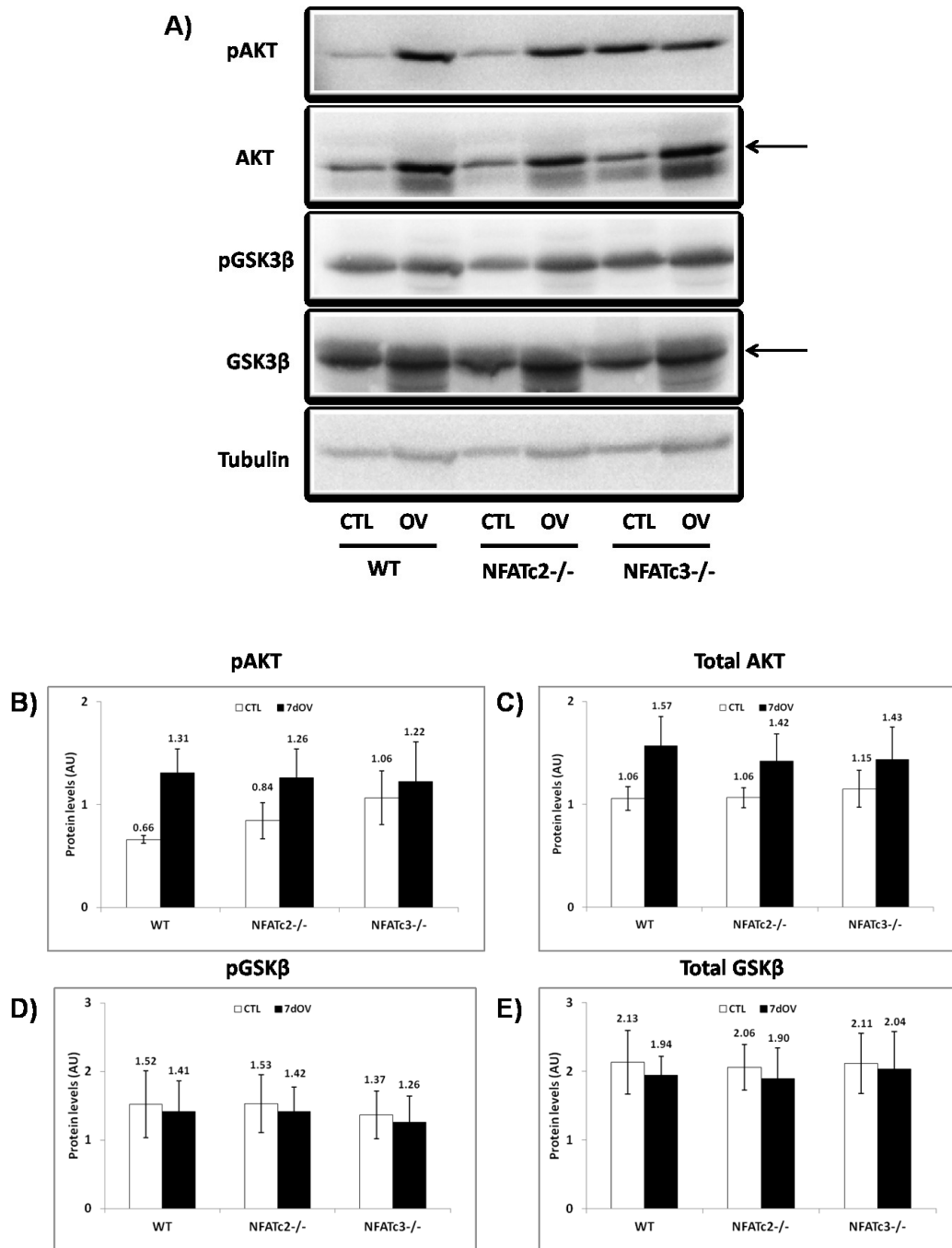


Figure 3.9: Akt signaling is not responsible for altered growth in NFAT knockout mice.

A) Representative Western blot images and quantification of protein levels for A) pAkt B) total Akt, C) pGSK3 β and D) total GSK3 β . Numbers above bars indicate the data value. All quantifications were standardized to tubulin loading control and are expressed as the mean \pm SE. ($p \leq 0.05$, $n=3$ per group)

3.6 Discussion

Skeletal muscle fibers are composed of myofibers that can adapt to meet functional demands. Cn/NFAT signaling has been implicated in modulation of skeletal muscle fiber growth and remodeling (reviewed in (Olson & Williams, 2000; Bassel-Duby & Olson, 2003, 2006; Michel *et al.*, 2007). In this study, the roles of the transcription factors NFATc2 and NFATc3, in the regulation of adaptive muscle growth, were investigated. The growth of the plantaris muscle was compared between wild-type and mice deficient for functional NFATc2 or NFATc3. This is the first study that explores the roles of NFATc2 and NFATc3 in functional compensatory muscle growth. The adaptive muscle growth was induced in this study using surgical synergistic muscle ablation, also called the overload model. This surgical model of muscle growth offers the advantage of inducing muscle adaptation by simultaneously increasing the nerve electrical activity and the muscle load. In addition, it offers the possibility of studying the malleability of adult muscle in a non-developmental setting. This muscle growth model has been characterized for promoting muscle fiber hypertrophy (Dunn & Michel, 1997; Dunn *et al.*, 1999) and hyperplasia (Antonio & Gonyea, 1993; Kelley, 1996), as well as remodeling toward oxidative phenotype (Dunn & Michel, 1997). In this study, 28 days of overload was used to study fiber size and fiber type remodeling, while 7 days of overload was used to study changes in the biochemical signaling pathways. A complete time course analysis of all properties was not possible in this study, due to the limitation of knockout animals available. Calcineurin signaling has been shown to mediate overload-induced muscle remodeling and we hypothesized that an absence of downstream signaling partners

NFATc2 or NFATc3 would prevent or blunt overload induced muscle growth. NFATc2 and NFATc3 knockout mice were chosen since these mice were previously described to display alteration in muscle mass (Horsley *et al.*, 2001; Kegley *et al.*, 2001).

NFATc2^{-/-} and NFATc3^{-/-} mice exhibit an adaptive muscle growth characterized by hyperplasia and an absence of hypertrophy

At first, plantaris muscle weights were compared between wild-type and NFATc2 or NFATc3 knockout mice following 7 or 28 days of functional overload. The results were expressed as relative muscle weights to control for intrinsic body weight differences between mice used. The results (Figure 3.2A) indicated that NFATc2^{-/-} and NFATc3^{-/-} mice displayed a reduced plantaris muscle growth as compared to wild-type mice. Notably, NFATc2 and NFATc3 knockout mice showed muscle weights comparable to wild-type mice in the initial phase (7 days) of the overload-induced remodeling. However, the greater muscle weight observed in the earlier phase of the overload period is probably caused by the surgical trauma that leads to muscle edema and an initial inflammatory response (Armstrong *et al.*, 1979) which is not a direct muscle growth response.

The growth of adult skeletal muscle can be described in two major steps. First, proliferating muscle precursor cells, called myoblasts, differentiate and fuse with one another to form nascent myotubes with a limited number of nuclei (Pavlati & Horsley, 2003). Secondly, the formed nascent myotubes fuse with additional myoblasts. This

allows the multinucleated myotubes to grow in CSA while maintaining a constant myonuclear domain (i.e. “the quantity of cytoplasm regulated by a single myonuclei” (Roy *et al.*, 1999)) (Roy *et al.*, 1999; Pavlath & Horsley, 2003). The first growth response is identified by an increase in fiber number (hyperplasia), while the second phase of growth is characterized by simultaneous hyperplasia and hypertrophy (Pavlath & Horsley, 2003).

Fiber size and fiber number were compared between wild-type and NFAT knockout mice after 28 days of functional overload to identify which step of muscle growth is compromised. The results indicated that hypertrophic fiber growth is inhibited in NFAT knockout mice and that this block is more pronounced in NFATc2^{-/-} mice (Figure 3.2B). This severe block of fiber hypertrophy in NFATc2^{-/-} mice is in agreement with published data that indicated that NFATc2^{-/-} mice display defects in prenatal and postnatal fiber growth (Horsley *et al.*, 2001). Specifically, using a model of muscle fiber regeneration following injury, NFATc2^{-/-} mice were shown to be capable of forming new fibers but displayed defects in secondary fusion (Horsley *et al.*, 2001; Mitchell & Pavlath, 2002; Pavlath, 2010). This lead to impaired nuclear addition and a block of fiber hypertrophy (Horsley *et al.*, 2001). In our study, the number of myonuclei per fiber was not counted and thus impaired nuclear addition was not assessed, but a block of fiber hypertrophy was observed (Figure 3.2B). In addition, our data implicate *Myf5* in this process since decrease levels of this myogenic regulator factor were detected in overloaded muscles of NFATc2^{-/-} mice (Figure 3.8A and B).

In this study, normal weight-bearing NFATc2 knockout mice did not display smaller muscle fiber CSA when compared to wild-type mice (Figure 3.2B), in contrast to what has previously been shown (Horsley *et al.*, 2001). Horsley *et al.* (2001) measured fiber size in NFATc2^{-/-} mice and described a decrease in fiber CSA in the load-bearing, predominantly oxidative, soleus (SOL) muscle and in the not load-bearing, mainly glycolytic, extensor digitorum longus (EDL) muscle. However, the SOL and EDL muscles differ in biochemical and physiological properties from the plantaris muscle investigated in this study. The plantaris muscle is a load-bearing muscle formed by a mixture of fiber types, displaying all types of oxidative and glycolytic profiles. This is an important aspect to keep in mind since muscle types differ in intrinsic abilities to adapt resulting from distinct embryonic myoblast lineages (Schiaffino & Serrano, 2002). In addition, differences in age, gender, species, and growth model used (functional overload, growth after atrophy, maintenance, regeneration, stimulus like IGF) may explain discrepancies between results presented in different studies (Mitchell & Pavlath, 2002; Schiaffino & Serrano, 2002; Konhilas *et al.*, 2004). Also, it was previously reported that calcineurin differentially influenced the growth of different muscle types (Mitchell *et al.*, 2002). More specifically, treatment of muscle with the pharmacological Cn inhibitor cyclosporine affected more severely the maintenance of growth in fast muscle plantaris than in slow muscle soleus (Mitchell *et al.*, 2002). As a result, caution should be taken when comparing results from different studies and, as performed in this study, all comparison should be made using the same species, muscle type, gender and animal age.

Next, in response to functional overload, both NFATc2^{-/-} and NFATc3^{-/-} mice displayed an increase in the number of muscle fibers per midbelly area (Figure 3.2C). This indicates that NFAT deficient muscles are able to carry out fiber hyperplasia. A significant decrease in fiber number was observed in normal weight-bearing muscles of NFATc3^{-/-} mice as compared to wild-type mice (Figure 3.2C) and as reported in the literature (Kegley *et al.*, 2001) it is caused by a defect in primary myogenesis. This decrease in the number of fibers observed in NFATc3^{-/-} mice (Figure 3.2C) could be mediated by decrease levels of *Mgn* in normal weight-bearing condition (Figure 3.8A and E). Nevertheless, following 28 days of functional overload, NFATc3 knockout mice reached a similar cell number as wild-type overloaded mice indicating that hyperplasia is not impaired (Figure 3.2C).

This is the first study to investigate the role of NFATc2 and NFATc3 in the adaptive growth response of adult muscles. Overall, our findings demonstrate that in the plantaris muscle, functional overload-induced muscle growth is mediated by hypertrophy and hyperplasia in wild-type mice, whereas in mice lacking functional NFATc2 or NFATc3 the hypertrophic fiber growth is blocked. Also, the data illustrate a differential adaptive growth response between NFATc2 and NFATc3 mice.

NFATc2^{-/-} and NFATc3^{-/-} mice maintain metabolic plasticity and display a block hypertrophic growth specific to glycolytic fibers

An analysis of fiber types was carried out and the size and percentage expression of each fiber type compared between normal weight-bearing and 28 days overloaded plantaris muscles in wild-type, NFATc2^{-/-} and NFATc3^{-/-} mice. This analysis seeks to determine if different NFAT isoforms may regulate the growth of different fiber types during adaptive muscle growth. The results indicated that NFATc2 and NFATc3 play important roles in the regulation of hypertrophic muscle growth predominantly in glycolytic fibers (Figure 3.3B and Figure 3.4B). Indeed, the overload-induced fiber hypertrophy of oxidative fibers expressing MyHC type IIa was maintained (Figure 3.3B) in knockout mice while the growth of glycolytic fibers expressing MyHC type IIb was blocked (Figure 3.4B). The blocked fiber size growth is in agreement with previous studies that implicated calcineurin signaling in the regulation of skeletal muscle hypertrophic growth (Dunn *et al.*, 1999; Musaro *et al.*, 1999; Semsarian *et al.*, 1999; Mitchell *et al.*, 2002; Miyazaki *et al.*, 2006; Oishi *et al.*, 2008; Sakuma *et al.*, 2008). In addition, another study has implicated a Cn downstream signaling partner NFATc1, together with the four-and-a-half Lim protein 1 (FHL1), in the regulation of skeletal muscle hypertrophic growth (Cowling *et al.*, 2008). In the latter study, it was shown that FHL1 complexes with NFATc1 and increases its transcriptional activity, promoting both skeletal muscle hypertrophy and oxidative fiber type remodeling (Cowling *et al.*, 2008). In contrast, other groups have indicated that calcineurin is not involved in skeletal muscle

hypertrophy (Bodine *et al.*, 2001; Rommel *et al.*, 2001; Parsons *et al.*, 2004) but numerous review papers (Schiaffino & Serrano, 2002; Bassel-Duby & Olson, 2003; Tidball, 2005; Sakuma & Yamaguchi, 2010) have provided possible explanations for the observed discrepancies between these two different conclusions. In our study, the divergent growth response of oxidative and glycolytic fibers in mice deficient for functional NFATc2 or NFATc3 serves to provide additional insight into the previously observed contrasting roles of Cn in muscle growth. Furthermore, the observed reduced growth of oxidative, MyHC IIa, fibers in NFATc2 knockout mice, as compared to wild-type or NFATc3^{-/-} mice (Figure 3.3B), is in agreement with impaired nuclear addition and a block of fiber hypertrophy observed previously in injury-induced regenerating fibers of NFATc2^{-/-} mice (Horsley *et al.*, 2001). In addition, the more pronounced block of fiber hypertrophy in NFATc2^{-/-} mice, as compared to NFATc3^{-/-} mice, suggests that NFAT proteins regulate distinct mechanisms. A differential regulation of the adaptive muscle growth response also is suggested by a different amount of Myf5 in the overloaded muscles of NFATc2^{-/-} mice (Figure 3.8A and C). The results suggest that different combinations of NFAT isoforms regulate the hypertrophy of specific fiber types, in the same way that previous research has shown that different combinations of NFAT isoforms are necessary for maintenance of both slow and fast muscle fibers (Calabria *et al.*, 2009). Overall, these data reveal that NFATc2 and NFATc3 transcription factors can selectively regulate hypertrophy of glycolytic fibers.

The comparison in the percentage expression of fibers compared between normal weight-bearing and 28 days overloaded plantaris muscles in wild-type, NFATc2^{-/-} and NFATc3^{-/-} mice indicated that both NFATc2 and NFATc3 knockout mice maintain the ability of oxidative fiber type remodeling (Figure 3.3C and Figure 3.4C). Yet, the fiber type remodeling observed in our study did not produce a complete sequential transition of MyHC towards oxidative fiber types. The absence of a significant transition in MyHC profiles (*i.e.* a reduction in expression of MyHC Iia fibers and an increase in expression of MyHC Iib fibers) indicates that longer overload periods and/or forced exercise (Gregory *et al.*, 1986) are necessary. The levels of mRNA encoding MyHC Iia and MyHC Iib were measured to corroborate an oxidative fiber type remodeling, that was implied by the histological assessments of fiber type expression. The preliminary data showed that, in the overloaded muscles of all animals investigated, the amount of *MyHC Iib* mRNA are decreased (Figure 3.5B) while the levels of *MyHC Iia* mRNA remained unchanged (Figure 3.5A). As a modification in the expression of muscle metabolic profiles often precedes changes in the expression of myosin heavy chain genes or proteins (Gundersen, 1998), the levels of mRNA encoding TnIs were measured. This contractile protein is associated with the expression of a slow muscle profile and its expression is promoted in conditions of oxidative muscle adaptation (Calvo *et al.*, 1996; Nakayama *et al.*, 1996; Chin *et al.*, 1998; Dunn *et al.*, 1999). As expected, an increase amount of *TnIs* mRNA was detected in overloaded muscles of all mice investigated (Figure 3.5C). Additionally, myogenin (*Mgn*), a gene recognized for its

roles in myogenesis, also has been implicated in mediating muscle remodeling toward oxidative metabolism (Hughes *et al.*, 1999). All mice investigated displayed an up-regulation in *Mgn* mRNA levels (Figure 3.8A and E). The ability of NFATc2 and NFATc3 knockout mice to experience oxidative fiber type remodeling under conditions of functional overload is in agreement with recent findings that indicated that a combination of different NFATs are required to mediate fiber type specification (Calabria *et al.*, 2009). The research carried out by Calabria *et al.* (2009) indicated that NFAT transcription factors act synergistically to regulate specification of muscle fibers and that a combination of NFATc1, NFATc2, NFATc3 and NFATc4 act together to promote expression of oxidative MyHC muscle fibers.

Overall, our results imply that the absence of one NFAT isoform does not prevent metabolic remodeling of muscles. Collectively these findings suggest that NFAT isoforms have a limited capacity to substitute for one another in muscle fiber type metabolic remodeling. Meanwhile, NFATc2 and NFATc3 isoforms are important in mediating skeletal muscle adaptive hypertrophic growth response of glycolytic muscle fibers. These findings provide new knowledge about the functions the different NFAT family members in skeletal muscles.

NFATc2^{-/-} and NFATc3^{-/-} mice display altered nuclear localization of surviving NFAT isoforms

All four isoforms of calcium regulated NFAT are present in skeletal muscles (Hoey *et al.*, 1995; Calabria *et al.*, 2009). To assess the capacity of NFAT proteins to substitute for one another, the levels of mRNA encoding NFATs were compared between wild-type and knockout mice, in normal weight-bearing or 7 days overloaded conditions. This comparison did not show compensatory changes in the amounts of surviving *NFAT* mRNA in muscles of NFATc2 or NFATc3 knockout mice (Figure 3.6). This is in agreement with previous studies that investigated *NFAT* mRNA levels in normal weight-bearing muscles or muscle cell cultures that lacked NFATc2 or NFATc3 expression (Horsley *et al.*, 2001; Kegley *et al.*, 2001). These findings indicate that compensatory regulation of surviving NFAT isoform mRNA is not occurring in NFATc2 or NFATc3 knockout mice in normal weight-bearing or adaptive muscle growth conditions.

NFAT proteins are transcription factors whose activities are regulated by dephosphorylation and subsequent localization to the nucleus. Previously, it has been reported that the translocation of some NFAT isoforms occurs at specific stages of muscle development (Abbott *et al.*, 1998). In addition, more recently it was shown that in response to distinct muscle electrical activity patterns, different combinations of NFAT proteins translocate to the nucleus and act to regulate the expression of specific muscle fiber types (Calabria *et al.*, 2009). It also has been described that nuclear shuttling of NFATc1 is linked to the activation of a slow muscle profile (Liu *et al.*, 2001; Shen *et al.*,

2006) and an increase in nuclear localization of NFATc1 was observed in the functional overload model (Dunn *et al.*, 2000; Dunn *et al.*, 2001). This study represents the first examination of the cellular distribution of all four calcium-regulated NFAT isoforms in conditions of adaptive muscle growth. Immunofluorescence was used to compare the nuclear localization of NFAT isoforms between normal weight-bearing and 7 days functional overloaded conditions in wild-type, NFATc2^{-/-} and NFATc3^{-/-} mice.

In the wild-type mice an increase in nuclear-localized NFATc1 isoform was detected in the overloaded plantaris as compared to normal weight-bearing levels (Figure 3.7A and B), corresponding to results previously reported in the literature (Dunn *et al.*, 2000; Dunn *et al.*, 2001). While our data demonstrated that NFATc2 and NFATc3 isoforms participate in muscle hypertrophic growth (Figure 3.2), these two isoforms did not show greater nuclear localization in response to overload in wild-type mice, versus the normal weight-bearing condition (Figure 3.7A and B). This finding suggests that nuclear shuttling of NFATc2 or NFATc3 might be implicated at earlier or later stages of the overload response. Consequently, future experiments should look at the expression of NFAT protein localization in a functional overload time course experiment.

The assessment of nuclear localization of NFATc1 in NFATc2^{-/-} mice did not indicate a significant increase in the nuclear localized NFATc1 in the overloaded muscle, but larger variability was detected for this isoform in the normal weight-bearing condition (Figure 3.7C and D). This may indicate that collaborative regulation occurs between NFATc1 and NFATc2 in wild-type mice hence the absence of functional NFATc2 in the

knockout mice leads to impaired nuclear shuttling of NFATc1 during the normal weight-bearing condition. Structural analysis of the NFAT proteins (Hogan *et al.*, 2003; Macian, 2005) has indicated that they can form cooperative transcriptional complexes as homo- or hetero-dimers with other NFAT isoforms, or with other transcription factors. In the NFATc2^{-/-} mice, the other NFAT isoforms did not exhibit alteration in nuclear localization in the overloaded condition (Figure 3.7C and D).

Finally, NFATc3^{-/-} mice displayed an increase in nuclear localization of both NFATc1 and NFATc4 isoforms (Figure 3.7E and F). This indicates that an absence of functional NFATc3 protein promotes a faster or greater nuclear trafficking of NFATc4. Notably, the nuclear import of NFATc1 with overload is reduced as compared to wild-type mice (1.3 in wild-type versus 1.1 in NFATc3^{-/-} mice) (Figure 3.7B and F) and NFATc4 might be recruited to substitute for NFATc1. NFATc4 is an isoform that has not been investigated in depth in skeletal muscles. NFATc4 knockout mice do not display defects in their muscle phenotype (Graef *et al.*, 2001) and the expression of NFATc4 is very low in skeletal muscles (Hoey *et al.*, 1995; McCullagh *et al.*, 2004; Calabria *et al.*, 2009). Nevertheless, NFATc4 was shown to play roles in the specification of all four types of skeletal muscle fibers (Calabria *et al.*, 2009) and results presented here also implicate NFATc4 in the regulation of adaptive muscle growth.

In summary, these results imply that NFATc1 requires the presence of both NFATc2 and NFATc3 to fine tune its correct nuclear localization during the overload response. These data point out that more detailed analyses are required to elucidate the

exact mechanisms of NFAT nuclear trafficking in the functional overload model. Of foremost importance would be to carry out a detailed time-course investigation of NFAT localization over a large overload time period. In addition, immunoprecipitation experiments should be performed to study the formation of NFAT dimers in the nucleus, comparing wild-type and NFAT knockout mice in normal weight-bearing or overloaded conditions. It would also be interesting to compare the nuclear localization of NFATs in different fiber types since NFAT knockout mice displayed a block of growth of glycolytic (Figure 3.4B), but not oxidative fibers (Figure 3.3B). The latter experiments would strengthen the idea that NFATc2 and NFATc3 are essential to mediate hypertrophic growth in selected fiber types. Overall, immunofluorescence experiments suggest that a lack of functional NFATc2 or NFATc3 influences NFATc1 cellular distribution and suggest that NFAT isoforms might act collectively to influence muscle fiber hypertrophic growth. The absence of NFATc2 or NFATc3 could alter the import/export dynamics of surviving NFAT isoforms or it could affect the formation of NFAT cooperative transcriptional complexes. These results also imply distinct nuclear trafficking dynamics of surviving NFAT family members during the adaptive muscle growth in NFATc2^{-/-} or NFATc3^{-/-} mice. More detailed experiments are required to clearly elucidate the cellular distribution of NFAT isoforms and to better understand NFAT transcription factors functions during the adaptive overload-induced remodeling of skeletal muscles.

NFATc2 and NFATc3 regulate the expression of myogenic regulatory factors

As NFATc2 and NFATc3 knockout mice have been shown to display defects in various steps of developmental myogenesis (Horsley *et al.*, 2001; Kegley *et al.*, 2001), the mRNA coding for some myogenic factors were measured using RT-PCR. More precisely, in our study *Pax7* was used as a marker of muscle precursor cells called satellite cells. Satellite cells become activated under conditions of muscle regeneration or growth. The transcription factor *Pax7* is expressed in all satellite cells and it ensures survival of these cells (Seale *et al.*, 2000; Kuang *et al.*, 2006; Buckingham, 2007; Buckingham & Relaix, 2007). The myogenic factors *Myf5* and *MyoD* served as markers of satellite cells activation and determination of the formation of myoblasts (Rudnicki *et al.*, 1993; Megeney & Rudnicki, 1995; Sabourin & Rudnicki, 2000; Charge & Rudnicki, 2004). Finally, *Mgn* was used as a marker of myoblast differentiation into myotubes that will form and grow into mature muscle fibers (Hasty *et al.*, 1993; Nabeshima *et al.*, 1993; Megeney & Rudnicki, 1995; Sabourin & Rudnicki, 2000).

The levels of *Pax7* gene showed a slight, but not significant, increase in the overloaded muscles of all mice investigated (Figure 3.8A and B). This result is in agreement with the literature since in the functional overload model the levels of this transcription factor displayed a rapid increase in the first 12 hours, peaked at 2 days and then exhibited a progressive decrease in expression (Hyatt *et al.*, 2008). The lack of differential expression of the *Pax7* gene between wild-type and NFAT knockout mice indicates that the expression of satellite cells is not altered in these animals.

Next, the levels of *Myf5* and *MyoD* were determined and the results indicated an up-regulation of *Myf5* levels in overloaded muscles of wild-type and NFATc3 knockout mice in comparison to normal weight-bearing muscles (Figure 3.8A and C). In contrast, a higher expression of *Myf5* was not seen in overloaded muscles of NFATc2^{-/-} mice. This finding could possibly relate to the impaired nuclear addition seen in NFATc2^{-/-} mice (Horsley *et al.*, 2001) since higher levels of Myf5 have been shown to promote satellite cell self-renewal (Charge & Rudnicki, 2004). An absence of satellite cells self-renewal could lead to impaired nuclear addition in growing muscle fibers and this would prevent the maintenance of a constant nuclear domain. In addition, Myf5 was shown to be regulated by a Cn/NFATc1 dependent mechanism in cell culture experiments (Friday & Pavlath, 2001) and our immunofluorescence assays suggested possible formation of cooperative transcriptional complexes between NFAT isoforms.

In contrast, the levels of *MyoD* did not show significant differences in the overloaded condition for all animals investigated (Figure 3.8A and D). This finding was expected since *MyoD* was shown to follow a similar time course of expression as the *Pax7* gene in the functional overload; it thus returns to control expression levels after 7 days of overload (Hyatt *et al.*, 2008). It should also be noted that a difference in gene expression was not observed for Pax7, Myf5 or MyoD between animals, in normal weight-bearing conditions. This finding is consistent with previous reports that did not detect changes in the expression of MyoD in NFATc2^{-/-} mice (Horsley *et al.*, 2001).

Meanwhile, this study represents the first analysis of the expression levels of myogenic regulatory factors in NFATc3^{-/-} mice.

Myogenin (Mgn) is a myogenic factor essential for the transition from proliferative myoblasts to differentiated cells that will fuse and form myotubes (Hasty *et al.*, 1993; Nabeshima *et al.*, 1993; Rawls *et al.*, 1995). Analysis of the levels of *Mgn* indicated a large increase in *Mgn* mRNA levels in all mice investigated (Figure 3.8A and E) indicating that formation of nascent myotubes is not blocked in NFAT knockout mice and in good agreement with the observed hyperplasia in our model. It is also important to note a decrease in the amount of *Mgn* in normal weight-bearing muscle of NFATc3^{-/-} mice (Figure 3.8A and E). This finding is consistent with a study that implicated NFATc3 in the induction of myogenin expression (Armand *et al.*, 2008) and supports the finding of a reduced number of fibers in NFATc3^{-/-} mice in the normal weight-bearing condition (Figure 3.2C) and (Kegley *et al.*, 2001). In the functional overloaded condition, the levels of *Mgn* are increased and this is also consistent with the ability of NFATc3^{-/-} mice to display overload induced fiber hyperplasia (Figure 3.2C). These data indicate that *Mgn* is not regulated by NFATc2 or NFATc3 during adaptive muscle growth yet NFATc3 controls *Mgn* expression during developmental myogenesis.

Collectively, these preliminary results suggest that during adaptive muscle growth, NFATc2 regulates the expression of *Myf5*, and this can possibly relate to the more pronounced block of fiber hypertrophy seen in NFATc2^{-/-} mice (Figure 3.2B) Meanwhile, NFATc3 appears to influence the levels of *Mgn* during the developmental

growth of muscles, and this can be associated to the reduced number of fibers in NFATc3^{-/-} mice (Figure 3.2C).

Signaling via Akt pathway is not altered in overloaded NFATc2^{-/-} or NFATc3^{-/-} mice

The Akt signaling pathway is well characterized in its role to promote skeletal muscle hypertrophy and prevent muscle atrophy (Bodine *et al.*, 2001; Rommel *et al.*, 2001; Glass, 2005; Sandri, 2008; Glass, 2010). Akt becomes activated by phosphorylation and an increase in the expression of total Akt and phosphorylated protein have been reported in various models of muscle growth such as exercise (Nader & Esser, 2001; Sakamoto *et al.*, 2003; Sakamoto *et al.*, 2004), electrical stimulation (Nader & Esser, 2001; Sakamoto *et al.*, 2002) or the functional overload model (Bodine *et al.*, 2001; Miyazaki *et al.*, 2011). The glycogen synthase kinase-3 β (GSK-3 β) is a target of Akt signaling and Akt-induced phosphorylation of GSK-3 β leads to inhibition of GSK-3 β activity (Cross *et al.*, 1995; Proud & Denton, 1997; Harwood, 2001). GSK-3 β is a negative regulator of protein translation and a reduction in its activity leads to muscle growth (Rommel *et al.*, 2001; Vyas *et al.*, 2002). In addition, GSK-3 β has been shown to regulate NFAT transcription factors transcriptional activity during condition of muscle growth (Rommel *et al.*, 2001; Vyas *et al.*, 2002)

The levels of phosphorylated and total Akt and GSK-3 β proteins were measured using Western blotting and compared between normal weight-bearing and overloaded conditions in wild-type and 7 days functional overloaded animals (Figure 3.9).

Quantification of these results indicated an increase in total and phosphorylated levels of Akt in the overloaded condition in all animals investigated. Meanwhile, total or phosphorylated levels of GSK-3 β did not change in the overloaded condition. It is also interesting to observe a subtle increase in the levels of pAkt in NFATc3 knockout mice in the normal weight-bearing muscles as compared to wild-type and NFATc2^{-/-} mice (Figure 3.9A and B). This could be a way for NFATc3^{-/-} mice to compensate for a decreased number of fibers in the normal weight-bearing condition (Figure 3.2C).

The results presented in this section should be re-confirmed and strengthened using a larger sample size to try to achieve statistically significant differences in the data. Nevertheless, these results indicate that Akt / GSK-3 β signaling events are most likely not responsible for the reduced growth of glycolytic fibers in NFATc2 or NFATc3 knockout mice in conditions of adaptive muscle growth.

Summary

This is the first study to use NFATc2 and NFATc3 knockout mice to investigate the roles of NFAT transcription factors in the adaptive muscle growth induced by surgical synergistic muscles ablation. The findings indicated that NFATc2 and NFATc3 transcription factors are important in the regulation of glycolytic fiber hypertrophy. Furthermore, NFATc2 and NFATc3 knockout mice displayed differences in their adaptive growth responses. More precisely, the hypertrophic growth was more severely blunted in NFATc2^{-/-} than NFATc3^{-/-} mice. Meanwhile, both knockout mice maintained

the ability to carry out the overload-induced oxidative metabolic remodeling. The results demonstrated that NFATc2^{-/-} and NFATc3^{-/-} mice display alteration in nuclear shuttling of NFAT isoforms and implicated the less documented NFATc4 isoform in the regulation of muscle adaptive growth. The outcomes also showed that NFATc2 and NFATc3 knockout mice differ in expression and regulation of myogenic factors *Myf5* and *Mgn* and this provided insight into the different growth response of these animals. In short, NFATc2 may regulate the expression of *Myf5* during adaptive muscle growth, while NFATc3 could influence the levels of *Mgn* during the developmental growth of muscles. Finally, mice deficient for functional NFATc2 or NFATc3 did not display impaired Akt signaling in response to the overload induced adaptive muscle growth.

In conclusion, our findings illustrate the importance of NFATc2 and NFATc3 in the regulation of muscle hypertrophy. Although many questions still remain unanswered and require future study, these results demonstrate that both NFATc2 and NFATc3 control adaptive growth of adult muscles. Our results also highlight the significance of different muscle growth models and distinct muscle and / or fiber types in decoding signaling events that stimulate muscle growth. A better understanding of molecular pathways regulating muscle growth can help identify future therapeutic targets for the treatment of various diseases displaying symptoms of muscle atrophy or wasting, such as cancer induced cachexia or various forms of muscular dystrophy.

3.7 Future Directions

Currently an ongoing project involves the investigation of muscle growth in mice deficient simultaneously for both functional NFATc2 and NFATc3 isoforms. Our laboratory is at this time breeding these transgenic mice, but as in the case of NFATc3^{-/-} mice, the breeding success is very low. Indeed, it was reported that NFATc3^{-/-} mice undergo fetal death and thus the chances of obtaining homozygous offspring is only about 12% (Oukka *et al.*, 1998). Furthermore, NFATc2^{-/-}c3^{-/-} mice are often sick and frail due to the weakness of their immune system, and this leads to younger death before surgery age or death following overload surgery. Nevertheless, it would be a very interesting to evaluate the response of these double null mice to the surgical overload model.

In this chapter, due to the limited number of animals available, the signaling events were investigated following 7 days of functional overload, while histological phenotypic comparison were carried out after 28 days of functional overload. The future experiments should aim to evaluate a detailed time course of events for the observed data. As explained in the discussion, it appears important to investigate both the signaling and phenotypic alterations at 3 days, 1 week (7 days), 4 weeks (28 days) and 8 weeks. These experiments would require a large number of mutant mice and this is definitely a limitation to this study, but it would provide a clear and in depth understanding of NFAT roles in the regulation of adaptive muscle growth.

Finally, in the short-term it would also be important to perform an in depth immunofluorescent analysis of NFAT nuclear localization, not only at different overload time periods but also by fiber type. Our results indicated that NFATc2 or NFATc3 knockout mice display defects in growth of glycolytic but not oxidative fiber types. In NFATc2^{-/-} or NFATc3^{-/-} mice alterations in the nuclear trafficking of NFATs proteins were detected hence a detailed time and fiber type analysis of the nuclear trafficking is important.

Furthermore, Western blotting analysis of the expression of NFAT transcription factors in different cellular compartments is still pending due to the untidy results obtained in preliminary experiments. The analysis of Western blot detection is complicated by the presence of various splice variants of a single NFAT isoform, by the numerous phosphorylation sites present on NFAT proteins and by the detection of unspecific bands from other proteins containing a Rel homology domain. Additionally, immunoprecipitation experiments should be carried out to confirm the formation of transcriptional complexes between the different NFAT isoforms during muscle growth.

Finally, the experiments carried out using semi-quantitative PCR should be re-analyzed using real-time PCR. This equipment would provide a more precise and quantitative analysis of gene expression and would refine and support the results presented in this chapter. As an alternative, gene arrays could also be performed but caution should be taken in selecting gene array targets. The gene array assay would

provide a global analysis of possible changes in gene expression of numerous targets in a single experiment.

Overall, to achieve a detail and clear understanding of the precise roles of NFATc2 and NFATc3 in the overload growth model more experiments are awaiting. An in depth understanding requires long term careful planning due to the limitations of the animals available.

Chapter 4: **Agrin regulates skeletal muscle signaling**

Ewa M. Kulig¹ and Robin N. Michel²

1. *Department of Chemistry and Biochemistry, Concordia University, Montreal, Quebec, Canada*
2. *Department of Exercise Science, Concordia University, Montreal, Quebec, Canada*

4.1 Background

In this Chapter the possibility that the trophic factor agrin can regulate skeletal muscle growth is explored. A recombinant neural agrin is injected directly into the tibialis anterior muscle of wild-type, aging and dystrophic mice. The results illustrate that agrin may regulate Akt signaling, a major muscle growth pathway. Yet, agrin failed to induce fiber hypertrophy in wild-type mice, it does not regulate Akt signaling in aging muscle, and it only showed a partial rescue of dystrophic muscle pathology.

These results represent preliminary data that aim to discover novel roles for agrin. This protein is well recognized for its function in the maintenance and formation of NMJ but recent research has also highlighted some possible new functions for agrin.

4.2 Abstract

The plasticity of skeletal muscle is a complex mechanism controlled by signals coming from the nerve and from within the muscle. Agrin is a large heparan sulfate proteoglycan released by the motor neuron. The best characterized function of agrin in skeletal muscle is its ability to form and stabilize the NMJ. Recent investigations indicate that agrin also has novel roles in muscles, beyond the maintenance of the NMJ.

In this study, a recombinant neural agrin was injected *in vivo* into the tibialis anterior muscle of mice. In wild-type adult, healthy mice results showed that agrin may regulate Akt signaling, a major muscle growth pathway. Yet, histological assessment of wild-type muscle fibers did not indicate fiber hypertrophy or fiber type remodeling following agrin injection. In addition, the roles of agrin were assessed in two models displaying degeneration of skeletal muscles. Agrin administration failed to activate Akt signaling in mice displaying sarcopenia; the progressive decline of muscle mass and function that occurs with age. On the other hand, agrin treatment decreased the number of centrally nucleated fibers in a mouse model for Duchenne Muscular Dystrophy (DMD) indicating a modest rescue of muscle wasting.

While these results are preliminary they suggest new functions for agrin in skeletal muscles. More in depth assessments of mechanical and biochemical properties of muscles are necessary to obtain a detailed picture of agrin's roles in the regulation of muscle diseases and/or growth. Nevertheless, this investigation identifies novel research avenues to pursue in this field.

4.3 Introduction

The plasticity of skeletal muscles is a complex mechanism controlled by signals coming from the nerve and from within the muscle. Agrin is a large heparan sulfate proteoglycan that exists in numerous different splice variants displaying different biological activities and tissue distributions (Ferns *et al.*, 1993; Hoch *et al.*, 1993). Currently, neural agrin, that contains an insert at splice site Z, is the sole isoform recognized to display biological activity (Ferns *et al.*, 1993; Bezakova & Lomo, 2001; Williams *et al.*, 2008).

Agrin is released by the motor neuron into the presynaptic cleft and on the muscle surface agrin interacts with two receptors (Hoch, 1999). Firstly, the association of agrin with α -dystroglycan (α -DG) (Gee *et al.*, 1994) serves to aggregate the dystrophin-associated glycoprotein complex (DGC) (Campanelli *et al.*, 1994; Hoch, 1999). The main functions of this complex are to stabilize the skeletal muscle structure and to serve as a scaffold for various signaling molecules (Pilgram *et al.*, 2010). Secondly, agrin interacts with LDL-receptor related protein 4 (LRP4) (Kim *et al.*, 2008; Zhang *et al.*, 2008) that forms a complex with the muscle specific kinase (MuSK) and initiates a signaling cascade that drives the aggregation of AChR (DeChiara *et al.*, 1996; Glass *et al.*, 1996a; Glass *et al.*, 1996b).

Agrin is widely expressed in different tissues such as brain, spinal cord, retina, muscle, liver, kidney or lung (Ferns *et al.*, 1993; Hoch *et al.*, 1993) and its broad expression indicates that it also can regulate processes other than NMJ maintenance

(reviewed in (Bezakova & Ruegg, 2003; Williams *et al.*, 2008)). Similarly, novel roles for agrin are emerging in the regulation of skeletal muscles. For instance, over-expression of agrin in mice was beneficial in the treatment of congenital muscular dystrophy (CMD) characterized by an absence of extracellular matrix structural protein laminin- α 2 (Moll *et al.*, 2001; Bentzinger *et al.*, 2005; Qiao *et al.*, 2005). In addition, agrin was shown to regulate properties of skeletal muscle cells *in vitro* by altering excitation-contraction coupling via regulation in the expression of various ion channels (Bandi *et al.*, 2008; Jurdana *et al.*, 2009). Finally, agrin was shown to enhance the contractile functions of an engineered aneural muscle tissue system (Bian & Bursac, 2011). These findings indicate that agrin might have novel roles in skeletal muscles, beyond its well characterized function in the maintenance of NMJ.

In this study, two models displaying degeneration of skeletal muscles were used. Firstly, sarcopenia is the age-dependent progressive decline in skeletal muscle mass and contractile function (Balagopal *et al.*, 1997). The average life-span of mice is about two years, thus animals older than 24 months are an adequate model to represent elderly mice. Secondly, Duchenne Muscular Dystrophy (DMD) is caused by the absence of a functional dystrophin. This dystrophin deficiency destabilizes the DGC and leads to progressive weakness and deterioration of skeletal muscle functions and structures. In research, *mdx* mice are commonly used as a model for DMD (Bulfield *et al.*, 1984; Carnwath & Shotton, 1987; Coulton *et al.*, 1988a; Coulton *et al.*, 1988b; Pastoret & Sebille, 1995). The hypothesis explored in this study was that agrin can promote muscle

growth or it can prevent muscle decline. To investigate the roles of agrin in the regulation of skeletal muscles a direct intramuscular injection of a recombinant C-terminal half of neural agrin was performed in young, old and dystrophic mice.

While preliminary data presented indicate that agrin may regulate the expression of Akt and S6K proteins, two major signaling targets of skeletal muscle growth, the data also suggest that agrin treatment does not improve the pathology observed in sarcopenic muscles. Meanwhile, deteriorating *mdx* muscles displayed a limited improvement in some of the disease symptoms. Taken together, these results illustrate innovative roles for the trophic factor agrin in skeletal muscles and demand further research to better understand agrin involvement in muscle plasticity.

4.4 Methods

4.4.1 Animal Care, Surgeries and Extractions

All animal care and experimental procedures were performed in accordance with the guidelines established by the Canadian Council of Animal Care. These procedures were approved by the University Animal Research Ethics Committee (UAREC) of Concordia University. Animals were housed in temperature and humidity controlled conditions on a 14:10 hour light: dark cycle and had access to water and food *ad libitum*. In all experimental procedures male mice were used. Young and dystrophic mice were 3 months old while aged mice were between 24 and 29 months of age.

4.4.2 Animal Surgeries and Extractions

All surgical procedures were performed under aseptic conditions on animals anesthetized by intramuscular injection (1.2 μ l / g) of 100 mg/ml ketamine hydrochloride and 10 mg/ml xylazine in a volume ratio of 1.6:1. A small incision was performed exposing the muscle surface, and the recombinant C-terminal half of rat agrin (R&D systems, Minneapolis, MN, USA) was injected directly into the tibialis anterior (TA) muscle. This ~90 kDa protein fragment contained an 8 amino acid insert at the Z site that induces clustering of AChRs at NMJ and is the neural isoform of agrin. Recombinant agrin was injected at a concentration of 10 μ M in a sterile carrier solution consisting of 25 mM PBS with 0.1% BSA. A single injection of 2.5 μ l of recombinant agrin was performed in the left TA muscles and the contralateral limb served as a control and was injected with the carrier solution. The muscles of mice were extracted 7 days post-injection, either frozen directly in liquid nitrogen or embedded in OCT (Tissue-Tek, Torrance, CA, USA) and frozen in melting isopentane. Upon completion of tissues extraction, mice were euthanized by cervical dislocation under anesthesia and all tissues were stored at -86°C until processed.

4.4.3 Immunohistochemistry

To determine muscle fiber type and size, muscle cryosections (10 μ m) were cut from TA muscle midbelly anatomical location. Sections were blocked for 30 minutes in 5% goat serum in a carrier solution consisting of 0.5% bovine serum albumin (BSA) in

25 mM phosphate buffer solution (PBS) (pH = 7.4). Subsequently, the sections were incubated overnight at 4°C in carrier solution with a primary antibody raised against the appropriate MyHC type. All antibodies used (MyHC I: A4.840 using 1:25 dilution; MyHC IIa: SC71 using 2:25 dilution; MyHC IIx: 6H1 without dilution; MyHC IIb: BF-F3 using 1:25 dilution) were from the Developmental Study Hybridoma Bank (DSHB, University of Iowa, Iowa city, IA). After three 10 minutes rinses in PBS, sections were incubated for two hours in secondary antibodies, horseradish peroxidase-conjugated goat anti-mouse IgG (MyHC type IIa) or IgM (MyHC type I, IIx, IIb) (Sigma-Aldrich, St-Louis, MO, USA) using a 1:25 dilution. The sections then were rinsed three times with PBS for ten minutes, and the bound antibody complexes were visualized using 1 mg/ml of diaminobenzidine tetrahydrochloride (DAB). Additionally, hematoxylin and eosin staining was carried out to analyse fiber damage and central nucleation. Briefly, slides were incubated in 0.5% Harris haematoxylin (Sigma-Aldrich, MO, USA) for five minutes, rinsed with water, and immediately dipped in 1% HCl / 70% EtOH solution and rinsed again with water. Subsequently slides were incubated in 1% eosin (Fisher Scientific, ON, Canada) for three minutes, rinsed with water, incubated successively in 70%, 80% and 90% EtOH solutions for two minutes each, and finally immersed in xylene (Fisher Scientific, ON, Canada) for thirty seconds. Slides were air dried and mounted in Permount (Fisher Scientific, ON, Canada). All slides were analyzed with an Olympus BX-60 light microscope. Three distinct regions were selected randomly from the midbelly of each TA muscle and images were captured across serial sections using a

Retiga SRV camera (QImaging, Surrey, ON, Canada). All fibers in those regions were classified according to the type of MyHC expressed and fiber cross sectional size was measured using ImagePro Plus version 6.2 software (Olympus, Markham, ON, Canada). In all analysis, the researcher was blinded to the experimental condition.

4.4.4 Protein extraction and Western Blotting

Muscles were homogenized using a hand-held Tissue Tearor homogenizer (ColeParmer, Montreal, QC, Canada) in RIPA buffer consisting of 1XPBS, 1% igepal, 0.5% sodium deoxycholate, 0.1% sodium dodecyl sulfate (SDS), 0.001 M sodium orthovanadate, 0.01 M sodium fluoride, 0.01 mg/ml aprotinin, 0.01 mg/ml leupetin and 1 mM phenylmethanesulfonyl fluoride (all reagents from Sigma-Aldrich, St-Louis, MO, USA). Homogenates were incubated on ice for 30 minutes followed by two 4°C centrifugations at 15 000 x g for 20 minutes. The supernatants were collected and the protein concentration determined using Quick Start Bradford dye reagent (Bio-Rad, Mississauga, ON, Canada).

For protein expression analysis, 150 µg of protein were separated by SDS polyacrylamide gel electrophoresis (SDS-PAGE) on a gel consisting of a 5% stacking gel and an 8% separating gel. Samples were electrophoresed (buffer: 25 mM Tris, 192 mM glycine, 0.1% SDS, pH 8.3) at 120V and Amersham Full-Range Rainbow (GE Healthcare, Baie d'Urfe, QC, Canada) molecular weight markers were used to define the protein sizes. Subsequently, proteins were transferred (buffer: 25 mM Tris, 192 mM

glycine and 20% methanol) to a PVDF membrane (Millipore, Billerica, MA, USA) at 100V for one hour and a successful transfer was confirmed using Ponceau S staining. Membranes were blocked for one hour using 5% non-fat milk in 0.1% Tween-Tris Buffered Saline (T-TBS) and incubated with primary antibody overnight at 4°C on a shaker as indicated in Table 3.2. The following day, the membranes were washed three times five minutes using 0.1% T-TBS and were then incubated with the appropriate horseradish peroxidase-conjugated secondary antibody: anti-rabbit IgG #7074 (Cell Signaling Technology, Danvers, MA, USA) or anti-mouse IgG #A8924 (Sigma-Aldrich, St-Louis, MO, USA). Subsequently, membranes were developed using the chemiluminescent Immobilon HRP substrate kit (Millipore, MA, USA) as per the manufacturer's instructions. Images were captured and protein expression quantified by densitometry with the AlphaInnotech system and FluorChem software (San Leonardo, CA, USA).

PROTEIN NAME	SUPPLIER	SIZE (kDa)	1°ANTIBODY	2°ANTIBODY
α-tubulin	Cell Signaling #2125	52	1:2000 in 5% milk	1:2000 in 5% milk for 1hr (anti-rabbit)
pAkt (ser473)	Cell Signaling #4060	60	1:1000 in 5% BSA	1:2000 in 5% milk for 2hrs (anti-rabbit)
Akt	BD Bioscience #610861	60	1:1000 in 5% milk	1:2000 in 5% milk for 2hrs (anti-mouse)
pS6K (thr389)	Cell Signaling #9206	70	1:1000 in 5% milk	1:2000 in 5% milk for 2hrs (anti-mouse)
S6K	Santa Cruz #sc-230	70	1:1000 in 5% milk	1:1000 in 5% milk for 1hr (anti-rabbit)

Table 4-1: Western Blotting Conditions

4.4.5 Statistical Analysis

All data were analyzed using independent samples two-tailed Student's T-test. All statistics were performed using SPSS statistics software version 17.0 (IBM SPSS, Chicago, IL, USA).

4.5 Results

4.5.1 Agrin injection is not regulating muscle fiber growth in healthy adult mice

In this study, we seek to determine if agrin can regulate the growth of skeletal muscles. A recombinant C-terminal half of agrin (AGR), sufficient to carry out agrin induced AChR clustering *in vivo* (Bezakova *et al.*, 2001), was injected directly into the TA muscle of adult, healthy mice. The contralateral limb was injected with a saline solution (PBS) and served as a control. A week post surgery, muscles were extracted and muscle weights, expressed relative to total body weight, were compared between PBS and AGR treated muscles. The data showed that agrin injection did not alter the relative muscle mass (Figure 4.1A). In addition, fiber typing was carried out based on the type of MyHC expressed. The cross sectional area (CSA) and percentage expression of muscle fibers were compared between PBS and AGR injected muscles. Agrin injection did not modify the CSA of oxidative fibers expressing MyHC IIa or glycolytic muscle fibers expressing MyHC IIb as compared to PBS treated muscles (Figure 4.1B). In addition, AGR treatment did not change the percentage expression of oxidative or glycolytic fibers (Figure 4.1C) versus PBS injected muscles.

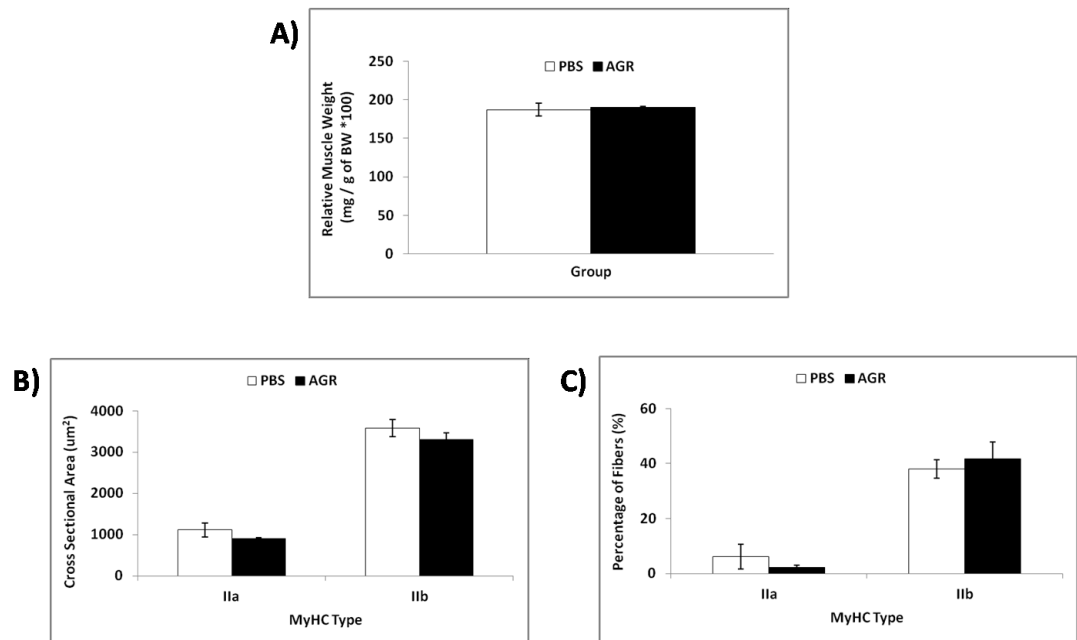


Figure 4.1: Agrin is not promoting muscle growth in adult, healthy mice.

A) Comparison of relative muscle weights between PBS (saline control) and AGR injected muscles of adult, healthy mice. Muscle fibers, classified to express MyHC IIa or MyHC IIb, were compared between PBS and AGR injected muscle. B) Quantification of fiber cross sectional area and C) quantification of fiber type's percentage expression. All results are expressed as the mean \pm SE. ($p < 0.05$, $n=3$ per group)

4.5.2 Agrin may regulate Akt signaling in muscles of healthy adult mice

Akt signaling is the major signaling pathway described to regulate muscle growth. Akt expression and phosphorylation levels are rapidly activated in conditions of muscle growth (Bodine *et al.*, 2001; Rommel *et al.*, 2001; Pallafacchina *et al.*, 2002) and this in turn leads to phosphorylation and activation of the downstream target S6K (ribosomal protein S6 kinase) (also known as $p70^{S6K}$) (reviewed in (Glass, 2003a, b). Western blotting analysis indicated that injection of AGR in muscles of wild-type adult, healthy mice increased the expression of phosphorylated and total Akt protein by 1.6 fold

compared to PBS injected muscles (Figure 4.2A and B). In addition, the levels of phosphorylated and total S6K protein were measured. The administration of agrin did not alter the expression of phosphorylated S6K but levels of total S6K expression were increased 1.3 fold as compared to PBS treated muscles. It is essential to note that these findings are not significant and an analysis with a larger sample size is necessary. In summary, our data suggest that in adult, healthy mice agrin may regulate Akt signaling but it does not modify muscle fiber size.

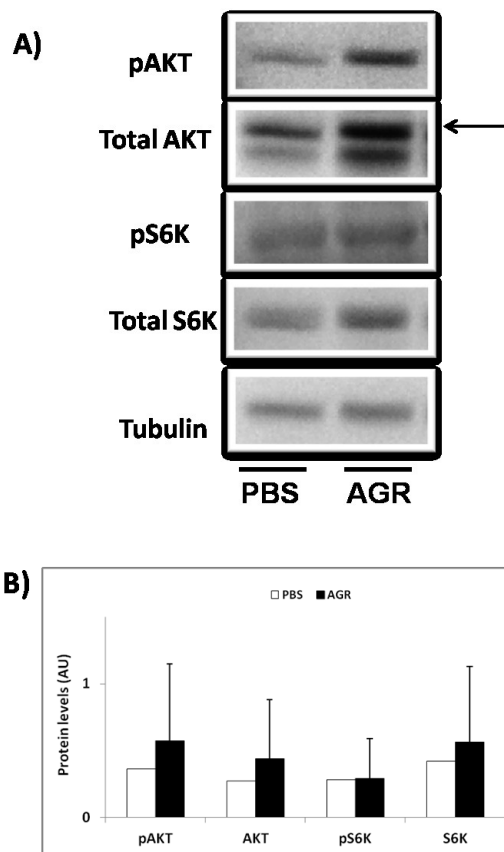


Figure 4.2: Agrin may regulate Akt signaling in muscles of adult, healthy mice.

A) Representative Western blot images comparing protein expression in PBS (saline control) and AGR injected wild-type muscle of adult, healthy mice. B) Quantification of protein levels. All quantifications were standardized to tubulin loading control and are expressed as the mean \pm SE ($p < 0.05$, $n=3$ per group).

4.5.3 Agrin does not activate Akt signaling in a sarcopenia model

Next the ability of agrin to rescue the progressive muscle decline observed in sarcopenia was investigated. Firstly, aging mice were characterized to confirm the phenotypic changes normally observed in sarcopenia. Aging mice displayed a marked increase in total body weight (Figure 4.3A) and a notable decrease in absolute muscle weight (Figure 4.3B), but these results were not significant. The relative muscle weights were compared between young and old mice and a significant 40% decrease was measured in sarcopenia (Figure 4.3C). In addition, sarcopenia is characterized by a decrease in fiber CSA size. In this study, mice displayed a 45% decrease in fiber size (Figure 4.3D and E). These results confirmed a decline of muscle mass in the aging mice used in this study.

Next, to determine if agrin can prevent the progressive muscle atrophy observed in sarcopenia, this trophic factor was injected into aging muscles. The comparison of the relative muscle weights between PBS and AGR injected muscles did not show a recovery of muscle mass (Figure 4.4A). Furthermore, Akt activated signaling can not only induce muscle hypertrophy, but it also prevents muscle atrophy (Bodine *et al.*, 2001). Agrin's ability to regulate Akt signaling in sarcopenia was assessed using immunoblotting. The results indicated that AGR administration did not change the expression of total or phosphorylated Akt or S6K protein in comparison to PBS injected muscles (Figure 4.4B and C). Overall, these preliminary data failed to show a role for agrin in the regulation of Akt signaling in sarcopenia.

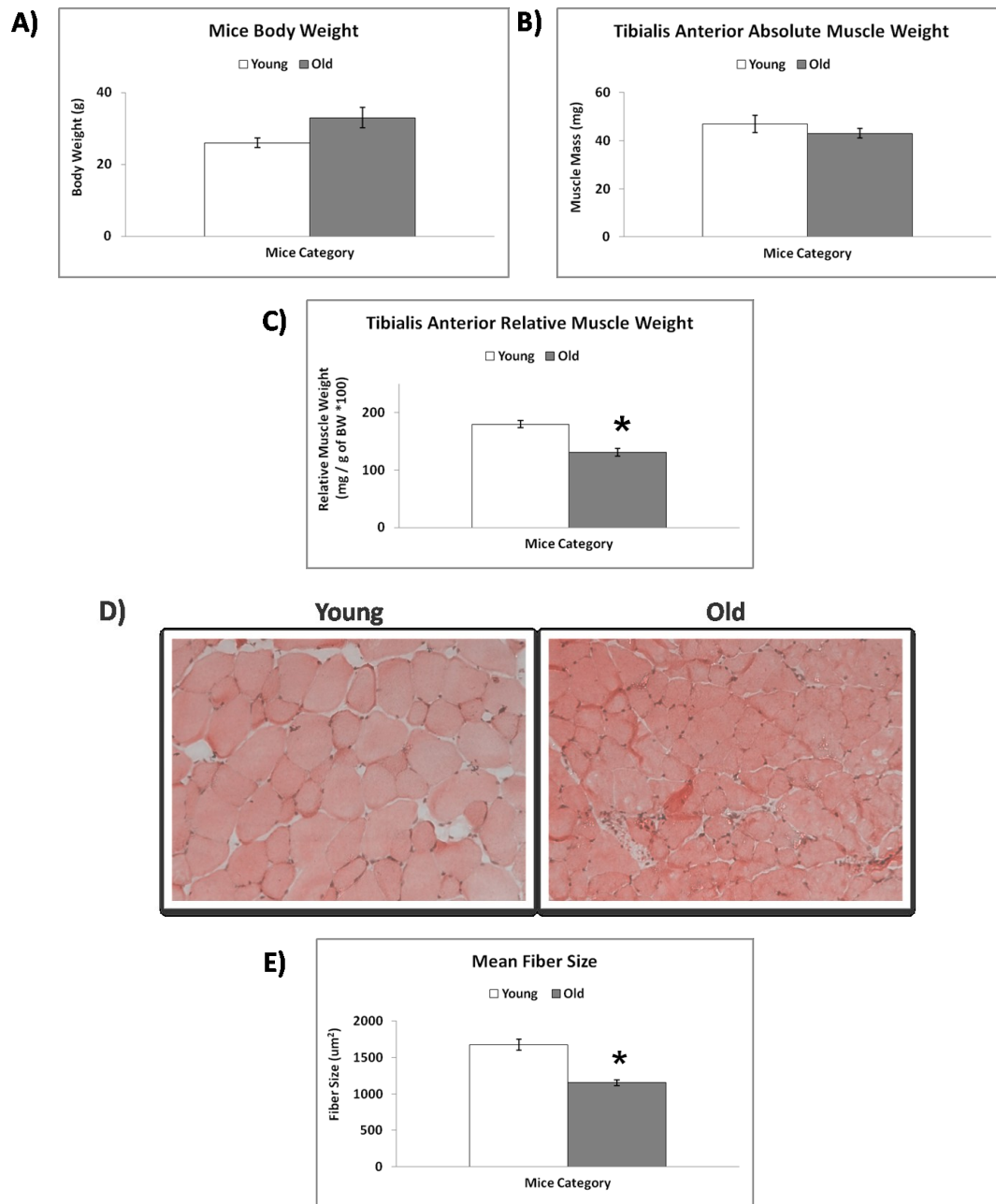


Figure 4.3: Characterization of the sarcopenia model

A) Quantification of total mouse body weight, B) absolute TA muscle weight and C) TA muscle weight relative to total body weight comparing young (3 months) and aging (>24months) mice D) Representative images stained for H&E illustrating the progressive atrophy observed in aging muscles. E) Quantification of muscle fiber size comparing young and aging muscles. All quantifications are expressed as mean \pm SE (* sig. diff. from young, $p < 0.05$, $n=3$ per group).

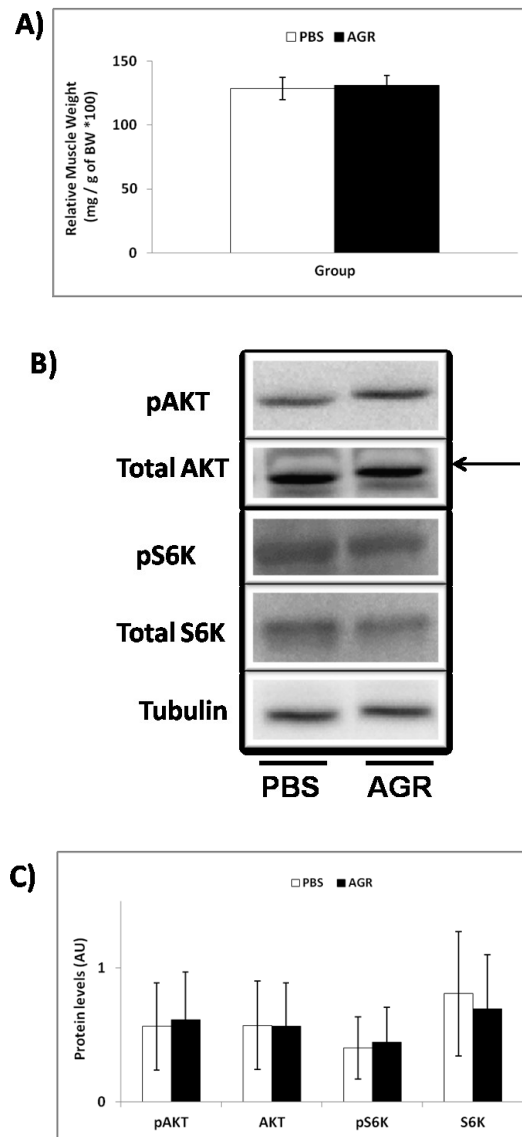


Figure 4.4: Agrin does not activate Akt signaling in aging muscles

A) Representative Western blot images comparing protein expression in PBS (saline control) and AGR injected wild-type muscles of old mice displaying symptoms of sarcopenia. B) Quantification of protein levels. All quantifications were standardized to tubulin loading control and are expressed as the mean \pm SE ($p < 0.05$, $n=3$ per group).

4.5.4 Agrin treatment regulates central nucleation in dystrophic muscles

Previous research has shown that agrin can improve the pathology observed in CMD (Moll *et al.*, 2001; Bentzinger *et al.*, 2005; Qiao *et al.*, 2005), yet the roles of agrin in DMD were not investigated. In the next experiments, a preliminary analysis of agrin's role in DMD was carried out using *mdx* mice. Previously, histological parameters that are hallmarks of DMD have been characterized in *mdx* mice (Briguet *et al.*, 2004). They included a large number of muscle fibers displaying central nucleation and an increase in fiber CSA variability versus healthy mice. In this investigation, a histological assay confirmed a large number of centrally nucleated fibers in dystrophic muscles of *mdx* mice (Figure 4.5A), in contrast to the absence of centrally nucleated fibers in wild-type mice. The presence of centrally nucleated fibers confirms that muscle regeneration is occurring in the diseased muscles. In addition, a frequency distribution of fiber CSA indicated a significant increase in small ($<1000 \mu\text{m}^2$) fibers in muscles of dystrophic mice but failed to demonstrate a major increase in fiber size variability (Figure 4.5B). The smaller-sized fibers are most likely new regenerating fibers. Finally, a quantitative measurement of the coefficient of variation (ratio of standard deviation to the mean) showed that *mdx* mice display a larger variability in their fiber size in comparison to wild-type mice (Figure 4.5C). The coefficient of variation is a normalized measure of fiber size dispersion as compared to the alternative standard deviation that could be use for this type of assay.

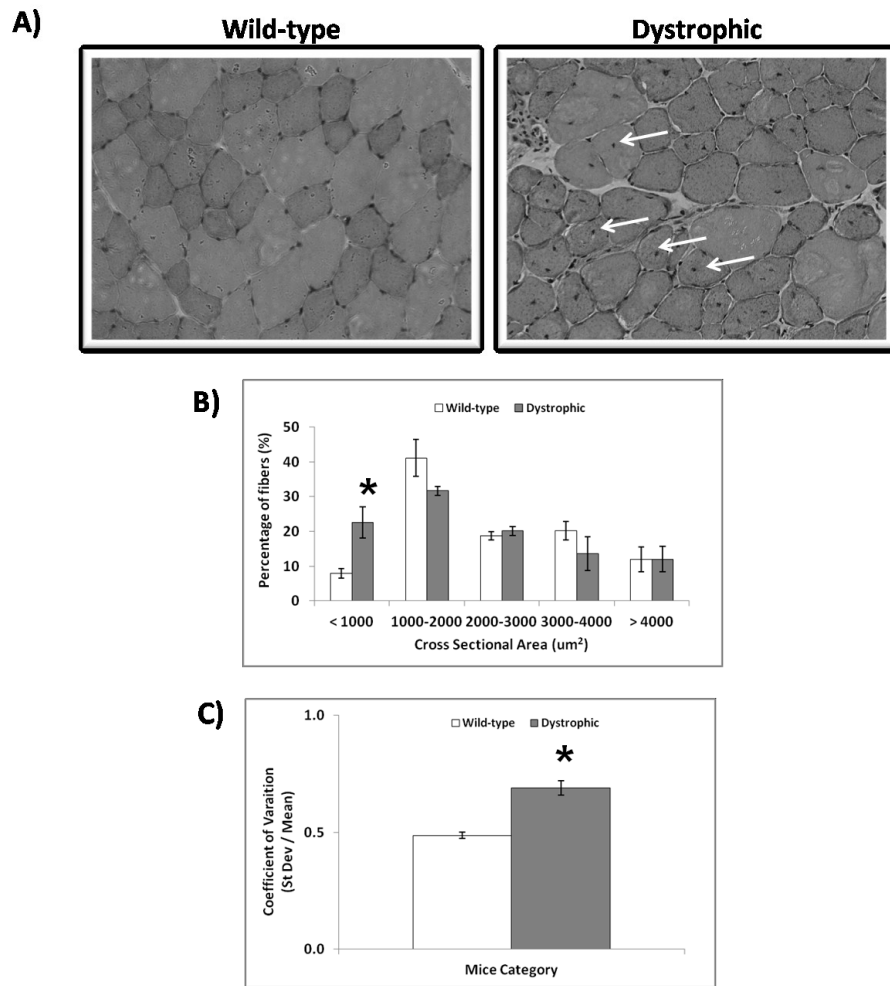


Figure 4.5: Characterization of the dystrophic model

A) Representative images stained for H&E illustrating the higher fiber size variability and the increased central nucleation observed in muscles of *mdx* mice. The arrows point to some centrally nucleated fibers. B) Frequency distribution of fiber size comparing wild-type and dystrophic muscles. C) Quantification of fiber size variability expressed using the coefficient of variation. All quantifications are expressed as mean \pm SE (* sig. diff. from wild-type, $p < 0.05$, $n=3$ per group).

Next, these same histological parameters were used to assess the hallmarks of DMD in *mdx* mice that were administered an intramuscular injection of agrin. The frequency distribution of fibers CSA failed to identify changes between PBS and AGR

injected muscles (Figure 4.6A). Similarly, the coefficient of variation did not show alterations between PBS and AGR administrated dystrophic muscles (Figure 4.6B). In addition, a fiber typing analysis (based on the expression of MyHC) did not show modifications in fiber size or fiber percentage expression in *mdx* mice following agrin

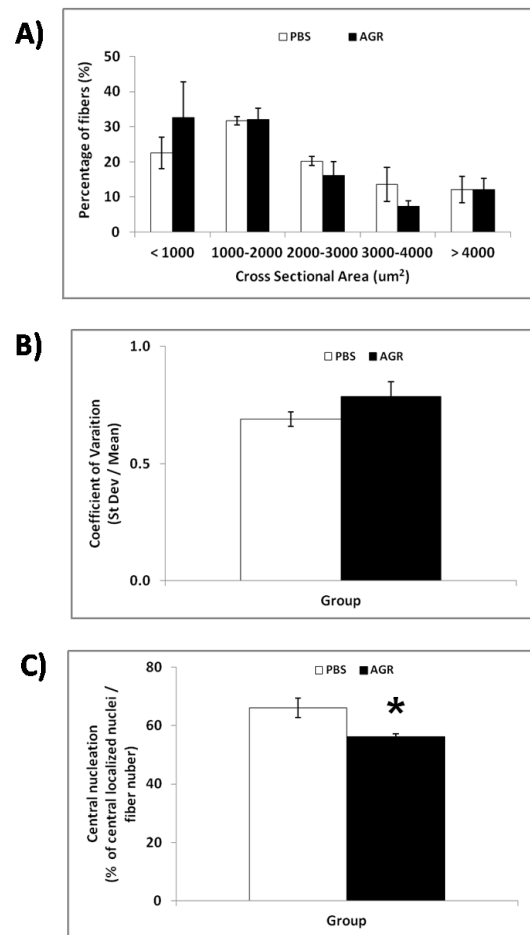


Figure 4.6: Agrin decrease central nucleation in *mdx* mice

A) Frequency distribution of fiber size comparing PBS (control saline) and AGR injected dystrophic muscles. B) Quantification of fiber size variability expressed using the coefficient of variation. C) Quantification of the number of fibers displaying central nucleation. All quantifications are expressed as mean \pm SE. (* sig. diff. from control PBS, $p < 0.05$, $n=3$).

injection (data not shown). Finally, fibers displaying central nucleation were counted and compared between PBS and AGR treated muscles. The administration of AGR promoted a subtle, yet significant decrease in central nucleation: from 66% \pm 5 in PBS muscles to 56% \pm 1 in AGR treated muscles (Figure 4.6C). These results suggest that agrin could be beneficial in the treatment of DMD.

4.6 Discussion

The roles of the nerve-derived factor agrin in the regulation of NMJ development and maintenance are well documented. Recent research has also illustrated novel functions for agrin in skeletal muscles (Moll *et al.*, 2001; Bentzinger *et al.*, 2005; Qiao *et al.*, 2005; Bandi *et al.*, 2008; Jurdana *et al.*, 2009; Bian & Bursac, 2011). In addition, agrin injection *in vivo* is able to rescue overload-induced muscle growth in a surgical model displaying a blocked transport of trophic factors from the nerve to the muscle (Michel & Kulig, 2008). In this investigation, we sought to determine if agrin can regulate muscle mass in adult mice. Furthermore, roles for agrin in the improvement of muscle wasting observed in sarcopenia and DMD were investigated.

A recombinant C-terminal half of rat agrin was injected directly into the tibialis anterior (TA) muscle of wild-type, healthy, adult mice. The injected protein contained an 8 amino acid insert at the Z site sufficient to induce clustering of AChRs at NMJ. This recombinant protein was a fragment of the “neural agrin”; the sole agrin isoform currently characterized to display biological activity (Ferns *et al.*, 1993; Bezakova &

Lomo, 2001; Williams *et al.*, 2008). In this study, the TA muscle of one side was injected with AGR while the contralateral TA muscle served as a control and was injected with a saline PBS solution. This permitted controlling for intrinsic differences that might exist between animals and it allowed for the minimization of both animal and recombinant protein usage. The TA muscle was chosen because of its ease of access and compartmentalized localization in mice hind limbs. A week post-injection, muscle weights were compared and the data failed to show a change following agrin treatment (Figure 4.1A). The results were expressed as relative muscle weights to control for intrinsic body weight differences between mice. Since the measurement of muscle weights is a crude method that cannot detect subtle alterations in muscle fiber growth, fiber typing analysis was performed based on MyHC expression. The fiber typing analysis allowed the comparison of fiber cross sectional area (CSA) and the percentage expression of different fiber types. Yet again, a comparison between PBS and AGR injected muscles did not indicate a remodeling in muscle fiber size (Figure 4.1B) or fiber type (Figure 4.1C).

The major pathway shown to regulate muscle growth is the Akt signaling cascade. This pathway is rapidly activated under conditions of muscle growth and the activity of this pathway persists for many days to promote muscle fiber hypertrophy (Bodine *et al.*, 2001; Rommel *et al.*, 2001; Pallafacchina *et al.*, 2002). Briefly, this pathway is activated through insulin growth factor (IGF-1) signaling that phosphorylates and triggers the activation of Akt via the phosphatidyl inositol 3-kinase (PI3K). This signaling leads to

downstream phosphorylation and activation of S6K (p70^{S6K}) a positive regulator of protein translation (reviewed in (Glass, 2003a, b, 2005, 2010). The results presented here indicated that AGR injection may increase the levels of phosphorylated and total Akt protein in comparison to PBS treated muscles (Figure 4.2A and B). Yet, the phosphorylation of Akt's downstream signaling partner S6K was not observed following AGR administration (Figure 4.2A and B). This finding indicates that protein synthesis via S6K signaling is probably not regulated by agrin in adult mice. However, since an increase in the expression of total S6K protein was observed in agrin treated muscles, this could indicate a delayed activation of this signaling partner. Alternatively, Akt signaling could block protein degradation mediated by ubiquitin ligases (Stitt *et al.*, 2004). Indeed, Akt phosphorylates forkhead box (FOXO) transcription factors preventing their entry into the nucleus (Stitt *et al.*, 2004). Normally, FOXO transcription factors induce the expression of ubiquitin liagases MuRF1 (muscle specific ring finger protein 1) and MAFbx (muscle specific F-box protein; also called atrogen-1) leading to protein degradation and muscle atrophy (Stitt *et al.*, 2004). This signaling was not investigated in this study but should be considered in future experiments.

Also, it cannot be ruled out that a longer agrin treatment period and/or increased dosage of agrin are necessary to observe a hypertrophic muscle growth response. In this study, the dosage used was previously shown to induce AChR clustering *in vivo* (Bezakova *et al.*, 2001). In addition, the recombinant agrin used in this study had a similar size to a mini-agrin that when over-expressed in mice had a half-life of 4.5 days

(Meinen *et al.*, 2007). This suggests that agrin was biologically active in our model over the experimental time course. In spite of that, it is possible that muscles require a longer time period to display fiber type remodeling and/or fiber growth following intramuscular agrin injection. Future studies should carry out a time course investigation of possible roles for agrin in the regulation of muscle mass. In addition, in future experiments recombinant agrin should be fluorescent-labeled, prior to injection, to permit the tracking of the recombinant protein expression and localization. Collectively, the results presented indicate that a week post-agrin injection, skeletal muscles are not displaying fiber growth, yet agrin may modulate the signaling of Akt pathway. Future agrin injection experiments should be performed using a larger sample size and with consideration of the above mentioned improvements.

Numerous critical events such as muscle fiber atrophy, oxidative fiber type remodeling and alteration in NMJ structure, occur during skeletal muscle aging (reviewed in (Nair, 2005; Doran *et al.*, 2009). This investigation examines the possibility that an intramuscular injection of recombinant agrin could rescue the progressive muscle decline observed in sarcopenia. Firstly, measurements of body and muscle weights were compared between young adult (3 months) and older mice (< 24 months). The older mice displayed subtle increases in overall body weights (Figure 4.3A) mediated by an increase in fat accumulation due to a reduced activity of aging animals. Meanwhile, the absolute and relative muscle weights were both reduced in old mice in comparison to young mice (Figure 4.3B and C). In addition, histological analysis confirmed muscle fiber atrophy

(Figure 4.3E) and other symptoms of sarcopenia (reviewed in (Nair, 2005; Doran *et al.*, 2009) were noted such as fibers with central nucleation and an increase infiltration of fat and connective tissue between fibers (Figure 4.3D). Subsequently, the activation of Akt signaling was compared between PBS and AGR injected muscle. The results indicated that agrin administration did not trigger, or that it delayed, the activation of Akt signaling in sarcopenia (Figure 4.4B and C). These results are in agreement with an investigation that used the overload induced muscle growth model and showed a reduced or delayed activation of Akt signaling in older mice (Hwee & Bodine, 2009). A time course experiment would differentiate between a blocked or delayed activation of this signaling pathway. Alternatively, these explorative results may indicate that agrin administration is not beneficial in the treatment of sarcopenia. This conclusion would concur with a recent study that used transgenic over-expression of agrin and, by means of fiber size measurements, indicated that agrin did not prevent skeletal muscle atrophy (Butikofer *et al.*, 2011). Yet, other recent studies illustrated agrin's ability to regulate excitation-contraction coupling (Bandi *et al.*, 2008; Jurdana *et al.*, 2009) and agrin's ability to regulate contractile properties of muscle fibers (Bian & Bursac, 2011). In future experiments, measurements of muscle fiber strength and fatigability should be performed in sarcopenic muscles injected with agrin. The likelihood exists that agrin does not induce the hypertrophy or prevent the atrophy of aging skeletal muscles, but it might be capable of improving muscles mechanical properties.

Next, previous research indicated that transgenic over-expression of agrin in mice was beneficial in the treatment of congenital muscular dystrophy (CMD) characterized by an absence of extracellular matrix structural protein laminin- α 2 (Moll *et al.*, 2001; Bentzinger *et al.*, 2005; Qiao *et al.*, 2005). In CMD mice, agrin improved muscle structure, whole body growth, mouse motility and lifespan (Moll *et al.*, 2001; Bentzinger *et al.*, 2005; Qiao *et al.*, 2005). Since agrin expression levels are decreased in the muscles (Eusebio *et al.*, 2003) and brain (Nico *et al.*, 2010) of *mdx* mice, in the next experiments, agrin was injected into the TA muscle of this mouse model of DMD. Firstly, using histological parameters that are hallmarks of dystrophy in *mdx* mice (Briguet *et al.*, 2004), dystrophy-induced muscle wasting was confirmed in animals used in this study. The results indicated a large number of centrally nucleated fibers and an increased variability in fiber size in the TA muscles of *mdx* mice, in comparison to wild-type mice (Figure 4.5). Subsequently, using the same histological comparison parameters, the data indicated that while AGR injection did not modify the fiber size variability (Figure 4.6A and B), AGR administration led to a decrease in the number of centrally nucleated fibers in *mdx* muscles versus PBS treated muscles (Figure 4.6C). This finding suggests a partial improvement of the dystrophic phenotype. A reduction in centrally nucleated fibers suggests a decrease in fiber regeneration. This could indicate a reduce speed in the cyclic events of fiber degeneration/regeneration observed in *mdx* mice. Previously, agrin was shown to promote the expression of the utrophin gene in cell cultures (Gramolini *et al.*, 1998; Gramolini *et al.*, 1999). Utrophin is a dystrophin homologue that has been shown

to be naturally upregulated in dystrophic models and a genetic over-expression of utrophin improves biochemical and morphological aspects of DMD (reviewed in (Gramolini & Jasmin, 1998; Jasmin *et al.*, 2002). Agrin intramuscular injection could regulate utrophin expression in *mdx* mice or, alternatively, agrin may stabilize the DAC and thus improve muscle strength in disease mice. In light of these points, future experiments should focus on assessing muscle fiber regeneration, damage and mechanical properties, in addition to determining the expression of utrophin in agrin injected muscles of *mdx* mice.

In conclusion, results presented here provide an explorative assessment of potential novel roles for agrin in skeletal muscles. The data presented serve as a survey of possible research targets and indicate that agrin may regulate muscle signaling. In this study, the results suggested that agrin regulates the activation of Akt signaling in adult, healthy muscles. In addition, a partial improvement of the dystrophic phenotype was observed in *mdx* mice administered with agrin. Since recent studies have shown that activation of Akt attenuates dystrophic symptoms (Blaauw *et al.*, 2008; Kim *et al.*, 2011), this path should be investigated in detail in *mdx* mice. Agrin signaling via Akt could be a novel therapeutic avenue for the treatment of DMD.

4.7 Future Directions

Currently, a project has been initiated that involves the blocking of agrin expression in skeletal muscles. The hypothesis is that blocking agrin expression will prevent or reduce muscle growth. Muscle growth can be induced using the functional overload model. Meanwhile, agrin expression can be reduced in skeletal muscles by electroporation of plasmids that would generate short hairpin RNAs (shRNA) that target agrin (McCroskery *et al.*, 2006; McCroskery *et al.*, 2009). Alternatively, the expression of agrin could be decreased via injection of an antibody against agrin (although preliminary experiments using this model lead to mice death).

As indicated previously, the involvement of agrin in the regulation of DMD pathology is an interesting research path. Agrin has the potential to promote expression of the dystrophin homologue utrophin (Gramolini *et al.*, 1998; Gramolini *et al.*, 1999) and in addition agrin can activate Akt signaling (this study). Both utrophin (reviewed in (Gramolini & Jasmin, 1998; Jasmin *et al.*, 2002) and Akt (Blaauw *et al.*, 2008; Kim *et al.*, 2011) are potential therapeutic targets for the treatment of DMD. The investigation of agrin roles in *mdx* mice is thus a particularly attractive research model.

Chapter 5: ***Conclusion***

Skeletal muscles play a central role in the overall health of individuals. Defects in muscles lead to various diseases, and in addition numerous disease symptoms include a progressive wasting of muscles called cachexia. A better understanding of muscle plasticity can help in the prevention and treatment of a vast number of diseases.

Skeletal muscle can adapt its properties to respond to various demands such as mechanical loads, neural activity, hormones circulation and availability of nutrients and/or growth factors. This ability of adult muscle to change in response to various stimuli is called muscle plasticity and it can lead to alterations in muscle fiber type, size and signaling. Furthermore, skeletal muscles are in continuous communication with nerves by means of the NMJ, and the properties of the motor neuron can be remodel to match the properties of the muscle fibers it innervates. Collectively, neuromuscular plasticity is influenced by both anterograde (from the nerve) and retrograde (from the muscle fiber) mechanisms illustrating the importance of the communication that occurs at the NMJ.

Animal models are frequently used to study molecular and cellular mechanisms that regulate muscle growth. The research presented in this thesis illustrates the use of diverse mouse models to explore various events that influence neuromuscular plasticity. In this first study, the adaptability of NMJ to muscle's signals is illustrated using transgenic mice displaying compromised calmodulin signaling in skeletal muscles. These mice adapt by changing the organization of AChRs at their NMJ. A change in density or structure of NMJ can remodel synaptic communication. Abnormally localized AChRs

could represent fragmented endplates mediated by a loss of nerve terminals followed by novel nerve sprouting. Furthermore, a dysregulation in synaptic communication leads to muscle disease, such as Myasthenia Gravis where a loss of AChR leads to muscle fatigue and wasting. In the second study, mice knockout for NFATc2 or NFATc3 are used. These mouse models demonstrate the importance of NFAT transcription factors in compensatory muscle growth and illustrate the ability of muscle to fine tune its growth response. This work also shows that signaling partners described to have important function in other tissues, can regulate muscle mass. A better understanding of the signaling that regulates muscle growth serves to identify therapeutic targets to improve deteriorating muscles mass observed in numerous diseases. Finally, the third study explored the roles of the nerve-derived trophic factor agrin in the modulation of muscle fiber mass. Agrin may regulate signaling pathways that mediate muscle growth or it could improve muscle contractile functions by stabilizing the DGC. A large number of muscle disorders, such as Duchenne Muscular Dystrophy or sarcopenia, are awaiting treatment and original research can help pinpoint novel beneficial therapeutic strategies.

Collectively, the research presented in this thesis illustrates the inter-dependence between the motor nerve and skeletal muscle fibers. In addition, this work highlights the complexity of skeletal muscle plasticity and shows that research in this field is an ongoing process. As new discoveries are made, new signaling targets are identified, novel links between signaling pathways emerge and the original roles for old signaling targets are revealed. The research in the field of neuromuscular plasticity has a double objective

of providing a better understanding of signaling pathways in skeletal muscles and identifying novel pharmacological targets for the treatment of neuromuscular disorders. Appropriate synaptic communication and normal muscle function are key aspects in the overall health and well-being of humans.

Statistical Analysis

Chapter 2: PCR

Group Statistics

Gene	Genotype	N	Mean	Std. Deviation	Std. Error Mean
HDAC4	WT	5	1.0000	.29536	.13209
	TG	5	1.0732	.13422	.06002
Dach2	WT	5	1.0000	.42455	.18986
	TG	5	1.0737	.19736	.08826
Mgn	WT	5	1.0000	.24936	.11152
	TG	5	.9012	.33058	.14784
AGR	WT	3	1.0000	.18047	.10419
	TG	4	.7341	.25136	.12568
MuSK	WT	3	1.0000	.24558	.14179
	TG	4	1.1226	.19054	.09527
NRG	WT	3	1.0000	.42430	.24497
	TG	4	1.0347	.20012	.10006
GABP	WT	3	1.0001	.36040	.20808
	TG	3	.9611	.13812	.07975
AChRalpha	WT	3	1.0000	.17670	.10202
	TG	4	1.0204	.27341	.13670
AChRgamma	WT	3	1.0000	.16402	.09470
	TG	4	1.0918	.18677	.09339
AChRepsilon	WT	3	1.0000	.17946	.10361
	TG	4	.8108	.30122	.15061

Independent Samples Test

		Levene's Test for		t-test for Equality of Means						
		Equality of Variances							95% Confidence Interval of the Difference	
		F	Sig.	t	df	Sig. (2-tailed)	Mean Difference	Std. Error Difference	Lower	Upper
HDAC4	Equal variances assumed	3.020	.120	-.505	8	.627	-.07323	.14509	-.40780	.26134
	Equal variances not assumed			-.505	5.584	.633	-.07323	.14509	-.43475	.28828
Dach2	Equal variances assumed	2.407	.159	-.352	8	.734	-.07367	.20938	-.55649	.40915
	Equal variances not assumed			-.352	5.652	.738	-.07367	.20938	-.59374	.44640
Mgn	Equal variances assumed	.155	.704	.533	8	.608	.09879	.18518	-.32825	.52582
	Equal variances not assumed			.533	7.439	.609	.09879	.18518	-.33392	.53149
AGR	Equal variances assumed	.257	.633	1.543	5	.184	.26595	.17237	-.17715	.70905
	Equal variances not assumed			1.629	4.999	.164	.26595	.16325	-.15373	.68563
MuSK	Equal variances assumed	.423	.544	-.749	5	.488	-.12256	.16365	-.54322	.29811
	Equal variances not assumed			-.717	3.710	.516	-.12256	.17082	-.61185	.36674
NRG	Equal variances assumed	4.299	.093	-.147	5	.889	-.03474	.23669	-.64318	.57370
	Equal variances not assumed			-.131	2.673	.905	-.03474	.26462	-.93817	.86868

GABP	Equal variances assumed	4.171	.111	.175	4	.870	.03897	.22284	-.57972	.65767
	Equal variances not assumed			.175	2.575	.874	.03897	.22284	-.74121	.81916
AChRalpha	Equal variances assumed	.657	.455	-.112	5	.915	-.02047	.18289	-.49061	.44966
	Equal variances not assumed			-.120	4.963	.909	-.02047	.17058	-.45993	.41899
AChRgamma	Equal variances assumed	1.162	.330	-.675	5	.529	-.09183	.13597	-.44134	.25768
	Equal variances not assumed			-.690	4.772	.522	-.09183	.13300	-.43868	.25502
AChRbeta	Equal variances assumed	2.634	.166	.955	5	.384	.18921	.19817	-.32021	.69863
	Equal variances not assumed			1.035	4.874	.349	.18921	.18281	-.28439	.66282

Chapter 2: Western Blotting

Group Statistics

	Genotype	N	Mean	Std. Deviation	Std. Error Mean
pCaMKII	SOL WT	3	.2111	.02155	.01244
	SOL TG	3	.1488	.02710	.01565
CaMKII	SOL WT	3	.2352	.07221	.04169
	SOL TG	3	.2477	.05618	.03244

Independent Samples Test

	Levene's Test for Equality of Variances	t-test for Equality of Means	
			95% Confidence Interval of the Difference

		F	Sig.	t	df	Sig. (2-tailed)	Mean Difference	Std. Error Difference	Lower	Upper
pCaMKII	Equal variances assumed	.146	.722	3.116	4	.036	.06230	.01999	.00679	.11781
	Equal variances not assumed			3.116	3.807	.038	.06230	.01999	.00567	.11893
CaMKII	Equal variances assumed	.254	.641	-.235	4	.825	-.01243	.05282	-.15909	.13423
	Equal variances not assumed			-.235	3.772	.826	-.01243	.05282	-.16266	.13779

Group Statistics

Genotype		N	Mean	Std. Deviation	Std. Error Mean
pCaMKII	EDL WT	3	.4398	.04666	.02694
	EDL TG	3	.3165	.10597	.06118
CaMKII	EDL WT	3	.3445	.11453	.06612
	EDL TG	3	.3069	.11390	.06576

Independent Samples Test

		Levene's Test for Equality of Variances		t-test for Equality of Means						
		F	Sig.	t	df	Sig. (2-tailed)	Mean Difference	Std. Error Difference	95% Confidence Interval of the Difference	
									Lower	Upper
pCaMKII	Equal variances assumed	2.480	.190	1.844	4	.139	.12327	.06685	-.06233	.30886
	Equal variances not assumed			1.844	2.747	.171	.12327	.06685	-.10098	.34751
CaMKII	Equal variances assumed	.001	.974	.403	4	.707	.03760	.09326	-.22132	.29652

Group Statistics

Genotype		N	Mean	Std. Deviation	Std. Error Mean					
pCaMKII	EDL WT	3	.4398	.04666	.02694					
	EDL TG	3	.3165	.10597	.06118					
CaMKII	EDL WT	3	.3445	.11453	.06612					
	EDL TG	3	.3165	.10597	.06118					
Equal variances not assumed				.403	4.000	.707	.03760	.09326	-.22132	.29652

Group Statistics

Genotype		N	Mean	Std. Deviation	Std. Error Mean
pERK1	SOL WT	3	.5179	.03731	.02154
	SOL TG	3	.7058	.12551	.07246
ERK1	SOL WT	3	.8937	.12331	.07119
	SOL TG	3	.9271	.10545	.06088
pERK2	SOL WT	3	.7978	.06000	.03464
	SOL TG	3	.9606	.17381	.10035
ERK2	SOL WT	3	.9996	.12355	.07133
	SOL TG	3	1.0355	.13157	.07596
pJNK	SOL WT	3	.6514	.13902	.08026
	SOL TG	3	.5039	.07491	.04325
JNK	SOL WT	3	.7476	.39373	.22732
	SOL TG	3	.4702	.05132	.02963
AChRalpha	SOL WT	3	.8614	.29267	.16897
	SOL TG	3	.8788	.21610	.12477

Independent Samples Test

	Levene's Test for Equality of Variances	t-test for Equality of Means
--	--	------------------------------

									95% Confidence Interval of the Difference	
		F	Sig.	t	df	Sig. (2-tailed)	Mean Difference	Std. Error Difference	Lower	Upper
pERK1	Equal variances assumed	4.390	.104	-2.485	4	.068	-.18787	.07560	-.39775	.02202
	Equal variances not assumed			-2.485	2.351	.112	-.18787	.07560	-.47077	.09503
ERK1	Equal variances assumed	.135	.732	-.357	4	.739	-.03340	.09367	-.29348	.22668
	Equal variances not assumed			-.357	3.906	.740	-.03340	.09367	-.29597	.22917
pERK2	Equal variances assumed	6.032	.070	-1.533	4	.200	-.16277	.10616	-.45752	.13198
	Equal variances not assumed			-1.533	2.470	.241	-.16277	.10616	-.54559	.22005
ERK2	Equal variances assumed	.119	.748	-.345	4	.748	-.03593	.10420	-.32525	.25338
	Equal variances not assumed			-.345	3.984	.748	-.03593	.10420	-.32570	.25383
pJNK	Equal variances assumed	1.975	.233	1.618	4	.181	.14753	.09117	-.10560	.40067
	Equal variances not assumed			1.618	3.071	.202	.14753	.09117	-.13885	.43392
JNK	Equal variances assumed	5.517	.079	1.210	4	.293	.27740	.22924	-.35908	.91388
	Equal variances not assumed			1.210	2.068	.346	.27740	.22924	-.67854	1.23334
AChRalpha	Equal variances assumed	.516	.512	-.083	4	.938	-.01737	.21005	-.60055	.56581

Group Statistics

Genotype		N	Mean	Std. Deviation	Std. Error Mean					
pERK1	SOL WT	3	.5179	.03731	.02154					
	SOL TG	3	.7058	.12551	.07246					
ERK1	SOL WT	3	.8937	.12331	.07119					
	SOL TG	3	.9271	.10545	.06088					
pERK2	SOL WT	3	.7978	.06000	.03464					
	SOL TG	3	.9606	.17381	.10035					
ERK2	SOL WT	3	.9996	.12355	.07133					
	SOL TG	3	1.0355	.13157	.07596					
pJNK	SOL WT	3	.6514	.13902	.08026					
	SOL TG	3	.5039	.07491	.04325					
JNK	SOL WT	3	.7476	.39373	.22732					
	SOL TG	3	.4702	.05132	.02963					
AChRalpha	SOL WT	3	.8614	.29267	.16897					
Equal variances not assumed				-.083	3.681	.938	-.01737	.21005	-.62102	.58629

Chapter 3: Muscle Weights

Descriptives

Relative Muscle Weight

	N	Mean	Std. Deviation	Std. Error	95% Confidence Interval for Mean		Minimum	Maximum
					Lower Bound	Upper Bound		
					WT CTL	6		
WT 7dOV	3	.8533	.00577	.00333	.8390	.8677	.85	.86
WT 28dOV	4	1.2000	.09309	.04655	1.0519	1.3481	1.07	1.29
NFATc2-/- CTL	7	.5171	.04271	.01614	.4776	.5566	.45	.58

NFATc2-/- 7dOV	3	.6833	.14012	.08090	.3353	1.0314	.57	.84
NFATc2-/- 28dOV	4	.8775	.12393	.06196	.6803	1.0747	.80	1.06
NFATc3-/- CTL	5	.5020	.02950	.01319	.4654	.5386	.46	.53
NFATc3-/- 7dOV	3	.7967	.09018	.05207	.5726	1.0207	.71	.89
NFATc3-/- 28dOV	3	.9600	.19157	.11060	.4841	1.4359	.83	1.18
Total	38	.7303	.24077	.03906	.6511	.8094	.45	1.29

Test of Homogeneity of Variances

Relative Muscle Weight

Levene Statistic	df1	df2	Sig.
4.423	8	29	.001

Robust Tests of Equality of Means

Relative Muscle Weight

	Statistic ^a	df1	df2	Sig.
Welch	114.999	8	9.771	.000

Post Hoc Tests

Multiple Comparisons

Dependent Variable:Relative Muscle Weight

(I) Genotype	(J) Genotype	Mean Difference (I-J)	Std. Error	Sig.	95% Confidence Interval		
					Lower Bound	Upper Bound	
Dunnett T3	WT CTL	WT 7dOV	-.28167 [*]	.01572	.000	-.3608	-.2026
		WT 28dOV	-.62833 [*]	.04902	.004	-.9331	-.3236
		NFATc2-/- CTL	.05452	.02229	.495	-.0352	.1443
		NFATc2-/- 7dOV	-.11167	.08234	.936	-.9240	.7007
		NFATc2-/- 28dOV	-.30583	.06384	.125	-.7255	.1138
		NFATc3-/- CTL	.06967	.02025	.147	-.0160	.1553
		NFATc3-/- 7dOV	-.22500	.05429	.252	-.7093	.2593
		NFATc3-/- 28dOV	-.38833	.11167	.370	-1.5316	.7550
	WT 7dOV	WT CTL	.28167 [*]	.01572	.000	.2026	.3608

	WT 28dOV	-.34667*	.04667	.044	-.6788	-.0146
	NFATc2-/- CTL	.33619*	.01648	.000	.2589	.4135
	NFATc2-/- 7dOV	.17000	.08097	.708	-.6940	1.0340
	NFATc2-/- 28dOV	-.02417	.06205	1.000	-.4673	.4190
	NFATc3-/- CTL	.35133*	.01361	.000	.2762	.4264
	NFATc3-/- 7dOV	.05667	.05217	.980	-.4969	.6102
	NFATc3-/- 28dOV	-.10667	.11065	.992	-1.2897	1.0764
WT 28dOV	WT CTL	.62833*	.04902	.004	.3236	.9331
	WT 7dOV	.34667*	.04667	.044	.0146	.6788
	NFATc2-/- CTL	.68286*	.04927	.003	.3805	.9853
	NFATc2-/- 7dOV	.51667	.09333	.086	-.1061	1.1395
	NFATc2-/- 28dOV	.32250	.07750	.105	-.0638	.7088
	NFATc3-/- CTL	.69800*	.04838	.003	.3870	1.0090
	NFATc3-/- 7dOV	.40333*	.06984	.041	.0200	.7867
	NFATc3-/- 28dOV	.24000	.12000	.739	-.6959	1.1759
NFATc2-/- CTL	WT CTL	-.05452	.02229	.495	-.1443	.0352
	WT 7dOV	-.33619*	.01648	.000	-.4135	-.2589
	WT 28dOV	-.68286*	.04927	.003	-.9853	-.3805
	NFATc2-/- 7dOV	-.16619	.08249	.735	-.9734	.6411
	NFATc2-/- 28dOV	-.36036	.06403	.078	-.7778	.0571
	NFATc3-/- CTL	.01514	.02085	1.000	-.0707	.1009
	NFATc3-/- 7dOV	-.27952	.05451	.162	-.7577	.1987
	NFATc3-/- 28dOV	-.44286	.11178	.299	-1.5821	.6963
NFATc2-/- 7dOV	WT CTL	.11167	.08234	.936	-.7007	.9240
	WT 7dOV	-.17000	.08097	.708	-1.0340	.6940
	WT 28dOV	-.51667	.09333	.086	-1.1395	.1061
	NFATc2-/- CTL	.16619	.08249	.735	-.6411	.9734
	NFATc2-/- 28dOV	-.19417	.10190	.782	-.7860	.3977
	NFATc3-/- CTL	.18133	.08197	.671	-.6443	1.0070

	NFATc3-/- 7dOV	-.11333	.09621	.983	-.7404	.5137
	NFATc3-/- 28dOV	-.27667	.13703	.732	-1.1286	.5753
NFATc2-/- 28dOV	WT CTL	.30583	.06384	.125	-.1138	.7255
	WT 7dOV	.02417	.06205	1.000	-.4190	.4673
	WT 28dOV	-.32250	.07750	.105	-.7088	.0638
	NFATc2-/- CTL	.36036	.06403	.078	-.0571	.7778
	NFATc2-/- 7dOV	.19417	.10190	.782	-.3977	.7860
	NFATc3-/- CTL	.37550	.06335	.072	-.0500	.8010
	NFATc3-/- 7dOV	.08083	.08094	.998	-.3428	.5044
	NFATc3-/- 28dOV	-.08250	.12678	1.000	-.9403	.7753
NFATc3-/- CTL	WT CTL	-.06967	.02025	.147	-.1553	.0160
	WT 7dOV	-.35133	.01361	.000	-.4264	-.2762
	WT 28dOV	-.69800	.04838	.003	-1.0090	-.3870
	NFATc2-/- CTL	-.01514	.02085	1.000	-.1009	.0707
	NFATc2-/- 7dOV	-.18133	.08197	.671	-1.0070	.6443
	NFATc2-/- 28dOV	-.37550	.06335	.072	-.8010	.0500
	NFATc3-/- 7dOV	-.29467	.05371	.152	-.7951	.2058
	NFATc3-/- 28dOV	-.45800	.11139	.283	-1.6119	.6959
NFATc3-/- 7dOV	WT CTL	.22500	.05429	.252	-.2593	.7093
	WT 7dOV	-.05667	.05217	.980	-.6102	.4969
	WT 28dOV	-.40333	.06984	.041	-.7867	-.0200
	NFATc2-/- CTL	.27952	.05451	.162	-.1987	.7577
	NFATc2-/- 7dOV	.11333	.09621	.983	-.5137	.7404
	NFATc2-/- 28dOV	-.08083	.08094	.998	-.5044	.3428
	NFATc3-/- CTL	.29467	.05371	.152	-.2058	.7951
	NFATc3-/- 28dOV	-.16333	.12225	.952	-1.0791	.7524
NFATc3-/- 28dOV	WT CTL	.38833	.11167	.370	-.7550	1.5316
	WT 7dOV	.10667	.11065	.992	-1.0764	1.2897
	WT 28dOV	-.24000	.12000	.739	-1.1759	.6959

NFATc2-/- CTL	.44286	.11178	.299	-.6963	1.5821
NFATc2-/- 7dOV	.27667	.13703	.732	-.5753	1.1286
NFATc2-/- 28dOV	.08250	.12678	1.000	-.7753	.9403
NFATc3-/- CTL	.45800	.11139	.283	-.6959	1.6119
NFATc3-/- 7dOV	.16333	.12225	.952	-.7524	1.0791

Chapter 3: Fibers Size

Descriptives

Fiber Size

	N	Mean	Std. Deviation	Std. Error	95% Confidence Interval for Mean		Minimum	Maximum
					Lower Bound	Upper Bound		
					WT CTL	3		
WT OV	4	2403.75	201.888	100.944	2082.50	2725.00	2200	2622
NFATc2-/- CTL	4	1636.75	179.673	89.836	1350.85	1922.65	1383	1798
NFATc2-/- OV	4	1803.00	299.744	149.872	1326.04	2279.96	1590	2244
NFATc3-/- CTL	3	1889.00	318.679	183.989	1097.36	2680.64	1559	2195
NFATc3-/- OV	3	2283.00	176.570	101.943	1844.38	2721.62	2139	2480
Total	21	1960.19	374.348	81.689	1789.79	2130.59	1341	2622

Test of Homogeneity of Variances

Fiber Size

Levene Statistic	df1	df2	Sig.
.704	5	15	.629

ANOVA

Fiber Size

	Sum of Squares	df	Mean Square	F	Sig.
Between Groups	1754735.738	5	350947.148	5.023	.007
Within Groups	1047987.500	15	69865.833		
Total	2802723.238	20			

Post Hoc Tests

Multiple Comparisons

Dependent Variable:Fiber Size

	(I) Group	(J) Group	Mean Difference (I-J)	Std. Error	Sig.	95% Confidence Interval	
						Lower Bound	Upper Bound
Tukey HSD	WT CTL	WT OV	-645.750	201.879	.055	-1301.65	10.15
		NFATc2-/- CTL	121.250	201.879	.989	-534.65	777.15
		NFATc2-/- OV	-45.000	201.879	1.000	-700.90	610.90
		NFATc3-/- CTL	-131.000	215.818	.989	-832.18	570.18
		NFATc3-/- OV	-525.000	215.818	.206	-1226.18	176.18
	WT OV	WT CTL	645.750	201.879	.055	-10.15	1301.65
		NFATc2-/- CTL	767.000	186.903	.010	159.76	1374.24
		NFATc2-/- OV	600.750	186.903	.053	-6.49	1207.99
		NFATc3-/- CTL	514.750	201.879	.171	-141.15	1170.65
		NFATc3-/- OV	120.750	201.879	.990	-535.15	776.65
	NFATc2-/- CTL	WT CTL	-121.250	201.879	.989	-777.15	534.65
		WT OV	-767.000	186.903	.010	-1374.24	-159.76
		NFATc2-/- OV	-166.250	186.903	.943	-773.49	440.99
		NFATc3-/- CTL	-252.250	201.879	.806	-908.15	403.65
		NFATc3-/- OV	-646.250	201.879	.055	-1302.15	9.65
	NFATc2-/- OV	WT CTL	45.000	201.879	1.000	-610.90	700.90
		WT OV	-600.750	186.903	.053	-1207.99	6.49
		NFATc2-/- CTL	166.250	186.903	.943	-440.99	773.49
		NFATc3-/- CTL	-86.000	201.879	.998	-741.90	569.90
		NFATc3-/- OV	-480.000	201.879	.225	-1135.90	175.90
NFATc3-/- CTL	WT CTL	131.000	215.818	.989	-570.18	832.18	
	WT OV	-514.750	201.879	.171	-1170.65	141.15	
	NFATc2-/- CTL	252.250	201.879	.806	-403.65	908.15	

	NFATc2-/- OV	86.000	201.879	.998	-569.90	741.90
	NFATc3-/- OV	-394.000	215.818	.480	-1095.18	307.18
NFATc3-/- OV	WT CTL	525.000	215.818	.206	-176.18	1226.18
	WT OV	-120.750	201.879	.990	-776.65	535.15
	NFATc2-/- CTL	646.250	201.879	.055	-9.65	1302.15
	NFATc2-/- OV	480.000	201.879	.225	-175.90	1135.90
	NFATc3-/- CTL	394.000	215.818	.480	-307.18	1095.18

Chapter 3: Fiber Number

Descriptives

Fiber Number

	N	Mean	Std. Deviation	Std. Error	95% Confidence Interval for Mean		Minimum	Maximum
					Lower Bound	Upper Bound		
					WT CTL	3		
WT OV	4	864.25	62.334	31.167	765.06	963.44	786	938
NFATc2-/- CTL	4	730.75	114.284	57.142	548.90	912.60	637	890
NFATc2-/- OV	4	1016.25	93.578	46.789	867.35	1165.15	921	1145
NFATc3-/- CTL	3	444.67	58.046	33.513	300.47	588.86	394	508
NFATc3-/- OV	3	891.67	76.350	44.081	702.00	1081.33	805	949
Total	21	782.48	199.891	43.620	691.49	873.47	394	1145

Test of Homogeneity of Variances

Fiber Number

Levene Statistic	df1	df2	Sig.
.564	5	15	.726

ANOVA

Fiber Number

	Sum of Squares	df	Mean Square	F	Sig.
Between Groups	679656.988	5	135931.398	17.066	.000

Within Groups	119472.250	15	7964.817		
Total	799129.238	20			

Post Hoc Tests

Multiple Comparisons

Dependent Variable:Fiber Number

(I) Group	(J) Group	Mean Difference (I-J)	Std. Error	Sig.	95% Confidence Interval		
					Lower Bound	Upper Bound	
Tukey HSD	WT CTL	WT OV	-204.917	68.163	.078	-426.37	16.54
		NFATc2-/- CTL	-71.417	68.163	.894	-292.87	150.04
		NFATc2-/- OV	-356.917 [*]	68.163	.001	-578.37	-135.46
		NFATc3-/- CTL	214.667	72.869	.087	-22.08	451.42
		NFATc3-/- OV	-232.333	72.869	.056	-469.08	4.42
WT OV	WT CTL	WT CTL	204.917	68.163	.078	-16.54	426.37
		NFATc2-/- CTL	133.500	63.106	.331	-71.53	338.53
		NFATc2-/- OV	-152.000	63.106	.214	-357.03	53.03
		NFATc3-/- CTL	419.583 [*]	68.163	.000	198.13	641.04
		NFATc3-/- OV	-27.417	68.163	.998	-248.87	194.04
NFATc2-/- CTL	WT CTL	WT CTL	71.417	68.163	.894	-150.04	292.87
		WT OV	-133.500	63.106	.331	-338.53	71.53
		NFATc2-/- OV	-285.500 [*]	63.106	.004	-490.53	-80.47
		NFATc3-/- CTL	286.083 [*]	68.163	.008	64.63	507.54
		NFATc3-/- OV	-160.917	68.163	.231	-382.37	60.54
NFATc2-/- OV	WT CTL	WT CTL	356.917 [*]	68.163	.001	135.46	578.37
		WT OV	152.000	63.106	.214	-53.03	357.03
		NFATc2-/- CTL	285.500 [*]	63.106	.004	80.47	490.53
		NFATc3-/- CTL	571.583 [*]	68.163	.000	350.13	793.04
		NFATc3-/- OV	124.583	68.163	.478	-96.87	346.04
NFATc3-/- CTL	WT CTL	WT CTL	-214.667	72.869	.087	-451.42	22.08

	WT OV	-419.583 [*]	68.163	.000	-641.04	-198.13
	NFATc2-/- CTL	-286.083 [*]	68.163	.008	-507.54	-64.63
	NFATc2-/- OV	-571.583 [*]	68.163	.000	-793.04	-350.13
	NFATc3-/- OV	-447.000 [*]	72.869	.000	-683.75	-210.25
NFATc3-/- OV	WT CTL	232.333	72.869	.056	-4.42	469.08
	WT OV	27.417	68.163	.998	-194.04	248.87
	NFATc2-/- CTL	160.917	68.163	.231	-60.54	382.37
	NFATc2-/- OV	-124.583	68.163	.478	-346.04	96.87
	NFATc3-/- CTL	447.000 [*]	72.869	.000	210.25	683.75

Chapter 3: Analysis of MyHC IIa fibers

Descriptives

MyHC IIa Size

	N	Mean	Std. Deviation	Std. Error	95% Confidence Interval for Mean		Minimum	Maximum
					Lower Bound	Upper Bound		
					WT CTL	3		
WT 28dOV	4	2079.75	319.265	159.633	1571.73	2587.77	1805	2531
NFATc2-/- CTL	4	944.50	166.442	83.221	679.65	1209.35	743	1097
NFTAc2-/- 28dOV	4	1479.75	180.469	90.234	1192.58	1766.92	1221	1641
NFATc3-/- CTL	3	1113.33	63.815	36.844	954.81	1271.86	1042	1165
NFATc3-/- 28dOV	3	1995.67	120.608	69.633	1696.06	2295.27	1888	2126
Total	21	1476.76	491.219	107.193	1253.16	1700.36	743	2531

Test of Homogeneity of Variances

MyHC IIa Size

Levene Statistic	df1	df2	Sig.
1.962	5	15	.143

ANOVA

MyHC Ila Size

	Sum of Squares	df	Mean Square	F	Sig.
Between Groups	3984837.976	5	796967.595	14.213	.000
Within Groups	841081.833	15	56072.122		
Total	4825919.810	20			

Post Hoc Tests

Multiple Comparisons

Dependent Variable: MyHC Ila Size

(I) Group	(J) Group	Mean Difference (I-J)	Std. Error	Sig.	95% Confidence Interval	
					Lower Bound	Upper Bound
Tukey HSD WT CTL	WT 28dOV	-856.750*	180.856	.003	-1444.34	-269.16
	NFATc2-/- CTL	278.500	180.856	.646	-309.09	866.09
	NFTAc2-/- 28dOV	-256.750	180.856	.716	-844.34	330.84
	NFATc3-/- CTL	109.667	193.343	.992	-518.50	737.83
	NFATc3-/- 28dOV	-772.667*	193.343	.012	-1400.83	-144.50
WT 28dOV	WT CTL	856.750*	180.856	.003	269.16	1444.34
	NFATc2-/- CTL	1135.250*	167.440	.000	591.24	1679.26
	NFTAc2-/- 28dOV	600.000*	167.440	.027	55.99	1144.01
	NFATc3-/- CTL	966.417*	180.856	.001	378.82	1554.01
	NFATc3-/- 28dOV	84.083	180.856	.997	-503.51	671.68
NFATc2-/- CTL	WT CTL	-278.500	180.856	.646	-866.09	309.09
	WT 28dOV	-1135.250*	167.440	.000	-1679.26	-591.24
	NFTAc2-/- 28dOV	-535.250	167.440	.055	-1079.26	8.76
	NFATc3-/- CTL	-168.833	180.856	.931	-756.43	418.76
	NFATc3-/- 28dOV	-1051.167*	180.856	.000	-1638.76	-463.57
NFTAc2-/- 28dOV	WT CTL	256.750	180.856	.716	-330.84	844.34
	WT 28dOV	-600.000*	167.440	.027	-1144.01	-55.99

	NFATc2-/- CTL	535.250	167.440	.055	-8.76	1079.26
	NFATc3-/- CTL	366.417	180.856	.373	-221.18	954.01
	NFATc3-/- 28dOV	-515.917	180.856	.102	-1103.51	71.68
NFATc3-/- CTL	WT CTL	-109.667	193.343	.992	-737.83	518.50
	WT 28dOV	-966.417*	180.856	.001	-1554.01	-378.82
	NFATc2-/- CTL	168.833	180.856	.931	-418.76	756.43
	NFTAc2-/- 28dOV	-366.417	180.856	.373	-954.01	221.18
	NFATc3-/- 28dOV	-882.333*	193.343	.004	-1510.50	-254.17
NFATc3-/- 28dOV	WT CTL	772.667*	193.343	.012	144.50	1400.83
	WT 28dOV	-84.083	180.856	.997	-671.68	503.51
	NFATc2-/- CTL	1051.167*	180.856	.000	463.57	1638.76
	NFTAc2-/- 28dOV	515.917	180.856	.102	-71.68	1103.51
	NFATc3-/- CTL	882.333*	193.343	.004	254.17	1510.50

Descriptives

MyHC IIa Percentage

	N	Mean	Std. Deviation	Std. Error	95% Confidence Interval for Mean		Minimum	Maximum
					Lower Bound	Upper Bound		
					WT CTL	3		
WT 28dOV	4	61.00	6.831	3.416	50.13	71.87	52	68
NFATc2-/- CTL	4	35.25	13.500	6.750	13.77	56.73	18	46
NFTAc2-/- 28dOV	4	57.25	9.215	4.608	42.59	71.91	47	66
NFATc3-/- CTL	3	41.67	15.631	9.025	2.84	80.50	25	56
NFATc3-/- 28dOV	3	52.67	24.007	13.860	-6.97	112.30	29	77
Total	21	49.48	16.711	3.647	41.87	57.08	18	77

Test of Homogeneity of Variances

MyHC IIa Percentage

Levene Statistic	df1	df2	Sig.
1.560	5	15	.231

ANOVA

MyHC IIa Percentage

	Sum of Squares	df	Mean Square	F	Sig.
Between Groups	1809.738	5	361.948	1.438	.267
Within Groups	3775.500	15	251.700		
Total	5585.238	20			

Chapter 3: Analysis of MyHC IIb fibers

Descriptives

MyHC IIb Size

	N	Mean	Std. Deviation	Std. Error	95% Confidence Interval for Mean		Minimum	Maximum
					Lower Bound	Upper Bound		
					WT CTL	3		
WT 28dOV	4	3426.50	542.245	271.123	2563.67	4289.33	2914	4190
NFATc2-/- CTL	4	2109.75	242.625	121.313	1723.68	2495.82	1916	2460
NFTAc2-/- 28dOV	4	2378.75	241.956	120.978	1993.74	2763.76	2247	2741
NFATc3-/- CTL	3	2658.00	298.608	172.402	1916.22	3399.78	2335	2924
NFATc3-/- 28dOV	3	3208.67	223.768	129.193	2652.79	3764.54	3075	3467
Total	21	2683.71	588.759	128.478	2415.71	2951.71	1916	4190

Test of Homogeneity of Variances

MyHC IIb Size

Levene Statistic	df1	df2	Sig.
.716	5	15	.621

ANOVA

MyHC Ilb Size

	Sum of Squares	df	Mean Square	F	Sig.
Between Groups	5028211.119	5	1005642.224	7.920	.001
Within Groups	1904531.167	15	126968.744		
Total	6932742.286	20			

Post Hoc Tests

Multiple Comparisons

Dependent Variable: MyHC Ilb Size

(I) Group	(J) Group	Mean Difference (I-J)	Std. Error	Sig.	95% Confidence Interval	
					Lower Bound	Upper Bound
Tukey HSD WT CTL	WT 28dOV	-1060.500*	272.149	.015	-1944.70	-176.30
	NFATc2-/- CTL	256.250	272.149	.929	-627.95	1140.45
	NFTAc2-/- 28dOV	-12.750	272.149	1.000	-896.95	871.45
	NFATc3-/- CTL	-292.000	290.940	.910	-1237.25	653.25
	NFATc3-/- 28dOV	-842.667	290.940	.095	-1787.92	102.59
WT 28dOV	WT CTL	1060.500*	272.149	.015	176.30	1944.70
	NFATc2-/- CTL	1316.750*	251.961	.001	498.14	2135.36
	NFTAc2-/- 28dOV	1047.750*	251.961	.009	229.14	1866.36
	NFATc3-/- CTL	768.500	272.149	.107	-115.70	1652.70
	NFATc3-/- 28dOV	217.833	272.149	.963	-666.37	1102.04
NFATc2-/- CTL	WT CTL	-256.250	272.149	.929	-1140.45	627.95
	WT 28dOV	-1316.750*	251.961	.001	-2135.36	-498.14
	NFTAc2-/- 28dOV	-269.000	251.961	.887	-1087.61	549.61
	NFATc3-/- CTL	-548.250	272.149	.379	-1432.45	335.95
	NFATc3-/- 28dOV	-1098.917*	272.149	.011	-1983.12	-214.71
NFTAc2-/- 28dOV	WT CTL	12.750	272.149	1.000	-871.45	896.95
	WT 28dOV	-1047.750*	251.961	.009	-1866.36	-229.14
	NFATc2-/- CTL	269.000	251.961	.887	-549.61	1087.61

	NFATc3-/- CTL	-279.250	272.149	.902	-1163.45	604.95
	NFATc3-/- 28dOV	-829.917	272.149	.072	-1714.12	54.29
NFATc3-/- CTL	WT CTL	292.000	290.940	.910	-653.25	1237.25
	WT 28dOV	-768.500	272.149	.107	-1652.70	115.70
	NFATc2-/- CTL	548.250	272.149	.379	-335.95	1432.45
	NFTAc2-/- 28dOV	279.250	272.149	.902	-604.95	1163.45
	NFATc3-/- 28dOV	-550.667	290.940	.443	-1495.92	394.59
NFATc3-/- 28dOV	WT CTL	842.667	290.940	.095	-102.59	1787.92
	WT 28dOV	-217.833	272.149	.963	-1102.04	666.37
	NFATc2-/- CTL	1098.917	272.149	.011	214.71	1983.12
	NFTAc2-/- 28dOV	829.917	272.149	.072	-54.29	1714.12
	NFATc3-/- CTL	550.667	290.940	.443	-394.59	1495.92

Descriptives

MyHC IIb Percentage

	N	Mean	Std. Deviation	Std. Error	95% Confidence Interval for Mean		Minimum	Maximum
					Lower Bound	Upper Bound		
					WT CTL	3		
WT 28dOV	4	10.50	6.191	3.096	.65	20.35	5	19
NFATc2-/- CTL	4	40.75	19.363	9.681	9.94	71.56	23	58
NFTAc2-/- 28dOV	4	24.00	10.801	5.401	6.81	41.19	15	38
NFATc3-/- CTL	3	28.00	10.583	6.110	1.71	54.29	20	40
NFATc3-/- 28dOV	3	23.00	11.136	6.429	-4.66	50.66	13	35
Total	21	25.57	16.482	3.597	18.07	33.07	5	59

Test of Homogeneity of Variances

MyHC IIb Percentage

Levene Statistic	df1	df2	Sig.
5.658	5	15	.004

Robust Tests of Equality of Means

MyHC IIb Percentage

	Statistic ^a	df1	df2	Sig.
Welch	2.281	5	6.284	.167

Chapter 3: PCR

Descriptives

MyHC IIa

	N	Mean	Std. Deviation	Std. Error	95% Confidence Interval for Mean		Minimum	Maximum
					Lower Bound	Upper Bound		
					WT CTL	3		
WT 7dOV	3	1.7996	.43826	.25303	.7109	2.8883	1.30	2.11
NFATc2 ^{-/-} CTL	3	2.2801	.71211	.41114	.5111	4.0490	1.48	2.86
NFATc2 ^{-/-} 7dOV	3	2.0279	.79692	.46010	.0482	4.0075	1.11	2.57
NFATc3 ^{-/-} CTL	3	2.2445	.61708	.35627	.7116	3.7775	1.62	2.86
NFATc3 ^{-/-} 7dOV	3	1.7750	.56608	.32683	.3687	3.1812	1.44	2.43
Total	18	2.0188	.58766	.13851	1.7266	2.3110	1.11	2.86

Test of Homogeneity of Variances

MyHC IIa

Levene Statistic	df1	df2	Sig.
.428	5	12	.821

ANOVA

MyHC IIa

	Sum of Squares	df	Mean Square	F	Sig.

Between Groups	.684	5	.137	.316	.894
Within Groups	5.187	12	.432		
Total	5.871	17			

Descriptives

MyHC IIb

	N	Mean	Std. Deviation	Std. Error	95% Confidence Interval for Mean		Minimum	Maximum
					Lower Bound	Upper Bound		
					WT CTL	3		
WT 7dOV	3	.4870	.18648	.10766	.0237	.9502	.29	.66
NFATc2-/- CTL	3	.9739	.76771	.44324	-.9332	2.8810	.22	1.75
NFATc2-/- 7dOV	3	.3618	.22167	.12798	-.1888	.9125	.11	.53
NFATc3-/- CTL	3	.9551	1.05378	.60840	-1.6626	3.5729	.17	2.15
NFATc3-/- 7dOV	3	.4024	.26542	.15324	-.2569	1.0618	.13	.66
Total	18	.7309	.61470	.14489	.4252	1.0366	.11	2.15

Test of Homogeneity of Variances

MyHC IIb

Levene Statistic	df1	df2	Sig.
2.747	5	12	.070

ANOVA

MyHC IIb

	Sum of Squares	df	Mean Square	F	Sig.
Between Groups	1.913	5	.383	1.018	.449
Within Groups	4.511	12	.376		
Total	6.424	17			

Descriptives

Tnls

	N	Mean	Std. Deviation	Std. Error	95% Confidence Interval for Mean		Minimum	Maximum
					Lower Bound	Upper Bound		
					WT CTL	3		
WT 7dOV	3	1.9996	1.32512	.76506	-1.2921	5.2914	.95	3.49
NFATc2-/- CTL	3	.5501	.63934	.36912	-1.0381	2.1383	.17	1.29
NFATc2-/- 7dOV	3	1.7446	1.91822	1.10748	-3.0206	6.5097	.33	3.93
NFATc3-/- CTL	3	.2701	.11430	.06599	-.0138	.5541	.15	.37
NFATc3-/- 7dOV	3	1.5501	1.48259	.85597	-2.1329	5.2330	.39	3.22
Total	18	1.1011	1.20589	.28423	.5015	1.7008	.13	3.93

Test of Homogeneity of Variances

Tnls

Levene Statistic	df1	df2	Sig.
4.376	5	12	.017

Robust Tests of Equality of Means

Tnls

	Statistic ^a	df1	df2	Sig.
Welch	1.324	5	4.903	.385

Descriptives

NFATc1

	N	Mean	Std. Deviation	Std. Error	95% Confidence Interval for Mean		Minimum	Maximum
					Lower Bound	Upper Bound		
					WT CTL	3		
WT 7dOV	3	1.5797	.09236	.05332	1.3503	1.8091	1.48	1.67
NFATc2-/- CTL	3	1.8999	.23111	.13343	1.3258	2.4740	1.75	2.17

NFATc2-/- 7dOV	3	1.5745	.25109	.14497	.9507	2.1982	1.43	1.86
NFATc3-/- CTL	3	1.5644	.34671	.20017	.7031	2.4256	1.23	1.93
NFATc3-/- 7dOV	3	1.5891	.09519	.05496	1.3527	1.8256	1.48	1.67
Total	18	1.6512	.22739	.05360	1.5382	1.7643	1.23	2.17

Test of Homogeneity of Variances

NFATc1

Levene Statistic	df1	df2	Sig.
1.391	5	12	.295

ANOVA

NFATc1

	Sum of Squares	df	Mean Square	F	Sig.
Between Groups	.260	5	.052	1.007	.455
Within Groups	.619	12	.052		
Total	.879	17			

Descriptives

NFATc2

	N	Mean	Std. Deviation	Std. Error	95% Confidence Interval for Mean		Minimum	Maximum
					Lower Bound	Upper Bound		
					WT CTL	3		
WT 7dOV	3	1.0971	.09206	.05315	.8684	1.3258	1.02	1.20
NFATc2-/- CTL	3	.7902	.39137	.22596	-.1821	1.7624	.35	1.10
NFATc2-/- 7dOV	3	.7884	.45559	.26303	-.3433	1.9202	.35	1.26
NFATc3-/- CTL	3	.7402	.66261	.38256	-.9058	2.3862	.18	1.47
NFATc3-/- 7dOV	3	.6315	.35142	.20289	-.2414	1.5045	.27	.97

Descriptives

NFATc2

	N	Mean	Std. Deviation	Std. Error	95% Confidence Interval for Mean		Minimum	Maximum
					Lower Bound	Upper Bound		
					WT CTL	3		
WT 7dOV	3	1.0971	.09206	.05315	.8684	1.3258	1.02	1.20
NFATc2-/- CTL	3	.7902	.39137	.22596	-.1821	1.7624	.35	1.10
NFATc2-/- 7dOV	3	.7884	.45559	.26303	-.3433	1.9202	.35	1.26
NFATc3-/- CTL	3	.7402	.66261	.38256	-.9058	2.3862	.18	1.47
NFATc3-/- 7dOV	3	.6315	.35142	.20289	-.2414	1.5045	.27	.97
Total	18	.9057	.44664	.10527	.6836	1.1279	.18	1.81

Test of Homogeneity of Variances

NFATc2

Levene Statistic	df1	df2	Sig.
1.310	5	12	.323

ANOVA

NFATc2

	Sum of Squares	df	Mean Square	F	Sig.
Between Groups	1.194	5	.239	1.305	.325
Within Groups	2.197	12	.183		
Total	3.391	17			

Descriptives

NFATc3

	N	Mean	Std. Deviation	Std. Error	95% Confidence Interval for Mean		Minimum	Maximum
					Lower Bound	Upper Bound		

WT CTL	3	.6413	.05750	.03320	.4984	.7841	.58	.70
WT 7dOV	3	.5076	.04693	.02709	.3911	.6242	.48	.56
NFATc2-/- CTL	3	.7174	.28080	.16212	.0199	1.4150	.51	1.04
NFATc2-/- 7dOV	3	.4957	.28280	.16327	-.2068	1.1983	.29	.82
NFATc3-/- CTL	3	.3177	.09897	.05714	.0718	.5635	.23	.42
NFATc3-/- 7dOV	3	.3488	.08717	.05033	.1322	.5653	.29	.45
Total	18	.5048	.20769	.04895	.4015	.6080	.23	1.04

Test of Homogeneity of Variances

NFATc3

Levene Statistic	df1	df2	Sig.
4.911	5	12	.011

Robust Tests of Equality of Means

NFATc3

	Statistic ^a	df1	df2	Sig.
Welch	5.207	5	5.406	.041

Post Hoc Tests

Multiple Comparisons

Dependent Variable: NFATc3

(I) Group	(J) Group	Mean Difference (I-J)	Std. Error	Sig.	95% Confidence Interval		
					Lower Bound	Upper Bound	
Dunnett T3	WT CTL	WT 7dOV	.13361	.04285	.239	-.0929	.3601
		NFATc2-/- CTL	-.07617	.16548	1.000	-1.4761	1.3238
		NFATc2-/- 7dOV	.14551	.16661	.981	-1.2656	1.5567
		NFATc3-/- CTL	.32358	.06608	.087	-.0695	.7166
		NFATc3-/- 7dOV	.29246	.06029	.079	-.0479	.6329
WT 7dOV	WT CTL	-.13361	.04285	.239	-.3601	.0929	
		NFATc2-/- CTL	-.20978	.16437	.886	-1.6414	1.2218
		NFATc2-/- 7dOV	.01190	.16550	1.000	-1.4308	1.4546

	NFATc3-/- CTL	.18997	.06324	.311	-.2216	.6015
	NFATc3-/- 7dOV	.15885	.05716	.350	-.1927	.5104
NFATc2-/- CTL	WT CTL	.07617	.16548	1.000	-1.3238	1.4761
	WT 7dOV	.20978	.16437	.886	-1.2218	1.6414
	NFATc2-/- 7dOV	.22168	.23009	.981	-.9670	1.4104
	NFATc3-/- CTL	.39975	.17190	.505	-.8626	1.6621
	NFATc3-/- 7dOV	.36863	.16975	.558	-.9324	1.6697
NFATc2-/- 7dOV	WT CTL	-.14551	.16661	.981	-1.5567	1.2656
	WT 7dOV	-.01190	.16550	1.000	-1.4546	1.4308
	NFATc2-/- CTL	-.22168	.23009	.981	-1.4104	.9670
	NFATc3-/- CTL	.17807	.17298	.958	-1.0955	1.4516
	NFATc3-/- 7dOV	.14695	.17085	.984	-1.1654	1.4593
NFATc3-/- CTL	WT CTL	-.32358	.06608	.087	-.7166	.0695
	WT 7dOV	-.18997	.06324	.311	-.6015	.2216
	NFATc2-/- CTL	-.39975	.17190	.505	-1.6621	.8626
	NFATc2-/- 7dOV	-.17807	.17298	.958	-1.4516	1.0955
	NFATc3-/- 7dOV	-.03112	.07614	1.000	-.4281	.3659
NFATc3-/- 7dOV	WT CTL	-.29246	.06029	.079	-.6329	.0479
	WT 7dOV	-.15885	.05716	.350	-.5104	.1927
	NFATc2-/- CTL	-.36863	.16975	.558	-1.6697	.9324
	NFATc2-/- 7dOV	-.14695	.17085	.984	-1.4593	1.1654
	NFATc3-/- CTL	.03112	.07614	1.000	-.3659	.4281

Descriptives

NFATc4

	N	Mean	Std. Deviation	Std. Error	95% Confidence Interval for Mean		Minimum	Maximum
					Lower Bound	Upper Bound		
					WT CTL	3		

WT 7dOV	3	1.4535	.17955	.10366	1.0075	1.8995	1.25	1.58
NFATc2-/- CTL	3	.7882	.50879	.29375	-.4757	2.0521	.26	1.27
NFATc2-/- 7dOV	3	1.0078	.91951	.53088	-1.2764	3.2920	.39	2.06
NFATc3-/- CTL	3	.4593	.41810	.24139	-.5794	1.4979	.17	.94
NFATc3-/- 7dOV	3	.6113	.54834	.31658	-.7509	1.9734	.25	1.24
Total	18	.8617	.55352	.13047	.5864	1.1369	.17	2.06

Test of Homogeneity of Variances

NFATc4

Levene Statistic	df1	df2	Sig.
2.805	5	12	.067

ANOVA

NFATc4

	Sum of Squares	df	Mean Square	F	Sig.
Between Groups	1.805	5	.361	1.273	.337
Within Groups	3.403	12	.284		
Total	5.209	17			

Descriptives

Pax7

	N	Mean	Std. Deviation	Std. Error	95% Confidence Interval for Mean		Minimum	Maximum
					Lower Bound	Upper Bound		
					WT CTL	3		
WT 7dOV	3	1.2585	.34455	.19893	.4026	2.1144	.94	1.62
NFATc2-/- CTL	3	.7583	.27745	.16019	.0690	1.4475	.51	1.06
NFATc2-/- 7dOV	3	.8883	.15187	.08768	.5111	1.2656	.71	.99
NFATc3-/- CTL	2	.7352	.18685	.13212	-.9436	2.4140	.60	.87

NFATc3-/- 7dOV	3	1.0381	.26049	.15039	.3910	1.6852	.83	1.33
Total	17	.9470	.27837	.06752	.8039	1.0901	.51	1.62

Test of Homogeneity of Variances

Pax7

Levene Statistic	df1	df2	Sig.
.472	5	11	.790

ANOVA

Pax7

	Sum of Squares	df	Mean Square	F	Sig.
Between Groups	.523	5	.105	1.608	.237
Within Groups	.716	11	.065		
Total	1.240	16			

Descriptives

Myf5

	N	Mean	Std. Deviation	Std. Error	95% Confidence Interval for Mean		Minimum	Maximum
					Lower Bound	Upper Bound		
					WT CTL	3		
WT 7dOV	3	1.4918	.52584	.30359	.1856	2.7981	1.04	2.07
NFATc2-/- CTL	3	.7026	.45708	.26390	-.4329	1.8381	.40	1.23
NFATc2-/- 7dOV	3	1.0183	.67495	.38968	-.6584	2.6949	.26	1.55
NFATc3-/- CTL	3	.7624	.06431	.03713	.6027	.9222	.69	.81
NFATc3-/- 7dOV	3	1.4059	.49678	.28681	.1718	2.6399	.93	1.92
Total	18	1.0440	.50038	.11794	.7952	1.2928	.26	2.07

Test of Homogeneity of Variances

Myf5

Levene Statistic	df1	df2	Sig.
1.824	5	12	.182

ANOVA

Myf5

	Sum of Squares	df	Mean Square	F	Sig.
Between Groups	1.662	5	.332	1.537	.251
Within Groups	2.595	12	.216		
Total	4.256	17			

Descriptives

MyoD

	N	Mean	Std. Deviation	Std. Error	95% Confidence Interval for Mean		Minimum	Maximum
					Lower Bound	Upper Bound		
					WT CTL	3		
WT 7dOV	3	.7291	.09047	.05223	.5043	.9538	.64	.82
NFATc2-/- CTL	3	.5103	.11967	.06909	.2131	.8076	.42	.65
NFATc2-/- 7dOV	3	.6774	.13775	.07953	.3352	1.0196	.58	.84
NFATc3-/- CTL	2	.6415	.44350	.31360	-3.3432	4.6262	.33	.96
NFATc3-/- 7dOV	3	.4396	.04540	.02621	.3268	.5524	.41	.49
Total	17	.6121	.17759	.04307	.5208	.7034	.33	.96

Test of Homogeneity of Variances

MyoD

Levene Statistic	df1	df2	Sig.
13.302	5	11	.000

Robust Tests of Equality of Means

MyoD

	Statistic ^a	df1	df2	Sig.
Welch	4.322	5	4.321	.082

Descriptives

Myogenin

	N	Mean	Std. Deviation	Std. Error	95% Confidence Interval for Mean		Minimum	Maximum
					Lower Bound	Upper Bound		
					WT CTL	3		
WT 7dOV	3	1.6539	.57196	.33022	.2331	3.0747	1.09	2.24
NFATc2-/- CTL	3	.7238	.54871	.31680	-.6393	2.0868	.28	1.34
NFATc2-/- 7dOV	3	1.5083	1.26092	.72799	-1.6240	4.6406	.72	2.96
NFATc3-/- CTL	3	.3417	.33676	.19443	-.4949	1.1782	.00	.67
NFATc3-/- 7dOV	3	.8238	.53297	.30771	-.5001	2.1478	.33	1.39
Total	18	.9523	.75183	.17721	.5785	1.3262	.00	2.96

Test of Homogeneity of Variances

Myogenin

Levene Statistic	df1	df2	Sig.
2.534	5	12	.087

ANOVA

Myogenin

	Sum of Squares	df	Mean Square	F	Sig.
Between Groups	3.981	5	.796	1.698	.210
Within Groups	5.628	12	.469		
Total	9.609	17			

Chapter 3: Nuclear Localization

Wild type

Descriptives

	N	Mean	Std. Deviation	Std. Error	95% Confidence Interval for Mean		Minimum	Maximum
					Lower Bound	Upper Bound		
NFATc1 WT CTL	3	1.0200	.06557	.03786	.8571	1.1829	.96	1.09
WT 7dOV	3	1.3400	.03000	.01732	1.2655	1.4145	1.31	1.37
Total	6	1.1800	.18111	.07394	.9899	1.3701	.96	1.37
NFATc2 WT CTL	3	.9967	.48336	.27907	-.2041	2.1974	.47	1.42
WT 7dOV	3	1.3033	.28711	.16576	.5901	2.0166	1.06	1.62
Total	6	1.1500	.39324	.16054	.7373	1.5627	.47	1.62
NFATc3 WT CTL	3	1.0000	.52849	.30512	-.3128	2.3128	.68	1.61
WT 7dOV	3	1.0033	.23714	.13691	.4143	1.5924	.75	1.22
Total	6	1.0017	.36636	.14956	.6172	1.3861	.68	1.61
NFATc4 WT CTL	3	.9833	.20841	.12032	.4656	1.5010	.80	1.21
WT 7dOV	3	1.1433	.36460	.21050	.2376	2.0491	.75	1.47
Total	6	1.0633	.27969	.11418	.7698	1.3569	.75	1.47

Test of Homogeneity of Variances

	Levene Statistic	df1	df2	Sig.
NFATc1	1.600	1	4	.275
NFATc2	.915	1	4	.393
NFATc3	3.796	1	4	.123
NFATc4	.950	1	4	.385

ANOVA

	Sum of Squares	df	Mean Square	F	Sig.
NFATc1 Between Groups	.154	1	.154	59.077	.002
Within Groups	.010	4	.003		
Total	.164	5			

NFATc2	Between Groups	.141	1	.141	.893	.398
	Within Groups	.632	4	.158		
	Total	.773	5			
NFATc3	Between Groups	.000	1	.000	.000	.993
	Within Groups	.671	4	.168		
	Total	.671	5			
NFATc4	Between Groups	.038	1	.038	.435	.545
	Within Groups	.353	4	.088		
	Total	.391	5			

NFATc2-/-

Descriptives

	N	Mean	Std. Deviation	Std. Error	95% Confidence Interval for Mean		Minimum	Maximum
					Lower Bound	Upper Bound		
					NFATc1 NFATc2-/- CTL	3		
NFATc2-/- 7dOV	3	1.5300	.06557	.03786	1.3671	1.6929	1.46	1.59
Total	6	1.2750	.54782	.22365	.7001	1.8499	.17	1.59
NFATc2 NFATc2-/- CTL	3	1.0233	.44837	.25887	-.0905	2.1371	.61	1.50
NFATc2-/- 7dOV	3	.6800	.43486	.25106	-.4002	1.7602	.34	1.17
Total	6	.8517	.43751	.17861	.3925	1.3108	.34	1.50
NFATc3 NFATc2-/- CTL	3	.9700	.46776	.27006	-.1920	2.1320	.69	1.51
NFATc2-/- 7dOV	3	1.0767	.58398	.33716	-.3740	2.5274	.64	1.74
Total	6	1.0233	.47681	.19466	.5230	1.5237	.64	1.74

NFATc4 NFATc2-/- CTL	3	.9833	.22189	.12811	.4321	1.5345	.80	1.23
NFATc2-/- 7dOV	3	1.1167	.31565	.18224	.3326	1.9008	.91	1.48
Total	6	1.0500	.25472	.10399	.7827	1.3173	.80	1.48

Test of Homogeneity of Variances

	Levene Statistic	df1	df2	Sig.
NFATc1	11.545	1	4	.027
NFATc2	.003	1	4	.959
NFATc3	.281	1	4	.624
NFATc4	.894	1	4	.398

ANOVA

		Sum of Squares	df	Mean Square	F	Sig.
NFATc1	Between Groups	.390	1	.390	1.405	.301
	Within Groups	1.110	4	.278		
	Total	1.501	5			
NFATc2	Between Groups	.177	1	.177	.906	.395
	Within Groups	.780	4	.195		
	Total	.957	5			
NFATc3	Between Groups	.017	1	.017	.061	.817
	Within Groups	1.120	4	.280		
	Total	1.137	5			
NFATc4	Between Groups	.027	1	.027	.358	.582
	Within Groups	.298	4	.074		
	Total	.324	5			

Robust Tests of Equality of Means

		Statistic ^a	df1	df2	Sig.
NFATc1	Welch	1.405	1	2.031	.356
NFATc2	Welch	.906	1	3.996	.395

NFATc3	Welch	.061	1	3.818	.818
NFATc4	Welch	.358	1	3.589	.585

NFATc3-/-

Descriptives

	N	Mean	Std. Deviation	Std. Error	95% Confidence Interval for Mean		Minimum	Maximum
					Lower Bound	Upper Bound		
					NFATc1 NFATc3-/- CTL	3		
NFATc3-/- 7dOV	3	1.1567	.07024	.04055	.9822	1.3311	1.09	1.23
Total	6	1.0733	.10690	.04364	.9612	1.1855	.95	1.23
NFATc2 NFATc3-/- CTL	3	.9800	.13115	.07572	.6542	1.3058	.84	1.10
NFATc3-/- 7dOV	3	1.0833	.06506	.03756	.9217	1.2450	1.02	1.15
Total	6	1.0317	.10852	.04430	.9178	1.1456	.84	1.15
NFATc3 NFATc3-/- CTL	3	.9900	.21284	.12288	.4613	1.5187	.76	1.18
NFATc3-/- 7dOV	3	.8867	.09866	.05696	.6416	1.1317	.82	1.00
Total	6	.9383	.15880	.06483	.7717	1.1050	.76	1.18
NFATc4 NFATc3-/- CTL	3	1.0067	.18717	.10806	.5417	1.4716	.87	1.22
NFATc3-/- 7dOV	3	1.4400	.07000	.04041	1.2661	1.6139	1.37	1.51
Total	6	1.2233	.26890	.10978	.9411	1.5055	.87	1.51

Test of Homogeneity of Variances

	Levene Statistic	df1	df2	Sig.
NFATc1	.136	1	4	.731
NFATc2	1.327	1	4	.314
NFATc3	1.620	1	4	.272
NFATc4	4.330	1	4	.106

ANOVA

		Sum of Squares	Df	Mean Square	F	Sig.
NFATc1	Between Groups	.042	1	.042	10.776	.030
	Within Groups	.015	4	.004		
	Total	.057	5			
NFATc2	Between Groups	.016	1	.016	1.495	.289
	Within Groups	.043	4	.011		
	Total	.059	5			
NFATc3	Between Groups	.016	1	.016	.582	.488
	Within Groups	.110	4	.028		
	Total	.126	5			
NFATc4	Between Groups	.282	1	.282	14.107	.020
	Within Groups	.080	4	.020		
	Total	.362	5			

Chapter 3: Western Blotting

Descriptives

pAKT

	N	Mean	Std. Deviation	Std. Error	95% Confidence Interval for Mean		Minimum	Maximum
					Lower Bound	Upper Bound		
					WT CTL	3		
WT 7dOV	3	1.3100	.39947	.23063	.3176	2.3023	.85	1.57
NFATc2-/- CTL	3	.8425	.30226	.17451	.0916	1.5933	.59	1.18
NFATc2-/- 7dOV	3	1.2575	.48792	.28170	.0455	2.4696	.73	1.69
NFATc3-/- CTL	3	1.0658	.45049	.26009	-.0533	2.1849	.57	1.45
NFATc3-/- 7dOV	3	1.2235	.66370	.38319	-.4252	2.8722	.65	1.95

Descriptives

pAKT

	N	Mean	Std. Deviation	Std. Error	95% Confidence Interval for Mean		Minimum	Maximum
					Lower Bound	Upper Bound		
					WT CTL	3		
WT 7dOV	3	1.3100	.39947	.23063	.3176	2.3023	.85	1.57
NFATc2-/- CTL	3	.8425	.30226	.17451	.0916	1.5933	.59	1.18
NFATc2-/- 7dOV	3	1.2575	.48792	.28170	.0455	2.4696	.73	1.69
NFATc3-/- CTL	3	1.0658	.45049	.26009	-.0533	2.1849	.57	1.45
NFATc3-/- 7dOV	3	1.2235	.66370	.38319	-.4252	2.8722	.65	1.95
Total	18	1.0600	.43914	.10351	.8416	1.2784	.57	1.95

Test of Homogeneity of Variances

pAKT

Levene Statistic	df1	df2	Sig.
1.773	5	12	.193

ANOVA

pAKT

	Sum of Squares	Df	Mean Square	F	Sig.
Between Groups	1.005	5	.201	1.061	.428
Within Groups	2.273	12	.189		
Total	3.278	17			

Descriptives

AKT

	N	Mean	Std. Deviation	Std. Error	95% Confidence Interval for Mean		Minimum	Maximum
					Lower Bound	Upper Bound		

WT CTL	3	1.0556	.19975	.11532	.5594	1.5518	.87	1.27
WT 7dOV	3	1.5712	.48768	.28156	.3597	2.7827	1.16	2.11
NFATc2-/- CTL	3	1.0642	.17061	.09850	.6404	1.4880	.87	1.19
NFATc2-/- 7dOV	3	1.4178	.45754	.26416	.2812	2.5544	.92	1.82
NFATc3-/- CTL	3	1.1514	.30967	.17879	.3822	1.9207	.80	1.38
NFATc3-/- 7dOV	3	1.4351	.54303	.31352	.0862	2.7841	.81	1.79
Total	18	1.2826	.38636	.09107	1.0904	1.4747	.80	2.11

Test of Homogeneity of Variances

AKT

Levene Statistic	df1	df2	Sig.
1.700	5	12	.209

ANOVA

AKT

	Sum of Squares	df	Mean Square	F	Sig.
Between Groups	.724	5	.145	.958	.480
Within Groups	1.814	12	.151		
Total	2.538	17			

Chapter 4: Agrin in adult healthy mice

Group Statistics

	Mice Category	N	Mean	Std. Deviation	Std. Error Mean
Relative Muscle Weight	Adult PBS	3	187.00	13.892	8.021
	Adult AGR	3	189.67	3.055	1.764

Independent Samples Test

	Levene's Test for Equality of Variances	t-test for Equality of Means
--	---	------------------------------

								95% Confidence Interval of the Difference		
		F	Sig.	t	Df	Sig. (2-tailed)	Mean Difference	Std. Error Difference	Lower	Upper
Relative Muscle Weight	Equal variances assumed	8.818	.041	-.325	4	.762	-2.667	8.212	-25.468	20.135
	Equal variances not assumed			-.325	2.193	.774	-2.667	8.212	-35.183	29.850

Group Statistics

Mice Category		N	Mean	Std. Deviation	Std. Error Mean
Size MyHC IIa	Adult PBS	2	1112.50	289.207	204.500
	Adult AGR	3	897.67	36.116	20.851

Independent Samples Test

		Levene's Test for Equality of Variances		t-test for Equality of Means						
				95% Confidence Interval of the Difference						
		F	Sig.	t	Df	Sig. (2-tailed)	Mean Difference	Std. Error Difference	Lower	Upper
Size MyHC IIa	Equal variances assumed	382.610	.000	1.388	3	.259	214.833	154.784	-277.759	707.425
	Equal variances not assumed			1.045	1.021	.483	214.833	205.560	-2274.333	2704.000

Group Statistics

Mice Category		N	Mean	Std. Deviation	Std. Error Mean
---------------	--	---	------	----------------	-----------------

Size MyHC IIb	Adult PBS	3	3578.33	369.522	213.343
	Adult AGR	3	3308.00	280.343	161.856

Independent Samples Test

		Levene's Test for Equality of Variances		t-test for Equality of Means						
									95% Confidence Interval of the Difference	
		F	Sig.	t	Df	Sig. (2-tailed)	Mean Difference	Std. Error Difference	Lower	Upper
Size MyHC IIb	Equal variances assumed	.179	.694	1.009	4	.370	270.333	267.792	-473.178	1013.844
	Equal variances not assumed			1.009	3.729	.374	270.333	267.792	-494.947	1035.614

Group Statistics

Mice Category		N	Mean	Std. Deviation	Std. Error Mean
Percentage MyHC IIa	Adult PBS	3	6.33	7.767	4.485
	Adult AGR	3	2.67	1.155	.667

Independent Samples Test

		Levene's Test for Equality of Variances		t-test for Equality of Means						
									95% Confidence Interval of the Difference	
		F	Sig.	t	Df	Sig. (2-tailed)	Mean Difference	Std. Error Difference	Lower	Upper

		F	Sig.	t	Df	Sig. (2-tailed)	Mean Difference	Std. Error Difference	Lower	Upper
Percentage MyHC IIa	Equal variances assumed	6.890	.059	.809	4	.464	3.667	4.534	-8.921	16.255
	Equal variances not assumed			.809	2.088	.500	3.667	4.534	-15.071	22.404

Group Statistics

Mice Category	N	Mean	Std. Deviation	Std. Error Mean
Percentage MyHC IIb Adult PBS	3	38.00	5.568	3.215
Adult AGR	3	41.67	10.408	6.009

Independent Samples Test

		Levene's Test for Equality of Variances		t-test for Equality of Means						
									95% Confidence Interval of the Difference	
		F	Sig.	t	Df	Sig. (2-tailed)	Mean Difference	Std. Error Difference	Lower	Upper
Percentage MyHC IIb	Equal variances assumed	1.741	.257	-.538	4	.619	-3.667	6.815	-22.588	15.255
	Equal variances not assumed			-.538	3.058	.627	-3.667	6.815	-25.124	17.791

Group Statistics

Mice Category	N	Mean	Std. Deviation	Std. Error Mean
pAKT Adult PBS	3	.6257	.15581	.08996

	Adult AGR	3	.9923	.27832	.16069
Total AKT	Adult PBS	3	.4747	.14650	.08458
	Adult AGR	3	.7627	.35205	.20325
pS6K	Adult PBS	3	.4920	.16865	.09737
	Adult AGR	3	.5090	.09657	.05575
Total S6K	Adult PBS	3	.7297	.23276	.13438
	Adult AGR	3	.9760	.18385	.10614

Independent Samples Test

		Levene's Test for Equality of Variances		t-test for Equality of Means						
								95% Confidence Interval of the Difference		
		F	Sig.	t	df	Sig. (2-tailed)	Mean Difference	Std. Error Difference	Lower	Upper
pAKT	Equal variances assumed	1.323	.314	-1.991	4	.117	-.36667	.18416	-.87797	.14463
	Equal variances not assumed			-1.991	3.141	.136	-.36667	.18416	-.93809	.20475
Total AKT	Equal variances assumed	3.751	.125	-1.308	4	.261	-.28800	.22015	-.89924	.32324
	Equal variances not assumed			-1.308	2.673	.292	-.28800	.22015	-1.03978	.46378
pS6K	Equal variances assumed	1.340	.311	-.152	4	.887	-.01700	.11220	-.32853	.29453
	Equal variances not assumed			-.152	3.184	.889	-.01700	.11220	-.36268	.32868
Total S6K	Equal variances assumed	.456	.536	-1.438	4	.224	-.24633	.17125	-.72179	.22912
	Equal variances not assumed			-1.438	3.796	.227	-.24633	.17125	-.73202	.23935

Chapter 4: Characterization of sarcopenia

Group Statistics

Mice Category		N	Mean	Std. Deviation	Std. Error Mean
Body Weight	Young	3	26.000	2.2913	1.3229
	Old	3	32.733	4.8336	2.7907

Independent Samples Test

		Levene's Test for Equality of Variances		t-test for Equality of Means						
									95% Confidence Interval of the Difference	
		F	Sig.	t	df	Sig. (2-tailed)	Mean Difference	Std. Error Difference	Lower	Upper
Body Weight	Equal variances assumed	1.714	.261	-2.180	4	.095	-6.7333	3.0883	-15.3079	1.8412
	Equal variances not assumed			-2.180	2.856	.122	-6.7333	3.0883	-16.8489	3.3823

Group Statistics

Mice Category		N	Mean	Std. Deviation	Std. Error Mean
Absolute Muscle Weight	Young	3	46.900	4.8962	2.8268
	Old	3	42.700	3.1749	1.8330

Independent Samples Test

		Levene's Test for Equality of Variances		t-test for Equality of Means						
									95% Confidence Interval of the Difference	
		F	Sig.	t	df	Sig. (2-tailed)	Mean Difference	Std. Error Difference	Lower	Upper

		F	Sig.	t	df	Sig. (2-tailed)	Mean Difference	Std. Error Difference	Lower	Upper
Absolute Muscle Weight	Equal variances assumed	.723	.443	1.247	4	.281	4.2000	3.3691	-5.1541	13.5541
	Equal variances not assumed			1.247	3.429	.291	4.2000	3.3691	-5.8013	14.2013

Group Statistics

		Mice Category	N	Mean	Std. Deviation	Std. Error Mean
Relative Muscle Weight		Young	3	180.33	2.887	1.667
		Old	3	131.33	10.693	6.173

Independent Samples Test

		Levene's Test for Equality of Variances		t-test for Equality of Means						
									95% Confidence Interval of the Difference	
		F	Sig.	t	df	Sig. (2-tailed)	Mean Difference	Std. Error Difference	Lower	Upper
Relative Muscle Weight	Equal variances assumed	7.797	.049	7.663	4	.002	49.000	6.394	31.246	66.754
	Equal variances not assumed			7.663	2.290	.011	49.000	6.394	24.570	73.430

Group Statistics

		Mice Category	N	Mean	Std. Deviation	Std. Error Mean
Mean Fiber Size		Young	3	1674.55	136.824	78.995

Group Statistics

	Mice Category	N	Mean	Std. Deviation	Std. Error Mean
Mean Fiber Size	Young	3	1674.55	136.824	78.995
	Old	3	1154.41	65.863	38.026

Independent Samples Test

		Levene's Test for Equality of Variances		t-test for Equality of Means						
								95% Confidence Interval of the Difference		
		F	Sig.	t	df	Sig. (2-tailed)	Mean Difference	Std. Error Difference	Lower	Upper
Mean Fiber Size	Equal variances assumed	.944	.386	5.933	4	.004	520.137	87.671	276.723	763.552
	Equal variances not assumed			5.933	2.880	.011	520.137	87.671	234.413	805.862

Chapter 4: Agrin in sarcopenia

Group Statistics

	Mice Category	N	Mean	Std. Deviation	Std. Error Mean
Relative Muscle Weight	Old PBS	6	130.17	11.771	4.806
	Old AGR	3	131.00	13.892	8.021

Independent Samples Test

		Levene's Test for Equality of Variances		t-test for Equality of Means					

								95% Confidence Interval of the Difference		
		F	Sig.	t	df	Sig. (2-tailed)	Mean Difference	Std. Error Difference	Lower	Upper
Relative Muscle Weight	Equal variances assumed	.103	.757	-.095	7	.927	-.833	8.778	-21.591	19.924
	Equal variances not assumed			-.089	3.513	.934	-.833	9.350	-28.278	26.611

Group Statistics

Mice Category	N	Mean	Std. Deviation	Std. Error Mean
pAKT Old PBS	3	.5627	.06357	.03670
Old AGR	3	.6140	.03236	.01868
Total AKT Old PBS	3	.5720	.22188	.12810
Old AGR	3	.5643	.24553	.14176
pS6K Old PBS	3	.4033	.14066	.08121
Old AGR	3	.4473	.17957	.10367
Total S6K Old PBS	3	.8073	.05181	.02991
Old AGR	3	.6957	.18874	.10897

Independent Samples Test

		Levene's Test for Equality of Variances		t-test for Equality of Means						
								95% Confidence Interval of the Difference		
		F	Sig.	t	df	Sig. (2-tailed)	Mean Difference	Std. Error Difference	Lower	Upper

pAKT	Equal variances assumed	2.588	.183	-1.246	4	.281	-.05133	.04118	-.16568	.06301
	Equal variances not assumed			-1.246	2.971	.302	-.05133	.04118	-.18312	.08046
Total AKT	Equal variances assumed	.094	.775	.040	4	.970	.00767	.19106	-.52281	.53815
	Equal variances not assumed			.040	3.960	.970	.00767	.19106	-.52495	.54029
pS6K	Equal variances assumed	.465	.533	-.334	4	.755	-.04400	.13169	-.40964	.32164
	Equal variances not assumed			-.334	3.783	.756	-.04400	.13169	-.41806	.33006
Total S6K	Equal variances assumed	4.536	.100	.988	4	.379	.11167	.11300	-.20207	.42540
	Equal variances not assumed			.988	2.300	.415	.11167	.11300	-.31858	.54192

Chapter 4: Characterization of mdx mice

Group Statistics

Mice Category	N	Mean	Std. Deviation	Std. Error Mean	
< 1000	Wild-type	3	7.88	2.309	1.333
	Dystrophic	3	22.53	7.765	4.483
1000 - 2000	Wild-type	3	41.15	9.201	5.312
	Dystrophic	3	31.69	2.168	1.252
2000 - 3000	Wild-type	3	18.77	2.138	1.235
	Dystrophic	3	20.16	2.233	1.289
3000 - 4000	Wild-type	3	20.26	4.589	2.649
	Dystrophic	3	13.58	8.402	4.851
> 4000	Wild-type	3	11.95	6.069	3.504

Group Statistics

Mice Category		N	Mean	Std. Deviation	Std. Error Mean
< 1000	Wild-type	3	7.88	2.309	1.333
	Dystrophic	3	22.53	7.765	4.483
1000 - 2000	Wild-type	3	41.15	9.201	5.312
	Dystrophic	3	31.69	2.168	1.252
2000 - 3000	Wild-type	3	18.77	2.138	1.235
	Dystrophic	3	20.16	2.233	1.289
3000 - 4000	Wild-type	3	20.26	4.589	2.649
	Dystrophic	3	13.58	8.402	4.851
> 4000	Wild-type	3	11.95	6.069	3.504
	Dystrophic	3	12.04	6.481	3.742

Independent Samples Test

		Levene's Test for Equality of Variances		t-test for Equality of Means						
								95% Confidence Interval of the Difference		
		F	Sig.	t	df	Sig. (2-tailed)	Mean Difference	Std. Error Difference	Lower	Upper
< 1000	Equal variances assumed	6.985	.057	-3.132	4	.035	-14.650	4.677	-27.636	-1.664
	Equal variances not assumed			-3.132	2.351	.072	-14.650	4.677	-32.153	2.853
1000 - 2000	Equal variances assumed	8.681	.042	1.733	4	.158	9.460	5.457	-5.692	24.613
	Equal variances not assumed			1.733	2.221	.213	9.460	5.457	-11.915	30.836
2000 - 3000	Equal variances assumed	.013	.915	-.784	4	.477	-1.399	1.785	-6.355	3.557

	Equal variances not assumed			-0.784	3.993	.477	-1.399	1.785	-6.359	3.560
3000 - 4000	Equal variances assumed	1.995	.231	1.208	4	.294	6.677	5.527	-8.668	22.023
	Equal variances not assumed			1.208	3.096	.311	6.677	5.527	-10.609	23.963
> 4000	Equal variances assumed	.020	.895	-0.017	4	.987	-0.089	5.126	-14.322	14.144
	Equal variances not assumed			-0.017	3.983	.987	-0.089	5.126	-14.346	14.169

Group Statistics

Mice Category		N	Mean	Std. Deviation	Std. Error Mean
Coefficient Variation	Wild-type	3	.4869	.02217	.01280
	Dystrophic	3	.6891	.05448	.03146

Independent Samples Test

		Levene's Test for Equality of Variances		t-test for Equality of Means						
									95% Confidence Interval of the Difference	
		F	Sig.	t	df	Sig. (2-tailed)	Mean Difference	Std. Error Difference	Lower	Upper
Coefficient Variation	Equal variances assumed	3.617	.130	-5.955	4	.004	-.20223	.03396	-.29652	-.10794
	Equal variances not assumed			-5.955	2.645	.013	-.20223	.03396	-.31900	-.08545

Chapter 4: Agrin in mdx mice

Group Statistics

Mice Category	N	Mean	Std. Deviation	Std. Error Mean	
< 1000	MDX PBS	3	22.53	7.765	4.483
	MDX AGR	3	32.51	17.707	10.223
1000 - 2000	MDX PBS	3	31.69	2.168	1.252
	MDX AGR	3	32.04	5.507	3.179
2000 - 3000	MDX PBS	3	20.16	2.233	1.289
	MDX AGR	3	16.07	7.010	4.047
3000 - 4000	MDX PBS	3	13.58	8.402	4.851
	MDX AGR	3	7.32	2.813	1.624
> 4000	MDX PBS	3	12.04	6.481	3.742
	MDX AGR	3	12.07	5.711	3.297

Independent Samples Test

		Levene's Test for Equality of Variances		t-test for Equality of Means						
									95% Confidence Interval of the Difference	
		F	Sig.	t	df	Sig. (2-tailed)	Mean Difference	Std. Error Difference	Lower	Upper
< 1000	Equal variances assumed	3.281	.144	-.894	4	.422	-9.974	11.163	-40.967	21.019
	Equal variances not assumed			-.894	2.742	.443	-9.974	11.163	-47.468	27.520
1000 - 2000	Equal variances assumed	1.865	.244	-.103	4	.923	-.351	3.417	-9.838	9.135

	Equal variances not assumed			-.103	2.605	.926	-.351	3.417	-12.219	11.517
2000 - 3000	Equal variances assumed	4.150	.111	.965	4	.389	4.098	4.248	-7.695	15.892
	Equal variances not assumed			.965	2.402	.421	4.098	4.248	-11.540	19.737
3000 - 4000	Equal variances assumed	5.036	.088	1.224	4	.288	6.259	5.115	-7.943	20.462
	Equal variances not assumed			1.224	2.443	.326	6.259	5.115	-12.337	24.855
> 4000	Equal variances assumed	.000	.993	-.006	4	.995	-.032	4.987	-13.880	13.815
	Equal variances not assumed			-.006	3.938	.995	-.032	4.987	-13.967	13.902

Group Statistics

Mice Category	N	Mean	Std. Deviation	Std. Error Mean
Coefficient Variation MDX PBS	3	.6891	.05448	.03146
MDX AGR	3	.7872	.10927	.06309

Independent Samples Test

		Levene's Test for Equality of Variances		t-test for Equality of Means						
								95% Confidence Interval of the Difference		
		F	Sig.	t	df	Sig. (2-tailed)	Mean Difference	Std. Error Difference	Lower	Upper
Coefficient Variation	Equal variances assumed	2.565	.184	-1.392	4	.236	-.09812	.07050	-.29385	.09761

Group Statistics

Mice Category		N	Mean	Std. Deviation	Std. Error Mean				
Coefficient Variation	MDX PBS	3	.6891	.05448	.03146				
Equal variances assumed			-1.392	2.937	.260	-.09812	.07050	-.32524	.12899
Equal variances not assumed									

Group Statistics

Mice Category		N	Mean	Std. Deviation	Std. Error Mean
Central Nuclei	Mdx PBS	3	66.00	5.568	3.215
	Mdx AGR	3	56.33	1.155	.667

Independent Samples Test

		Levene's Test for Equality of Variances		t-test for Equality of Means						
								95% Confidence Interval of the Difference		
		F	Sig.	t	df	Sig. (2-tailed)	Mean Difference	Std. Error Difference	Lower	Upper
Central Nuclei	Equal variances assumed	4.062	.114	2.945	4	.042	9.667	3.283	.552	18.782
	Equal variances not assumed			2.945	2.172	.089	9.667	3.283	-3.441	22.774

References

- Abbott KL, Friday BB, Thaloor D, Murphy TJ & Pavlath GK. (1998). Activation and cellular localization of the cyclosporine A-sensitive transcription factor NF-AT in skeletal muscle cells. *Mol Biol Cell* **9**, 2905-2916.
- Al-Shanti N & Stewart CE. (2009). Ca²⁺/calmodulin-dependent transcriptional pathways: potential mediators of skeletal muscle growth and development. *Biol Rev Camb Philos Soc* **84**, 637-652.
- Angus LM, Chakkalakal JV, Mejat A, Eibl JK, Belanger G, Megeney LA, Chin ER, Schaeffer L, Michel RN & Jasmin BJ. (2005). Calcineurin-NFAT signaling, together with GABP and peroxisome PGC-1 {alpha}, drives utrophin gene expression at the neuromuscular junction. *Am J Physiol Cell Physiol* **289**, C908-917.
- Antonio J & Gonyea WJ. (1993). Skeletal muscle fiber hyperplasia. *Med Sci Sports Exerc* **25**, 1333-1345.
- Apel ED, Roberds SL, Campbell KP & Merlie JP. (1995). Rapsyn may function as a link between the acetylcholine receptor and the agrin-binding dystrophin-associated glycoprotein complex. *Neuron* **15**, 115-126.
- Armand AS, Bourajjaj M, Martinez-Martinez S, el Azzouzi H, da Costa Martins PA, Hatzis P, Seidler T, Redondo JM & De Windt LJ. (2008). Cooperative synergy between NFAT and MyoD regulates myogenin expression and myogenesis. *J Biol Chem* **283**, 29004-29010.
- Armstrong RB, Marum P, Tullson P & Saubert CWt. (1979). Acute hypertrophic response of skeletal muscle to removal of synergists. *J Appl Physiol* **46**, 835-842.
- Balagopal P, Rooyackers OE, Adey DB, Ades PA & Nair KS. (1997). Effects of aging on in vivo synthesis of skeletal muscle myosin heavy-chain and sarcoplasmic protein in humans. *Am J Physiol* **273**, E790-800.
- Balice-Gordon RJ & Lichtman JW. (1993). In vivo observations of pre- and postsynaptic changes during the transition from multiple to single innervation at developing neuromuscular junctions. *J Neurosci* **13**, 834-855.
- Bandi E, Jevsek M, Mars T, Jurdana M, Formaggio E, Sciancalepore M, Fumagalli G, Grubic Z, Ruzzier F & Lorenzon P. (2008). Neural agrin controls maturation of the excitation-contraction coupling mechanism in human myotubes developing in vitro. *Am J Physiol Cell Physiol* **294**, C66-73.
- Bartoli M, Ramarao MK & Cohen JB. (2001). Interactions of the rapsyn RING-H2 domain with dystroglycan. *J Biol Chem* **276**, 24911-24917.

- Bassel-Duby R & Olson EN. (2003). Role of calcineurin in striated muscle: development, adaptation, and disease. *Biochem Biophys Res Commun* **311**, 1133-1141.
- Bassel-Duby R & Olson EN. (2006). Signaling pathways in skeletal muscle remodeling. *Annu Rev Biochem* **75**, 19-37.
- Bayer KU, Harbers K & Schulman H. (1998). alphaKAP is an anchoring protein for a novel CaM kinase II isoform in skeletal muscle. *EMBO J* **17**, 5598-5605.
- Bentzinger CF, Barzagli P, Lin S & Ruegg MA. (2005). Overexpression of mini-agrin in skeletal muscle increases muscle integrity and regenerative capacity in laminin-alpha2-deficient mice. *FASEB J* **19**, 934-942.
- Berchtold MW, Brinkmeier H & Muntener M. (2000). Calcium ion in skeletal muscle: its crucial role for muscle function, plasticity, and disease. *Physiol Rev* **80**, 1215-1265.
- Bezakova G, Helm JP, Francolini M & Lomo T. (2001). Effects of purified recombinant neural and muscle agrin on skeletal muscle fibers in vivo. *J Cell Biol* **153**, 1441-1452.
- Bezakova G & Lomo T. (2001). Muscle activity and muscle agrin regulate the organization of cytoskeletal proteins and attached acetylcholine receptor (AChR) aggregates in skeletal muscle fibers. *J Cell Biol* **153**, 1453-1463.
- Bezakova G & Ruegg MA. (2003). New insights into the roles of agrin. *Nat Rev Mol Cell Biol* **4**, 295-308.
- Bian W & Bursac N. (2011). Soluble miniagrin enhances contractile function of engineered skeletal muscle. *FASEB J*.
- Bigard X, Sanchez H, Zoll J, Mateo P, Rousseau V, Veksler V & Ventura-Clapier R. (2000). Calcineurin Co-regulates contractile and metabolic components of slow muscle phenotype. *J Biol Chem* **275**, 19653-19660.
- Blaauw B, Mammucari C, Toniolo L, Agatea L, Abraham R, Sandri M, Reggiani C & Schiaffino S. (2008). Akt activation prevents the force drop induced by eccentric contractions in dystrophin-deficient skeletal muscle. *Hum Mol Genet* **17**, 3686-3696.
- Blake DJ, Weir A, Newey SE & Davies KE. (2002). Function and genetics of dystrophin and dystrophin-related proteins in muscle. *Physiol Rev* **82**, 291-329.
- Bodine SC, Stitt TN, Gonzalez M, Kline WO, Stover GL, Bauerlein R, Zlotchenko E, Scrimgeour A, Lawrence JC, Glass DJ & Yancopoulos GD. (2001). Akt/mTOR pathway is a crucial regulator of skeletal muscle hypertrophy and can prevent muscle atrophy in vivo. *Nat Cell Biol* **3**, 1014-1019.

- Borges LS & Ferns M. (2001). Agrin-induced phosphorylation of the acetylcholine receptor regulates cytoskeletal anchoring and clustering. *J Cell Biol* **153**, 1-12.
- Borges LS, Lee Y & Ferns M. (2002). Dual role for calcium in agrin signaling and acetylcholine receptor clustering. *J Neurobiol* **50**, 69-79.
- Borges LS, Yechikhov S, Lee YI, Rudell JB, Friese MB, Burden SJ & Ferns MJ. (2008). Identification of a motif in the acetylcholine receptor beta subunit whose phosphorylation regulates rapsyn association and postsynaptic receptor localization. *J Neurosci* **28**, 11468-11476.
- Braun AP & Schulman H. (1995). The multifunctional calcium/calmodulin-dependent protein kinase: from form to function. *Annu Rev Physiol* **57**, 417-445.
- Briguet A, Courdier-Fruh I, Foster M, Meier T & Magyar JP. (2004). Histological parameters for the quantitative assessment of muscular dystrophy in the mdx-mouse. *Neuromuscul Disord* **14**, 675-682.
- Briguet A & Ruegg MA. (2000). The Ets transcription factor GABP is required for postsynaptic differentiation in vivo. *J Neurosci* **20**, 5989-5996.
- Bruneau E, Sutter D, Hume RI & Akaaboune M. (2005a). Identification of nicotinic acetylcholine receptor recycling and its role in maintaining receptor density at the neuromuscular junction in vivo. *J Neurosci* **25**, 9949-9959.
- Bruneau EG & Akaaboune M. (2006a). The dynamics of recycled acetylcholine receptors at the neuromuscular junction in vivo. *Development* **133**, 4485-4493.
- Bruneau EG & Akaaboune M. (2006b). Running to stand still: ionotropic receptor dynamics at central and peripheral synapses. *Mol Neurobiol* **34**, 137-151.
- Bruneau EG, Esteban JA & Akaaboune M. (2009). Receptor-associated proteins and synaptic plasticity. *FASEB J* **23**, 679-688.
- Bruneau EG, Macpherson PC, Goldman D, Hume RI & Akaaboune M. (2005b). The effect of agrin and laminin on acetylcholine receptor dynamics in vitro. *Dev Biol* **288**, 248-258.
- Buckingham M. (2007). Skeletal muscle progenitor cells and the role of Pax genes. *C R Biol* **330**, 530-533.
- Buckingham M & Relaix F. (2007). The role of Pax genes in the development of tissues and organs: Pax3 and Pax7 regulate muscle progenitor cell functions. *Annu Rev Cell Dev Biol* **23**, 645-673.
- Bulfield G, Siller WG, Wight PA & Moore KJ. (1984). X chromosome-linked muscular dystrophy (mdx) in the mouse. *Proc Natl Acad Sci U S A* **81**, 1189-1192.

- Burgess RW, Skarnes WC & Sanes JR. (2000). Agrin isoforms with distinct amino termini: differential expression, localization, and function. *J Cell Biol* **151**, 41-52.
- Butikofer L, Zurlinden A, Bolliger MF, Kunz B & Sonderegger P. (2011). Destabilization of the neuromuscular junction by proteolytic cleavage of agrin results in precocious sarcopenia. *FASEB J* **25**, 4378-4393.
- Calabria E, Ciciliot S, Moretti I, Garcia M, Picard A, Dyar KA, Pallafacchina G, Tothova J, Schiaffino S & Murgia M. (2009). NFAT isoforms control activity-dependent muscle fiber type specification. *Proc Natl Acad Sci U S A* **106**, 13335-13340.
- Calvo S, Stauffer J, Nakayama M & Buonanno A. (1996). Transcriptional control of muscle plasticity: differential regulation of troponin I genes by electrical activity. *Dev Genet* **19**, 169-181.
- Campanelli JT, Roberds SL, Campbell KP & Scheller RH. (1994). A role for dystrophin-associated glycoproteins and utrophin in agrin-induced AChR clustering. *Cell* **77**, 663-674.
- Carafoli E & Klee CB. (1999). *Calcium as a cellular regulator*.
- Carnwath JW & Shotton DM. (1987). Muscular dystrophy in the mdx mouse: histopathology of the soleus and extensor digitorum longus muscles. *J Neurol Sci* **80**, 39-54.
- Chakkalakal JV, Nishimune H, Ruas JL, Spiegelman BM & Sanes JR. (2010). Retrograde influence of muscle fibers on their innervation revealed by a novel marker for slow motoneurons. *Development* **137**, 3489-3499.
- Charge SB & Rudnicki MA. (2004). Cellular and molecular regulation of muscle regeneration. *Physiol Rev* **84**, 209-238.
- Cheung ZH, Fu AK & Ip NY. (2006). Synaptic roles of Cdk5: implications in higher cognitive functions and neurodegenerative diseases. *Neuron* **50**, 13-18.
- Chin D & Means AR. (2000). Calmodulin: a prototypical calcium sensor. *Trends Cell Biol* **10**, 322-328.
- Chin D, Winkler KE & Means AR. (1997). Characterization of substrate phosphorylation and use of calmodulin mutants to address implications from the enzyme crystal structure of calmodulin-dependent protein kinase I. *J Biol Chem* **272**, 31235-31240.
- Chin ER. (2004). The role of calcium and calcium/calmodulin-dependent kinases in skeletal muscle plasticity and mitochondrial biogenesis. *Proc Nutr Soc* **63**, 279-286.

- Chin ER, Olson EN, Richardson JA, Yang Q, Humphries C, Shelton JM, Wu H, Zhu W, Bassel-Duby R & Williams RS. (1998). A calcineurin-dependent transcriptional pathway controls skeletal muscle fiber type. *Genes Dev* **12**, 2499-2509.
- Cohen TJ, Waddell DS, Barrientos T, Lu Z, Feng G, Cox GA, Bodine SC & Yao TP. (2007). The histone deacetylase HDAC4 connects neural activity to muscle transcriptional reprogramming. *J Biol Chem* **282**, 33752-33759.
- Constantin B, Sebillé S & Cognard C. (2006). New insights in the regulation of calcium transfers by muscle dystrophin-based cytoskeleton: implications in DMD. *J Muscle Res Cell Motil* **27**, 375-386.
- Corin SJ, Juhasz O, Zhu L, Conley P, Kedes L & Wade R. (1994). Structure and expression of the human slow twitch skeletal muscle troponin I gene. *J Biol Chem* **269**, 10651-10659.
- Corin SJ, Levitt LK, O'Mahoney JV, Joya JE, Hardeman EC & Wade R. (1995). Delineation of a slow-twitch-myofiber-specific transcriptional element by using in vivo somatic gene transfer. *Proc Natl Acad Sci U S A* **92**, 6185-6189.
- Coulton GR, Curtin NA, Morgan JE & Partridge TA. (1988a). The mdx mouse skeletal muscle myopathy: II. Contractile properties. *Neuropathol Appl Neurobiol* **14**, 299-314.
- Coulton GR, Morgan JE, Partridge TA & Sloper JC. (1988b). The mdx mouse skeletal muscle myopathy: I. A histological, morphometric and biochemical investigation. *Neuropathol Appl Neurobiol* **14**, 53-70.
- Cowling BS, McGrath MJ, Nguyen MA, Cottle DL, Kee AJ, Brown S, Schessl J, Zou Y, Joya J, Bonnemann CG, Hardeman EC & Mitchell CA. (2008). Identification of FHL1 as a regulator of skeletal muscle mass: implications for human myopathy. *J Cell Biol* **183**, 1033-1048.
- Crabtree GR & Olson EN. (2002). NFAT signaling: choreographing the social lives of cells. *Cell* **109 Suppl**, S67-79.
- Cross DA, Alessi DR, Cohen P, Andjelkovich M & Hemmings BA. (1995). Inhibition of glycogen synthase kinase-3 by insulin mediated by protein kinase B. *Nature* **378**, 785-789.
- de Gregorio R, Iniguez MA, Fresno M & Alemany S. (2001). Cot kinase induces cyclooxygenase-2 expression in T cells through activation of the nuclear factor of activated T cells. *J Biol Chem* **276**, 27003-27009.
- De Koninck P & Schulman H. (1998). Sensitivity of CaM kinase II to the frequency of Ca²⁺ oscillations. *Science* **279**, 227-230.

- de la Pompa JL, Timmerman LA, Takimoto H, Yoshida H, Elia AJ, Samper E, Potter J, Wakeham A, Marengere L, Langille BL, Crabtree GR & Mak TW. (1998). Role of the NF-ATc transcription factor in morphogenesis of cardiac valves and septum. *Nature* **392**, 182-186.
- Decarlo K, Emley A, Dadzie OE & Mahalingam M. (2011). Laser capture microdissection: methods and applications. *Methods Mol Biol* **755**, 1-15.
- DeChiara TM, Bowen DC, Valenzuela DM, Simmons MV, Poueymirou WT, Thomas S, Kinetz E, Compton DL, Rojas E, Park JS, Smith C, DiStefano PS, Glass DJ, Burden SJ & Yancopoulos GD. (1996). The receptor tyrosine kinase MuSK is required for neuromuscular junction formation in vivo. *Cell* **85**, 501-512.
- Delling U, Tureckova J, Lim HW, De Windt LJ, Rotwein P & Molkentin JD. (2000). A calcineurin-NFATc3-dependent pathway regulates skeletal muscle differentiation and slow myosin heavy-chain expression. *Mol Cell Biol* **20**, 6600-6611.
- Denzer AJ, Brandenberger R, Gesemann M, Chiquet M & Rugg MA. (1997). Agrin binds to the nerve-muscle basal lamina via laminin. *J Cell Biol* **137**, 671-683.
- Doran P, Donoghue P, O'Connell K, Gannon J & Ohlendieck K. (2009). Proteomics of skeletal muscle aging. *Proteomics* **9**, 989-1003.
- Dunn SE, Burns JL & Michel RN. (1999). Calcineurin is required for skeletal muscle hypertrophy. *J Biol Chem* **274**, 21908-21912.
- Dunn SE, Chin ER & Michel RN. (2000). Matching of calcineurin activity to upstream effectors is critical for skeletal muscle fiber growth. *J Cell Biol* **151**, 663-672.
- Dunn SE & Michel RN. (1997). Coordinated expression of myosin heavy chain isoforms and metabolic enzymes within overloaded rat muscle fibers. *Am J Physiol* **273**, C371-383.
- Dunn SE, Simard AR, Bassel-Duby R, Williams RS & Michel RN. (2001). Nerve activity-dependent modulation of calcineurin signaling in adult fast and slow skeletal muscle fibers. *J Biol Chem* **276**, 45243-45254.
- Dupont G & Goldbeter A. (1998). CaM kinase II as frequency decoder of Ca²⁺ oscillations. *Bioessays* **20**, 607-610.
- Espina V, Heiby M, Pierobon M & Liotta LA. (2007). Laser capture microdissection technology. *Expert Rev Mol Diagn* **7**, 647-657.
- Espina V, Milia J, Wu G, Cowherd S & Liotta LA. (2006a). Laser capture microdissection. *Methods Mol Biol* **319**, 213-229.

- Espina V, Wulfschuhle JD, Calvert VS, VanMeter A, Zhou W, Coukos G, Geho DH, Petricoin EF, 3rd & Liotta LA. (2006b). Laser-capture microdissection. *Nat Protoc* **1**, 586-603.
- Eusebio A, Oliveri F, Barzaghi P & Ruegg MA. (2003). Expression of mouse agrin in normal, denervated and dystrophic muscle. *Neuromuscul Disord* **13**, 408-415.
- Ferns M, Hoch W, Campanelli JT, Rupp F, Hall ZW & Scheller RH. (1992). RNA splicing regulates agrin-mediated acetylcholine receptor clustering activity on cultured myotubes. *Neuron* **8**, 1079-1086.
- Ferns MJ, Campanelli JT, Hoch W, Scheller RH & Hall Z. (1993). The ability of agrin to cluster AChRs depends on alternative splicing and on cell surface proteoglycans. *Neuron* **11**, 491-502.
- Fertuck HC & Salpeter MM. (1976). Quantitation of junctional and extrajunctional acetylcholine receptors by electron microscope autoradiography after ¹²⁵I-alpha-bungarotoxin binding at mouse neuromuscular junctions. *J Cell Biol* **69**, 144-158.
- Fluck M, Waxham MN, Hamilton MT & Booth FW. (2000). Skeletal muscle Ca(2+)-independent kinase activity increases during either hypertrophy or running. *J Appl Physiol* **88**, 352-358.
- Frank D, Kuhn C, Katus HA & Frey N. (2006). The sarcomeric Z-disc: a nodal point in signalling and disease. *J Mol Med (Berl)* **84**, 446-468.
- Friday BB, Horsley V & Pavlath GK. (2000). Calcineurin activity is required for the initiation of skeletal muscle differentiation. *J Cell Biol* **149**, 657-666.
- Friday BB, Mitchell PO, Kegley KM & Pavlath GK. (2003). Calcineurin initiates skeletal muscle differentiation by activating MEF2 and MyoD. *Differentiation* **71**, 217-227.
- Friday BB & Pavlath GK. (2001). A calcineurin- and NFAT-dependent pathway regulates Myf5 gene expression in skeletal muscle reserve cells. *J Cell Sci* **114**, 303-310.
- Friese MB, Blagden CS & Burden SJ. (2007). Synaptic differentiation is defective in mice lacking acetylcholine receptor beta-subunit tyrosine phosphorylation. *Development* **134**, 4167-4176.
- Fu AK, Ip FC, Fu WY, Cheung J, Wang JH, Yung WH & Ip NY. (2005). Aberrant motor axon projection, acetylcholine receptor clustering, and neurotransmission in cyclin-dependent kinase 5 null mice. *Proc Natl Acad Sci U S A* **102**, 15224-15229.
- Fuhrer C, Gautam M, Sugiyama JE & Hall ZW. (1999). Roles of rapsyn and agrin in interaction of postsynaptic proteins with acetylcholine receptors. *J Neurosci* **19**, 6405-6416.

- Gardiner P, Michel R, Browman C & Noble E. (1986). Increased EMG of rat plantaris during locomotion following surgical removal of its synergists. *Brain Res* **380**, 114-121.
- Gautam M, Noakes PG, Moscoso L, Rupp F, Scheller RH, Merlie JP & Sanes JR. (1996). Defective neuromuscular synaptogenesis in agrin-deficient mutant mice. *Cell* **85**, 525-535.
- Gauthier ER, Madison SD & Michel RN. (1997). Rapid RNA isolation without the use of commercial kits: application to small tissue samples. *Pflugers Arch* **433**, 664-668.
- Gee SH, Montanaro F, Lindenbaum MH & Carbonetto S. (1994). Dystroglycan-alpha, a dystrophin-associated glycoprotein, is a functional agrin receptor. *Cell* **77**, 675-686.
- Glass DJ. (2003a). Molecular mechanisms modulating muscle mass. *Trends Mol Med* **9**, 344-350.
- Glass DJ. (2003b). Signalling pathways that mediate skeletal muscle hypertrophy and atrophy. *Nat Cell Biol* **5**, 87-90.
- Glass DJ. (2005). Skeletal muscle hypertrophy and atrophy signaling pathways. *Int J Biochem Cell Biol* **37**, 1974-1984.
- Glass DJ. (2010). Signaling pathways perturbing muscle mass. *Curr Opin Clin Nutr Metab Care* **13**, 225-229.
- Glass DJ, Bowen DC, Stitt TN, Radziejewski C, Bruno J, Ryan TE, Gies DR, Shah S, Mattsson K, Burden SJ, DiStefano PS, Valenzuela DM, DeChiara TM & Yancopoulos GD. (1996a). Agrin acts via a MuSK receptor complex. *Cell* **85**, 513-523.
- Glass DJ, DeChiara TM, Stitt TN, DiStefano PS, Valenzuela DM & Yancopoulos GD. (1996b). The receptor tyrosine kinase MuSK is required for neuromuscular junction formation and is a functional receptor for agrin. *Cold Spring Harb Symp Quant Biol* **61**, 435-444.
- Godfrey EW, Nitkin RM, Wallace BG, Rubin LL & McMahan UJ. (1984). Components of Torpedo electric organ and muscle that cause aggregation of acetylcholine receptors on cultured muscle cells. *J Cell Biol* **99**, 615-627.
- Graef IA, Chen F, Chen L, Kuo A & Crabtree GR. (2001). Signals transduced by Ca(2+)/calcineurin and NFATc3/c4 pattern the developing vasculature. *Cell* **105**, 863-875.
- Gramolini AO, Angus LM, Schaeffer L, Burton EA, Tinsley JM, Davies KE, Changeux JP & Jasmin BJ. (1999). Induction of utrophin gene expression by heregulin in skeletal muscle cells: role of the N-box motif and GA binding protein. *Proc Natl Acad Sci U S A* **96**, 3223-3227.

- Gramolini AO, Burton EA, Tinsley JM, Ferns MJ, Cartaud A, Cartaud J, Davies KE, Lunde JA & Jasmin BJ. (1998). Muscle and neural isoforms of agrin increase utrophin expression in cultured myotubes via a transcriptional regulatory mechanism. *J Biol Chem* **273**, 736-743.
- Gramolini AO & Jasmin BJ. (1998). Molecular mechanisms and putative signalling events controlling utrophin expression in mammalian skeletal muscle fibres. *Neuromuscul Disord* **8**, 351-361.
- Gregory P, Low RB & Stirewalt WS. (1986). Changes in skeletal-muscle myosin isoenzymes with hypertrophy and exercise. *Biochem J* **238**, 55-63.
- Gu Y & Hall ZW. (1988). Characterization of acetylcholine receptor subunits in developing and in denervated mammalian muscle. *J Biol Chem* **263**, 12878-12885.
- Guerini D & Klee CB. (1989). Cloning of human calcineurin A: evidence for two isozymes and identification of a polyproline structural domain. *Proc Natl Acad Sci U S A* **86**, 9183-9187.
- Gundersen K. (1998). Determination of muscle contractile properties: the importance of the nerve. *Acta Physiol Scand* **162**, 333-341.
- Gundersen K. (2010). Excitation-transcription coupling in skeletal muscle: the molecular pathways of exercise. *Biol Rev Camb Philos Soc*.
- Hanson PI & Schulman H. (1992). Neuronal Ca²⁺/calmodulin-dependent protein kinases. *Annu Rev Biochem* **61**, 559-601.
- Harwood AJ. (2001). Regulation of GSK-3: a cellular multiprocessor. *Cell* **105**, 821-824.
- Hasty P, Bradley A, Morris JH, Edmondson DG, Venuti JM, Olson EN & Klein WH. (1993). Muscle deficiency and neonatal death in mice with a targeted mutation in the myogenin gene. *Nature* **364**, 501-506.
- Hausser HJ, Ruegg MA, Brenner RE & Ksiazek I. (2007). Agrin is highly expressed by chondrocytes and is required for normal growth. *Histochem Cell Biol* **127**, 363-374.
- Hoch W. (1999). Formation of the neuromuscular junction. Agrin and its unusual receptors. *Eur J Biochem* **265**, 1-10.
- Hoch W, Ferns M, Campanelli JT, Hall ZW & Scheller RH. (1993). Developmental regulation of highly active alternatively spliced forms of agrin. *Neuron* **11**, 479-490.
- Hoch W, McConville J, Helms S, Newsom-Davis J, Melms A & Vincent A. (2001). Auto-antibodies to the receptor tyrosine kinase MuSK in patients with myasthenia gravis without acetylcholine receptor antibodies. *Nat Med* **7**, 365-368.

- Hodge MR, Ranger AM, Charles de la Brousse F, Hoey T, Grusby MJ & Glimcher LH. (1996). Hyperproliferation and dysregulation of IL-4 expression in NF-ATp-deficient mice. *Immunity* **4**, 397-405.
- Hoey T, Sun YL, Williamson K & Xu X. (1995). Isolation of two new members of the NF-AT gene family and functional characterization of the NF-AT proteins. *Immunity* **2**, 461-472.
- Hogan PG, Chen L, Nardone J & Rao A. (2003). Transcriptional regulation by calcium, calcineurin, and NFAT. *Genes Dev* **17**, 2205-2232.
- Holt KH, Crosbie RH, Venzke DP & Campbell KP. (2000). Biosynthesis of dystroglycan: processing of a precursor propeptide. *FEBS Lett* **468**, 79-83.
- Hook SS & Means AR. (2001). Ca(2+)/CaM-dependent kinases: from activation to function. *Annu Rev Pharmacol Toxicol* **41**, 471-505.
- Hopf C & Hoch W. (1996). Agrin binding to alpha-dystroglycan. Domains of agrin necessary to induce acetylcholine receptor clustering are overlapping but not identical to the alpha-dystroglycan-binding region. *J Biol Chem* **271**, 5231-5236.
- Horsley V, Friday BB, Matteson S, Kegley KM, Gephart J & Pavlath GK. (2001). Regulation of the growth of multinucleated muscle cells by an NFATC2-dependent pathway. *J Cell Biol* **153**, 329-338.
- Horsley V & Pavlath GK. (2002). NFAT: ubiquitous regulator of cell differentiation and adaptation. *J Cell Biol* **156**, 771-774.
- Hughes SM, Chi MM, Lowry OH & Gundersen K. (1999). Myogenin induces a shift of enzyme activity from glycolytic to oxidative metabolism in muscles of transgenic mice. *J Cell Biol* **145**, 633-642.
- Hwee DT & Bodine SC. (2009). Age-related deficit in load-induced skeletal muscle growth. *J Gerontol A Biol Sci Med Sci* **64**, 618-628.
- Hyatt JP, McCall GE, Kander EM, Zhong H, Roy RR & Huey KA. (2008). PAX3/7 expression coincides with MyoD during chronic skeletal muscle overload. *Muscle Nerve* **38**, 861-866.
- Iozzo RV, Zoeller JJ & Nystrom A. (2009). Basement membrane proteoglycans: modulators Par Excellence of cancer growth and angiogenesis. *Mol Cells* **27**, 503-513.
- Ip FC, Glass DG, Gies DR, Cheung J, Lai KO, Fu AK, Yancopoulos GD & Ip NY. (2000). Cloning and characterization of muscle-specific kinase in chicken. *Mol Cell Neurosci* **16**, 661-673.

- Jacobson C, Cote PD, Rossi SG, Rotundo RL & Carbonetto S. (2001). The dystroglycan complex is necessary for stabilization of acetylcholine receptor clusters at neuromuscular junctions and formation of the synaptic basement membrane. *J Cell Biol* **152**, 435-450.
- Jain J, Burgeon E, Badalian TM, Hogan PG & Rao A. (1995). A similar DNA-binding motif in NFAT family proteins and the Rel homology region. *J Biol Chem* **270**, 4138-4145.
- Jasmin BJ, Angus LM, Belanger G, Chakkalakal JV, Gramolini AO, Lunde JA, Stocksley MA & Thompson J. (2002). Multiple regulatory events controlling the expression and localization of utrophin in skeletal muscle fibers: insights into a therapeutic strategy for Duchenne muscular dystrophy. *J Physiol Paris* **96**, 31-42.
- Jenkins GW, Kemnitz CP & Tortora GJ. (2010). *Anatomy and Physiology: from science to life*. John Wiley & Sons Inc.
- Jo SA, Zhu X, Marchionni MA & Burden SJ. (1995). Neuregulins are concentrated at nerve-muscle synapses and activate ACh-receptor gene expression. *Nature* **373**, 158-161.
- Jurdana M, Fumagalli G, Grubic Z, Lorenzon P, Mars T & Sciancalepore M. (2009). Neural agrin changes the electrical properties of developing human skeletal muscle cells. *Cell Mol Neurobiol* **29**, 123-131.
- Jury EC & Kabouridis PS. (2010). New role for Agrin in T cells and its potential importance in immune system regulation. *Arthritis Res Ther* **12**, 205.
- Kanaseki T, Ikeuchi Y, Sugiura H & Yamauchi T. (1991). Structural features of Ca²⁺/calmodulin-dependent protein kinase II revealed by electron microscopy. *J Cell Biol* **115**, 1049-1060.
- Karnovsky MJ & Roots L. (1964). A "Direct-Coloring" Thiocholine Method for Cholinesterases. *J Histochem Cytochem* **12**, 219-221.
- Kegley KM, Gephart J, Warren GL & Pavlath GK. (2001). Altered primary myogenesis in NFATC3(-/-) mice leads to decreased muscle size in the adult. *Dev Biol* **232**, 115-126.
- Kelley G. (1996). Mechanical overload and skeletal muscle fiber hyperplasia: a meta-analysis. *J Appl Physiol* **81**, 1584-1588.
- Ketterer C, Zeiger U, Budak MT, Rubinstein NA & Khurana TS. (2011). Identification of the neuromuscular junction transcriptome of extraocular muscle by laser capture microdissection. *Invest Ophthalmol Vis Sci* **51**, 4589-4599.
- Khan AA, Bose C, Yam LS, Soloski MJ & Rupp F. (2001). Physiological regulation of the immunological synapse by agrin. *Science* **292**, 1681-1686.

- Kim MH, Kay DI, Rudra RT, Chen BM, Hsu N, Izumiya Y, Martinez L, Spencer MJ, Walsh K, Grinnell AD & Crosbie RH. (2011). Myogenic Akt signaling attenuates muscular degeneration, promotes myofiber regeneration and improves muscle function in dystrophin-deficient mdx mice. *Hum Mol Genet* **20**, 1324-1338.
- Kim N, Stiegler AL, Cameron TO, Hallock PT, Gomez AM, Huang JH, Hubbard SR, Dustin ML & Burden SJ. (2008). Lrp4 is a receptor for Agrin and forms a complex with MuSK. *Cell* **135**, 334-342.
- Konhilas JP, Maass AH, Luckey SW, Stauffer BL, Olson EN & Leinwand LA. (2004). Sex modifies exercise and cardiac adaptation in mice. *Am J Physiol Heart Circ Physiol* **287**, H2768-2776.
- Kuang S, Charge SB, Seale P, Huh M & Rudnicki MA. (2006). Distinct roles for Pax7 and Pax3 in adult regenerative myogenesis. *J Cell Biol* **172**, 103-113.
- Kulig EM, Eibl JK, St-Louis M, Michel SA, Pavlath GK & Michel RN. (2009). Calcineurin/NFATc1-c3 signaling isoforms have distinct roles in the regulation of skeletal muscle fiber remodeling during compensatory growth. . In *Society for Neuroscience Annual Meeting 2009*. Neuroscience Meeting Planner 2009. Online. Program No.861.5, Chicago, IL.
- Kulig EM, St-Louis M, Michel SA, Pavlath GK & Michel RN. (2010). Differential calcineurin/NFATc1-c3 signaling in the regulation of the skeletal muscle fiber phenotype. . In *Experimental Biology 2010*. FASEB J; 24: 1b594 Anaheim, CA.
- Kummer TT, Misgeld T, Lichtman JW & Sanes JR. (2004). Nerve-independent formation of a topologically complex postsynaptic apparatus. *J Cell Biol* **164**, 1077-1087.
- Kummer TT, Misgeld T & Sanes JR. (2006). Assembly of the postsynaptic membrane at the neuromuscular junction: paradigm lost. *Curr Opin Neurobiol* **16**, 74-82.
- Lacazette E, Le Calvez S, Gajendran N & Brenner HR. (2003). A novel pathway for MuSK to induce key genes in neuromuscular synapse formation. *J Cell Biol* **161**, 727-736.
- Lane RJ, Roncaroli F, Charles P, McGonagle DG & Orrell RW. (2011). Acetylcholine receptor antibodies in patients with genetic myopathies: Clinical and biological significance. *Neuromuscul Disord*.
- Langenbach KJ & Rando TA. (2002). Inhibition of dystroglycan binding to laminin disrupts the PI3K/AKT pathway and survival signaling in muscle cells. *Muscle Nerve* **26**, 644-653.
- Lara-Pezzi E, Winn N, Paul A, McCullagh K, Slominsky E, Santini MP, Mourkioti F, Sarathchandra P, Fukushima S, Suzuki K & Rosenthal N. (2007). A naturally occurring calcineurin variant inhibits FoxO activity and enhances skeletal muscle regeneration. *J Cell Biol* **179**, 1205-1218.

- Levitt LK, O'Mahoney JV, Brennan KJ, Joya JE, Zhu L, Wade RP & Hardeman EC. (1995). The human troponin I slow promoter directs slow fiber-specific expression in transgenic mice. *DNA Cell Biol* **14**, 599-607.
- Li H, Rao A & Hogan PG. (2011). Interaction of calcineurin with substrates and targeting proteins. *Trends Cell Biol* **21**, 91-103.
- Liang P & MacRae TH. (1997). Molecular chaperones and the cytoskeleton. *J Cell Sci* **110** (Pt **13**), 1431-1440.
- Lieber RL. (2010). *Skeletal muscle structure, function & plasticity : the physiological basis of rehabilitation*. Lippincott Williams & Wilkins.
- Lin S, Maj M, Bezakova G, Magyar JP, Brenner HR & Ruegg MA. (2008). Muscle-wide secretion of a miniaturized form of neural agrin rescues focal neuromuscular innervation in agrin mutant mice. *Proc Natl Acad Sci U S A* **105**, 11406-11411.
- Lindstrom J. (2010). Nicotinic Acetylcholine Receptors. In *Encyclopedia of Life Sciences (ELS)*. John Wiley & Sons, Ltd.
- Linnoila J, Wang Y, Yao Y & Wang ZZ. (2008). A mammalian homolog of *Drosophila* tumorous imaginal discs, Tid1, mediates agrin signaling at the neuromuscular junction. *Neuron* **60**, 625-641.
- Lisman J, Schulman H & Cline H. (2002). The molecular basis of CaMKII function in synaptic and behavioural memory. *Nat Rev Neurosci* **3**, 175-190.
- Liu Y, Cseresnyes Z, Randall WR & Schneider MF. (2001). Activity-dependent nuclear translocation and intranuclear distribution of NFATc in adult skeletal muscle fibers. *J Cell Biol* **155**, 27-39.
- Lopez-Rodriguez C, Aramburu J, Rakeman AS & Rao A. (1999). NFAT5, a constitutively nuclear NFAT protein that does not cooperate with Fos and Jun. *Proc Natl Acad Sci U S A* **96**, 7214-7219.
- Luo C, Burgeon E, Carew JA, McCaffrey PG, Badalian TM, Lane WS, Hogan PG & Rao A. (1996a). Recombinant NFAT1 (NFATp) is regulated by calcineurin in T cells and mediates transcription of several cytokine genes. *Mol Cell Biol* **16**, 3955-3966.
- Luo C, Burgeon E & Rao A. (1996b). Mechanisms of transactivation by nuclear factor of activated T cells-1. *J Exp Med* **184**, 141-147.
- Macian F. (2005). NFAT proteins: key regulators of T-cell development and function. *Nat Rev Immunol* **5**, 472-484.

- Macpherson P, Kostrominova T, Tang H & Goldman D. (2002). Protein kinase C and calcium/calmodulin-activated protein kinase II (CaMK II) suppress nicotinic acetylcholine receptor gene expression in mammalian muscle. A specific role for CaMK II in activity-dependent gene expression. *J Biol Chem* **277**, 15638-15646.
- Madhavan R, Zhao XT, Chan F, Wu Z & Peng HB. (2003). The involvement of calcineurin in acetylcholine receptor redistribution in muscle. *Mol Cell Neurosci* **23**, 587-599.
- Malenka RC, Kauer JA, Perkel DJ, Mauk MD, Kelly PT, Nicoll RA & Waxham MN. (1989). An essential role for postsynaptic calmodulin and protein kinase activity in long-term potentiation. *Nature* **340**, 554-557.
- Marieb EN. (2001). *Human Anatomy & Physiology*. Benjamin Cummings.
- Martinez-Pena y Valenzuela I, Mouslim C & Akaaboune M. (2010). Calcium/calmodulin kinase II-dependent acetylcholine receptor cycling at the mammalian neuromuscular junction in vivo. *J Neurosci* **30**, 12455-12465.
- Martinou JC, Falls DL, Fischbach GD & Merlie JP. (1991). Acetylcholine receptor-inducing activity stimulates expression of the epsilon-subunit gene of the muscle acetylcholine receptor. *Proc Natl Acad Sci U S A* **88**, 7669-7673.
- Martinou JC & Merlie JP. (1991). Nerve-dependent modulation of acetylcholine receptor epsilon-subunit gene expression. *J Neurosci* **11**, 1291-1299.
- Maselli RA, Fernandez JM, Arredondo J, Navarro C, Ngo M, Beeson D, Cagney O, Williams DC, Wollmann RL, Yarov-Yarovoy V & Ferns MJ. (2011). LG2 agrin mutation causing severe congenital myasthenic syndrome mimics functional characteristics of non-neural (z-) agrin. *Hum Genet*.
- McConville J & Vincent A. (2002). Diseases of the neuromuscular junction. *Curr Opin Pharmacol* **2**, 296-301.
- McCroskery S, Bailey A, Lin L & Daniels MP. (2009). Transmembrane agrin regulates dendritic filopodia and synapse formation in mature hippocampal neuron cultures. *Neuroscience* **163**, 168-179.
- McCroskery S, Chaudhry A, Lin L & Daniels MP. (2006). Transmembrane agrin regulates filopodia in rat hippocampal neurons in culture. *Mol Cell Neurosci* **33**, 15-28.
- McCullagh KJ, Calabria E, Pallafacchina G, Ciciliot S, Serrano AL, Argentini C, Kalhovde JM, Lomo T & Schiaffino S. (2004). NFAT is a nerve activity sensor in skeletal muscle and controls activity-dependent myosin switching. *Proc Natl Acad Sci U S A* **101**, 10590-10595.

- McMullen CA & Andrade FH. (2009). Functional and morphological evidence of age-related denervation in rat laryngeal muscles. *J Gerontol A Biol Sci Med Sci* **64**, 435-442.
- Means AR. (2000). Regulatory cascades involving calmodulin-dependent protein kinases. *Mol Endocrinol* **14**, 4-13.
- Megeath LJ & Fallon JR. (1998). Intracellular calcium regulates agrin-induced acetylcholine receptor clustering. *J Neurosci* **18**, 672-678.
- Megeney LA & Rudnicki MA. (1995). Determination versus differentiation and the MyoD family of transcription factors. *Biochem Cell Biol* **73**, 723-732.
- Meier T, Masciulli F, Moore C, Schoumacher F, Eppenberger U, Denzer AJ, Jones G & Brenner HR. (1998). Agrin can mediate acetylcholine receptor gene expression in muscle by aggregation of muscle-derived neuregulins. *J Cell Biol* **141**, 715-726.
- Meinen S, Barzaghi P, Lin S, Lochmuller H & Ruegg MA. (2007). Linker molecules between laminins and dystroglycan ameliorate laminin- α 2-deficient muscular dystrophy at all disease stages. *J Cell Biol* **176**, 979-993.
- Meinen S, Lin S, Thurnherr R, Erb M, Meier T & Ruegg MA. (2011). Apoptosis inhibitors and mini-agrin have additive benefits in congenital muscular dystrophy mice. *EMBO Mol Med* **3**, 465-479.
- Meinen S & Ruegg MA. (2006). Congenital muscular dystrophy: mini-agrin delivers in mice. *Gene Ther* **13**, 869-870.
- Mejat A, Ravel-Chapuis A, Vandromme M & Schaeffer L. (2003). Synapse-specific gene expression at the neuromuscular junction. *Ann N Y Acad Sci* **998**, 53-65.
- Mendell LM, Collins WF, 3rd & Munson JB. (1994). Retrograde determination of motoneuron properties and their synaptic input. *J Neurobiol* **25**, 707-721.
- Michel RN, Chin ER, Chakkalakal JV, Eibl JK & Jasmin BJ. (2007). Ca²⁺/calmodulin-based signalling in the regulation of the muscle fibre phenotype and its therapeutic potential via modulation of utrophin A and myostatin expression. *Appl Physiol Nutr Metab* **32**, 921-929.
- Michel RN & Kulig EM. (2008). Nerve-derived agrin cooperates with neural activity to potentiate translational control of skeletal muscle growth via p70 S6K. In *Experimental Biology 2008*. FASEB J; 22: 959.24, San Diego, CA.
- Misgeld T, Burgess RW, Lewis RM, Cunningham JM, Lichtman JW & Sanes JR. (2002). Roles of neurotransmitter in synapse formation: development of neuromuscular junctions lacking choline acetyltransferase. *Neuron* **36**, 635-648.

- Misgeld T, Kummer TT, Lichtman JW & Sanes JR. (2005). Agrin promotes synaptic differentiation by counteracting an inhibitory effect of neurotransmitter. *Proc Natl Acad Sci U S A* **102**, 11088-11093.
- Mishina M, Takai T, Imoto K, Noda M, Takahashi T, Numa S, Methfessel C & Sakmann B. (1986). Molecular distinction between fetal and adult forms of muscle acetylcholine receptor. *Nature* **321**, 406-411.
- Mitchell PO, Mills ST & Pavlath GK. (2002). Calcineurin differentially regulates maintenance and growth of phenotypically distinct muscles. *Am J Physiol Cell Physiol* **282**, C984-992.
- Mitchell PO & Pavlath GK. (2002). Multiple roles of calcineurin in skeletal muscle growth. *Clin Orthop Relat Res*, S197-202.
- Miyazaki M, Hitomi Y, Kizaki T, Ohno H, Katsumura T, Haga S & Takemasa T. (2006). Calcineurin-mediated slow-type fiber expression and growth in reloading condition. *Med Sci Sports Exerc* **38**, 1065-1072.
- Miyazaki M, McCarthy JJ, Fedele MJ & Esser KA. (2011). Early activation of mTORC1 signalling in response to mechanical overload is independent of phosphoinositide 3-kinase/Akt signalling. *J Physiol* **589**, 1831-1846.
- Molkentin JD, Lu JR, Antos CL, Markham B, Richardson J, Robbins J, Grant SR & Olson EN. (1998). A calcineurin-dependent transcriptional pathway for cardiac hypertrophy. *Cell* **93**, 215-228.
- Moll J, Barzaghi P, Lin S, Bezakova G, Lochmuller H, Engvall E, Muller U & Ruegg MA. (2001). An agrin minigene rescues dystrophic symptoms in a mouse model for congenital muscular dystrophy. *Nature* **413**, 302-307.
- Montanaro F, Gee SH, Jacobson C, Lindenbaum MH, Froehner SC & Carbonetto S. (1998). Laminin and alpha-dystroglycan mediate acetylcholine receptor aggregation via a MuSK-independent pathway. *J Neurosci* **18**, 1250-1260.
- Moore C, Leu M, Muller U & Brenner HR. (2001). Induction of multiple signaling loops by MuSK during neuromuscular synapse formation. *Proc Natl Acad Sci U S A* **98**, 14655-14660.
- Moransard M, Borges LS, Willmann R, Marangi PA, Brenner HR, Ferns MJ & Fuhrer C. (2003). Agrin regulates rapsyn interaction with surface acetylcholine receptors, and this underlies cytoskeletal anchoring and clustering. *J Biol Chem* **278**, 7350-7359.
- Murphy KT, Koopman R, Naim T, Leger B, Trieu J, Ibebunjo C & Lynch GS. (2010). Antibody-directed myostatin inhibition in 21-mo-old mice reveals novel roles for myostatin signaling in skeletal muscle structure and function. *FASEB J* **24**, 4433-4442.

- Musaro A, McCullagh KJ, Naya FJ, Olson EN & Rosenthal N. (1999). IGF-1 induces skeletal myocyte hypertrophy through calcineurin in association with GATA-2 and NF-ATc1. *Nature* **400**, 581-585.
- Nabeshima Y, Hanaoka K, Hayasaka M, Esumi E, Li S & Nonaka I. (1993). Myogenin gene disruption results in perinatal lethality because of severe muscle defect. *Nature* **364**, 532-535.
- Nader GA & Esser KA. (2001). Intracellular signaling specificity in skeletal muscle in response to different modes of exercise. *J Appl Physiol* **90**, 1936-1942.
- Nair KS. (2005). Aging muscle. *Am J Clin Nutr* **81**, 953-963.
- Nakayama M, Stauffer J, Cheng J, Banerjee-Basu S, Wawrousek E & Buonanno A. (1996). Common core sequences are found in skeletal muscle slow- and fast-fiber-type-specific regulatory elements. *Mol Cell Biol* **16**, 2408-2417.
- Naya FJ, Mercer B, Shelton J, Richardson JA, Williams RS & Olson EN. (2000). Stimulation of slow skeletal muscle fiber gene expression by calcineurin in vivo. *J Biol Chem* **275**, 4545-4548.
- Nazarian J, Bouri K & Hoffman EP. (2005). Intracellular expression profiling by laser capture microdissection: three novel components of the neuromuscular junction. *Physiol Genomics* **21**, 70-80.
- Newsom-Davis J. (2007). The emerging diversity of neuromuscular junction disorders. *Acta Myol* **26**, 5-10.
- Ngo ST, Noakes PG & Phillips WD. (2007). Neural agrin: a synaptic stabiliser. *Int J Biochem Cell Biol* **39**, 863-867.
- Nico B, Tamma R, Annese T, Mangieri D, De Luca A, Corsi P, Benagiano V, Longo V, Crivellato E, Salmaggi A & Ribatti D. (2010). Glial dystrophin-associated proteins, laminin and agrin, are downregulated in the brain of mdx mouse. *Lab Invest* **90**, 1645-1660.
- Nishimune H, Valdez G, Jarad G, Moulson CL, Muller U, Miner JH & Sanes JR. (2008). Laminins promote postsynaptic maturation by an autocrine mechanism at the neuromuscular junction. *J Cell Biol* **182**, 1201-1215.
- Nitkin RM, Smith MA, Magill C, Fallon JR, Yao YM, Wallace BG & McMahan UJ. (1987). Identification of agrin, a synaptic organizing protein from Torpedo electric organ. *J Cell Biol* **105**, 2471-2478.

- Oishi Y, Ogata T, Yamamoto KI, Terada M, Ohira T, Ohira Y, Taniguchi K & Roy RR. (2008). Cellular adaptations in soleus muscle during recovery after hindlimb unloading. *Acta Physiol (Oxf)* **192**, 381-395.
- Okada K, Inoue A, Okada M, Murata Y, Kakuta S, Jigami T, Kubo S, Shiraishi H, Eguchi K, Motomura M, Akiyama T, Iwakura Y, Higuchi O & Yamanashi Y. (2006). The muscle protein Dok-7 is essential for neuromuscular synaptogenesis. *Science* **312**, 1802-1805.
- Okamura H, Aramburu J, Garcia-Rodriguez C, Viola JP, Raghavan A, Tahiliani M, Zhang X, Qin J, Hogan PG & Rao A. (2000). Concerted dephosphorylation of the transcription factor NFAT1 induces a conformational switch that regulates transcriptional activity. *Mol Cell* **6**, 539-550.
- Olson EN & Williams RS. (2000). Calcineurin signaling and muscle remodeling. *Cell* **101**, 689-692.
- Oukka M, Ho IC, de la Brousse FC, Hoey T, Grusby MJ & Glimcher LH. (1998). The transcription factor NFAT4 is involved in the generation and survival of T cells. *Immunity* **9**, 295-304.
- Pallafacchina G, Calabria E, Serrano AL, Kalhovde JM & Schiaffino S. (2002). A protein kinase B-dependent and rapamycin-sensitive pathway controls skeletal muscle growth but not fiber type specification. *Proc Natl Acad Sci U S A* **99**, 9213-9218.
- Parsons SA, Millay DP, Wilkins BJ, Bueno OF, Tsika GL, Neilson JR, Liberatore CM, Yutzey KE, Crabtree GR, Tsika RW & Molkentin JD. (2004). Genetic loss of calcineurin blocks mechanical overload-induced skeletal muscle fiber type switching but not hypertrophy. *J Biol Chem* **279**, 26192-26200.
- Parsons SA, Wilkins BJ, Bueno OF & Molkentin JD. (2003). Altered skeletal muscle phenotypes in calcineurin Aalpha and Abeta gene-targeted mice. *Mol Cell Biol* **23**, 4331-4343.
- Pastoret C & Sebillé A. (1995). mdx mice show progressive weakness and muscle deterioration with age. *J Neurol Sci* **129**, 97-105.
- Pavlath GK. (2010). Spatial and functional restriction of regulatory molecules during mammalian myoblast fusion. *Exp Cell Res* **316**, 3067-3072.
- Pavlath GK & Horsley V. (2003). Cell fusion in skeletal muscle--central role of NFATC2 in regulating muscle cell size. *Cell Cycle* **2**, 420-423.
- Peng HB. (1984). Participation of calcium and calmodulin in the formation of acetylcholine receptor clusters. *J Cell Biol* **98**, 550-557.
- Peng HB & Froehner SC. (1985). Association of the postsynaptic 43K protein with newly formed acetylcholine receptor clusters in cultured muscle cells. *J Cell Biol* **100**, 1698-1705.

- Pette D & Staron RS. (2001). Transitions of muscle fiber phenotypic profiles. *Histochem Cell Biol* **115**, 359-372.
- Pilgram GS, Potikanond S, Baines RA, Fradkin LG & Noordermeer JN. (2010). The roles of the dystrophin-associated glycoprotein complex at the synapse. *Mol Neurobiol* **41**, 1-21.
- Proud CG & Denton RM. (1997). Molecular mechanisms for the control of translation by insulin. *Biochem J* **328 (Pt 2)**, 329-341.
- Qiao C, Li J, Zhu T, Draviam R, Watkins S, Ye X, Chen C & Xiao X. (2005). Amelioration of laminin-alpha2-deficient congenital muscular dystrophy by somatic gene transfer of miniagrin. *Proc Natl Acad Sci U S A* **102**, 11999-12004.
- Rainio EM, Sandholm J & Koskinen PJ. (2002). Cutting edge: Transcriptional activity of NFATc1 is enhanced by the Pim-1 kinase. *J Immunol* **168**, 1524-1527.
- Rao A, Luo C & Hogan PG. (1997). Transcription factors of the NFAT family: regulation and function. *Annu Rev Immunol* **15**, 707-747.
- Rascher G, Fischmann A, Kroger S, Duffner F, Grote EH & Wolburg H. (2002). Extracellular matrix and the blood-brain barrier in glioblastoma multiforme: spatial segregation of tenascin and agrin. *Acta Neuropathol* **104**, 85-91.
- Rauch SM, Huen K, Miller MC, Chaudry H, Lau M, Sanes JR, Johanson CE, Stopa EG & Burgess RW. (2011). Changes in brain beta-amyloid deposition and aquaporin 4 levels in response to altered agrin expression in mice. *J Neuropathol Exp Neurol* **70**, 1124-1137.
- Rawls A, Morris JH, Rudnicki M, Braun T, Arnold HH, Klein WH & Olson EN. (1995). Myogenin's functions do not overlap with those of MyoD or Myf-5 during mouse embryogenesis. *Dev Biol* **172**, 37-50.
- Reilly CE. (2000). Crucial role of heparan sulfate proteoglycan (agrin) in beta-amyloid formation in Alzheimer's disease. *J Neurol* **247**, 663-664.
- Rimer M, Cohen I, Lomo T, Burden SJ & McMahan UJ. (1998). Neuregulins and erbB receptors at neuromuscular junctions and at agrin-induced postsynaptic-like apparatus in skeletal muscle. *Mol Cell Neurosci* **12**, 1-15.
- Rodriguez A, Roy J, Martinez-Martinez S, Lopez-Maderuelo MD, Nino-Moreno P, Orti L, Pantoja-Uceda D, Pineda-Lucena A, Cyert MS & Redondo JM. (2009). A conserved docking surface on calcineurin mediates interaction with substrates and immunosuppressants. *Mol Cell* **33**, 616-626.
- Romi FR, Gilhus NE & Luckman SP. (2008). Serum matrix metalloproteinase-3 levels are elevated in myasthenia gravis. *J Neuroimmunol* **195**, 96-99.

- Rommel C, Bodine SC, Clarke BA, Rossman R, Nunez L, Stitt TN, Yancopoulos GD & Glass DJ. (2001). Mediation of IGF-1-induced skeletal myotube hypertrophy by PI(3)K/Akt/mTOR and PI(3)K/Akt/GSK3 pathways. *Nat Cell Biol* **3**, 1009-1013.
- Rose AJ, Alsted TJ, Kobbero JB & Richter EA. (2007a). Regulation and function of Ca²⁺-calmodulin-dependent protein kinase II of fast-twitch rat skeletal muscle. *J Physiol* **580**, 993-1005.
- Rose AJ, Frosig C, Kiens B, Wojtaszewski JF & Richter EA. (2007b). Effect of endurance exercise training on Ca²⁺ calmodulin-dependent protein kinase II expression and signalling in skeletal muscle of humans. *J Physiol* **583**, 785-795.
- Rose AJ & Hargreaves M. (2003). Exercise increases Ca²⁺-calmodulin-dependent protein kinase II activity in human skeletal muscle. *J Physiol* **553**, 303-309.
- Rose AJ, Kiens B & Richter EA. (2006). Ca²⁺-calmodulin-dependent protein kinase expression and signalling in skeletal muscle during exercise. *J Physiol* **574**, 889-903.
- Roy RR, Monke SR, Allen DL & Edgerton VR. (1999). Modulation of myonuclear number in functionally overloaded and exercised rat plantaris fibers. *J Appl Physiol* **87**, 634-642.
- Rudnicki MA, Schnegelsberg PN, Stead RH, Braun T, Arnold HH & Jaenisch R. (1993). MyoD or Myf-5 is required for the formation of skeletal muscle. *Cell* **75**, 1351-1359.
- Rupp F, Payan DG, Magill-Solc C, Cowan DM & Scheller RH. (1991). Structure and expression of a rat agrin. *Neuron* **6**, 811-823.
- Sabourin LA & Rudnicki MA. (2000). The molecular regulation of myogenesis. *Clin Genet* **57**, 16-25.
- Sakamoto K, Arnolds DE, Ekberg I, Thorell A & Goodyear LJ. (2004). Exercise regulates Akt and glycogen synthase kinase-3 activities in human skeletal muscle. *Biochem Biophys Res Commun* **319**, 419-425.
- Sakamoto K, Aschenbach WG, Hirshman MF & Goodyear LJ. (2003). Akt signaling in skeletal muscle: regulation by exercise and passive stretch. *Am J Physiol Endocrinol Metab* **285**, E1081-1088.
- Sakamoto K, Hirshman MF, Aschenbach WG & Goodyear LJ. (2002). Contraction regulation of Akt in rat skeletal muscle. *J Biol Chem* **277**, 11910-11917.
- Sakuma K, Akiho M, Nakashima H, Nakao R, Hirata M, Inashima S, Yamaguchi A & Yasuhara M. (2008). Cyclosporin A modulates cellular localization of MEF2C protein and blocks fiber hypertrophy in the overloaded soleus muscle of mice. *Acta Neuropathol* **115**, 663-674.

- Sakuma K & Yamaguchi A. (2010). The functional role of calcineurin in hypertrophy, regeneration, and disorders of skeletal muscle. *J Biomed Biotechnol* **2010**, 721219.
- Sanchez H, Bigard X, Veksler V, Mettauer B, Lampert E, Lonsdorfer J & Ventura-Clapier R. (2000). Immunosuppressive treatment affects cardiac and skeletal muscle mitochondria by the toxic effect of vehicle. *J Mol Cell Cardiol* **32**, 323-331.
- Sandri M. (2008). Signaling in muscle atrophy and hypertrophy. *Physiology (Bethesda)* **23**, 160-170.
- Sanes JR, Johnson YR, Kotzbauer PT, Mudd J, Hanley T, Martinou JC & Merlie JP. (1991). Selective expression of an acetylcholine receptor-lacZ transgene in synaptic nuclei of adult muscle fibers. *Development* **113**, 1181-1191.
- Sanes JR & Lichtman JW. (1999). Development of the vertebrate neuromuscular junction. *Annu Rev Neurosci* **22**, 389-442.
- Sanes JR & Lichtman JW. (2001). Induction, assembly, maturation and maintenance of a postsynaptic apparatus. *Nat Rev Neurosci* **2**, 791-805.
- Sapru MK, Florance SK, Kirk C & Goldman D. (1998). Identification of a neuregulin and protein-tyrosine phosphatase response element in the nicotinic acetylcholine receptor epsilon subunit gene: regulatory role of an Rts transcription factor. *Proc Natl Acad Sci U S A* **95**, 1289-1294.
- Schaeffer L, de Kerchove d'Exaerde A & Changeux JP. (2001). Targeting transcription to the neuromuscular synapse. *Neuron* **31**, 15-22.
- Schaeffer L, Duclert N, Huchet-Dymanus M & Changeux JP. (1998). Implication of a multisubunit Ets-related transcription factor in synaptic expression of the nicotinic acetylcholine receptor. *EMBO J* **17**, 3078-3090.
- Schiaffino S, Sandri M & Murgia M. (2007). Activity-dependent signaling pathways controlling muscle diversity and plasticity. *Physiology (Bethesda)* **22**, 269-278.
- Schiaffino S & Serrano A. (2002). Calcineurin signaling and neural control of skeletal muscle fiber type and size. *Trends Pharmacol Sci* **23**, 569-575.
- Seale P, Sabourin LA, Girgis-Gabardo A, Mansouri A, Gruss P & Rudnicki MA. (2000). Pax7 is required for the specification of myogenic satellite cells. *Cell* **102**, 777-786.
- Semsarian C, Wu MJ, Ju YK, Marciniak T, Yeoh T, Allen DG, Harvey RP & Graham RM. (1999). Skeletal muscle hypertrophy is mediated by a Ca²⁺-dependent calcineurin signalling pathway. *Nature* **400**, 576-581.

- Shaw JP, Utz PJ, Durand DB, Toole JJ, Emmel EA & Crabtree GR. (1988). Identification of a putative regulator of early T cell activation genes. *Science* **241**, 202-205.
- Shen T, Liu Y, Cseresnyes Z, Hawkins A, Randall WR & Schneider MF. (2006). Activity- and calcineurin-independent nuclear shuttling of NFATc1, but not NFATc3, in adult skeletal muscle fibers. *Mol Biol Cell* **17**, 1570-1582.
- Simeone L, Straubinger M, Khan MA, Nalleweg N, Cheusova T & Hashemolhosseini S. (2010). Identification of Erbin interlinking MuSK and ErbB2 and its impact on acetylcholine receptor aggregation at the neuromuscular junction. *J Neurosci* **30**, 6620-6634.
- Singhal N & Martin PT. (2011). Role of extracellular matrix proteins and their receptors in the development of the vertebrate neuromuscular junction. *Dev Neurobiol*.
- Somoracz A, Tatrai P, Horvath G, Kiss A, Kupcsulik P, Kovalszky I & Schaff Z. (2010). Agrin immunohistochemistry facilitates the determination of primary versus metastatic origin of liver carcinomas. *Hum Pathol* **41**, 1310-1319.
- Song Y & Balice-Gordon R. (2008). New dogs in the dogma: Lrp4 and Tid1 in neuromuscular synapse formation. *Neuron* **60**, 526-528.
- Stetefeld J, Alexandrescu AT, Maciejewski MW, Jenny M, Rathgeb-Szabo K, Schulthess T, Landwehr R, Frank S, Ruegg MA & Kammerer RA. (2004). Modulation of agrin function by alternative splicing and Ca²⁺ binding. *Structure* **12**, 503-515.
- Stitt TN, Drujan D, Clarke BA, Panaro F, Timofeyva Y, Kline WO, Gonzalez M, Yancopoulos GD & Glass DJ. (2004). The IGF-1/PI3K/Akt pathway prevents expression of muscle atrophy-induced ubiquitin ligases by inhibiting FOXO transcription factors. *Mol Cell* **14**, 395-403.
- Strochlic L, Cartaud A & Cartaud J. (2005). The synaptic muscle-specific kinase (MuSK) complex: new partners, new functions. *Bioessays* **27**, 1129-1135.
- Sugiyama JE, Glass DJ, Yancopoulos GD & Hall ZW. (1997). Laminin-induced acetylcholine receptor clustering: an alternative pathway. *J Cell Biol* **139**, 181-191.
- Talmadge RJ, Otis JS, Rittler MR, Garcia ND, Spencer SR, Lees SJ & Naya FJ. (2004). Calcineurin activation influences muscle phenotype in a muscle-specific fashion. *BMC Cell Biol* **5**, 28.
- Tang H & Goldman D. (2006). Activity-dependent gene regulation in skeletal muscle is mediated by a histone deacetylase (HDAC)-Dach2-myogenin signal transduction cascade. *Proc Natl Acad Sci U S A* **103**, 16977-16982.
- Tang H, Macpherson P, Argetsinger LS, Cieslak D, Suhr ST, Carter-Su C & Goldman D. (2004). CaM kinase II-dependent phosphorylation of myogenin contributes to activity-dependent

- suppression of nAChR gene expression in developing rat myotubes. *Cell Signal* **16**, 551-563.
- Tang H, Macpherson P, Marvin M, Meadows E, Klein WH, Yang XJ & Goldman D. (2009). A histone deacetylase 4/myogenin positive feedback loop coordinates denervation-dependent gene induction and suppression. *Mol Biol Cell* **20**, 1120-1131.
- Tang H, Sun Z & Goldman D. (2001). CaM kinase II-dependent suppression of nicotinic acetylcholine receptor delta-subunit promoter activity. *J Biol Chem* **276**, 26057-26065.
- Taniguchi M, Kurahashi H, Noguchi S, Fukudome T, Okinaga T, Tsukahara T, Tajima Y, Ozono K, Nishino I, Nonaka I & Toda T. (2006). Aberrant neuromuscular junctions and delayed terminal muscle fiber maturation in alpha-dystroglycanopathies. *Hum Mol Genet* **15**, 1279-1289.
- Tansey MG, Chu GC & Merlie JP. (1996). ARIA/HRG regulates AChR epsilon subunit gene expression at the neuromuscular synapse via activation of phosphatidylinositol 3-kinase and Ras/MAPK pathway. *J Cell Biol* **134**, 465-476.
- Tidball JG. (2005). Mechanical signal transduction in skeletal muscle growth and adaptation. *J Appl Physiol* **98**, 1900-1908.
- Tremblay MR & Carbonetto S. (2006). An extracellular pathway for dystroglycan function in acetylcholine receptor aggregation and laminin deposition in skeletal myotubes. *J Biol Chem* **281**, 13365-13373.
- Tseng CN, Zhang L, Cascio M & Wang ZZ. (2003). Calcium plays a critical role in determining the acetylcholine receptor-clustering activities of alternatively spliced isoforms of Agrin. *J Biol Chem* **278**, 17236-17245.
- Tseng CN, Zhang L, Wu SL, Wang WF, Wang ZZ & Cascio M. (2011). Asparagine of z8 insert is critical for the affinity, conformation, and acetylcholine receptor-clustering activity of neural agrin. *J Biol Chem* **285**, 27641-27651.
- Valenzuela DM, Stitt TN, DiStefano PS, Rojas E, Mattsson K, Compton DL, Nunez L, Park JS, Stark JL, Gies DR & et al. (1995). Receptor tyrosine kinase specific for the skeletal muscle lineage: expression in embryonic muscle, at the neuromuscular junction, and after injury. *Neuron* **15**, 573-584.
- Verbeek MM, Otte-Holler I, van den Born J, van den Heuvel LP, David G, Wesseling P & de Waal RM. (1999). Agrin is a major heparan sulfate proteoglycan accumulating in Alzheimer's disease brain. *Am J Pathol* **155**, 2115-2125.
- Vezina-Audette R. (2009). Calcium/Calmodulin Kinase II downstream of muscle activity regulates the aggregation of acetylcholine receptors in response to laminin. In *Department of Biology*. McGill University, Montreal.

- Vogel Z, Christian CN, Vigny M, Bauer HC, Sonderegger P & Daniels MP. (1983). Laminin induces acetylcholine receptor aggregation on cultured myotubes and enhances the receptor aggregation activity of a neuronal factor. *J Neurosci* **3**, 1058-1068.
- Vyas DR, Spangenburg EE, Abraha TW, Childs TE & Booth FW. (2002). GSK-3beta negatively regulates skeletal myotube hypertrophy. *Am J Physiol Cell Physiol* **283**, C545-551.
- Walke W, Staple J, Adams L, Gnegy M, Chahine K & Goldman D. (1994). Calcium-dependent regulation of rat and chick muscle nicotinic acetylcholine receptor (nAChR) gene expression. *J Biol Chem* **269**, 19447-19456.
- Wallace BG, Qu Z & Haganir RL. (1991). Agrin induces phosphorylation of the nicotinic acetylcholine receptor. *Neuron* **6**, 869-878.
- Wang J, Campos B, Jamieson GA, Jr., Kaetzel MA & Dedman JR. (1995). Functional elimination of calmodulin within the nucleus by targeted expression of an inhibitor peptide. *J Biol Chem* **270**, 30245-30248.
- Wang J, Jing Z, Zhang L, Zhou G, Braun J, Yao Y & Wang ZZ. (2003). Regulation of acetylcholine receptor clustering by the tumor suppressor APC. *Nat Neurosci* **6**, 1017-1018.
- Weston C, Gordon C, Teresa G, Hod E, Ren XD & Prives J. (2003). Cooperative regulation by Rac and Rho of agrin-induced acetylcholine receptor clustering in muscle cells. *J Biol Chem* **278**, 6450-6455.
- Weston C, Yee B, Hod E & Prives J. (2000). Agrin-induced acetylcholine receptor clustering is mediated by the small guanosine triphosphatases Rac and Cdc42. *J Cell Biol* **150**, 205-212.
- Williams S, Ryan C & Jacobson C. (2008). Agrin and neuregulin, expanding roles and implications for therapeutics. *Biotechnol Adv* **26**, 187-201.
- Winzen U, Cole GJ & Halfter W. (2003). Agrin is a chimeric proteoglycan with the attachment sites for heparan sulfate/chondroitin sulfate located in two multiple serine-glycine clusters. *J Biol Chem* **278**, 30106-30114.
- Wu H, Xiong WC & Mei L. (2010). To build a synapse: signaling pathways in neuromuscular junction assembly. *Development* **137**, 1017-1033.
- Yokoyama S & Asahara H. (2011). The myogenic transcriptional network. *Cell Mol Life Sci* **68**, 1843-1849.
- Zhang B, Luo S, Wang Q, Suzuki T, Xiong WC & Mei L. (2008). LRP4 serves as a coreceptor of agrin. *Neuron* **60**, 285-297.

